Université d'Ottawa • University of Ottawa

Electrochemical Quartz Crystal Microbalance and Impedance Analysis Investigations of Surface Processes at Platinum Electrodes

by

Steve V. De Cliff

A thesis submitted to the School of Graduate Studies and Research in partial fulfilment of the requirements for the degree of

Doctor of Philosophy
(Ph.D)
in Chemistry

Ottawa-Carleton Chemistry Institute
Department of Chemistry
University of Ottawa
Ottawa, Ontario, Canada

August 1996

Dr. C. Paul Wilde
Research Supervisor

Steve V. De Cliff
Ph.D Candidate

To Kevin Steven, my son:
with love

To my Parents:
in memory

To Marie-Rose Kituro, my mother-in-law:
in memory

Acknowledgements

I would like to express my grateful thanks to Professor C. Paul Wilde, my research supervisor, for his help and guidance throughout the course of this work. Professor Wilde has always been available for discussions and help when I have had questions and problems. I can't thank him enough for the time he has spent and the patience he has demonstrated in course of the last four years, especially this last year when he had to travel from London (UK) to Ottawa.

I would like to thank my colleagues in this lab, Dr. Meijie Zhang, Devi Pisharodi, Hassan Al-Maznai, Dr. Dong-Fang Yang and Qu Deyu, with whom I have worked over the past years for their support, advice, discussions and the many enjoyable and memorable moments we shared.

My sincere thanks go to Dr. Mario Morin for so much help and advice, especially for his help during the preparation, practice and presentation of my research seminar.

My sincere thanks are in order to all the technical and support staff, including Mr. E. Kristoff and J. Hopkins for making the glass cells used in this work, Mr. F. Allard for building the electronic circuits, Mr. L. Sorensen for his help with mechanics and Mr. J.P. McCaffrey (NRC) for performing the SEM analyses of quartz crystals.

I would like to thank all the people in Science Store and all the chemistry department staff, especially Mme Lise Maisonneuve (OCCI), Mme Monique Levesque, Mme Anette Fournier, Mme Johanne Pilon and Mme Murielle Brazeau.

I would like to thank Mr. Robert Auger and his family (Nicole, Steve and Pascal) for their support and encouragement during the last ten years. A part of this thesis has been printed with a laser printer they gave me as a Christmas gift.

I am also grateful to the University of Ottawa for his financial support under which I was able to undertake this research work.

Above all, I am greatly indebted to my wife, Liliane, for her love, encouragement and support throughout this work. She agreed for the time being to stop her school studies and join the employment market in order to permit me to finish this Ph.D program. Also my thanks are to Kevin, my son, Anita and Rachelle, my little sisters-in-law.

* * *

Table of Contents

Chapter 2:
Fundamentals of the Electrochemical Quartz Crystal Microbalance (EQCM)

Chapter 3:
Experimental and Apparatus

Chapter 4:
Influence of Surface Pre-Treatment and Anions on the Electrochemical Quartz Crystal Microbalance (EQCM): Studies at Electrodeposited Platinum Electrodes (EDPE)

Chapter 5:
Adsorption and Oxidation of Thiourea at Electrodeposited Platinum Electrodes

Chapter 6:
Adsorption of Chloride on
Electrodeposited Platinum Electrodes

* * *

List of Figures

* * *

List of Tables

* * *

Abstract

This thesis is concerned with the application of the Electrochemical Quartz Crystal Microbalance (EQCM) and of Impedance Analysis (IA) of EQCM electrodes in investigations of surface processes, particularly adsorption, at electrodeposited platinum electrodes.

In the first part of the present work, we have studied effects that can influence the mass (frequency) response that is measured by the EQCM technique. The factors investigated include: the preparation (platinization) and pre-treatment (cycling) of the electrode material itself which changes the electrode area, the surface roughness of the electrode and the identity and concentration of the anions of the background electrolyte. Anions of the background electrolyte are found to influence the observed mass response, but analysis of the data is difficult. The most important discovery in this thesis is that the EQCM reveals large frequency changes in the region of adsorbed hydrogen at Pt electrodes that have been extensively cycled. While this has been noted before, it has not been investigated thoroughly and no quartz crystal impedance experiments have been performed before now. EQCM and impedance experiments carried out in different electrolytes across a range of pH suggest that the large change is due to an interaction

between weakly adsorbed hydrogen and water which leads to an increase in the structure of the solvent close to the interface. The existence of this interaction has been noted previously in FTIR studies. The effect may also be influenced by adsorbed anions.

This work has shown that the surface state of an electrode and its hydrophilicity or hydrophobicity can have large effects on the frequency (mass) response. These changes cannot be seen from the electrochemical response alone.

In addition to the study of the adsorption of anions from the supporting electrolytes, the adsorption of another strongly adsorbing anion (chloride) and of a neutral adsorbate (thiourea) has been investigated. Thiourea adsorbs strongly to Pt and when present at or close to monolayer coverage has the effect of removing mass changes seen in the background electrolyte. In solutions where thiourea is present and the potential of the electrode is slowly increased, the mass is constant until the electrode surface is oxidised. This suggests that re-adsorption of products of thiourea oxidation or reactant occurs when adsorbates are removed at potentials below those where the electrode surface is oxidised. When the bulk thiourea concentration is very small, the re-adsorption is prevented and a mass decrease is seen as the adsorbed species are removed from the electrode surface by oxidation. Complete removal of adsorbates requires several cycles under the conditions used because of product adsorption.

In contrast to thiourea, adsorbed chloride influences the mass response in the H adsorption region of potential but does not produce complete blocking of mass changes of the background electrolyte. The most interesting responses were in the region of

potential where the electrode is oxidised. A series of mass responses that change substantially with potential and chloride concentration were suggested to result from a shifting balance between chloride desorption, possible adsorption of Cl^-, oxide formation and electrode dissolution.

Finally, this study shows that the EQCM technique can be a useful complement to other more sophisticated spectroscopic techniques, such as FTIR, in giving relevant information on the surface processes such as hydrophilicity, and perhaps changes in the structure of the electrolyte and solvent close to an electrode, processes that cannot be easily detected by conventional electrochemical techniques.

* * *

Chapter 1:

General Introduction

1.1. OVERVIEW AND MOTIVATION

1.1.1. Objective of this Research Work

The objective of this work is the investigation of surface processes, particularly adsorption, at platinum electrodes. The technique used is a coupling of a series of electrochemical techniques, mainly Cyclic Voltammetry (CV), with the Quartz Crystal Microbalance (QCM), which is a mass sensing technique. Both together give the Electrochemical Quartz Crystal Microbalance (EQCM), an *in situ* technique.

The EQCM technique involves, as we will see in more detail in Chapter 2, the use of electrodes that are deposited onto quartz crystals. These crystals are stimulated

to oscillate in the thickness shear mode and if mass is added to the crystal, for example by electrodeposition of another metal, then the frequency of oscillation changes and a simple linear relationship can be used to calculate the added mass from the observed frequency change. However, when such systems are operated in solution, the shear wave of the crystal causes a shear wave to propagate into solution (this is pictured in Figure 2.7). A change in the nature of the electrode surface - for example if it is made hydrophobic or hydrophilic - can alter the interaction between the oscillating crystal/electrode surface and the solution and this can lead to a frequency change that is not due to a mass change. The power of the EQCM technique derives from the comparison of mass and electrochemical data (for example, solvent movement in polymer films on electrodes can be detected with the EQCM since it leads to a mass change but not to passage of charge). Thus the possibility of changes at an interface giving rise to a frequency shift that is not due to a mass change is a disadvantage of the EQCM technique. Even if the presence of the quartz crystal as the substrate for the electrode does not affect the conventional electrochemical measurable parameters (current and charge), little is known of how a change of the solution properties or of properties at the metal/ electrolyte interface, perhaps as a result of a variation of potential of the electrode, really affect the interaction between electrode and solution and thus the frequency signal.

The identification of the factors that influence the frequency response at an EQCM is a difficult task, but a study in this area has the potential to provide

interesting information of a type that is not available from any other experiment.

In effect, it is well recognized that several factors such as preparation (in other words whether or not the electrode is a polycrystal, a single crystal or is electrodeposited) and cleaning of the electrode (some treatments may leave the electrode in an oxidised state, or may increase the roughness of the surface) affect the behaviour of an electrode surface, particularly for example its catalytic activity. The work presented here employs electrodeposited Pt, and so the problem of preparation starts with the electroplating process itself and the conditions under which it is carried out. Some studies (described in Chapter 4) have used vapour deposited Pt electrodes on the EQCM and Pt electrodes can be cycled to give a preferred orientation but so far, no EQCM studies in single crystal or preferred orientation Pt EQCM electrodes have been reported. Then for a given electrodeposited Pt electrode, another complication arises during electrochemical cleaning (cycling) in order to recover a clean Pt surface (free of adsorbed chloride) after the plating process. In both cases, the electrode can undergo changes in roughness and microstructure. These factors could be expected to have an influence on the interaction between surface and solution and hence, as described above, on the QCM response. Thus, any EQCM measurement should start with a characterization of all the effects that may affect the mass response given by the EQCM measurement. This starts with the influence of the electrolyte itself, the concentration of anions from supporting electrolytes, the pH and the nature of the

electrolyte. This is, in fact, the prime objective of this research work. It is to explore the effect of anionic and neutral adsorbates on the electrochemical and frequency responses.

There is still much debate in the literature concerning whether or not the EQCM can monitor such processes effectively.

1.1.2. Presentation of Systems Investigated

The main surface process investigated in this work is the phenomenon of adsorption of different types at Pt electrodes. The choice of the substances for the study of adsorption has been judiciously oriented in the two sub-fields of organic and ionic species. The organic domain is represented by thiourea (TU), which is a strongly adsorbing S-containing molecule. As for inorganic ions, the study is varied because the electrolytes themselves are composed of anions and cations. Anions are typically larger (particularly polyatomic ions such as perchlorate and sulphate) and less solvated than cations and so have a greater tendency to adsorb specifically. However, there is still a great variability in the extent of adsorption of anions with ions such as fluoride and perchlorate regarded as weakly adsorbing species while ions such as chloride are known to adsorb more strongly. Typical supporting electrolytes for electrochemical studies employ those ions that adsorb least, such as perchlorate and sulphate, and so the adsorption of these anions from supporting electrolytes will be a starting point for

examining anionic adsorption before the adsorption of halide anions (chloride and bromide).

1.1.3. Presentation of the Technique Used

As mentioned above, the method used to study surface processes in this thesis is the Electrochemical Quartz Crystal Microbalance. The technique is a coupling between a *programmed potential voltammetry* (PPV) technique, mainly *Cyclic Voltammetry (CV)*, and the QCM technique, which involves mass sensing. Programmed potential voltammetry is a technique that has been extensively documented in the electrochemical literature[1] . Consequently, this technique will not be discussed here. But in the majority of our experiments, the potential has been *programmed* as following:

① After pre-treatment of the electrode, the potential is held at fixed potential (E_{hold}) for various holding times (t_{hold}). During that time, an adsorbate may be added to the electrolyte and transient responses (current or mass) may be recorded if necessary.

② The potential E_{hold} is then gradually modulated to higher potentials (oxidation) or lower potentials (reduction) and scanned back to the original potential. This

kind of potential programming is the well known *Cyclic Voltammetry (CV)* technique.

③ In certain cases, the potential E_{Hold} is just stepped to a single potential where it is expected that some desired electrode process (oxidation, reduction, adsorption or desorption of species) might occur.

In chapter 2, the theory of the EQCM will be presented, but it is important to re-iterate at this stage that the EQCM is sensitive to factors other than added mass. Thus in this thesis, the EQCM has been used to study adsorption processes and in addition, the factors that affect the response of the EQCM have also been studied. A more complete knowledge in this area is important for establishing the potential usefulness and limitations of the EQCM for the study of electrode processes.

1.2. *OVERVIEW OF ELECTRODE PROCESSES*

1.2.1. Introduction of Useful Concepts

Because adsorption of ions and neutral molecules is a major focus of this thesis, some background knowledge concerning the electrode/ electrolyte interface is

presented here. In the study of *electrode processes* the only diagnostic element of the existence of an electrode reaction process is the observation and the measurement of a *current flow* that is a result of a perturbation of the electrode/ electrolyte interface due to a change of one or several parameters. These parameters are: charge (electrons) across the interface, electrode potential, electrode area and solution composition. Among these parameters, it is the first parameter that serves to categorize all the processes that occur at the interface, depending on whether the charge (electrons) are transferred or not across the interface. Thus one distinguishes *faradaic processes*, those due to the passage of a charge *across* the interface leading to oxidation or reduction reactions according to the Faraday's law (the amount of chemical reaction caused by the flow of the current is proportional to the amount of electricity passed), and *non-faradaic processes*, those that do not lead to any passage of charge across the interface, even if a potential is applied. In the latter case of nonfaradaic processes, the observed current flow is due to the variation of other parameters such as electrode potential, electrode area and solution composition. Adsorption and desorption phenomena usually, but by no means always, fall in the latter category.

Many non-faradaic processes such as adsorption and desorption processes are of primary importance in the characterization of the structure of the electrode/ electrolyte interface. Unfortunately, it is difficult to find an electrode that only exhibits nonfaradaic processes. Otherwise, both faradaic and nonfaradaic processes will occur,

which is the *real* situation encountered in electrochemistry. If we consider an interface where there are no faradaic processes occurring, since charge cannot cross this interface when a potential is applied across it, this interface behaves (and is often modelled) as a capacitor composed of two main plates of equal surface area A: the metal itself with the charge density σ^M (or charge q^M, with $\sigma^M = q^M/A$) and the solution side with the charge density σ^S (or charge q^S, with $\sigma^S=q^S/A$). The charge in the solution is composed of ions attracted to the interface to balance the charge on the electrode. Since there may be some adsorbed species on the electrode (depending on the nature of the solution), the charge density σ^S comes from the contribution of charge densities generated by charged species, usually ions, and solvent molecules, that are located at specific distances from the metal electrode. The above capacitor appears then to be made of several capacitor plates. The whole array of charged species and oriented dipoles existing at the electrode/ solution interface is the so called *electrical double-layer* [2,3].

The electrode/ electrolyte interface is then referred to as the electrical double-layer. The electrode carries an excess or deficiency of charge and always attracts an equal and opposite excess of ions in the region of solution closest to it. However, there is a potential at which the electrode is free of excess charge. This potential is called the *potential of zero charge (pzc)* [2,3]. In addition to coulombic considerations, it is important to note that for most studies where the solvent will be water, the solvent

molecules are dipoles, and will be oriented at the electrode surface by the charge with the direction of orientation being dictated by the sign of the charge. Solvent dipoles, when the solvent is water, may serve as scale for evaluation of the *hydrophilicity/ hydrophobicity* [4b] of the interface. This is a concept that is difficult to quantify and yet it may play a strong role in the interaction between the electrode of the EQCM, which is oscillating, and the solution and may influence the frequency signal that is seen.

A short review of some important concepts in connection with the interface metal/ electrolyte is presented below. These concepts are:

① the structure of the double-layer,

② specific and non-specific adsorption,

③ the potential of zero charge, and,

④ hydrophilicity/ hydrophobicity.

It is only when these concepts are clarified that the electrochemistry of metal electrodes such as platinum can be discussed more clearly.

1.2.2. Structure of the Metal/ Electrolyte Interface

Given the fact that this thesis involves a study of adsorption at electrodes, an

understanding of the structure of the metal solution interface is an important starting point. Without embarking on a more complicated explanation, one can say that the electrochemical cell used in this work comprises the following collection of interfacial elements:

① a metal electrode (made of electrodeposited platinum);

② an aqueous solution of electrolyte (supporting electrolyte);

③ a quartz crystal resonator that serves as the mass sensing element.

The interfacial elements ① and ② define what is commonly called the metal/ electrolyte interface. This interface is purely electrochemical and as an interface, all its properties are governed by *excesses* and *deficiencies* in the concentrations of components.

Although the interfacial element ③ is present, it should play no role in the response that is observed, as it is only in the region where the quartz crystal is covered by a metal that oscillation occurs in the EQCM method. The most relevant interface for this work is the *metal/ electrolyte* interface.

Various factors can affect such an interface. However, at the interface a sudden interruption of the positive field due to the positive nuclei causes the distributed

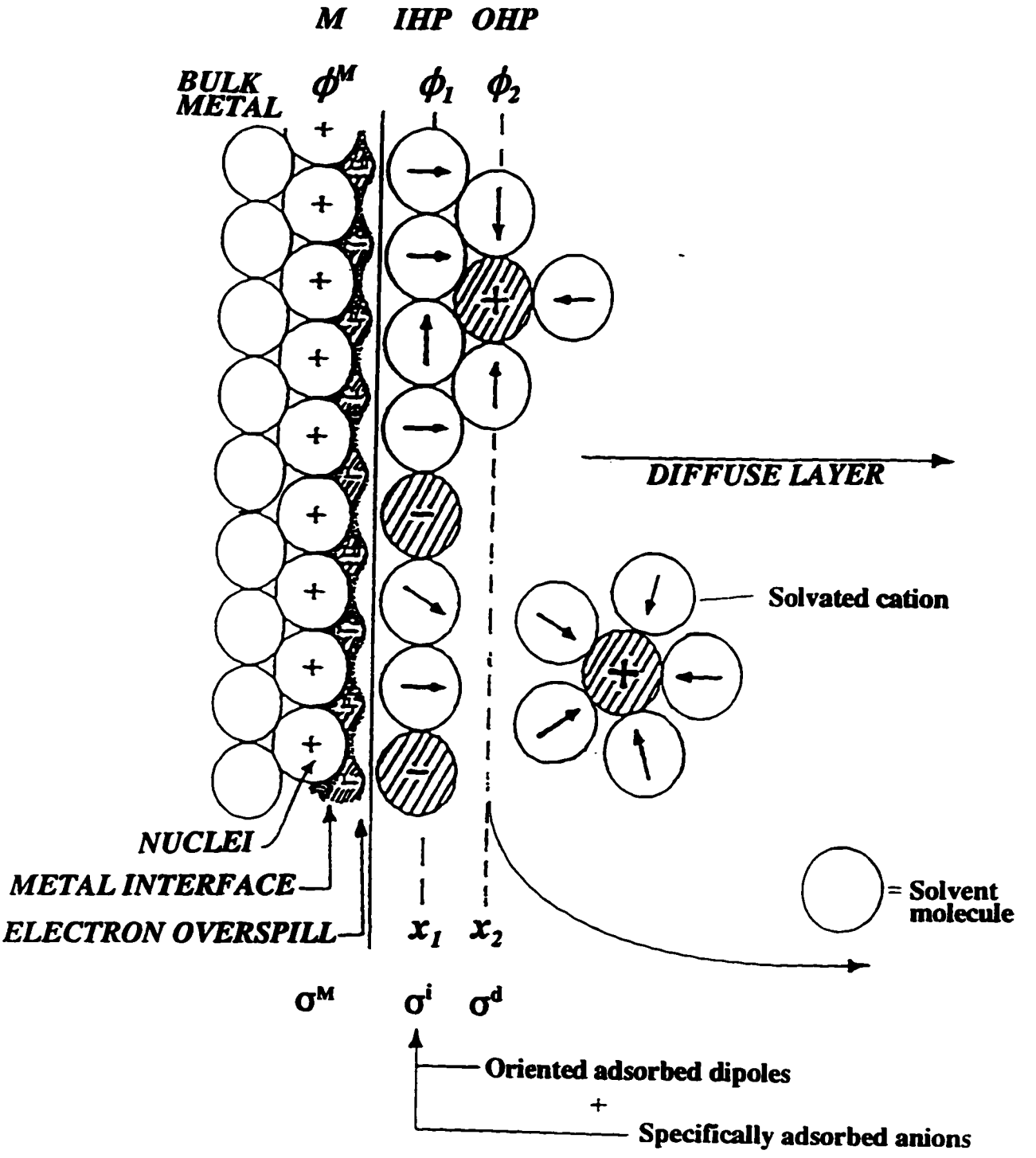

Figure 1-1:

Schematic diagram of the complex interphase at a metal/ electrolyte boundary with solvent molecules and ions present (*adapted from refs. 1 and 16*).

electrons to "overspill" the edge of the lattice (Figure 1-1). As result, there is creation of a deficiency or excess of negative charge in the metal surface layer, either outward or inward from the nominal surface. This leads to a separation of charges that defines the intrinsic surface potential, ϕ^M, of the metal in contact with the considered physical medium. Both the charge at the metal and the potential of the metal are defined on the basis of the concept of the electrified interface, also called the *electric double-layer* or simply the *double-layer.*

In the double-layer region, the field created by the potential ϕ^M (due to the charge q^M) can polarise any adsorbate species in the vicinity of the double-layer. Thus, the electron overspill effect is potential dependent. For the metal/solution interface, composed in this case of a platinum electrode and the electrolyte solution, the essential elements of the influence of the solution on the properties of the metal/solution interface have been well established. On the basis of the analysis of results of capacity measurements in various solvents, Frumkin was the first to point out that the properties of the solvent at the metal/ solution interface are different from those in the bulk solution even when the charge at the metal is zero[6]. For example, capacity measurements for adsorbed water on solids[7] and density measurements of water at solids/ water interfaces show that the state of water molecules is more ordered and more structured at most interfaces investigated than in the bulk solution [8]. Thus the metal/ solution interface is very complex when compared to the metal/vacuum interface.

Some possible structural features of the interface between an electrode and solution are:

① The existence of oriented solvent dipoles at the interface;

② The existence of specifically adsorbed anions and neutral molecules;

③ The existence of electrostatic adsorption of some ions;

④ Adsorption of solvated ions and lateral interactions at the interface between adsorbed species.

All these features show the complexity of the electrical double-layer and exerts a great influence on the electrode processes such as the adsorption of desired substrates. In electrochemistry, many efforts are made in order to know in which conditions all these interactions are minimized. It has been established that this condition is met at potential known as the *potential of zero charge (pzc).*

1.2.3. Potential of Zero Charge (pzc)

The best way of characterizing the double-layer is by a thermodynamic treatment since most of electrochemical quantities can be defined as extensible variables. One of the most often used extensible variables in electrochemistry is the electrochemical free energy $G = (T,P,A,n_i)$ whose total differentials with respect to

thermodynamical variables (A,n_i) gives the evolution of the system (the interface) at constant pressure and temperature. One partial derivative of particular importance is, $(\partial G/\partial A)$, called the *surface tension* γ [1-3].

Measurements of surface tension have played an important role in elucidating the interfacial structure at electrodes particularly for mercury electrodes because good measurements of surface tension are better achieved on liquid electrodes which can be confined in a capillary tube. The variation of the interfacial tension γ with the polarization of the electrode, i.e., its variation with the applied potential E, yields electrocapillary curves, which are simply plots of surface tension versus potential. Plots of these curves give the charge density σ^M of the metal at any potential.

Whatever the system studied, the common feature to all is the existence of a potential at which the surface tension is maximum. This potential is called the *electro-capillary maximum (ECM)* and is an extremely important point in the system. This point is defined as the *potential of zero charge (pzc)* which corresponds to a state of zero excess surface charge density at the electrode. From the above definition, one can say that $\sigma^M > 0$ for $E < pzc$, and $\sigma^M < 0$ for $E > pzc$. This means that, for $\sigma^M > 0$, anions will be attracted to the electrode and for $\sigma^M < 0$, cations will be attracted. Such anions or cations in the double-layer are said to be *specifically adsorbed* on the electrode if their presence on the electrode responds only to the excess or deficiency of charge.

Therefore, measurements of specific adsorption will give information on the potential of zero charge (pzc), and the measurement of the pzc will give information about specific adsorption.

There are many factors that may affect the potential of zero charge (pzc). The most important are[4a,4b]: the nature of the metal electrode, the solution composition, the pH of the medium, the crystallinity and hydrophilicity of the metal electrode. The influence of mechanical properties has also been reported in some electrochemical literatures[19-23].

a) Influence of the nature of the metal electrode on pzc

The influence of the nature of the metal electrode on its pzc can be better investigated if one examines the behaviour of a variety metals in the same solvent electrolytes taken such that the interactions of their ions with the electrode are governed by only electrostatic forces. Thus, the ions that are approaching the electrode surface retain their hydration sheath. When such ions are present on the electrode surface, they are said to be *non-specifically* adsorbed. Practically, all ions to a greater or lesser degree show specific adsorbability at the electrode/ solution interface. As a result, the pzc is shifted (for example, the pzc is shifted in a negative direction if anions adsorb)[1].

b) Influence of the solution composition on pzc

We only consider here the liquid electrolyte medium, so that the solution composition will be made of anions and cations. Among the anions, the specific adsorbability is the least pronounced in the following order [9-12]: ClO_4^- <F^- < SO_x^{2-}<Cl^-< Br^- < SCN^- < I^-. Cations of alkali and alkali-earth metals belong to the group of weakly adsorbable ions. For the same equimolar solution of sodium halide salts (NaX), the specific anion adsorption shifts the pzc in the negative direction in the sequence F^-, Cl^-, Br^-, I^-.

c) Influence of the alkalinity of the medium on pzc

From the definition of the pH, the only direct effect of pH on the pzc should be from specific adsorption of OH^- and H_3O^+. However, some metal electrodes may have hydrogen or oxygen adsorbed on their surface at the pzc in addition to solvent molecules and ions. As a result, the polarity of the metal-H or the metal-O bond contributes an additional term to the pzc. Unfortunately, platinum metal electrodes belong to this category and this does not make the determination of the pzc easy for these kind of metal electrodes. On these kind of electrodes, the surface charge caused by ionization of adsorbed hydrogen or oxygen to form H^+ or OH^- ions or by discharge of the latter is accompanied by a change in the solution acidity. In the case of the

platinum metal electrode, at the potentials $E_{\sigma=0}$, anion adsorption and hydrogen adsorption are mutually antagonistic. This is associated with the polarity of the Pt-H_{ads} bond which has a negative end turned toward the solution. Therefore, for a hydrogen adsorbing metal electrode such as platinum, $E_{Q=0}$ and $E_{\sigma=0}$ are equal only for pH≈7 [4a].

d) Influence of the crystallinity on pzc

There is no doubt that the crystallinity has a great influence on the pzc. A polycrystalline metal electrode appears as a combination or mixture of the electrical properties from the individual single crystal. One of these properties is the potential of zero charge (pzc), whose value for a polycrystalline metal electrode will depend on the composition of single crystal faces in the polycrystal. This has been demonstrated for the highest indexes of platinum (111 and 100) [4a]. When a polycrystalline metal electrode is undergoing ageing (cycling and repetitive experiments), the process can be compared to the electro-dissolution process of the metal electrode since the process has the effect of changing the micro-structure of the electrode surface (roughness), and thus its crystallinity. Therefore, one can say that ageing a polycrystalline metal electrode such as an electrodeposited platinum is the analog of the annealing process for a single crystal, and if the crystallinity of the surface changes during this process, then the pzc of the electrode may change with repetitive use of the electrode.

Since the hydrophilicity is deeply connected to the potential of zero charge

(pzc), its change will result in the shift of the potential of zero charge (pzc), which depends on the nature and alkalinity of the electrolyte.

e) Influence of Hydrophilicity on pzc

Another factor that is usually ignored is the role of the solvent dipole contribution to the inner-layer potential (thus the electrode potential). It has been established that the existence of solvent dipole has the effect of causing a shift in the pzc. When the solvent is water, for aqueous solution electrolytes, this interaction between the water dipole and the surface of a metal electrode defines what is known as hydrophilicity[4b]. In surface chemistry, surfaces with acid sites (OH groups) are generally defined as hydrophilic in the sense that they strongly bind other water molecules by acting as proton donors[13-16]. In contrast, surfaces with exposed oxygen groups (strongly dehydroxylated) often exhibit hydrophobic behaviour[17,18]. In general, a metal surface that easily bind water molecules through the oxygen atom (of water) may be defined as hydrophilic.

The problem of hydrophilicity is made difficult to investigate when the concerned metal reacts with the solvent (water). This is the case for Pt which reacts with water molecules to form Pt-O and Pt-H chemical bonds. Therefore, the dipole of water will interact with the dipoles of the Pt-O and Pt-H bonds. This makes Pt electrodes more difficult to characterize and the electrochemistry of Pt electrodes more

complicated.

f) Influence of mechanical properties on pzc

There is no definitive evidence of the theoretical justification for identifying the maximum of a mechanical property such as creep, deformation under stress or friction of a metal electrode with the pzc. Rebinder and Venstrem[19] were the first to investigate this effect while Bowden and Young[20] were the first to measure the friction between two polarized bodies of platinum. An increase in friction was associated with a reduction of repulsion between the double-layers of the two bodies as the concentration of positively charged species in the diffuse layer decreased on approaching the pzc. In the extreme of cathodic and anodic regions, the effect of adsorbed hydrogen and oxygen in reducing friction was recognized, and this effect was absent in the region of the pzc. The effect of adsorbed layers on the friction measurements has been confirmed by many other researchers[21,22], including Bockris[23].

1.2.4. Adsorption Phenomena at Metal Electrodes

The term "adsorption" usually refers to a phenomenon involving the transfer of material from one phase to an interface, with a change in the concentration of the

substance undergoing adsorption. The interface may be liquid/gas, solid/gas, liquid/liquid or solid/ liquid. In our work, the interface is a solid/ liquid interface composed of an electrodeposited Pt coated on a quartz crystal surrounded by an electrolyte.

From the above definition, adsorption is a result of the accumulation of the adsorbate at the interface. The interactions that govern such an accumulation can be either chemical or physical. Adsorption can thus result from a range of interactions between adsorbate and electrode, or in some cases the presence of one adsorbate may induce adsorption of another species. For example, the adsorption of alkaline earth cations by pre-adsorbed OH^- anions belongs to the latter category.

The study of adsorption at the metal/ electrolyte interface provides information about the knowledge on the structure of the interface and the distribution of the electric field across the interface. One important type of adsorption is *specific adsorption*[24].

From simple *coulombic considerations*, the specific adsorption is the amount of adsorbed species which is in excess or deficit of the amount which would be expected to be present at the interface between an electronic and ionic conductor[25]. This means that if there is an excess charge of σ^M on the metal, the coulombic adsorption is $-\sigma^M/nF$ mol per unit area. Then the excess or deficit of adsorption (the amount of adsorption that exceeds $-\sigma^M$ or is less than it) is called specific adsorption.

The most straightforward experimental approach to detecting specific adsorption is the measure of surface excesses or surface tensions. This concept arises from the

fact that a decrease in surface tension is known to be a good indication of adsorption. The excess charge or the surface tension on the electrode can be better defined by the slope of the electrocapillary curve at any potential. For the same coulombic charge, it has been established that this decrease in surface tension changes with the nature of anion[26]. This simply implies that the definition of specific adsorption must be considered beyond the simple coulombic considerations. Therefore, a practical definition of specific adsorption is that takes into account the concept of the potential of zero charge (pzc) which is developed from the Gibbs adsorption concept that better defines the concept of the surface excess. At the potential of zero charge (pzc), specific adsorption will occur when the measured surface excess for *any ionic species* is positive. At potential more positive than the pzc ($\sigma^M > 0$), there is a specific adsorption if the surface excess of *any cation* is positive. At potentials more negative than the pzc ($\sigma^M < 0$), there is a specific adsorption when the surface excess of *any anion* is positive.

1.3. ELECTROCHEMISTRY OF Pt ELECTRODES

1.3.1. Electrodeposited Platinum Electrodes

Electrodeposited Pt electrodes are used in this work and so it is important to review the electrochemistry of Pt. There are three main uses of an electrodeposited (or platinized) platinum electrode: as hydrogen reference electrodes, as inert surfaces of

high area in conductance work, and as catalysts and electro-catalysts particularly for important reactions such as those involved in fuel cells (oxidation of fuels such as hydrogen and methanol coupled with the reduction of oxygen).

Before the review of the aspects of electrodeposition of Pt by Feltham and Spiro[27], the electroplating was considered more of an art than a science. According to Feltham and Spiro, the electrodeposition of platinum, when performed from a chloroplatinic acid solution (2 mM H_2PtCl_6/ 0.2 M H_2SO_4) involves three couples:

$$Pt^{IV}Cl_6^{2-} + 2\,e^- \rightarrow Pt^{II}Cl_4^{2-} + 2\,Cl^- \qquad (1)$$

$$Pt^{II}Cl_4^{2-} + 2\,e^- \rightarrow Pt + 4\,Cl^- \qquad (2)$$

$$Pt^{IV}Cl_6^{2-} + 4\,e^- \rightarrow Pt + 6\,Cl^- \qquad (3)$$

The process involves a successive breaking of several Pt-Cl bonds and is thought to be kinetically slow with extremely low exchange current densities. The electrodeposition of Pt from such a plating bath is generally performed under potentiostatic control. The deposition potential influences the voltammetric behaviour of potentiostatically formed platinized electrodes [28].

1.3.2. Presentation of Some Quantitative Values

Contrarily to liquid metals, solid metals suffer from surface heterogeneity (their

surface are difficult to reproduce and keep clean) and a lack of electrostatic interactions between the metal and the solution species. This makes the double-layer of a metal such as platinum more complex than it is for liquid metals (i.e., Hg). For platinum, the situation is made more complicated by the strong adsorption of hydrogen and oxygen, and the fact the charges easily leak across the interface in the so-called double-layer region of potential, which defines the potential range where there is no adsorbed O or H at the electrode surface. All these aspects make the investigation of the structure of the double-layer at Pt difficult.

The experimental data needed to characterize the double-layer on Pt electrodes are mainly the double-layer capacity, potential of zero charge (pzc), and the amount of specifically adsorbed species. The measurement of the double-layer capacity alone should be sufficient to provide all the information needed to describe the surface excesses (surface tension, surface excess concentration) electrical parameters (potential of zero charge). However, one must know the pzc and its evaluation for a solid electrode such a platinum is, unfortunately, far from straightforward.

A review of the methods used for the evaluation of the pzc on solid metals has been given by Andersen and Perkins[29] and an evaluation of these methods has been done by Bockris *et al*[30]. The determination of the pzc and the double-layer capacity has been a subject of great debate between the Russian School[31-34] and the American

School, under the leadership of Frumkin and Bockris, respectively, with no final consensus being reached. The Russian school preferred the use of methods based on adsorption rather than other methods derived from the electrocapillary method and proposed a value 0.16 to 0.19 V (NHE) as the more correct pzc for Pt in aqueous solution[31]. However, the results proposed by the Russian school have been strongly contested by Bockris *et al*[30,35] who proposed a value of 0.565 ± 0.025 V (NHE). Frumkin's approach allows evaluation of the dependence of the pzc on the pH and fair agreement has been observed between theoretical and experimental results for a wide range of solutions, both in acid and alkali concentrations[34-38].

It is then clear that the determination of the pzc for Pt electrodes is not easy. This makes the development of the exact structure of the double-layer of Pt/ electrolyte interfaces difficult. This is why the characterization of the Pt electrodes should be a research priority for this metal of strategic importance in the industrial catalysis.

1.3.3. Electrosorption of Hydrogen and Oxygen

As noted above in several places, the surface electrochemistry of Pt is complex because it involves both the adsorption of hydrogen and oxygen in different potential ranges. The processes that occur at a Pt surface will now be described in more detail. In principle, there is little difference between a current voltage curve obtained for a

bulk Pt electrode that has been polished smooth and a current voltage curve obtained for an electrodeposited Pt electrode. The standard cyclic voltammogram of Pt is that observed in 0.5M H_2SO_4 for a bare Pt electrode (Fig.1-2, from Ref. 39). From the figure, one can distinguish three regions (potential scale: normal hydrogen electrode, nhe). Region I is the region of hydrogen adsorption/desorption that extends from 0.00 V to 0.40 V; Region II is the double-layer region (from 0.40 to 0.80 V) where there are no surface processes and where there is no faradaic current passed in a background electrolyte such as sulphuric acid. The current passed in this region merely serves to change the charge at the electrode surface. Region III is the surface (Pt) oxide region that extends from 0.80 V to 1.25 V. Below the potential of 0.00 V hydrogen gas is evolved, and above a potential of 1.25 V oxygen gas is evolved, as the solvent of the electrolyte is subject to cathodic and anodic decomposition.

The mechanism of the electrodeposition of H and the formation of the Pt oxide has been discussed extensively in the literature of the electrochemistry of Pt [39,40]:

$$Pt + H_3O^+ + e^- \rightleftharpoons Pt\text{-}H_{ads} + H_2O \qquad (1)$$

$$Pt + H_2O \rightleftharpoons Pt\text{-}OH + H^+ + e^- \qquad (2a)$$

$$Pt\text{-}OH \rightleftharpoons Pt\text{-}O + H^+ + e^- \qquad (2b)$$

The adsorption of hydrogen corresponds to a deposition process that occurs

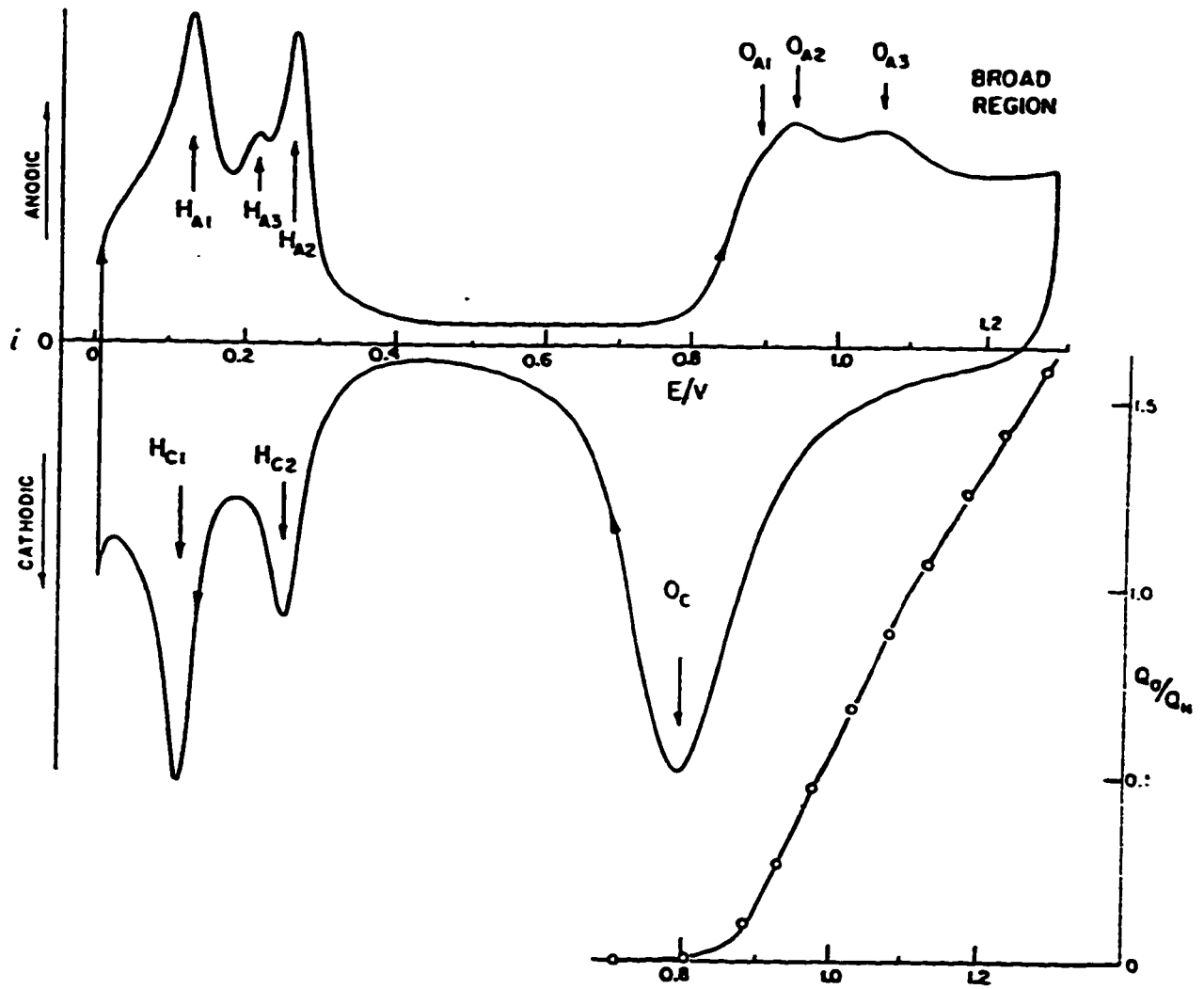

Figure 1-2:

Potentiodynamic i-E profile for Pt surface oxide formation and reduction in high purity 0.5 M aq. H_2SO_4 (25 °C). Scan rate: 100 mV/s. Also shown is the integrated oxide formation charge Q_O/Q_H as a function of anodic potential (*from Conway et al* [39]).

during a negative going scan and is followed by a removal of the previously adsorbed hydrogen when the potential is reversed. The adsorption of H atoms at the lower potential range is an under potential deposition (upd) process because it occurs at potentials more positive than the thermodynamic value for hydrogen evolution. At more positive potentials the formation of the oxide proceeds via a water molecule that is adsorbed in the sites previously occupied by hydrogen and released during the oxidation. The process is a two-electron process during which a Pt-hydroxide (Pt-OH) is first formed, then oxidised to form the Pt-oxide (Pt-O). The broad region before the oxygen evolution corresponds to the potential where the maximum oxide is formed. According to the above mechanism, one electron is transferred during the hydrogen desorption process whereas two electrons are transferred in the oxide formation.

Therefore, the real surface area (and the roughness factor) can be determined since the charge required for electrodeposited H and for electrodeposited O species is well known.

1.3.4. Determination of the Real Surface Area

The determination of the real surface area is very important in electrochemistry especially for adsorption studies for which the amount of adsorbed species is directly dependent on the surface area of the electrode. This is particularly important when a

smooth metal electrode is used because the surface is subjected to change with the repetitive use of a such electrode and the area may change with time.

The real surface area (Fig. 1-3) is calculated either by direct integration (using a charge integrator) or by graphical integration of anodic linear sweep i-E profiles by weighing cut-out i-E profiles of photocopied graph papers (accuracy: ±1%) using the charge value for one monolayer for hydrogen region or for oxide region[41-44]. For Pt electrodes, this charge is 210 μC and 420 per real cm^2 for the hydrogen and oxide regions, respectively. The charge in the oxide region is the double that of the hydrogen region, which agrees with the mechanism given above. In general, the hydrogen region is used for determination of real surface area for Pt, while the oxide region is used for gold which does not show a region of hydrogen adsorption. In this case, the real areas of gold electrodes are determined by taking a value of 400 μC real cm^2 as the charge required for the formation of a monolayer of oxide, according to the procedure of Burshtein *et al* [44].

For electrodes whose the geometric area can be known, the most useful quantity is the *roughness factor* ϕ (R_f or). It is a dimensionless quantity defined as $\phi = A/A'$, where A is the *real surface area*, and A' the *geometric area*. The roughness factor is the most used instead of the real surface area since it better relies the extent of the change of the real surface area with the amount of performed experiments.

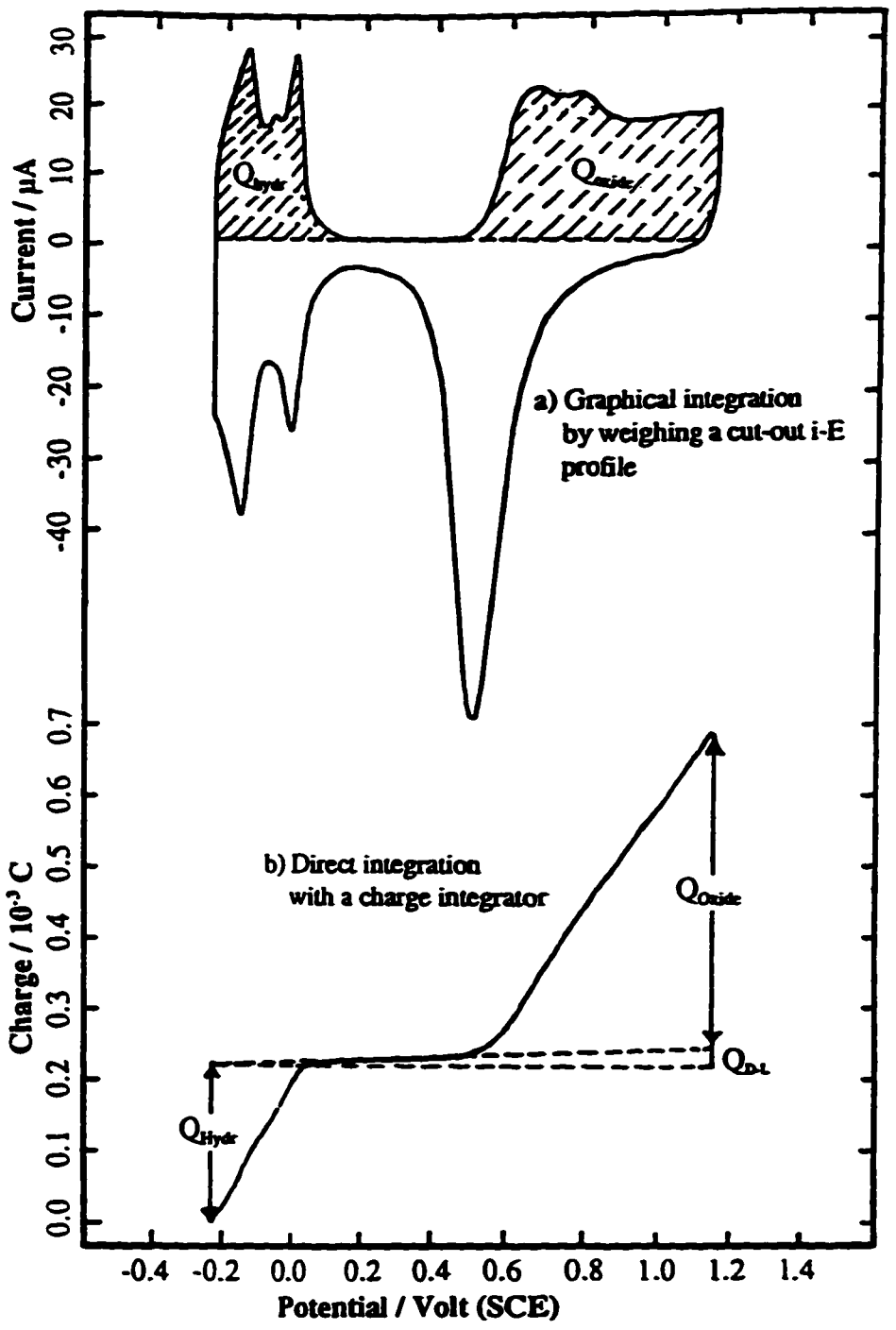

Figure 1-3:

Linear sweep i-E profiles for a platinized Pt electrode. The real surface area is calculated either by direct or graphical integration of the charge value for one monolayer of adsorbed hydrogen.

1.4. ORGANIZATION OF THE CHAPTERS OF THE THESIS

This thesis is organised as follows. Chapter 2, titled "*Fundamentals of the Electrochemical Quartz Crystal Microbalance*", describes the essential elements on the theory of the EQCM. In the first and second sections, an historical introduction of the background of the original QCM (the non electro-chemical aspect) is presented. This includes the piezoelectric effects of the quartz crystal and other materials that are able to exhibit it. The third section is devoted to the physical origins of mass sensing and how this mass sensing is related to the electrochemical measurements, in other words, the description of the electrochemical aspect of the QCM. Circuit and impedance analyses of quartz crystals are naturally introduced in the fourth section.

The experimental and apparatus are briefly presented in chapter 3. The research work is compiled in four experimental chapters (chapter 4 to 7). Chapter 4 is devoted to the characterization of the EQCM technique and presents the essentials on the influence of pre-treatment and anions (from supporting electrolytes) on the EQCM on electrodeposited Pt electrodes (EDP). The results for the study of the adsorption on electrodeposited Pt electrodes using the previously characterized EQCM (chapter 4) are summarised in chapter 5 for the adsorption of thiourea in acid electrolytes and in chapter 6 for halide anions.

* * *

Chapter 2:

Fundamentals of the Electrochemical Quartz Crystal Microbalance (EQCM)

2.1. INTRODUCTION

The piezoelectric quartz crystal microbalance (QCM)[45,46] and, in the last ten years, its electrochemical applications (EQCM)[47-53] have been extensively discussed in the literature. In this chapter we will discuss the theory of operation of the QCM with particular attention to the operation of the QCM in solution. More detailed treatments can be found in several different review articles and books [54-56].

In this section, we will briefly introduce the subject matter of this chapter. The significance of interfacial processes in electrochemical research and also often a lack of

fundamental understanding of how interfacial chemistry affects, for example, electron transfer and adsorption processes, has stimulated the development of methodologies that couple surface-sensitive probes (typically spectroscopic) to conventional electrochemical experiments. For example, the use of a wide range of *in-situ* IR reflectance spectroscopies [57-63], the FTIR in particular and other spectroscopies such as SERS, are now an almost routine part of an electrochemical investigation in many laboratories. Besides IR, other spectroscopies such as mass spectroscopy ("on-line" mass spectroscopy)[64-67], and some *ex situ* UHV techniques [68-71] have also been used to study the intermediates species formed on electrodes. "On-line" liquid chromatography has been efficiently applied to the analysis of species accumulated in the solution [72-75]. The electrochemical quartz crystal microbalance (EQCM), pioneered by Bruckenstein and Shay [47] and Kaufman *et al* [49], is one *non-spectroscopic* method that has been applied to the study of electrode-solution interfaces and it is this technique that has been applied in this thesis. The EQCM is a derivative of the quartz crystal microbalance or QCM and so a brief description of this latter method is presented first.

The quartz crystal microbalance (QCM) is an extremely sensitive probe that can measure mass changes in the nanogram range. It comprises an oscillating piezoelectric quartz crystal wafer that is sandwiched between two metal electrodes deposited in some way on the two faces of the crystal. The QCM was originally used in vacuum and air[45,76], and later adapted to be used in solution. Although the QCM responds (in general) only to

interfacial mass changes (and so is not necessarily a very selective detector), it still provides information that would be difficult to obtain with other conventional methods. Studies performed with the QCM technique include the detection of air pollutants (CO, SO_2, H_2S, HCl, etc.) [54], the electrosorption of oxides and halides [77-79], the electrocatalytic oxidations of organic molecules [80-82], dissolution and oxidation of metals [83-85], under-potential deposition of metals [86-92], electrodeposition of conductive polymers and molecular metals [93-97], the formation of Langmuir-Blodgett films [98], enzymatic studies [99-101], immunoassay techniques [102,103], and characterization of bulk liquid phase properties (density, viscosity and conductivity) [104,105]. When the QCM is coupled with electrochemical techniques, it is referred to as the "electrochemical quartz crystal microbalance" (EQCM) technique. A top view of a typical QCM/EQCM electrode in its enclosure is shown in Figure 2-1.

The use of the QCM in electrochemistry was first demonstrated by Jones and Meiure [106,107] who determined trace metals by deposition of the metal onto a QCM electrode in an electrochemical cell followed by the *ex situ* (in air) analysis of the deposited mass. Successful operation in the liquid environment was demonstrated by Konash and Bastiaans[108] in 1980, and a year later by Nomura[109]. The first *in situ* electrochemical application of the QCM was initiated by Nomura and co-workers [110,111]. These authors used an electrochemical QCM cell to investigate the electrochemical reduction of copper (II) and silver (I) in electrolyte solutions.

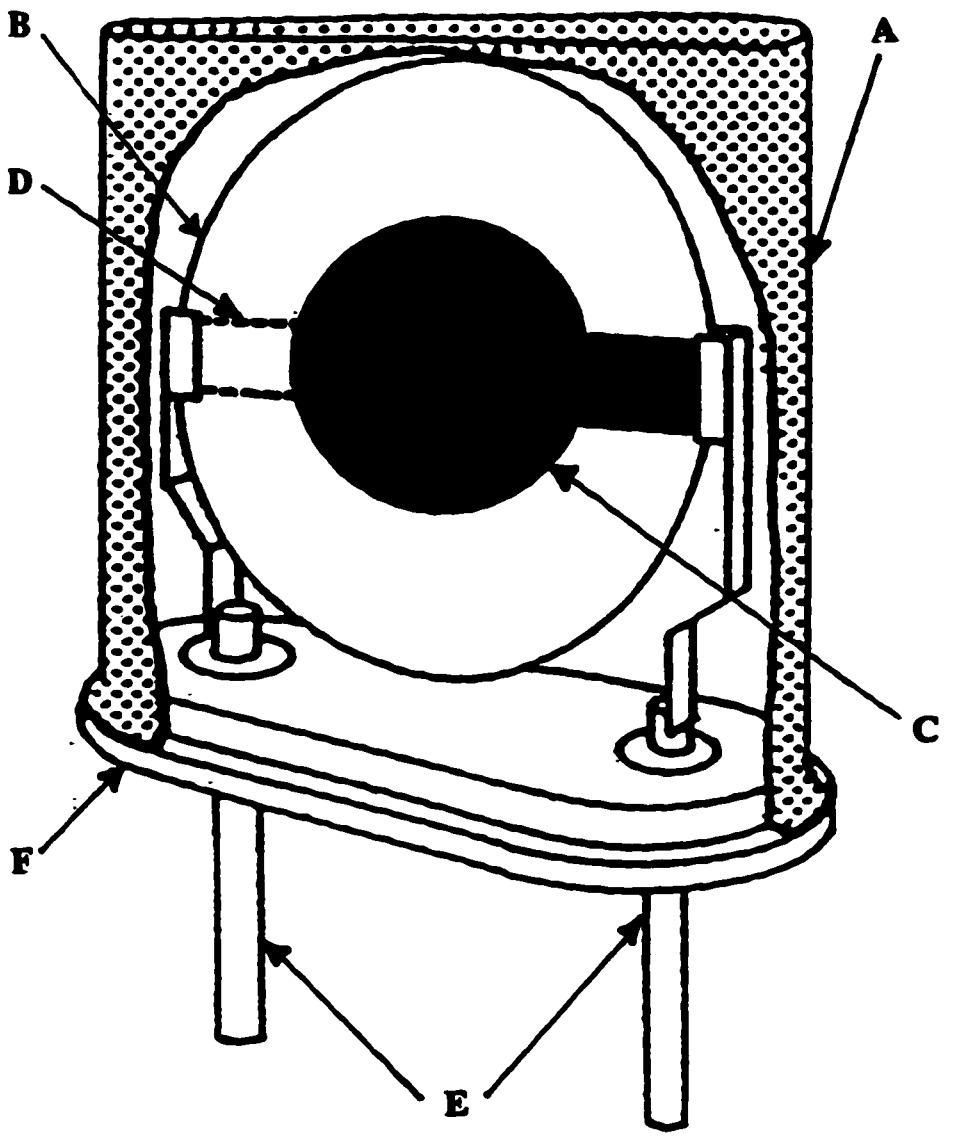

Figure 2-1:

A top view of a typical EQCM electrode in its enclosure (A). The electrode is purchased with deposited gold on both sides of the quartz wafer (B) in the pattern shown. The circular shaded area (C), which is the mass sensing area of the crystal, opposes an identical gold electrode on the other side of the quartz wafer (D). These circular regions are connected to the electrical circuitry (E) by means of an insulated mounting system (F).

When used as an *in situ* technique for measuring mass changes at electrode surfaces, one of the EQCM electrodes is exposed to the solution and simultaneously provides the alternating electric field which drives the oscillation of the crystal *and* acts as the working electrode in a conventional electrochemical cell. The other electrode remains exposed to air and serves only to complete the oscillation circuit. Thus, the EQCM experiment involves the measurement of the various electrochemical parameters, such as potential, current, and charge, at one of the EQCM electrodes and the simultaneous measurement of the oscillation frequency of the piezoelectric crystal from which, in favourable cases, minute mass changes at the electrode may be inferred.

Finally, equivalent circuit analysis (where the quartz crystal and its motion is modelled as a combination of electrical circuit elements) and impedance analysis (as a diagnostic tool of non-ideal behaviour) are extensively treated in section 2.5.

2.2. PROPERTIES OF PIEZOELECTRIC MATERIALS

2.2.1. Piezoelectric Effect

It is well known that when a mechanical stress is applied to certain crystals, an electrical polarization is produced. This phenomenon is called piezoelectricity. Literally, *piezoelectricity* is "pressure electricity", the prefix *piezo* being derived from the Greek "to press". Piezoelectricity is a reversible phenomenon. The *direct* piezoelectric effect occurs

when an applied stress produces an electric polarization. This induced polarization is proportional to the stress and changes sign with it. In turn, the *converse* piezoelectric effect occurs when a piezoelectric crystal becomes deformed (i.e. develops a strain) when placed in an electric field.

In 1880, the brothers Pierre and Jacques Curie were the first to observe the phenomenon of piezoelectricity in a series of substances. They demonstrated that pressure (stress) exerted on a small piece of quartz crystal [112] caused not only its deformation, but also an electrical potential across the deformed crystal. They attributed this electric potential to the charges generated in the stressed piezoelectric materials due to the formation of dipoles that result from the displacement of atoms in the crystalline material. The magnitude of the potential was proportional to the applied stress.

A year after their initial discovery, the Curies demonstrated what was called "the converse piezoelectric effect". By applying a voltage (electrical field) to a quartz crystal, they observed a physical distortion of that crystal, the converse phenomenon of piezoelectricity. *This converse piezoelectric effect is the basis of the quartz crystal microbalance (QCM).*

2.2.2. *Piezoelectric Materials*

The phenomenon of piezoelectricity is not particular to quartz crystals. The brothers Curie also observed the same piezoelectric effect for a series of other substances,

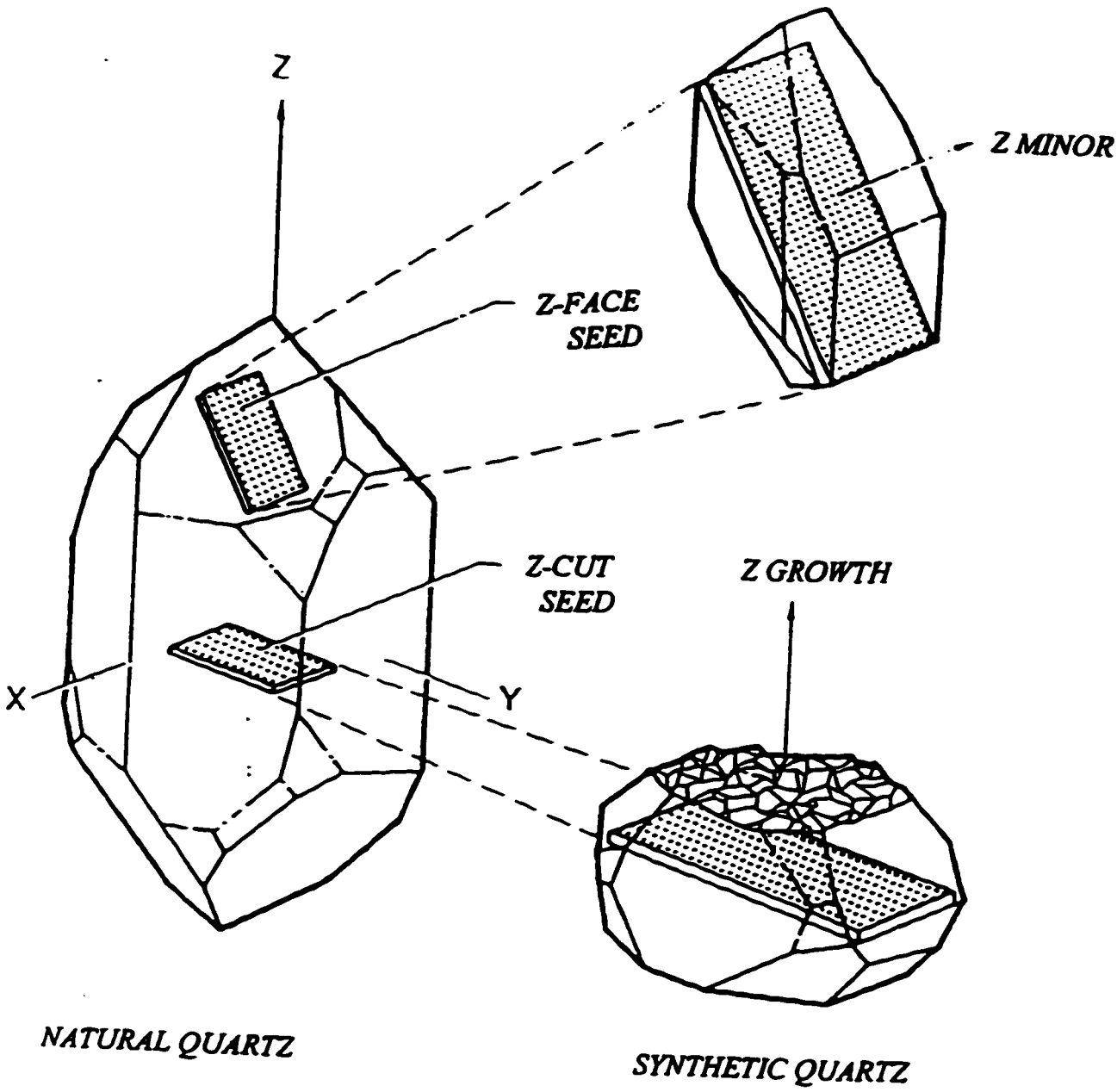

Figure 2-2:

Two seed plates commonly used in quartz synthesis from a perfect natural quartz (left) with assignment of axes (*from Gerber and Ballato* [113]).

such as Rochelle salt ($NaKC_4H_4O_6.4H_2O$) and tourmaline. The common property for all the substances for which a piezoelectric effect was observed has been found to be structural anisotropy in the solid materials . It so happens that the essential condition for a material to be piezoelectric is that it must be an ionic crystalline solid that crystallizes in a non-centro-symmetric structure (i.e., have no centre of symmetry). Figure 2-2 shows a perfect natural quartz crystal with assignment of axes and a synthetic quartz crystal cultured from a natural quartz [113,114].

Since piezoelectric materials must be anisotropic, their physical properties must depend on directions within the material since the stresses that result from the electromechanical coupling (the interaction of the electric field to induce mechanical effects such as stress and strain) depend upon the crystal symmetry, the configuration and orientation of electrical field, and the angle of cut of the crystal rod with respect of the crystallographic axes. Therefore, the axes of a such crystal must be well defined. This is provided by the science of Crystallography. The crystals used in this study are stimulated to oscillate in the thickness shear mode and only crystals cut with the proper angles exhibit shear motions and vibrations that occur as result of the establishment of a transverse acoustic wave that propagates in the direction perpendicular to the plane of the shear strain. Among the factors that can affect the stability of a quartz resonator, temperature and pressure are the most well known.

Crystal symmetry dictates that strain induced in a piezoelectric material by an applied electrical field (applied potential) of one polarity will be equal and opposite in

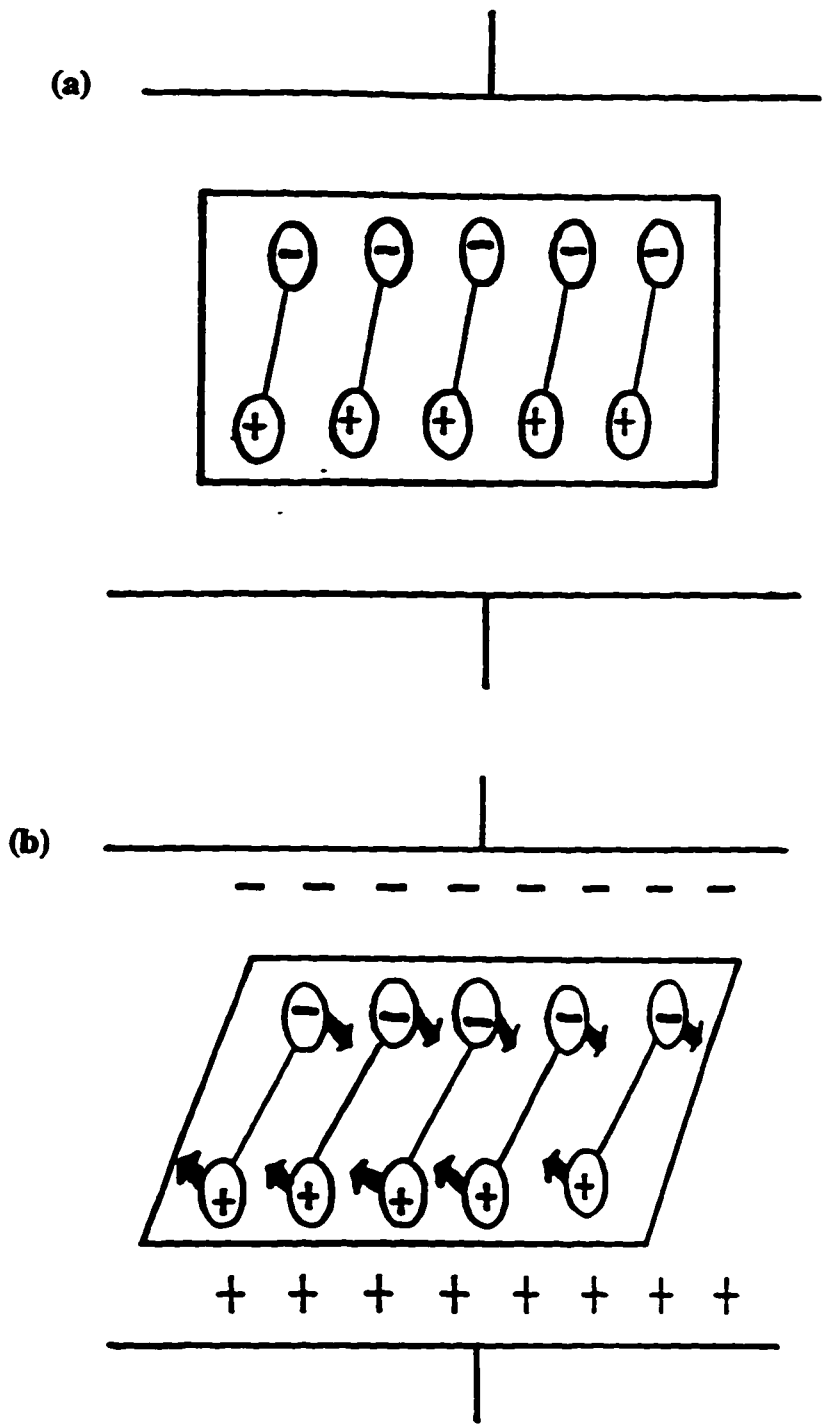

Figure 2-3:

Schematic representation of the converse piezoelectric effect for shear motion. The top figure (a) shows the dipoles with no applied electric field. The lower figure (b) shows the dipole motion when an electric field is applied (*from Buttry and Ward* [53]).

direction to that may result from the opposite polarity. Thus the converse piezoelectric effect appears as a result of the distribution of charges that move in the acentric material, followed by a reorientation of the dipoles induced by an applied electric field. The result is a *lattice strain* and a *shear deformation* (distortion) of the piezoelectric material (Figure 2.3). The direction of shear is dependent on the applied potential (electrical field) while the extent of shear depends on the magnitude of the applied potential.

The wavelength of the acoustic wave depends on the thickness of the quartz plate. In effect, of the many different modes of vibration that may exist in a piezoelectric body, it is only those that are capable of being driven by an applied electric field that are of direct relevance in resonator applications. Thickness mode resonators are currently the most important type in frequency control applications, especially *thickness-shear* mode resonators for which the acoustic shear wave propagates in the direction of the thickness along the Z axis while the shear strain developed by a field along the Y axis moves in the XY plane (Figure 2.4). The next section gives details of how the thickness can be correlated to the frequency of a quartz resonator cut in thickness-shear mode.

2.2.3. Thickness Shear Stress

For a crystal cut along the Y axis (Y-cut - see Figure 2-5), the principal displacement in the thickness shear deformation is in the XY plane and therefore

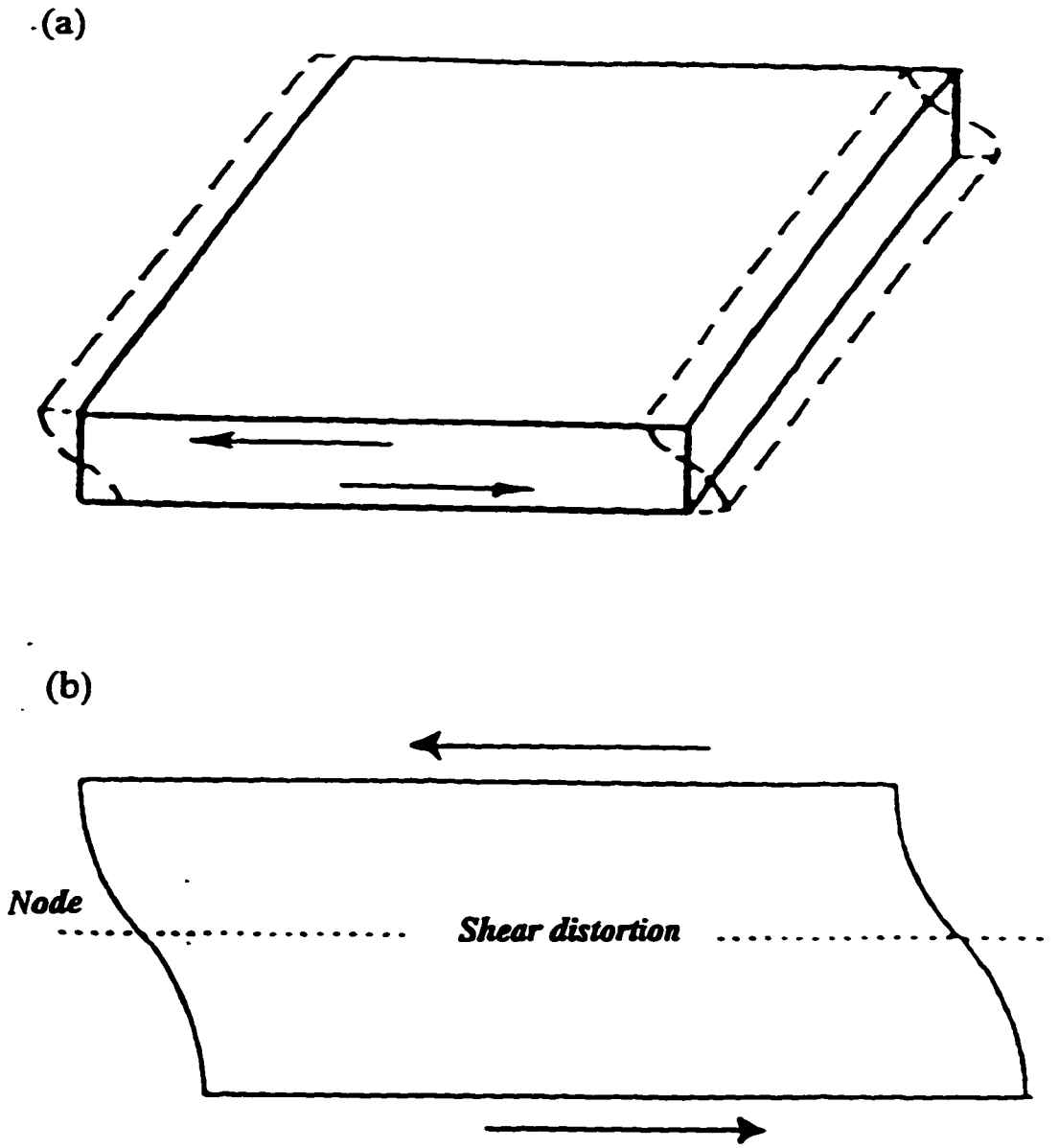

Figure 2-4:

(a) A three-dimensional and (b) a two-dimensional representation of the thickness-shear distortion of vibrations of a quartz crystal resonator (*a: from Lu and Czanderna* [53], *b: from Buttry* [52]).

perpendicular to the thickness. An alternating field can thus be thought of as generating transverse waves propagating along the thickness with a velocity v_Q and resonance will occur when the thickness contains an integral number of half wavelengths. For this model, the resonance frequencies are given by the expression

$$f_Q = \frac{nv_Q}{2t_Q} \tag{2.1}$$

where t_Q is the thickness of the plate and n is an odd integer. Thus the resonance frequencies are inversely proportional to the thickness t_Q. The product $k = f_Q t_Q$, known as the frequency-thickness constant, is $nv_Q/2$.

For a Y-cut resonator, k is approximately 1950 kHz.mm and the temperature coefficient of frequency is about +75 ppm/°C, which is very large. Consequently, the Y-cut is no longer used in frequency control applications. However, it is possible to minimize the effect of temperature by making a cut at an angle θ relative to the Y direction. This produces the rotated Y-cut family of quartz wafers (Figure 2.5). In fact, there are two angles (when negative and positive rotation are considered) which lead to a near zero temperature coefficient of frequency at room temperature.

The principle of how mass is extracted from the frequency (which is extracted from the thickness), i.e, the origins of mass sensing, is extensively treated in the next section.

2.3. *PHYSICAL PRINCIPLES OF THE QCM*

2.3.1. Origins of Mass Sensing

The monitoring of a surface process on the basis of a change in weight is a classical but not very specific approach. The sensitivity of quartz resonators to added mass has been widely studied and used to measure the deposition rate, thickness, etc., of various materials deposited onto a QCM electrode in a vacuum or in the gas phase. This technique was first suggested by Sauerbrey[115] in 1959.

It has been mentioned earlier that when a piezoelectric crystal resonator is used as mass sensor, the variation of the mass is deduced from the variation of its resonant frequency. The thickness-shear mode of vibration is particularly useful for QCM applications because it operates at high frequencies, especially the AT- and BT-cuts modes which have been shown to be sensitive to the addition or removal of mass at an electrode deposited onto the surface of the quartz crystal plate. It is thus important that the relationship between the mass and frequency is known quantitatively.

For rotated crystal cuts represented by the AT-and BT-cuts of figure 2-5, the equation (2.1) is still valid, and if one can take the first overtone (n = 1), one can write the equation (2.2) as follows:

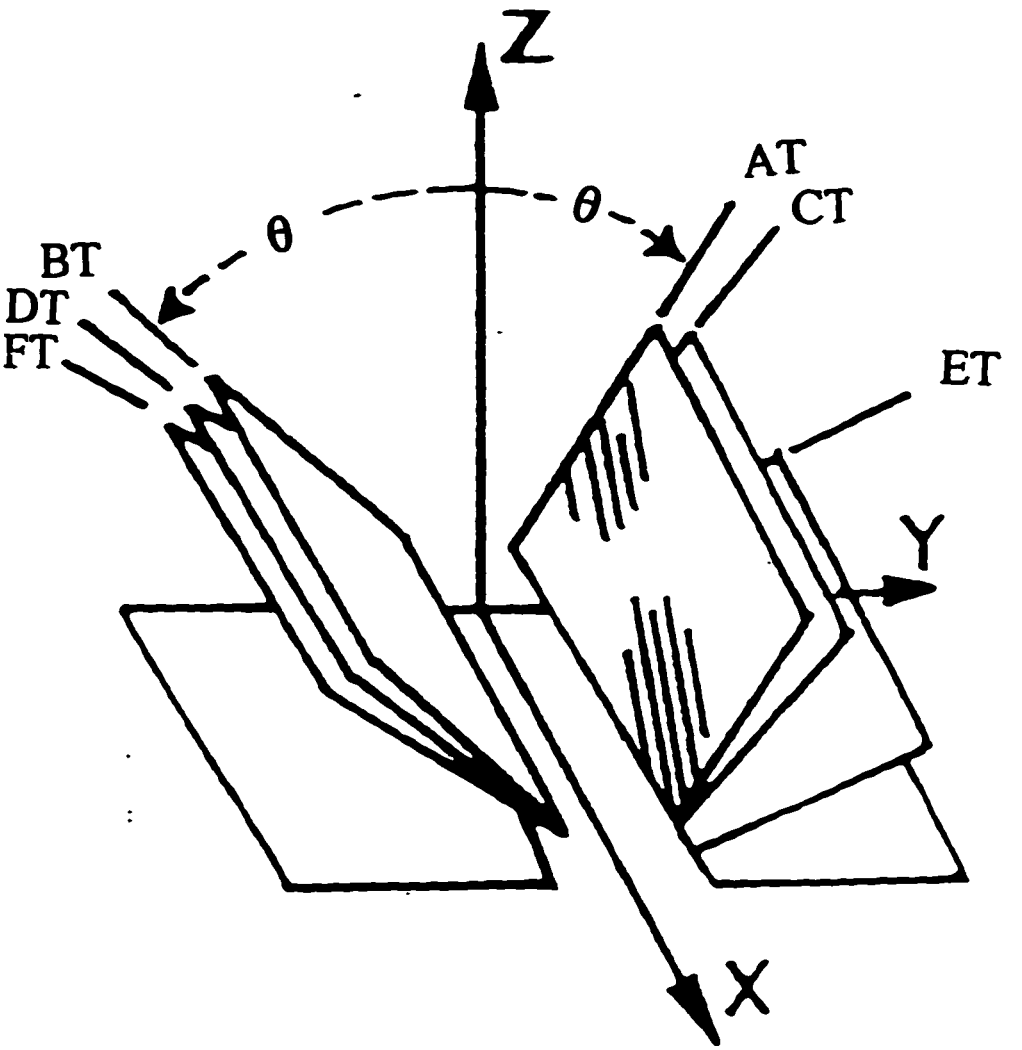

Figure 2-5:

Principal rotated Y-cuts modes of quartz crystal resonators (*from Gerber and Ballato* [114]).

$$f_Q t_Q = v_Q/2 \tag{2.2}$$

or

$$f_Q \lambda_Q = v_Q \tag{2.3}$$

where λ_Q is the wavelength of the shear-mode elastic wave in the thickness direction. Since v_Q is kept constant, the frequency change (df_Q) due to an infinitesimal change in the crystal thickness (dt_Q) will keep the product $f_Q t_Q$ always constant:

$$(f_Q+df_Q)\,(t_Q+dt_Q) = v_Q/2 \tag{2.4}$$

$$f_Q t_Q + f_Q dt_Q + t_Q df_Q + df_Q dt_Q = v_Q/2 \tag{2.5}$$

In the equation (2.5), the quantity $v_Q/2$ (right hand side) cancels with $f_Q t_Q$ (left hand side) according to equation (2.2). Also, one can take the term $df_Q dt_Q$ as zero in the first approximation since it is a product of two infinitesimal quantities. Thus, the equation (2.5) becomes

$$f_Q dt + t_Q df_Q = 0 \tag{2.6}$$

From (2.6) with appropriate algebraic manipulations, the resonant frequency shift df_Q caused by an infinitesimal change in the crystal thickness dt_Q is found to be

$$\frac{df_Q}{f_Q} = -\frac{dt_Q}{t_Q} \tag{2.7}$$

for which the negative sign means that an increase in the thickness of the quartz plate is followed by a correspondent decrease in its resonant frequency.

The possibility of using piezoelectric quartz crystal resonators as quantitative mass measuring devices was first developed by Sauerbrey [115,116] who postulated an operating principle of a QCM using the physical model of the figure (2-6) for a quartz crystal plate oscillating in the thickness-shear mode of the AT- and BT-cuts. For a quartz crystal cut in a regular geometrical figure as is the case for a cylindrical or rectangular plate of surface A and thickness t_Q, the volume V_Q of the quartz crystal can simply calculated as:

$$V_Q = At_Q \tag{2.8}$$

If the density ρ_Q of the quartz is known, its mass M_Q is related to its volume V_Q by $M_Q = V_Q\rho_Q$, and one can write the relationship that exists between the mass and thickness as

$$t_Q = \frac{M_Q}{A\rho_Q} \tag{2.9}$$

The equation (2.9), substituted in its differential form of the equation (2.7), yields

$$\frac{df_Q}{f_Q} = -\frac{dM}{M_Q} \tag{2.10}$$

where dM is an infinitesimal amount of foreign mass uniformly distributed over the crystal surface, as is the case of the film deposit in electrochemistry.

Sauerbrey made the assumption that for small mass changes, the addition of foreign mass can be treated as an equivalent mass change of the quartz crystal itself. If M_f is the mass of that deposited thin film, the equation 2.10 can be written as:

$$\frac{f_0 - f_Q}{f_Q} = -\frac{M_F}{M_Q} \tag{2.11}$$

where f_0 is the resonant frequency of quartz crystal with deposited mass M_F.

For the one-dimensional resonator model shown in figure (2.6), one can define the areal densities m_Q and m_F as the mass per unit area for the quartz crystal and deposited film, respectively:

$$m_Q = \frac{M_Q}{A} \tag{2.12}$$

$$m_F = \frac{M_F}{A} \tag{2.13}$$

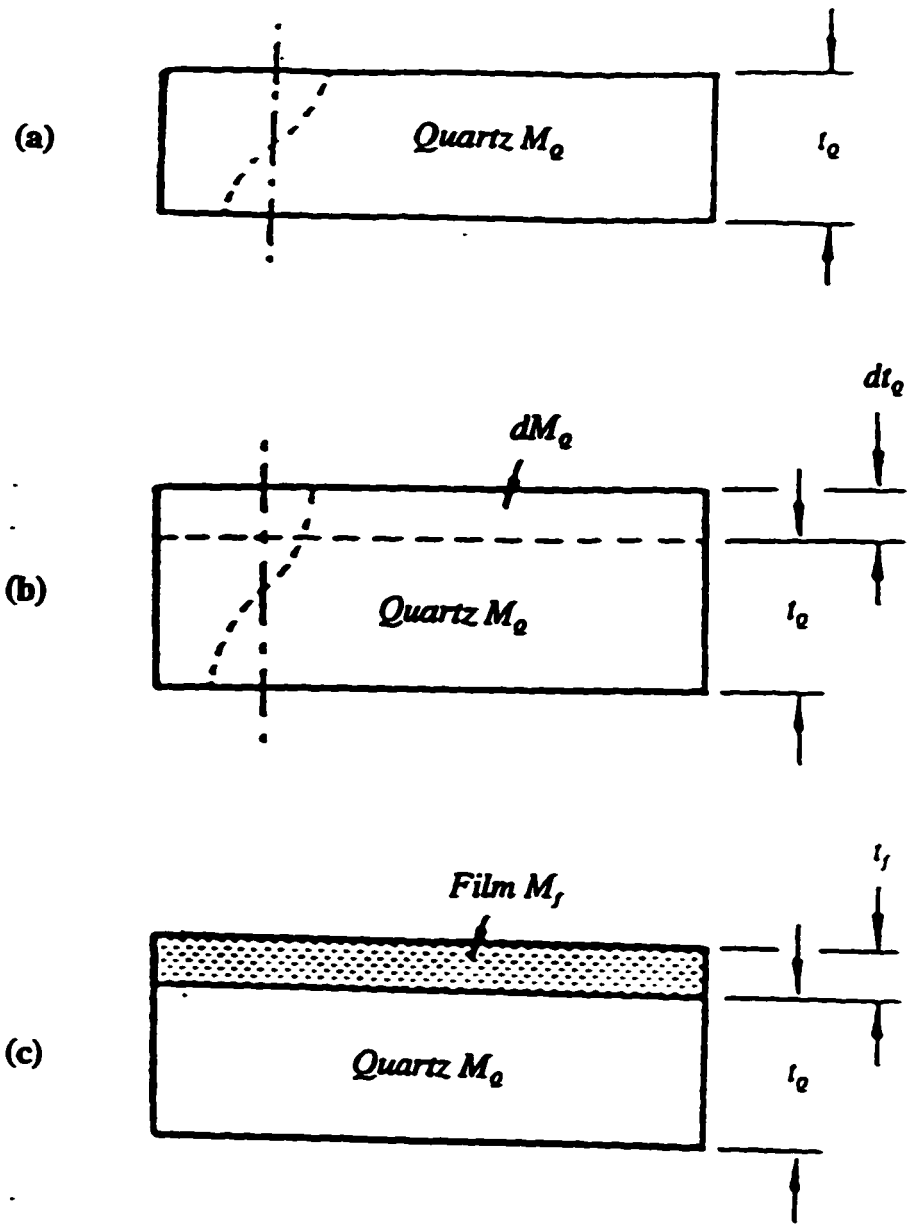

Figure 2-6:

A simplified model of a quartz crystal microbalance (the principle of mass sensing): a) At resonance, the wavelength is equal to the half of quartz plate thickness; b) An increase in the quartz plate thickness results in the decrease in the resonant frequency (an increase in the wavelength); c) The mass of a deposited film is treated as an equivalent amount of the quartz mass (*from Lu and Czanderna* [54]).

Thus, the equation (2.11) can be written in the following form:

$$\frac{f_0 - f_Q}{f_Q} = -\frac{m_F}{m_Q} \tag{2.14}$$

Combining Eq.(2.9) together with Eqs. (2.12) and (2.13), one can see that the areal density is equivalent to the product of thickness and density. This assumption is, of course, valid for materials having a density which is spatially uniform (uniform mass condition):

$$m_F = t_F \rho_F \tag{2.15}$$

and

$$m_Q = t_Q \rho_Q \tag{2.16}$$

where ρ_F and ρ_Q are the densities of film and quartz crystal plate, respectively, and t_F is the thickness of the deposited film. A substitution of Eqs. (2.2) and (2.16) into Eq. (2.14) yields

$$f_0 - f_Q = -\frac{2 f_Q^2 m_F}{\rho_Q v_Q} \tag{2.17}$$

$$\Delta f_F = -\frac{2 f_Q^2 m_F}{\rho_Q v_Q} \tag{2.18}$$

In general, the difference $\Delta f_F = f_0 - f_Q$ in Eq, (2.18) will be measured relative to the resonant

frequency f_o, instead of f_Q. The AT-cut crystals that are used have a resonant frequency of between 1-15 MHz, and Δf_F is often just a few hertz. Therefore, f_Q^2 in Eq.(2.18) can be easily expressed as $f_Q^2 = (f_o - \Delta f_F)^2 \approx f_o^2$, the second and third terms being negligible compared to the first one (f_o^2). Thus Eq.(2.18) can be written as

$$\Delta f_F = -\frac{2 f_0^2 m_F}{\rho_Q \upsilon_Q} \tag{2.19}$$

The shear wave velocity υ_Q is related to the shear modulus μ_Q (2.947×10^{11} g.cm^{-1}.s^{-2}) of the quartz crystal through the equation:

$$\upsilon_Q = (\mu_Q / \rho_Q)^{1/2} \tag{2.20}$$

Finally, by substitution of Eq.(2.20) into Eq.(2.19) we find the following equation

$$\Delta f_F = -\frac{2 n f_0^2}{\sqrt{\mu_Q \rho_Q}} \times \Delta m_F \tag{2.21}$$

called ***Sauerbrey's equation***, in which Δm_F (g.cm^{-2}) is the interfacial mass change of a rigid attachment of a film to the crystal of surface A/cm^2. In this equation, one can see that the frequency decreases as the mass increases. The overtone number n (see Eq.2.1) is introduced again to take into account the cases of quartz crystals that may vibrate at higher overtones.

The Sauerbrey equation (Eq.(2.21) is often expressed in a simplified form as following (Eq.2.22):

$$\Delta f_F = -C_F \Delta m_F \qquad (2.22)$$

where C_F is defined as the mass sensitivity or calibration constant of a QCM. Hence, Δf_F is linearly related to Δm_F and this simple relationship is the basis of the quartz crystal microbalance (QCM).

The constant C_F is evaluated with knowledge of the oscillation frequency of the fundamental mode of the QCM (f_0/MHz), the overtone number (n = 1), the density of the quartz ($\rho_Q = 2.648$ g.cm^{-3}) and the shear modulus of quartz ($\mu_Q = 2.947 \times 10^{11}$ g.cm^{-1}. s^{-2}). For a 10 MHz AT-cut quartz crystal, the theoretical mass sensitivity obtained from Eq.(2.22) is 226.4 MHz m^2/kg. This means that the addition of a material with an areal density of 4.425 ng/cm^2 onto a such resonator will cause a frequency shift of 1 Hz.

Equations 2.21 and 2.22 are alternative forms of the Sauerbrey equation and are the central equations that are applicable to the Quartz Crystal Microbalance and the Electrochemical Quartz Crystal Microbalance. All mass changes calculated or displayed in this thesis are calculated using these equations.

The outstanding features of Eq.(2.22) are that the mass sensitivity is dependent on the square of resonant frequency f_0 and can be calculated if the intrinsic properties of the

quartz crystal are known. Thus operating at higher frequency will offer the advantage of greater mass sensitivity, and no individual calibration is required provided that the deposited material covers the active vibrating area entirely. However, since f_0 is inversely proportional to the thickness, t_Q , of the quartz crystal, an increase of the fundamental frequency to obtain higher sensitivity will be limited by the difficulty of handling the fragile thin crystal required. In general, crystals which can be easily handled have fundamental frequencies that range between 1-15 MHz. For example, a 15 MHz-cut crystal has a thickness of about 100 μm.

Although most of the research involving sensors based on the Sauerbrey's equation has been concerned with gas phase operation, recent times have seen increased attention being paid to the operation in liquids under appropriate conditions. Bruckenstein and Shay[47], and in the same year, Kanazawa and Gordon[48], were the first to derive an appropriate equation that takes into account the effects due to liquid loading.

We consider it necessary to reserve an entire section to this important effect of liquid loading that opens the possibility of the use of the QCM in electrolyte solutions for the study of electrochemical processes.

2.3.2. Effects of Liquid Loading

When one face of a "smooth" crystal is in contact with a viscous liquid or a

viscoelastic film of thickness t_L, the energy flows out of the quartz crystal into the liquid in the form of damping acoustic waves as represented in figure 2-7. This energy loss is dependent on the properties of the interface between the Newtonian liquid and the quartz resonator.

In 1985 two physical models of a QCM in contact with a liquid were developed first by Bruckenstein and Shay [47], then by Kanazawa and Gordon [48]. These models are separately treated in the following sub-sections.

a) The Model of Bruckenstein and Shay

Using an approach based on an analogy with the ac polarographic diffusion-layer thickness, Bruckenstein and Shay [47] developed a simple expression for the thickness t_L of the liquid layer that oscillates with the crystal:

$$t_{L(BS)} = \left(\frac{\nu}{f_L} \right)^{\frac{1}{2}} \tag{2.23}$$

where ν ($cm^2\ s^{-1}$) is the kinematic viscosity of the liquid, f_L the frequency of oscillation in the liquid, and the subscript *(BS)* indicates the model of Bruckenstein and Shay.

If ρ_L is the density of the liquid, the effective additional liquid interfacial mass Δm_L

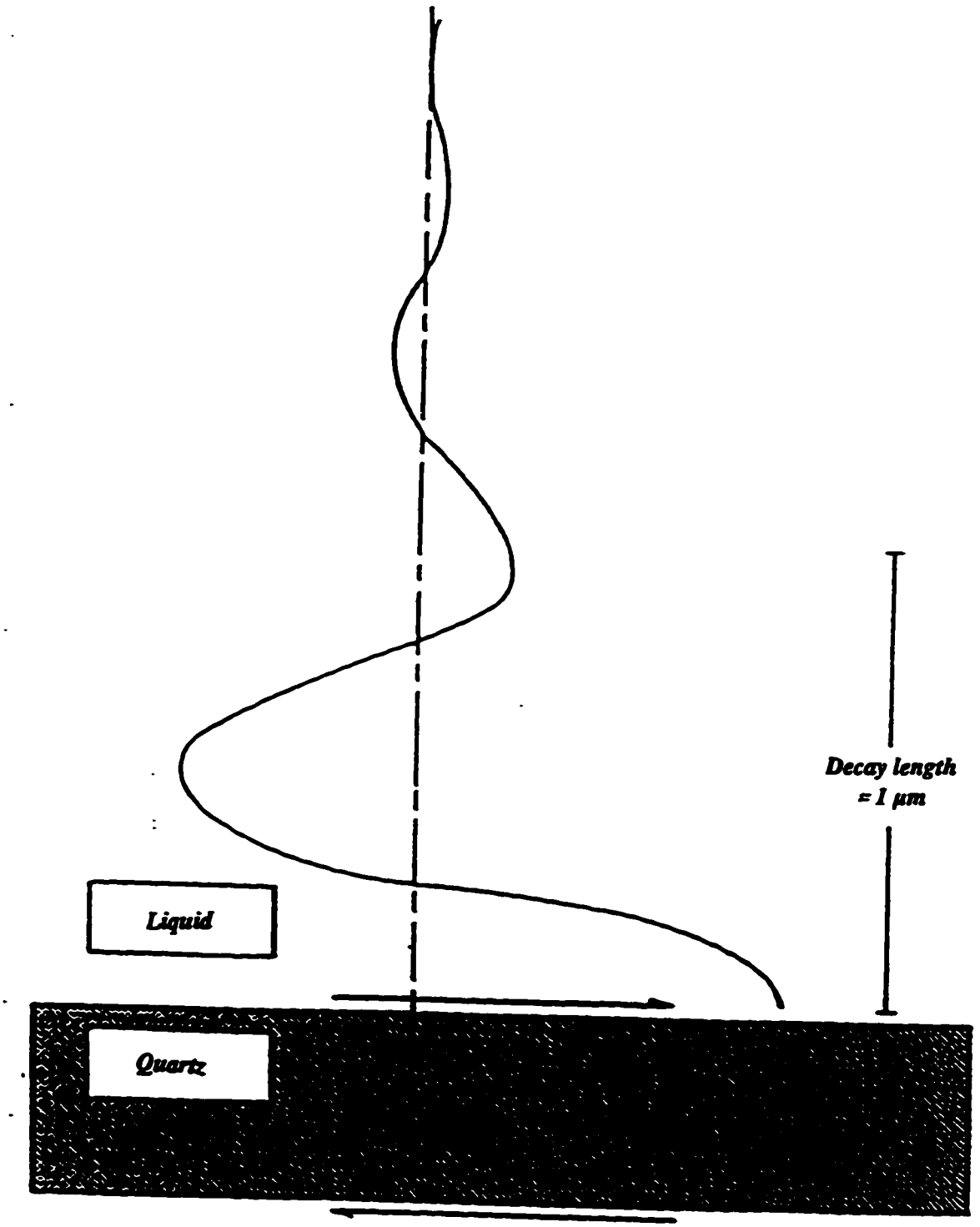

Figure 2-7:

The shear wave propagation in a newtonian liquid (*from Thompson et al* [51]).

attached to the face of the crystal in contact with the liquid is

$$\Delta m_L = \rho_L \left(\frac{\nu}{f_L} \right)^{\frac{1}{2}} \tag{2.24}$$

The kinematic viscosity ν is related to the density ρ_L of the liquid and its conventional viscosity η_L by the following relationship:

$$\nu = \left(\frac{\eta_L}{\rho_L} \right)^{\frac{1}{2}} \tag{2.25}$$

Provided $f_L = f_q$, substitution of Eqs. (2.24) and (2.25) into Eq. (2.21) yields the following relationship for the frequency change of the liquid loaded quartz:

$$\Delta f_{L(BS)} = -\frac{2nf_0^{3/2}}{\sqrt{\mu_Q \rho_Q}} \times (\rho_L \eta_L)^{1/2} \tag{2.26}$$

where n=1 or 2 depending on whether one or two faces of the crystal contact the solution.

The equation (2.26) is often written in its simplified form (2.27) after replacing the intrinsic constants of the quartz crystal:

$$\Delta f_{L(BS)} = -2.26 \times 10^{-6} n f_0^{3/2} \sqrt{\eta_L \rho_L} \tag{2.27}$$

For a 10 MHz AT-cut crystal, Eq.(2.27) predicts shifts in frequency of the order of 7 kHz if one face is in contact with the liquid.

b) The Model of Kanazawa and Gordon

In a similar physical model, Kanazawa and Gordon [48] treat the quartz as a totally lossless elastic solid and the liquid as a purely viscous medium. In the liquid, the solutions for the differential equation describing the shear waves are highly damped sinusoidal shear waves travelling in the z direction, away from the resonator surface. This damped shear wave can be located at point $[z,v_x(z,t)]$ at anytime, where $v_x(z,t)$ is the instantaneous velocity of the liquid that propagates with a propagation constant k. This latter can be written in terms of the density ρ_L and viscosity η_L:

$$k=\left(\frac{\omega\rho_L}{2\eta_L}\right)^{\frac{1}{2}} \tag{2.28}$$

In the above equation, one can recognize the definition of ν, the kinematic viscosity of the liquid (viscosity divided by density). Also, the reciprocal of the propagation constant 1/k has the dimensions of length and is the characteristic distance describing the envelope of the decay function (Figure 2.7). Therefore, the quantity 1/k can be treated as the thickness of the diffusion layer as for the equation (2.23)

$$t_{L(KG)} = \frac{1}{k} = \left(\frac{2\eta_L}{\omega \rho_L} \right)^{\frac{1}{2}} \tag{2.29}$$

With $\omega = 2\pi f_L$, Eq.(2.29) becomes:

$$t_{L(KG)} = \left(\frac{\eta_L}{\pi f_L \rho_L} \right)^{\frac{1}{2}} \tag{2.30.a}$$

$$= \left(\frac{\upsilon}{\pi f_L} \right)^{\frac{1}{2}} \tag{2.30.b}$$

Now, one can see that the equation (2.30) for the model of Kanazawa and Gordon is similar to that of Bruckenstein and Shay (Eq.2.23), the difference being the presence of π in the thickness equation of Kanazawa and Gordon. Therefore, the frequency change for a liquid loaded quartz crystal is

$$\Delta f_{L(KG)} = -\frac{2\pi f_0^{3/2}}{\sqrt{\mu_Q \rho_Q}} \times \left(\frac{\rho_L \eta_L}{\pi} \right)^{1/2} \tag{2.31}$$

It appears that both theories introduced new parameters for the mass of a thin boundary film, in this instance a liquid film which oscillates with the crystal when it is immersed in a liquid. It is also clear that η_L and ρ_L are the parameters which are relevant

to the operation and characterization of these devices in the liquid phase. However, none of these approaches considers the microscopic *boundaries* between the crystal surface and liquid, and it is these boundaries that are suspected to be responsible of some non-ideal behaviour of the QCM that will be summarized in the next sub-section.

However, before proceeding to this section, it is worth noting that the equations derived from the two theories differ by a factor of π so that the predicted mass decrease upon immersion of a QCM in liquid is calculated to be about 7 kHz by Bruckenstein and Shay, whereas the value predicted by Kanazawa and Gordon is about 2 kHz. While this may appear disconcerting, it is not particularly important because both theories predict a dependence of frequency on $(\eta_L \rho_L)^{1/2}$. In other words, if the QCM is operated in solution, then provided the properties of the solution do not change during the course of the experiment then the effect of liquid is simply to produce a constant offset of frequency (relative to the value observed in air) and the size of this offset is not important. Thus the Sauerbrey equation may be applied to the QCM in solution as well, provided that the added mass is rigid and that there are no significant changes in the composition of the solution during the course of an experiment.

2.3.3. Non-Ideal Behaviour

The Sauerbrey equation, as noted above, relies on several assumptions and in any QCM or EQCM investigation, one must keep in mind that the QCM/EQCM measures the

frequency change not the mass change. The mass change is inferred from the Sauerbrey equation. The conversion from the frequency to its equivalent mass supposes that the propagation of the shear wave from the crystal surface into solution is not disrupted and ideally, all the properties of any deposited layer should be comparable to that of the quartz crystal itself. There are circumstances when either the nature of any added mass, or a change in the surface of the crystal and the way it interacts with the solution cause unusual or non-ideal QCM/EQCM behaviour. These effects are illustrated in Figure 2-8.

We briefly report here some of these effects. We have divided these effects in two categories: those that are due to mass effects, and those that are due to surface effects. For more details the interested reader is referred to Ref. 53 and references therein.

a) Viscoelastic Effects

Viscoelastic effects are a common cause of unexpected behaviour in the category of non-ideal effects due to added mass. Such effects usually arise in studies of redox polymer films attached to electrodes when the viscosity and elasticity of the film change during redox cycling [117,118]. This is often due to changes in the morphology and swelling as ions and solvent move into and out of the film. Ordinarily the film would be treated as a rigid layer but if viscoelastic changes occur in the film then the total frequency change will contain two components, one due to the mass change as ions and solvent move in and

out of the film and a second as a result of the viscoelastic changes that are occurring. This behaviour thus appears as an erroneous evaluation of the mass change when establishing the number of counter ions and solvent molecules involved in the mass transport process *if* the frequency change is assumed to represent only a mass change.

This type of a non-ideal behaviour is easily investigated by impedance analysis (which is discussed later in this chapter).

b) High Mass Loading

In EQCM measurements, the mass of the film should not exceed 2% of the total mass of the quartz crystal. Otherwise, non-idealities as a result of *high mass loadings* will appear. This affects the sensitivity of the QCM, because this quantity decreases with large mass increases according to equation (2.22).

This non-ideal behaviour can be easily overcome when the investigator can control the mass deposit during an experiment. If this is not possible, an alternative is to use the "Z-match" [118,119] method which is an impedance analysis of the film and the quartz and is beyond the scope of this thesis. Unfortunately, the "Z-match" method requires that the shear modulus μ_f and the density ρ_f of the attached mass be known in advance, which is not always the case in EQCM applications. Thus, no applications of the "Z-match"

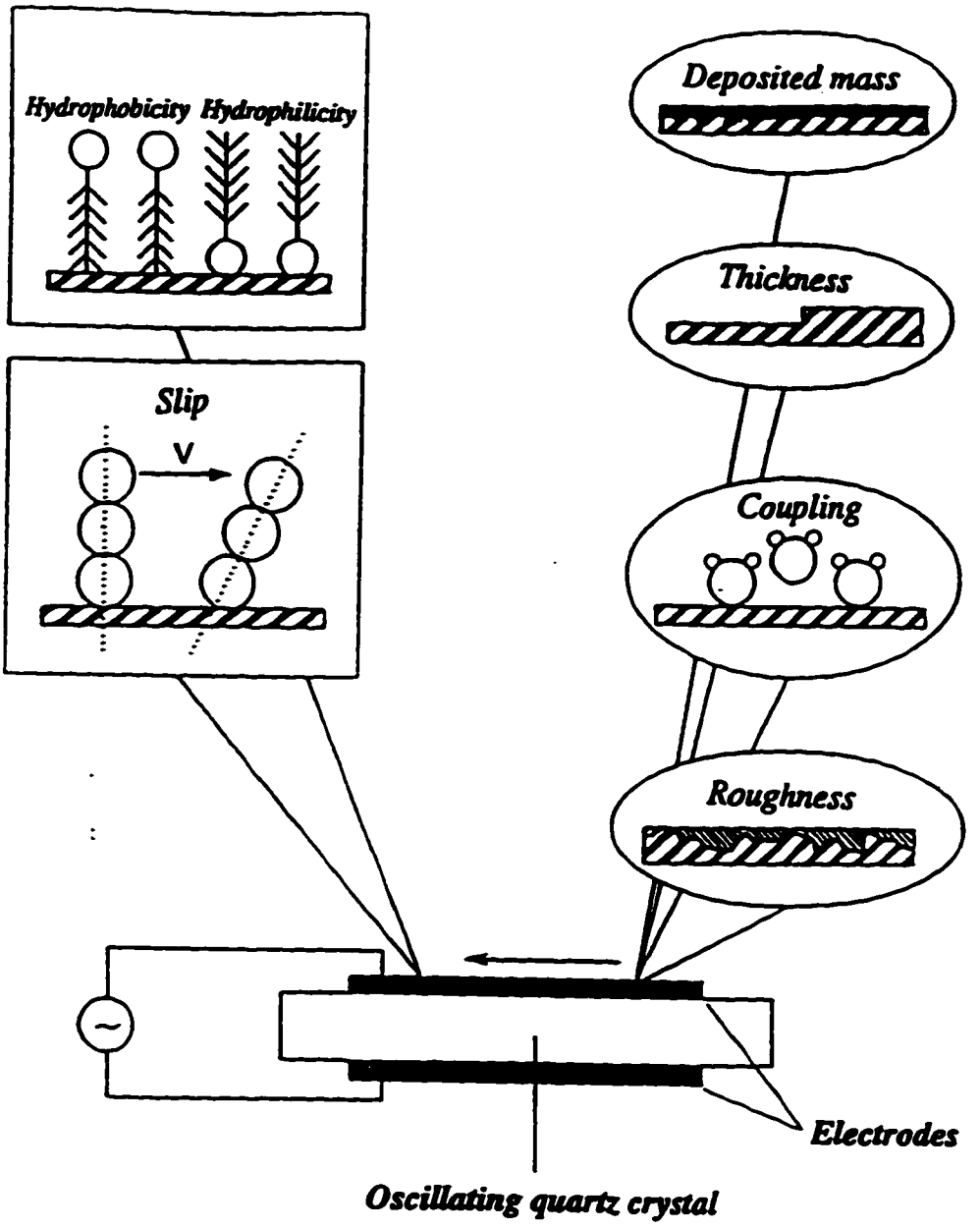

Figure 2-8:

Schematic diagram of interfacial factors that govern the behaviour of oscillating quartz crystal in liquid phase (*from Thompson et al* [51]).

method to electrochemical studies with the QCM have yet appeared.

c) *Non-Uniform Mass Distribution*

Finally in the category of mass effects leading to non-idealities, a *non-uniform mass distribution* can cause an error in EQCM investigations [120,121]. In EQCM measurements where the electrode is coated onto the quartz crystal either by vacuum sputtering or by electro-deposition, these non-uniformities will always be present to some extent. However Buttry and Ward[53] have concluded from an analysis of the literature that it is likely that deviations from the Sauerbrey equation as a result of non-uniformity occur only in extreme cases.

d) *Surface Roughness and Porosity*

The surface roughness effect is the first in this series that can be regarded as a non-ideality arising from a surface effect and is observed when an electrode process (typically a cycle which involves formation and then reduction of an oxide surface) leads to the formation of microscopic cavities in which liquid (generally water) can be trapped [122-124]. The cause of this effect is thought to be the fact that oxidation and subsequent reduction of the electrode results in a reduced surface that is rougher than the *initial* reduced surface (before the oxidation-reduction cycle).

e) Surface Stress/ Strain

Stress effects will almost always be present in EQCM measurements for which only one face of the quartz crystal contacts a volume of the liquid while the opposite side contacts the air. In a such arrangement, stress effects arise because the liquid exerts a hydrostatic pressure on the side faced to the liquid [54,125]. However, given that the hydrostatic pressure will not normally change during an experiment then there should not be any significant effect on EQCM results.

A second type of stress effect can be seen when there is compressive stress in thick films [54,126,127]. For example, hydrogen gas generated electrochemically can be absorbed into the bulk of some electrode materials such as palladium [128] and gives rise to stress in the metal which in turn leads to frequency changes that are much larger than those that could be expected if the EQCM were acting as a mass sensor. These effects can generally be eliminated by studying the same system with both an AT-cut crystal and a BT-cut crystal which have stress coefficients that are equal and opposite [129-131].

f) Interfacial Slippage

The application of the Sauerbrey equation also supposes that the *non-slip condition* applies. This means that the vibrating EQCM electrode and the adjacent molecular layer

of solution/electrolyte must move at the same velocity. This supposes that this adjacent solvent layer is tightly bound on the metal electrode. If it is not the case, the coupling between this adjacent solvent and the electrode will be altered. This affects the decay length of the shear wave which propagates into the liquid and thus the effective thickness of the liquid layer at the interface between electrode and solution and hence the frequency offset that is seen when crystal is immersed in a solution.

It has been reported that interfacial slippage is closely connected to changes in hydrophobicity and hydrophilicity [126,132-135] but such effects are very hard to identify with any certainty. Impedance analysis (described later in this chapter) may be of some use in this area. It should be noted that this effect is expected to be of interest at electrode surfaces, particularly because the nature of the surface can be changed with potential. For example, the conventional model of the interface involves a potential dependent re-orientation of adsorbed water at an electrode surface when the net charge carried by the electrode changes from positive to negative. In addition, processes such as surface oxidation and the adsorption of a monolayer of hydrogen, both of which are observed at platinum electrodes may influence the interaction between electrode surface and solution. This particular effect will be discussed in more detail later in this thesis, particularly in Chapter 4.

At this stage, we have presented the essentials that must be known for the

understanding the EQCM, as a complementary technique for investigation of surface processes. It is now the time to show how this technique is linked to the electrochemical techniques, mainly Cyclic Voltammetry, used in this thesis.

2.4. EQCM AND ELECTROCHEMICAL QUANTITIES

When looking at the equation (2.22), one can see that the measured frequency change f is linearly related to its equivalent mass change m, the minus sign meaning that when one is increasing, the other one is decreasing. The question now is how can this frequency change be related to the electrochemical measured quantities, mainly the current i, when a potential E is applied to the electrode that is undergoing an oxidation/ reduction reaction. The answer to this question is straightforward.

2.4.1. Mass Change and Charge

Application of a potential E to the electrode results in the passage of a current, i. The charge Q, which is a cumulative quantity, can be obtained by integration of the current i.

$$dQ = i\,dt \tag{2.32}$$

This is easily accomplished by means of an integrator of current (based on a simple operational amplifier circuit). Thus the charge Q represents the total number of electrons transferred in a given electrochemical process and corresponds to mass changes occurring at the electrode surface.

Secondly, the charge Q is related to the total mass change m that appears in the equation (2.22) by the following linear relationship

$$m=\frac{M_w Q}{nF} \tag{2.33}$$

where M_w (g mol^{-1}) is the apparent molar mass, n the number of electrons involved in the electrochemical process, and F the Faraday constant. Under ideal conditions, the frequency change f measured with the EQCM will be proportional to the charge Q and will be related to the apparent molar mass by the following equation (eqs.2.22 and 2.33 rearranged together):

$$\Delta f=-\frac{C_f M_w Q}{nF} \tag{2.34}$$

Inspection of equation (2.34) reveals that plots of mass vs charge are particularly useful in the determination of M_w/n, which represents the molar mass per electron transferred. The term *apparent molar mass* is stressed because the measured value of M_w will not be that expected based on the simple stoichiometric relationship, but will contain

contributions from solvent or coadsorbed species (anions) that often completely alter the true value of M_w. Therefore, non-linearities of plots of mass vs charge will be particularly useful for diagnosing non-ideal behaviour of the EQCM. We have given some examples of these unexpected behaviour in the sub-section 2.3.3 of chapter 2.

2.4.2. Mass Change and Cyclic Voltammetry

In the most of our results, the cyclic voltammetry (CV) has been used as the main electrochemical technique with the EQCM. In cyclic voltammetry, a *current I* is measured for a modulating applied *potential E*, which varies linearly with time at a *sweep rate* s (defined as s = dE/dt) which, in combination with Eq.2.32, gives the following relationship of the current that is being measured at scan rate or *sweep rate s*:

$$i = s\frac{dQ}{dE} \tag{2.35}$$

Combination of eqs. (2.34) and (2.35) gives the following relationship

$$i = \frac{nsF}{M_w C_f}\frac{d(\Delta f)}{dE} \tag{2.36}$$

which is an alternative approach to the mass vs cyclic voltammetry data analysis that involves the relationship between the *current I* measured by cyclic voltammetry and the

first derivative of the frequency change with respect to time.

In certain cases where mass or current transients are measured at a fixed potential E, the mass change will follow the same pattern as that of the charge because of the intrinsic linearity between mass and charge according to the equation (2.33).

2.5. CIRCUIT AND IMPEDANCE ANALYSES

In the previous section, it has been shown that quartz crystals cut in the thickness-shear mode can be applied to the determination of mass measurements and that the Sauerbrey equation that is derived from the direct relationship between the frequency and the thickness of a quartz crystal is, in general, applicable to both gas phase and solution operation. However, the possibility of non-ideal behaviour has also been raised in this chapter. It has also been stated that impedance analysis can often be used to identify non-ideal EQCM behaviour where an observed frequency change does not result from a mass change. The remainder of this chapter will be devoted to a discussion of impedance analysis and the information that it can yield, but before continuing with a discussion of impedance analysis, it is important to clarify the types of experiments that can be performed with the EQCM. These fall into two categories:

① In the first type (which is used most often) a circuit is used to allow the crystal to

oscillate and the frequency of the crystal is measured as it changes in response to changes in mass (or to alterations in surface properties such as roughness or hydrophilicity etc.). However, because the frequency of the crystal is the *only* quantity that is measured, it is difficult to establish without doubt that the Sauerbrey equation is being obeyed and that no non-ideal effects are present. In a few cases (e.g. deposition of a metal) the expected mass change can be calculated on the basis of a simple model involving say deposition of a film of known identity and by a known mechanism. Thus verification of the Sauerbrey equation by comparison of observed and expected values is possible. Unfortunately, checks of this type are not possible for most experiments.

② The second type of experiment involves impedance analysis of the quartz crystal. Here the frequency of the crystal is not measured as it responds to added mass but it is *driven* (by an external frequency generator) over a range of frequencies that spans the natural resonance frequency. The impedance of the crystal is recorded as a function of frequency. Physically impedance, Z ,is the voltage V across the crystal divided by the current i flowing through the crystal ($Z = V/i$) - it is the equivalent of resistance but for alternating currents. Impedance analysis is more powerful and informative than the normal EQCM experiment and can reveal the presence of non-ideal EQCM behaviour.

2.5.1. Equivalent Circuits

In many areas of electrochemistry, it is conventional to make use of equivalent circuits to model the behaviour of an electrode or electrode/solution interface. An equivalent circuit is simply a representation of the electrode-solution interface or electrochemical cell in terms of a series of circuit elements (resistors, capacitors and so on). This equivalent circuit serves as a model for the real system, and can be used to predict the response of the real system to particular perturbations. In addition, different physical properties can be associated with specific circuit elements and the changes that are seen in the values of these elements can be correlated to physical changes occurring in the system. The oscillating properties of the EQCM/QCM can also be discussed on the basis of an equivalent circuit and this circuit is introduced below.

The equivalent circuit for piezoelectric crystals and the detailed theory of its operation were discussed by Cady [136] in 1964. This theory was used until 1982 when Bottom [137] presented a much simplified version in his book "*Introduction to Quartz Crystal Circuit Design*". A simple and clear discussion of the equivalent circuit is also presented in the review paper by Buttry and Ward [53]. In their review paper, a series of references are related to the impedance analysis that uses a simplified electrical representation of an unperturbed QCM and an electrical circuit representation that includes the effects of mass and liquid loading of the quartz crystal [138-143]. Following publication of this review paper by Buttry and Ward, research aimed at understanding the effects of interfacial properties (especially viscoelastic effects) on the response of the

QCM, has increased and characterization of a quartz crystal microbalance by impedance analysis has become more common [144-147].

The quartz crystal is normally represented by an equivalent circuit such as that of figure (2.9.a) in which there are two branches. The LCR branch constitutes what is known as the motional arm of the circuit (since it is responsible for the oscillation properties of the circuit and thus mimics the oscillation of the crystal). The $L_m C_m$ series combination determines the resonance frequency f_m of this *motional arm* that defines the electro-mechanical characteristics of the quartz resonator. In addition, this branch includes a resistive component R_m that is a measure of the energy dissipation of the vibrating quartz and mechanical losses in the mounting system. For example, if the crystal is mounted in air then R_m will be smaller than if the crystal contacts a liquid where, as we have seen, energy flows out of the crystal as a damping wave into solution. The second part of the circuit contains a parallel capacitance, C_o, that includes any stray capacity (for example associated with contacts and leads to the crystal) and all the static effects (i.e those not associated with crystal motion) that arise between the coated metal-electrodes and the quartz crystal.

The equivalent circuit described in figure (2.9.a) is called the "BVD circuit" (Butterworth and Van Dyke) [137], and was developed to describe the behaviour of crystals exposed to air but it has been employed by a number of workers who have tried to show

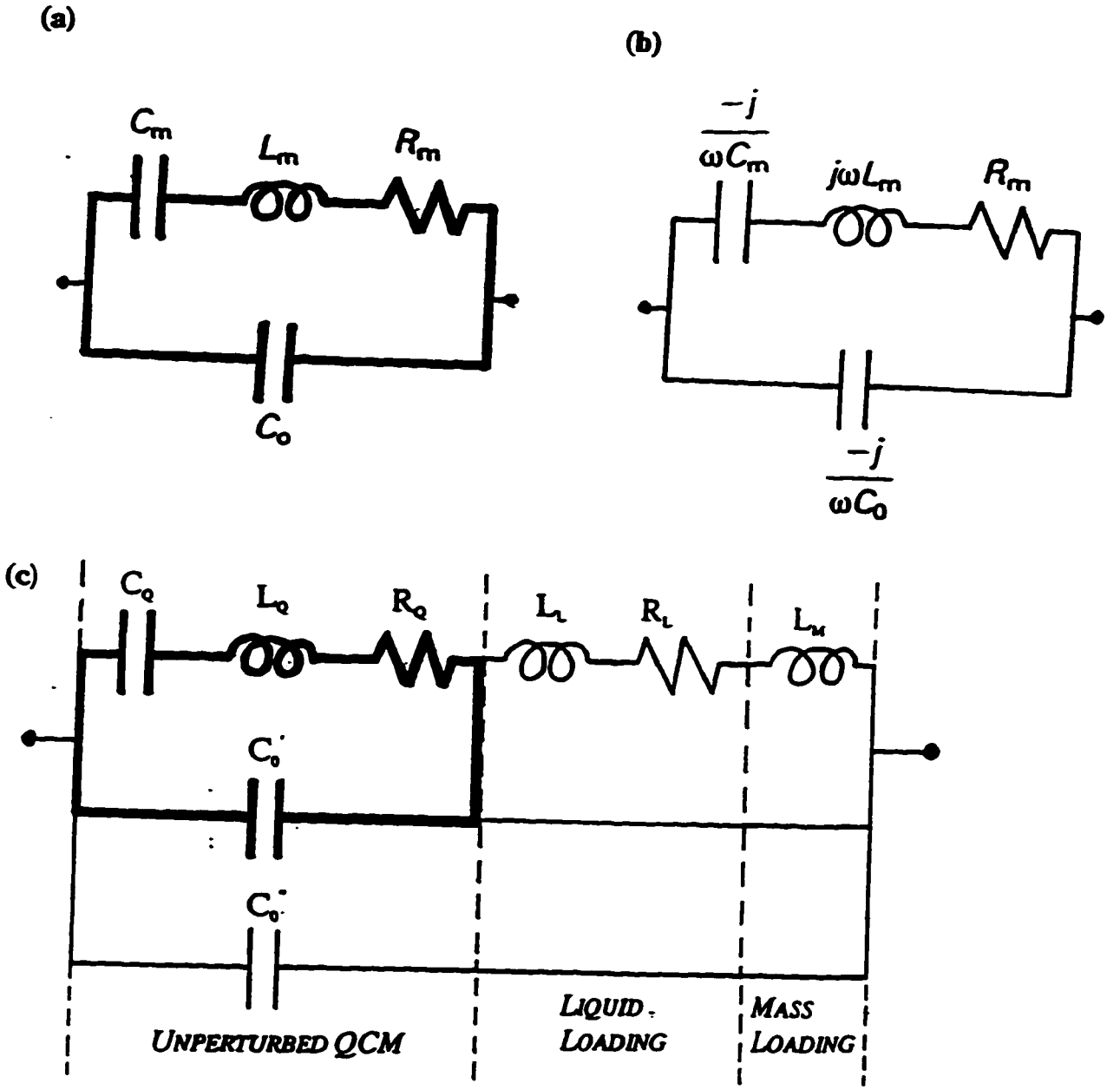

Figure 2-9:

a) A Butterworth-Van Dyke (BVD) equivalent circuit for the unperturbed QCM with parameters; b) Impedances elements of the unperturbed BVD equivalent circuit; c) Equivalent circuit for a perturbed QCM by mass and liquid loading (*from Martin et al* [143]).

that impedance measurements made on liquid-loaded QCM (or EQCM) can be fitted with this model [138-147]. Unfortunately, this circuit does not take into account the extra effects of mass and liquid loading when the quartz crystal is operating in solution. Figure (2.9.b) shows an equivalent circuit for a quartz crystal that is perturbed by the presence of a thin mass layer and a contacting liquid. This circuit contains another additional parallel capacitance C_0'' due to parasitic capacitance in the test fixture (connection to the impedance analyser). For the unperturbed QCM (by which we mean a quartz crystal exposed to air with no added mass), the components L_M, L_L and R_L reduce to zero and the BVD circuit is used.

Because of the presence of many circuit elements in the circuit representation of the figure (2.9.b), its mathematical characterization is difficult. However, it is important to see that the elements L_L, R_L and L_M, that arise from liquid and mass loading are additively related in series to the unperturbed QCM parameters of the circuit of the figure (2.9.a) as following:

$$R_m = R_Q + R_L \qquad \text{and} \qquad L_m = L_Q + L_M + L_L \tag{2.37}$$

This also applies for the parallel capacitive branches C_0' and C_0'':

$$C_0 = C_0' + C_0'' \tag{2.38}$$

By substituting the subscript m (m for motional arm, not for mass) and 0 to the new RLC circuit elements given by expressions (2.37-38), we obtain the unperturbed BVD circuit of the figure (2.9.a). Consequently, characterizing the unperturbed QCM fully determines the response of any perturbed QCM.

The overall impedance Z (the reciprocal of the admittance Y) of the equivalent circuit is then a combination of a series impedance Z_m due to motional branch that is parallel with Z_0, the impedance of the parallel branch C_0. It is a complex quantity that can be written in the following simplified form:

$$Z=\frac{Z_m Z_0}{Z_m+Z_0} \tag{2.39}$$

The impedances Z_m and Z_0 can be written in terms of their corresponding reactance X_m and X_0:

$$Z_m = R_m + X_m \qquad \text{and} \qquad Z_0 = jX_0 \tag{2.40}$$

with:

$$X_0=-\frac{1}{\omega C_0} \tag{2.41}$$

$$X_m=\omega L_m-\frac{1}{\omega C_m} \tag{2.42}$$

The quantity ω is the angular frequency (in rad s^{-1}) and is defined as $\omega = 2\pi f$, where f is the frequency (in Hz).

In general, the equation (2.39) will be written in the following standard form after multiplying the numerator and denominator by the complex conjugate of the denominator:

$$Z = R + jX \tag{2.43}$$

It is often simpler however to use the reciprocal of impedance, or the admittance Y = 1/Z:

$$Y = G + jB \tag{2.44}$$

with

$$|Y| = (G^2 + B^2)^{1/2} \tag{2.45}$$

where the conductance G and the susceptance B are the real and imaginary parts of the admittance Y, respectively. Both G and B are complicated expressions that are functions of R_m, L_m, C_m, C_0 and the angular frequency ω related to the frequency f through the following universal definition:

$$f = \frac{1}{2\pi\sqrt{LC}} \tag{2.46}$$

where LC represents the vibrating (oscillating) element part of the *motional arm* in the BVD circuit.

2.5.2. Model Prediction

Having described the equivalent circuit for an unperturbed QCM, it is now time to consider frequency changes that occur in the real situation of a perturbed QCM. From the definition of the frequency (Eq. 2.46), one can see that the capacitance C is not affected by mass or liquid loading. Frequency changes are only due to changes in the inertial mass component represented by L_M and L_L in the equation 2.37. Thus, the fractional change in f_s can be find by solving the equation given by $\partial f/\partial L$:

$$\frac{\partial f}{\partial L} = -\frac{1}{4\pi L\sqrt{LC}} \tag{2.47}$$

By multiplying the numerator by ∂L and by dividing by f at left and by the expression for the f at the right, one get the relationship between the fractional change in frequency and its corresponding fractional change in L by

$$\frac{\Delta f_s}{f_s} = -\frac{\Delta L}{2L} = -\frac{1}{2}\frac{L_M + L_L}{L_Q + L_M + L_L} \tag{2.48}$$

When mass and liquid loading are small ($L_M+L_L \ll L_Q$), the fractional change in resonant frequency of the series circuit (motional arm) is given by the following equation:

$$\Delta f_s = -\frac{2f_s^2}{\sqrt{\mu_Q \rho_Q}} \frac{\Delta M}{A} - \frac{f_s^{3/2}}{\sqrt{\rho_Q \mu_Q}} \sqrt{\frac{\rho_L \eta_L}{\pi}} \qquad (2.49)$$

in which ΔM is the change in mass, and A the surface area. The other parameters keep their previous meanings. In effect, one can recognize that this equation is a combination of the Sauerbrey equation (first term) and the Kanazawa-Gordon and Bruckenstein and Shay equations (second term) reflecting the effects of added mass and solution respectively.

The equation 2.44 is generally considered for polymer films for which the shift in frequency due to viscous coupling through the product $\eta_L\rho_L$ is important. If the product $\eta_L\rho_L$ is constant (in absence of liquid loading), the the equation (2.49) reduces to the first term which is the well known Sauerbrey equation (Eq. 2.21).

The key of the impedance analysis is then to derive the circuit parameters for an unperturbed QCM although it may mean that the perturbed QCM circuit parameters will be extracted later.

2.5.3. Impedance Analysis

The direct and converse piezoelectric effects are conjugate effects. This means that

when a quartz crystal is in oscillation, there will be an electrical field ***E*** generated by an applied voltage ***V*** across the crystal and a corresponding current density ***i*** flowing through the crystal. The relationship between i and V has the form of Ohm's law (i = YV), where Y is the admittance of the crystal. Admittance is the reciprocal of the impedance Z so that impedance is the equivalent of resistance for circuits involving alternating current.

Impedance analysis involves the measurement of current at a known applied voltage over a specified range of frequencies. This is accomplished in our laboratory with a Solartron Instruments 1260 Impedance/Gain-Phase Analyser.

a) Admittance diagrams

The properties of the series branch of a quartz resonator are conveniently described by the admittance of the resonator by the equation (2.44). Each element of the equivalent circuit represented by the figure 2-9 has an admittance. Among these elements, only the resistive component R is non frequency dependent. The capacitance C_0 and inductance L_m components are frequency dependent according to the equation 2.46. Consequently, the current flowing into the quartz crystal will depend on both the frequency and applied voltage.

Admittance plots are very useful to decern the frequency-dependent properties of the quartz crystal resonator. In these diagrams, the magnitude of the resultant admittance,

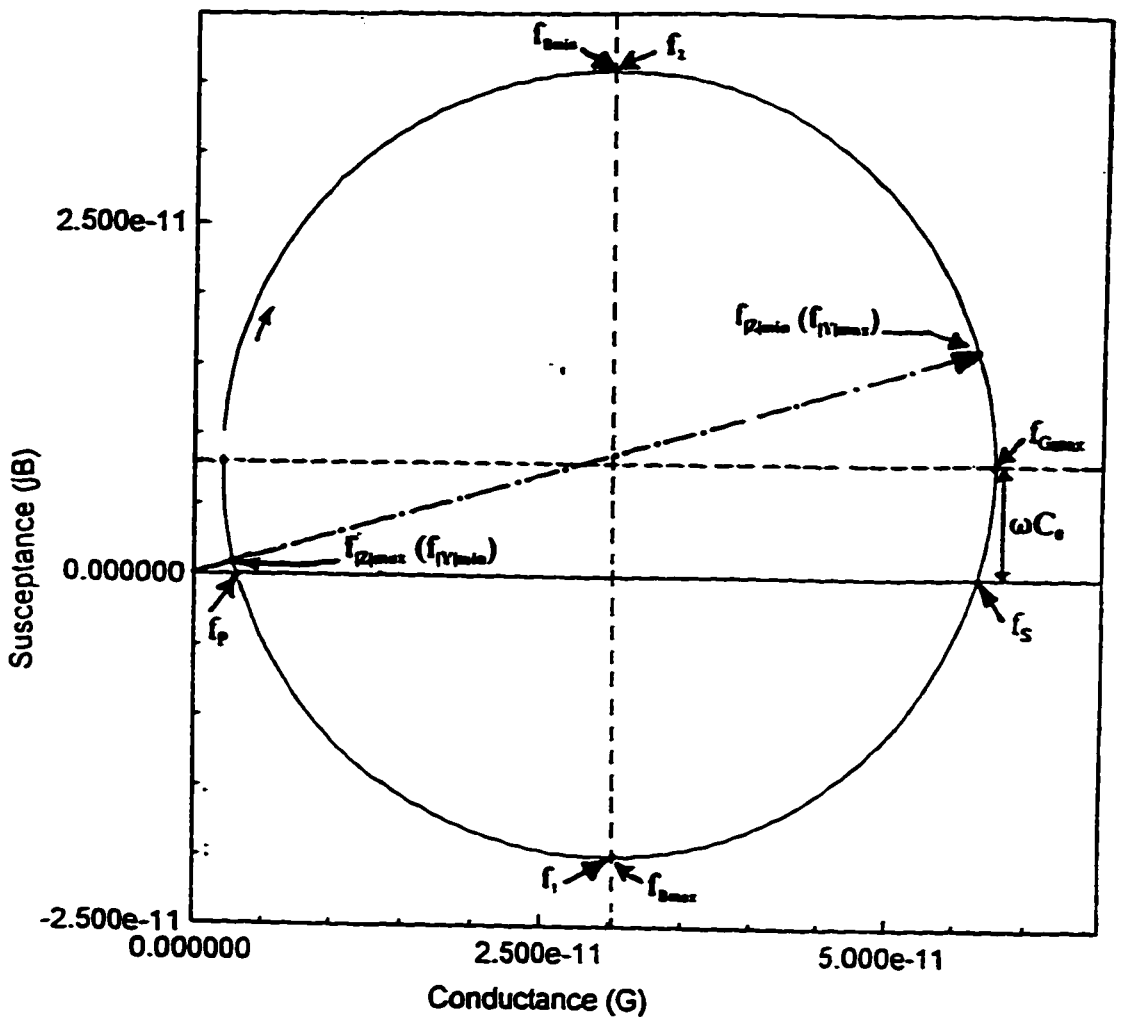

Figure 2-10:

Typical admittance plot (Nyquist plot) in the resonance region of an electrodeposited platinum quartz crystal in a 0.2 M H_2SO_4 electrolyte solution.

|Y|, is given by equation (2.45) and can be determined from the resultant of the real and imaginary vectors which affords the equation for a circle of radius G/2. Admittance diagrams, also called Nyquist plots, are simply plotting in which the real part of the admittance (the conductance) is plotted as abscissa and the imaginary part (the susceptance) is plotted as the ordinate. On the figure 2.10, one can see that as the frequency is increased from f = 0, the imaginary component of the admittance (jB) and the admittance itself reaches maximal values at f_{max}. By increasing the frequency, the real component of G reaches a maximum at the frequency $f_{G_{max}}$, which is the actual series resonance frequency. This frequency has two important characteristics: the impedance attains its minimum value (maximum value for admittance) and the series and parallel components are in a phase. Therefore, current flows easily at this point. In general, impedance analyses are driven at frequencies around f_{max}. Finally, another frequency of importance is f_{min} and corresponds to the point where the admittance and the imaginary component B reach minima.

Another characteristic of admittance plots is that because of the existence of the capacitance C_o, the frequency f_{max} is no longer located at the intersection point with the abscissa, as it is for an LCR circuit without static capacitance. For a quartz crystal resonator, the frequency f_{max} is raised along the imaginary axis (ordinate) from the real axis (abscissa) by an amount $\omega(C_o' + C_o'')$. Therefore, admittance plots can be useful to detect the extent of static effects (non conductive film would have more static effects

since they have the tendency to accumulate charge as for a condenser).

While admittance plots are useful, transformations of extracted data to Cartesian plots are still more important in elucidating the behaviour of the quartz crystal. These are generally given by the B-G and Z-θ plots, respectively.

b) The B-G plots

Because B and G are frequency dependent, functions $\partial B/\partial f$ and $\partial G/\partial f$ will be useful to extract some characteristic quantities. These quantities are simply the optimum values obtained after a Cartesian transformation of the data extracted from admittance plots by solving $\partial B/\partial f = 0$. The function of B has then two maxima at frequencies $f_{B_{max}}$ and $f_{B_{min}}$ while the function G has one maximum at the frequency $f_{G_{max}}$ (Figure 2.11).

The B-G plots of the figure (2.11) are very useful as diagnostic tools of the critical properties of a quartz crystal: these are the resonant frequency $f_{G_{max}}$ which is close to $f_{G_{max}}$ extracted from the G-curve, the frequencies $f_{B_{max}}$ and $f_{B_{min}}$ extracted from the B-curves. The sharpness of the conductance curves is delimited by two frequencies f_1 and f_2, so that $f_{G_{max}}$ is positioned exactly at half point between these two frequencies. From the G-curve, G_{Max} is the conductance, the inverse of the real reactance (the resistance). Therefore, this point corresponds to a minimum of the resistance, i.e. a maximum of current according to i =

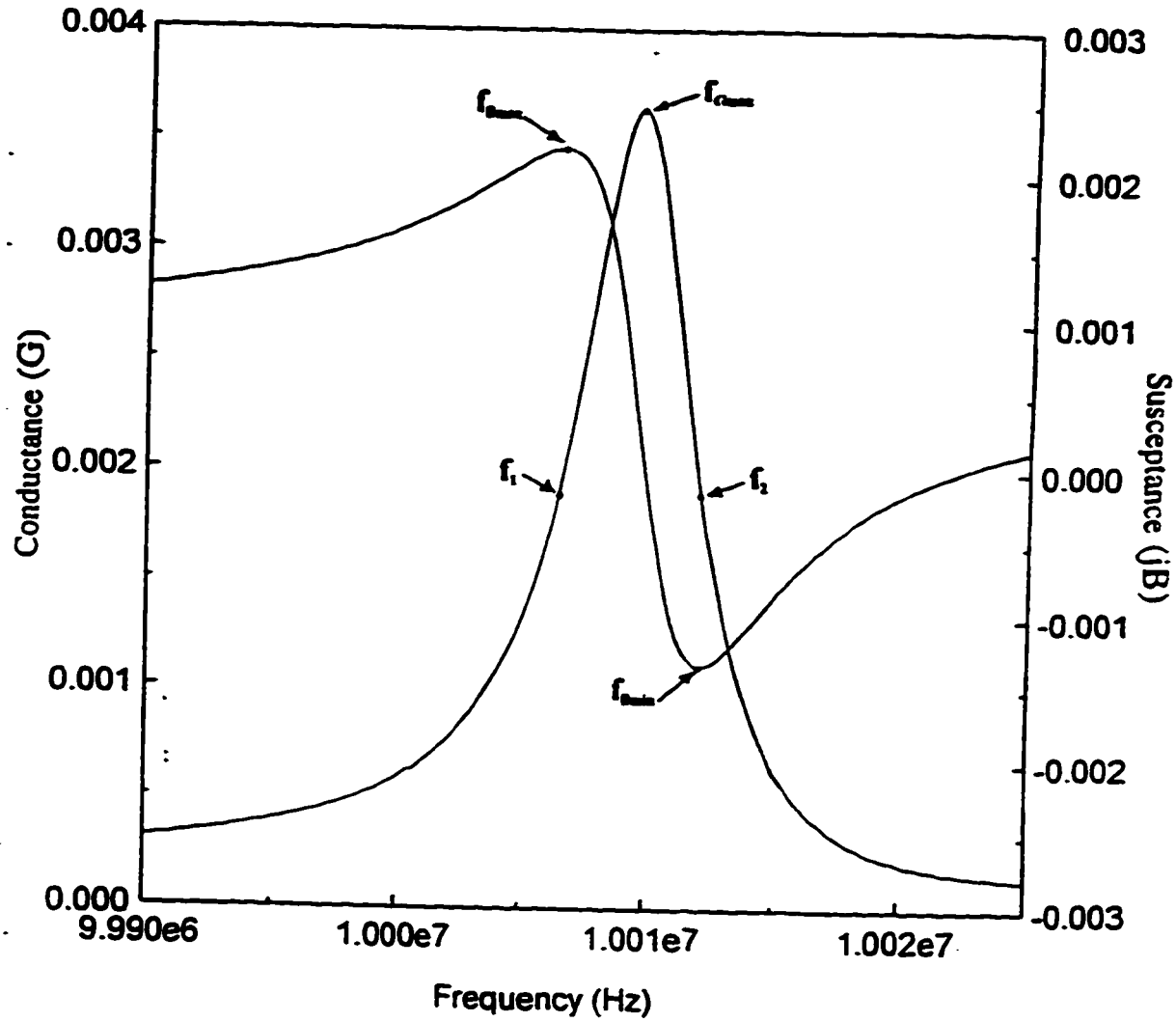

Figure 2-11:

Typical B-G plots in the resonance region of an electrodeposited platinum quartz crystal in a 0.2 M H_2SO_4 electrolyte solution.

V/R. Thus, current flows most easily at frequencies in the vicinity of $f_s \approx f_{G_{max}}$ which is equally positioned between two frequencies f_1 and f_2 (half-points). Therefore, quartz crystals behave as bandpass filters with a bandwidth defined as the difference f_2-f_1 of the half-power points on the G-curve. Unfortunately, it is not easy to extract the f_1 and f_2 values from the G-curve with a good accuracy. But since the frequencies $f_{B_{max}}$ and $f_{B_{max}}$ on the B-curves coincide with f_1 and f_2 on G-curves, the bandwidth of the filter can be easily replaced by:

$$f_{PWHH} = f_{B_{min}} - f_{B_{max}} \tag{2.50}$$

which is the *peak-width-at-half-height*, f_{PWHH}, defined by the difference between $f_{B_{min}}$ and $f_{B_{max}}$extracted from B-curves. The more f_{PWHH} is larger, the more the quartz crystal uses a large band of its frequencies. In terms of energy, since the current flows easily at the vicinity of $f_{G_{max}}$, a large bandwidth means a big dissipation of energy. Therefore, the *peak-width-at-half-height*, f_{PWHH}, together with the resonant frequency at G maximum, $f_{G_{max}}$, will serve as a diagnostic criteria for the extent of energy dissipation through the so-called *quality factor* Q of the quartz resonator.

c) *The Quality Factor Q*

The *peak-width-at-half-height* and the resonant frequencies are important quantities

that determine the quality factor Q which is the ratio of the energy stored to the energy lost during oscillation. So that, change in energy means change in the compliance element C_m of the quartz that represents the energy stored during oscillation of a vibrating mass represented by the circuit element L_m. From the expression of the series or motional resonant frequency f_p one can relate the series resonant frequency f_s and the quality factor Q as following:

$$f_{Gmax} \approx f_s = \frac{1}{2\pi\sqrt{L_m C_m}} \tag{2.51}$$

and

$$Q = \frac{f_s}{f_{Bmin} - f_{Bmax}} \approx \frac{f_{Gmax}}{f_{Bmin} - f_{Bmax}} = \frac{f_{Gmax}}{f_{PWHH}} \tag{2.52}$$

Alternatively, Q can be expressed in terms of L_m and R_m, which better define the concept of stored and lost energy:

$$Q = 2\pi f_{Gmax} \frac{L_m}{R_m} \tag{2.53}$$

with $L_m = L_Q + L_M + L_L$ and $R_m = R_Q + R_L$ being those that are shown on the figure (2.9.b) of the perturbed EQCM circuit that takes in account the effects of mass and liquid loading. Consequently, equations 2.46-48 are very pertinent and the conductance spectrum where the related quantities are extracted are a useful diagnostic tool because

a shift in f_{max} will be an indication of mass change at the surface of the quartz crystal while changes in energy dissipation will be discerned from the values of the peak-width-at-half-height (bandwidth). In the same order of idea, a high quality factor will be attributed to the high effective L values coupled with very low values of R. This allows B-G plots to be very useful for examining quartz crystals.

In general, when doing impedance analysis, one has to localize the series resonant frequency f_{max}, frequencies f_{max} and f_{max} on the B-G plots. The position of f_{max}, if shifted left (low frequencies), will be an indication of the existence of tightly bounded foreign material on an electrode. From the same B-G plots, a decrease in the conductance G means an increase of the resistive part in a circuit. Thus, the quality factor can be calculated. The value of Q and other parameters such as R_m can be used to check if the mass change observed is due to frequency change or not.

c) The Z-θ plots

In certain cases, we will be also interested to know the impedance Z rather than the admittance Y. The magnitude of the impedance Z, |Z| (in ohms), is defined by the inverse of |Y| (see Eq. 2.40)

$$|Z| = (R^2 + X^2)^{1/2} \tag{2.54}$$

and the phase angle θ (in radians) of impedance are simply defined as

$$\theta = \tan^{-1}\left(-\frac{X}{R}\right) \tag{2.55}$$

The phase angle θ is proportional to the difference in the time between when the voltage across the crystal is maximum and the current flowing through the crystal is a maximum. By solving θ = 0, which is a quadratic function of frequency, one can find the theoretical values of f_s and f_p, the series and parallel resonant frequencies, respectively.

Physically, impedance Z is the voltage V across the crystal divided by the current i flowing through the crystal (Z = V/i). Impedance analysis involves the measurement of current at a known applied voltage over a specified range of frequencies. Because of the presence of a series and a parallel branch, the resonance will be satisfied at two frequencies f_s and f_p, which are the series and parallel resonance frequencies, respectively. At these two frequencies, the phase angle θ crosses zero. The Z-θ plot contains $f_{z_{max}}$ and $f_{z_{min}}$ where the admittance magnitude is at a maximum and minimum, respectively (Figure 2.12). These quantities are found by solving $\partial|Z|/\partial f = 0$, while the solution of $\partial\theta/\partial f = 0$ gives only a maximum frequency $f_{\theta_{max}}$ for the maximum of the phase angle θ.

While B-G plots are useful to examine the behaviour of a quartz crystal resonator (interfacial and viscoelastic properties), Z-θ plots are generally used for investigation of

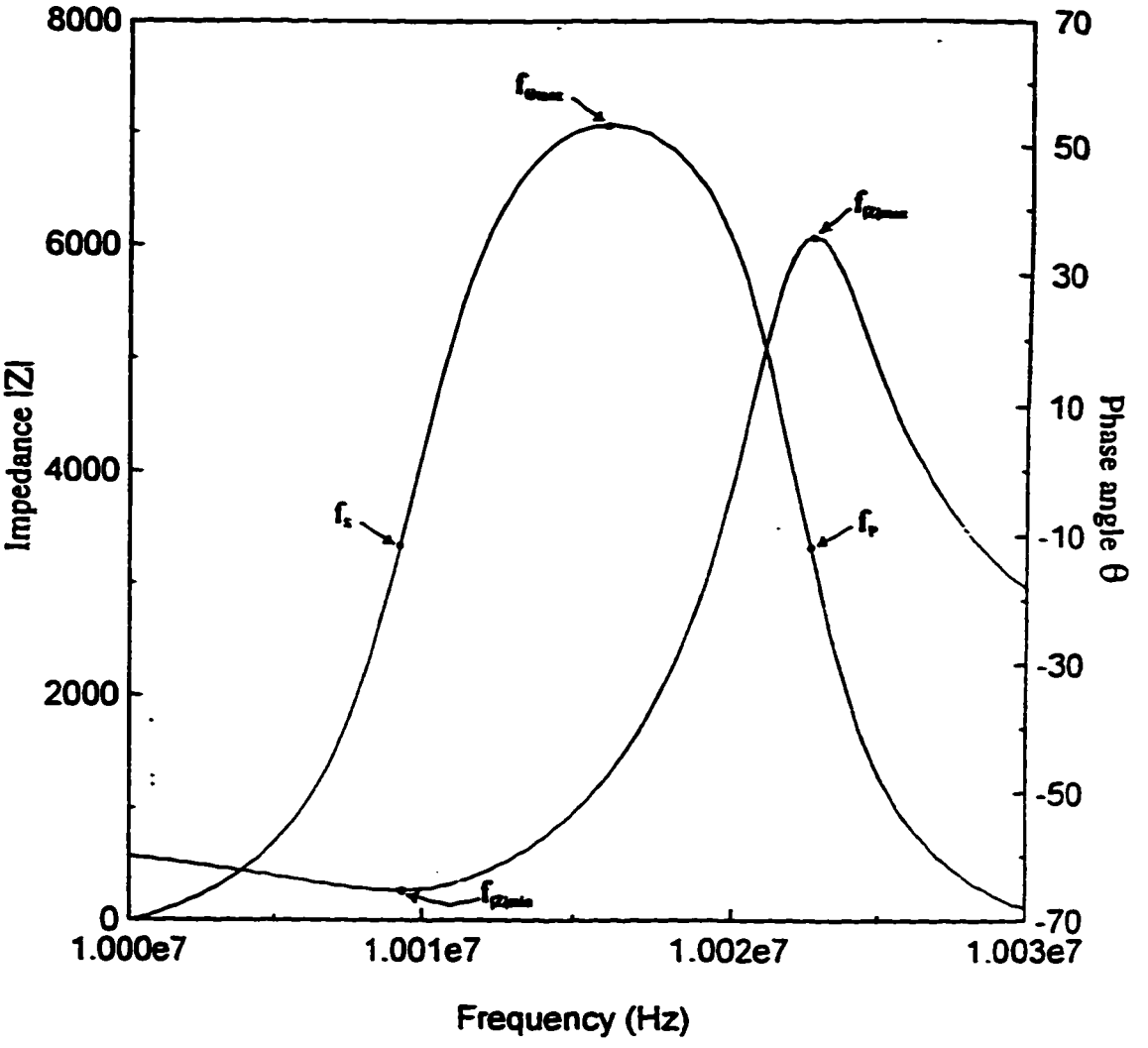

Figure 2-12:

Typical Z-θ plots in the resonance region of an electrodeposited platinum quartz crystal in a 0.2 M H_2SO_4 electrolyte solution.

the *analyzing the behaviour of the equivalent circuit* of a quartz crystal resonator, which is not the purpose of this study.

In general, when doing impedance analysis, one has to localise the series resonant frequency f_{max} , frequencies f_{max} and f_{min} on the B-G plots, then switch to the Z-θ plots bode to extract the numerical values of Z and θ for each of the above frequencies. Thus the quality factor can be calculated. The value of Q and other parameters such as R_m can be used to check if the mass change observed is due to frequency change or not.

* * *

Chapter 3:

Experimental and Apparatus

3.1. INTRODUCTION

In the work described in this thesis, adsorption processes involving both ions (principally halides) and neutral molecules (thiourea) have been studied using the Electrochemical Quartz Crystal Microbalance (EQCM) technique. In addition, other techniques such as Scanning Electron Microscopy (SEM) and Impedance Spectroscopy (IS) (as distinct from Electrochemical Impedance Spectroscopy or EIS) have been applied to address particular questions where appropriate. The principles of the EQCM have been fully introduced in the preceding chapter and Impedance Spectroscopy (IS), which is used in this work as a complementary diagnostic tool, has been treated in Chapter 2. This chapter describes instrumental aspects of both the EQCM technique and other related apparatus that has been employed in this thesis.

3.2. *QUARTZ CRYSTALS*

All quartz crystals used were nominal 10 MHz fundamental AT-cut crystals with gold electrodes deposited on both sides of the quartz plate. The quartz crystals are attached to a mount with a metallic enclosure that offers protection against damage (see Figure 2-1, chapter 2). All crystals used in this work were purchased from International Crystal Manufacturing Co, Inc., Oklahoma City (USA). The gold layer was vacuum deposited (by the manufacturer) without any adhesive layer between quartz and gold and has a typical thickness of about 0.09 μ. The gold is finished (again by the manufacturer) with 5 μ abrasive. An SEM picture of a gold electrode on the quartz crystal substrate is shown in Figure (3-1).

The quartz crystals are sealed onto the electrochemical cell using a silicone sealant and any mass changes resulting from electrochemical or non-electrochemical processes are monitored in terms of the corresponding frequency change. The frequency change is converted to a voltage for display onto a chart recorder as described below.

3.3. *ELECTROCHEMICAL CELL*

The electrochemical cell used in this work is made of Pyrex glass and has two main parts (Figure 3-2). The lower section can be considered as the main part in the sense that

it is the part of the cell to which the quartz crystal is attached. The upper part constitutes the cover for the lower part and has four-ports. Two ports are for the counter electrode compartment and for the Luggin capillary (that extends outside the cell to a beaker in which the reference electrode is placed). The other two ports are for the supply and removal of nitrogen gas that serves in this work either to deoxygenate the solution (when it is bubbled through the electrolyte) or to maintain a nitrogen atmosphere above the solution to avoid possible noise from the bubbling process.

As noted above, the quartz crystal is sealed on the lower part of the cell by means of a silicone sealant. Care must be taken to avoid any contact of the silicone sealant with the gold surface on the centre of the crystal electrode, as this is the mass sensing area. Finally, rigid leads are used to make the connection between the sealed quartz crystal and a box containing electronic circuitry that has two sockets for connection to the cell. One connection (to the electrode exposed to the solution) has a dual function, making contact for both the oscillator circuit and the electrochemical circuit while the other connection (to the electrode exposed to the air) is for the oscillation circuit alone.

3.4. ELECTRODES

As mentioned in the preceding section, a three-electrode cell was used for all experiments. These electrodes are: the working electrode, the counter or auxiliary electrode, and the reference electrode.

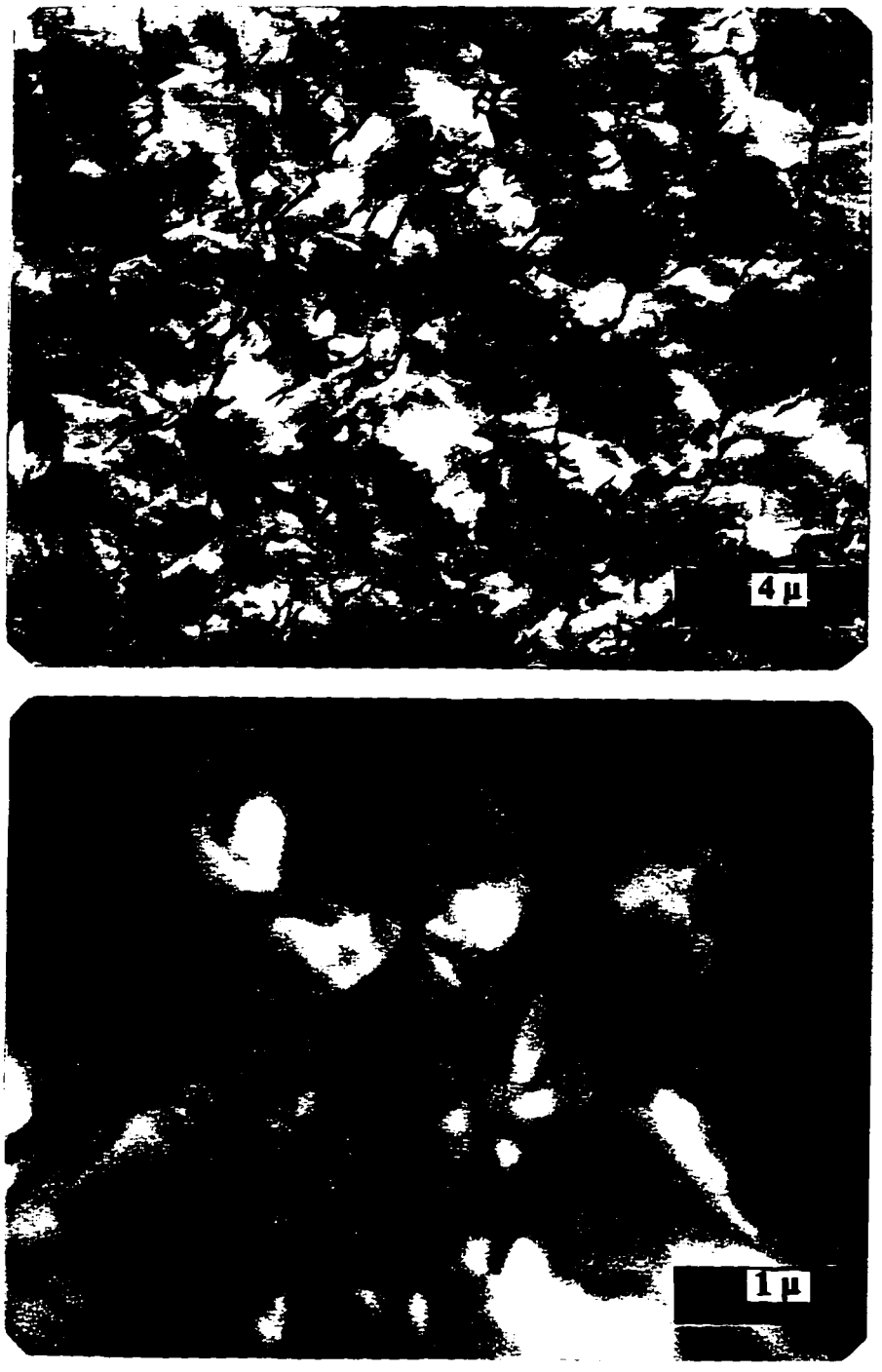

Figure 3-1:

Scanning Electron Micrograph (SEM) pictures of a gold electrodedeposited on the quartz crystal (*purchased from International Crystal Manufacturing Co., Inc,Oklahoma City, USA*).

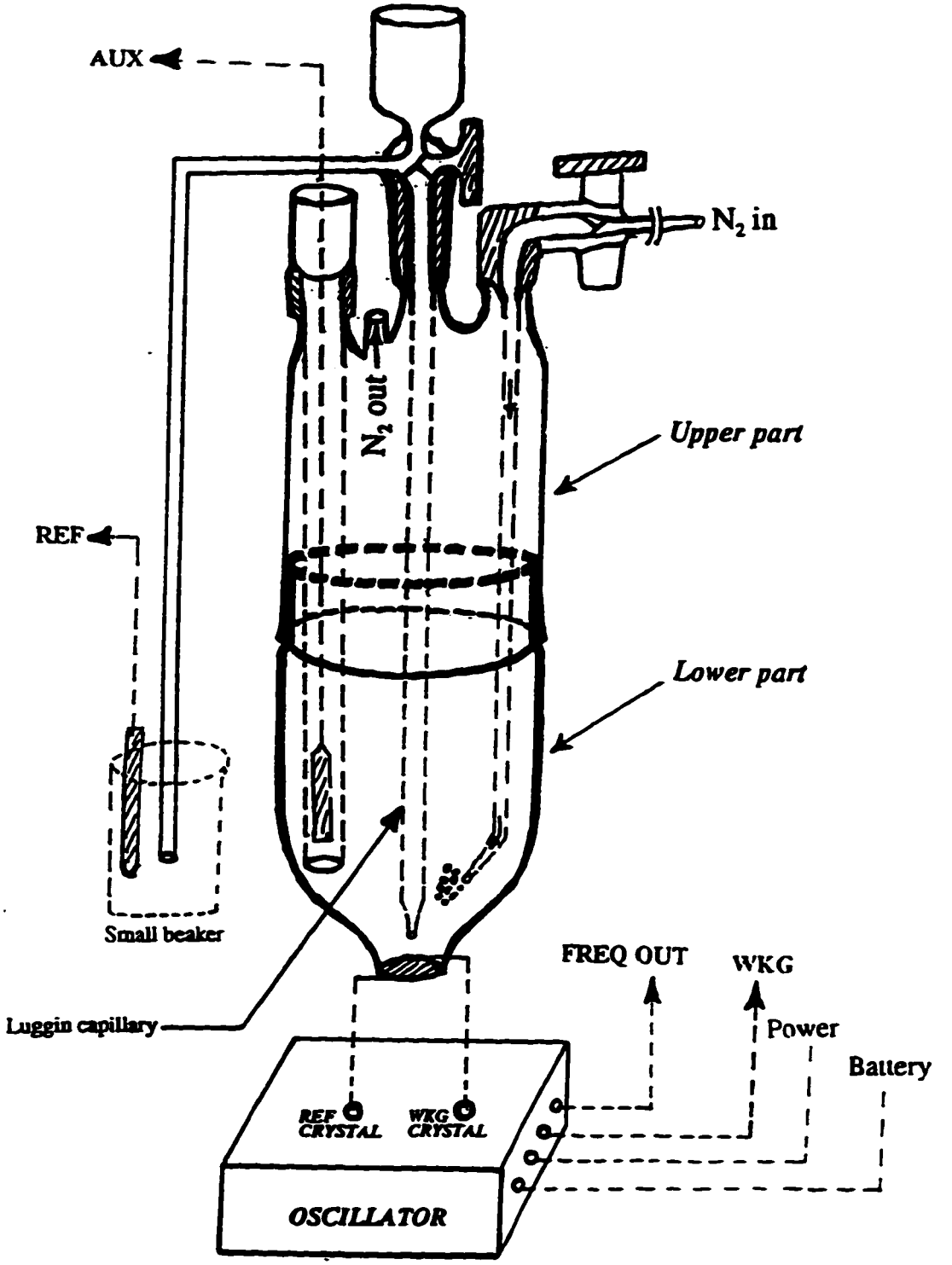

Figure 3-2:

Electrochemical quartz crystal microbalance cell with plug-jacks of the sealed quartz crystal connected to the oscillator circuit box.

The working electrode (WKG) is a platinized platinum electrode prepared by electrodeposition from a solution of 2 mM H_2PtCl_6 in 0.2 M H_2SO_4. The plating (onto the gold electrode on one face of the quartz crystal plate) was performed in a potentiostatic regime at +0.350 volts (SCE). Prior to plating the gold electrode was cleaned electrochemically by cycling between potentials where hydrogen and oxygen gases evolve (-0.30 to 1.45 V/SCE). The time of plating depended on the amount of platinum required. However, in general, an amount equivalent to 20 to 25 μg of platinum was deposited onto the gold electrode. This calculation is based on a frequency sensitivity of 61.5 mV/kHz or 16.2 Hz/mV for the frequency to voltage converter previously obtained by Wilde and Zhang who used the same electronic circuit[148].

The counter or auxiliary electrode (AUX) was a platinum wire of a large surface area that was placed in one of the ports of the upper part of the cell. The compartment is made of a Pyrex glass tube which is finished with a fine glass frit that separates the tube from the main part of the cell so that any undesirable products of the counter electrode reaction are prevented from entering the main body of the electrolyte. All potentials are referred to a reference (REF) electrode. It is a home made saturated calomel electrode (SCE) immersed in a small beaker and separated from the cell by a Luggin capillary. For some experiments a silver-silver chloride electrode (SSCE) was used but all potentials reported in this work are referred to the SCE scale.

The real surface area of the platinized Pt electrode was determined either by using an integrator or by simply photocopying and weighing the area of the hydrogen UPD charge of a CV taken in 0.2 M H_2SO_4. As has been mentioned in the chapter 1, it has been assumed that a charge of 210 $\mu C/cm^2$ corresponds to a monolayer of hydrogen adsorbed on Pt. After cycling in 0.2 M H_2SO_4, the platinum electrode has a starting roughness factor of 20 to 35 (ratio of real area to geometric area), assuming that the geometric area of the plated surface is 0.25 cm^2.

3.5. CHEMICALS AND SOLUTIONS

All experiments were performed at room temperature (23 ± 2 °C). Electrolyte solutions were prepared using high grade water (18 $M\Omega.cm^{-1}$) from a Millipore Milli-Q or Milli-Q Plus system.

The following chemicals were Analytical Reagents (Analar®) and were obtained from BDH: H_2PtCl_6, KBr, KOH, NaOH, $CaSO_4$, $PbSO_4$, Na_2SO_4, Na_2HPO_4, H_3PO_4 and $HClO_4$. Potassium chloride (KCl) was Suprapure® from Merck, and sulphuric acid (H_2SO_4) was either Suprapure® (from Merck) or Seastar™ , (from Seastar Chemicals Inc). Thiourea and Urea were certified from Fisher Scientific Company.

All the above chemicals were used as received without further purification. In some

cases, an ultrasonic bath (Branson 2210) was used to clean glassware. In cases where the solution was degassed with nitrogen, dried nitrogen (Ultra purity 99.99%) supplied by Air Products was used.

3.6. OSCILLATORY CIRCUITS

The quartz crystals used in our laboratory have a reasonable quality factor (see Section 2.5.3, Chapter 2). Before sealing the crystal on the cell, the quality factor is about 2×10^4, in air. The sealing process reduces this value by a factor of 2 ($Q_{seal} = 10^4$) crystal. Complications arise when the crystal is placed in an aqueous solution. A typical range for the quality factor of a gold-coated quartz crystal placed in a solution of 0.2 M H_2SO_4 is 1.25×10^3 to 2.0×10^3. All these measured values agree with reported literature values for similar quartz crystals in air and in solution[53]. Figure (3-3) shows conductance diagrams for the three situations: a gold quartz crystal before and after sealing up a cell (in air), the same sealed crystal but in a 0.2 M H_2SO_4 solution. The presence of a viscous solution reduces the quality factor of the quartz crystal in air by a factor of 5 to 8. This mechanically damps the crystal to a point where there is a lack of feedback to sustain oscillations.

To compensate for this drawback, the circuit must be designed so that the oscillation is supplemented with a high-gain amplifier in its feedback loop to allow the

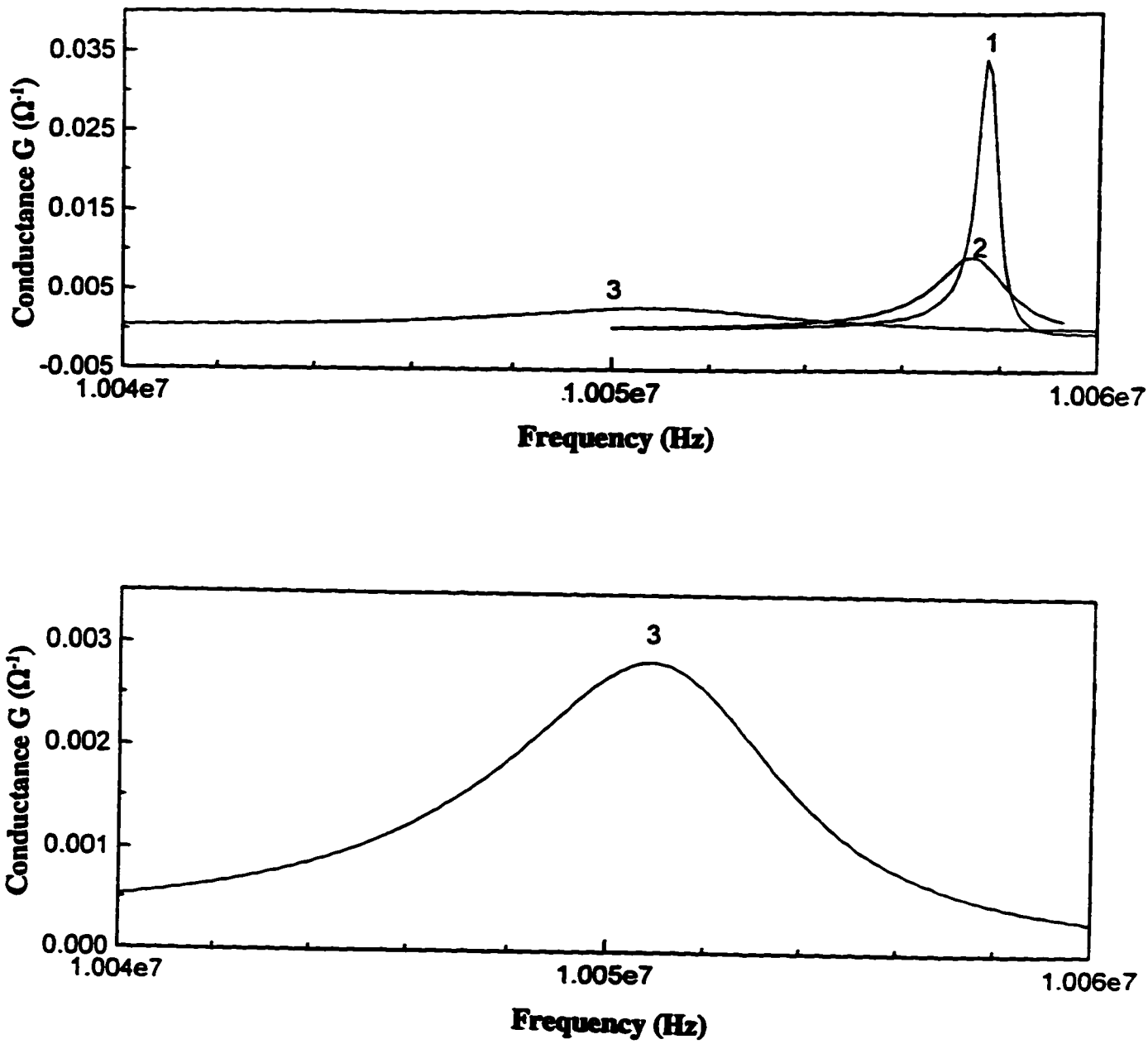

Figure 3-3:

Plots of conductance vs frequency (admittance diagrams or G-plots) for a 10 MHZ AT-cut gold-coated quartz crystal: 1: in air, before sealing up a cell; 2: the same crystal sealed up a cell but in air, and; 3: the same sealed crystal surrounded by 50 mL of a 0.2M H_2SO_4 solution. The diagram 3 (bottom) has been magnified.

oscillation of the crystal in the solution. There are several models that have been proposed to monitor mass changes while one face of the quartz crystal is immersed in the solutions while the reference crystal is external to the electrochemical cell. The more well-known are those of Bruckenstein and Shay [47], and of Kanazawa and Gordon [48].

Recently, Bruckenstein *et al* have built a new QCM circuit in which both the working and reference crystals are immersed in the same solution in order to minimize viscoelastic and density effects [149,150]. They called this new QCM a "*dual quartz crystal microbalance, DQCM*" and refer to the "*single quartz crystal microbalance, SQCM*" that uses one face of the only working crystal in contact of the liquid solution. In this work, we will continue to use the original denomination of EQCM instead of SQCM, even if both refer to the same circuit principle.

The oscillatory circuit used in our experiments is identical to that of Bruckenstein and Shay [47] as shown in figure (3-4). The circuit is composed of four blocks of electronic components: U1 (7404 HEX), U2 (7414 HEX), U3 (7474) and U4 (HP2630). The role of these elements is to control and synchronize the oscillations of the reference and working crystals to allow the difference between the oscillations of the reference and working crystals to be found by subtraction. It is assumed that the frequency of the reference crystal does not change. The components U1A-C (for the reference crystal) and U1D-F (for the working crystal) are made of inverter amplifiers of type HEX INVERT. Their role

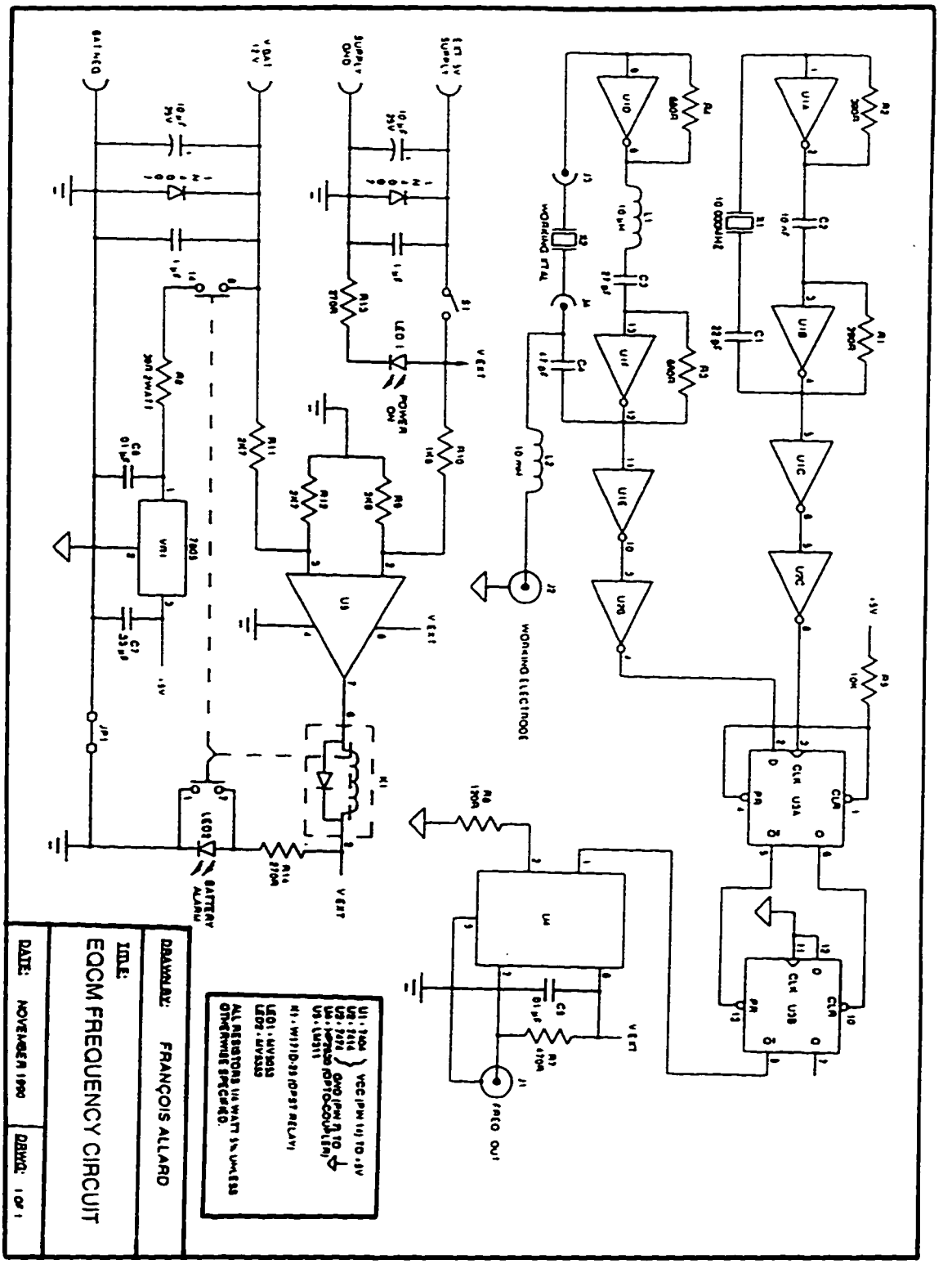

Figure 3-4:

The EQCM circuit with two separate reference and working quartz crystal oscillators: U1=7404 HEX INVERT; U2=7414 HEX Schmitt trigger; U3=7474 Dual D Flip-Flop; U4=HP2630 Dual Optically Isolated; Circuit of separate power supplies (lower part).

is to extract the individual oscillations generated by the two separated crystals. While the reference crystal is coupled to simple capacitors C_1 and C_2 to drive it at the desired 10 MHz frequency, the working crystal oscillator is coupled with two inductor-capacitor combinations L_1C_3 and L_2C_4 to take into account mass and liquid loading effects. Once these two oscillations are obtained, they are separated and inverted by means of two circuits U2B and U2C (Schmitt trigger inverters) and fed to a dual D flip-flop circuit (U3A and U3B) that measures only the absolute difference. Finally, since the difference of frequency between the reference and the working crystals is desired, care must be taken to avoid any complications from noise (e.g other instrumentation). This is assisted with a dual optically isolated gate of the circuit U4 that isolates the difference frequency between the reference and the working crystals from the undesired frequencies that may come from the whole of the EQCM setup. Ideally, one expects to measure frequency difference in the range 2-30 kHz, depending on the experiments that are carried out.

The remainder of the circuit involves the connection of the output-frequency to a frequency-to-voltage converter to allow the use of an analog voltage recorder to display results. In order to obtain accurate mass signals from the crystals, both the frequency-to-voltage and the frequency-to-mass must be calibrated. This has already done in our laboratory by Wilde and Zhang [148]. The frequency sensitivity obtained by the calibration of the frequency-to-voltage converter was found to be 16.2 Hz/mV, and the mass sensitivity obtained by galvanostatic deposition of silver onto the gold substrate from an

$AgNO_3$ solution is 19.6 ng/mV. Thus, in the results shown in later chapters, this figure has been used to convert the recorder scale (in mV) to a value in ng.

3.7. ELECTROCHEMICAL APPARATUS

Figure (3-5) shows a block diagram of the EQCM apparatus used in the present work. The potential was controlled by means of an Oxford Electrodes bipotentiostat from Abingdton, England. The working crystal is mounted to the electrochemical cell with one face (the working electrode) connected to the potentiostat for electrochemical control but with the two faces connected to the oscillatory circuit for the frequency measurement. The current was converted to a charge signal by means of a home-made integrator using an operational amplifier (Figure 3-6). The frequency difference between the reference and working crystals was converted to a voltage signal by a home-made frequency-to-voltage converter also shown in the block diagram of the EQCM instrument of the figure (3-5).

The frequency, the current and charge are recorded in form of voltages on a Philips PM 8272 XYt or a Kipp and Zonen BD91 XYY' chart recorder. When impedance measurements are made, only the lower part of the cell is connected to the Impedance/ Gain-Phase Analyser (Model SI 1260 of Schlumberger) by means of two short wires, i.e. all impedance measurements were made at open circuit, not under potential control.

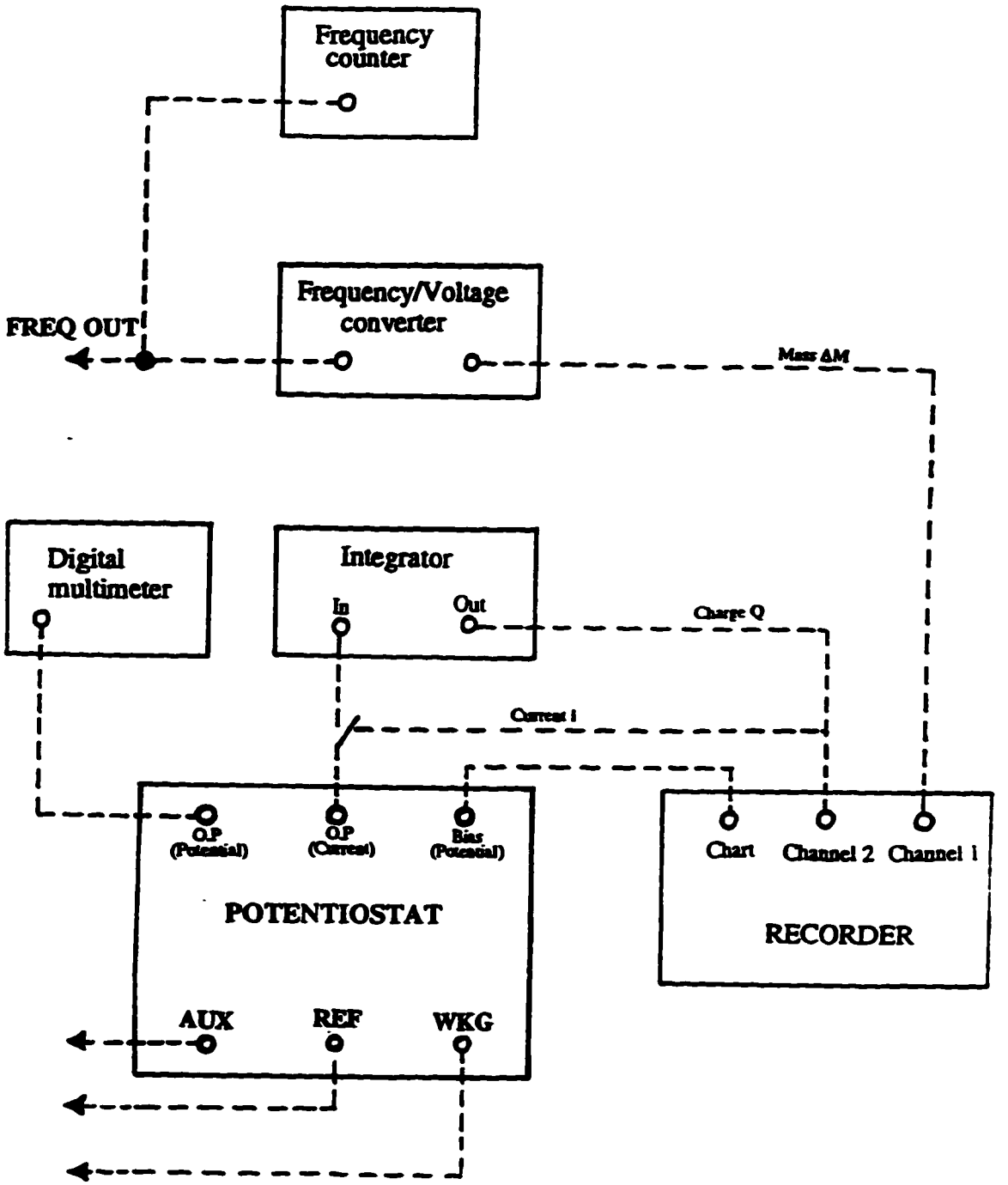

Figure 3-5:

Bloc diagram of main elements of the electrochemical apparatus: a bi-potentiostat, a frequency/ voltage converter, an integrator (see figure 3-6).

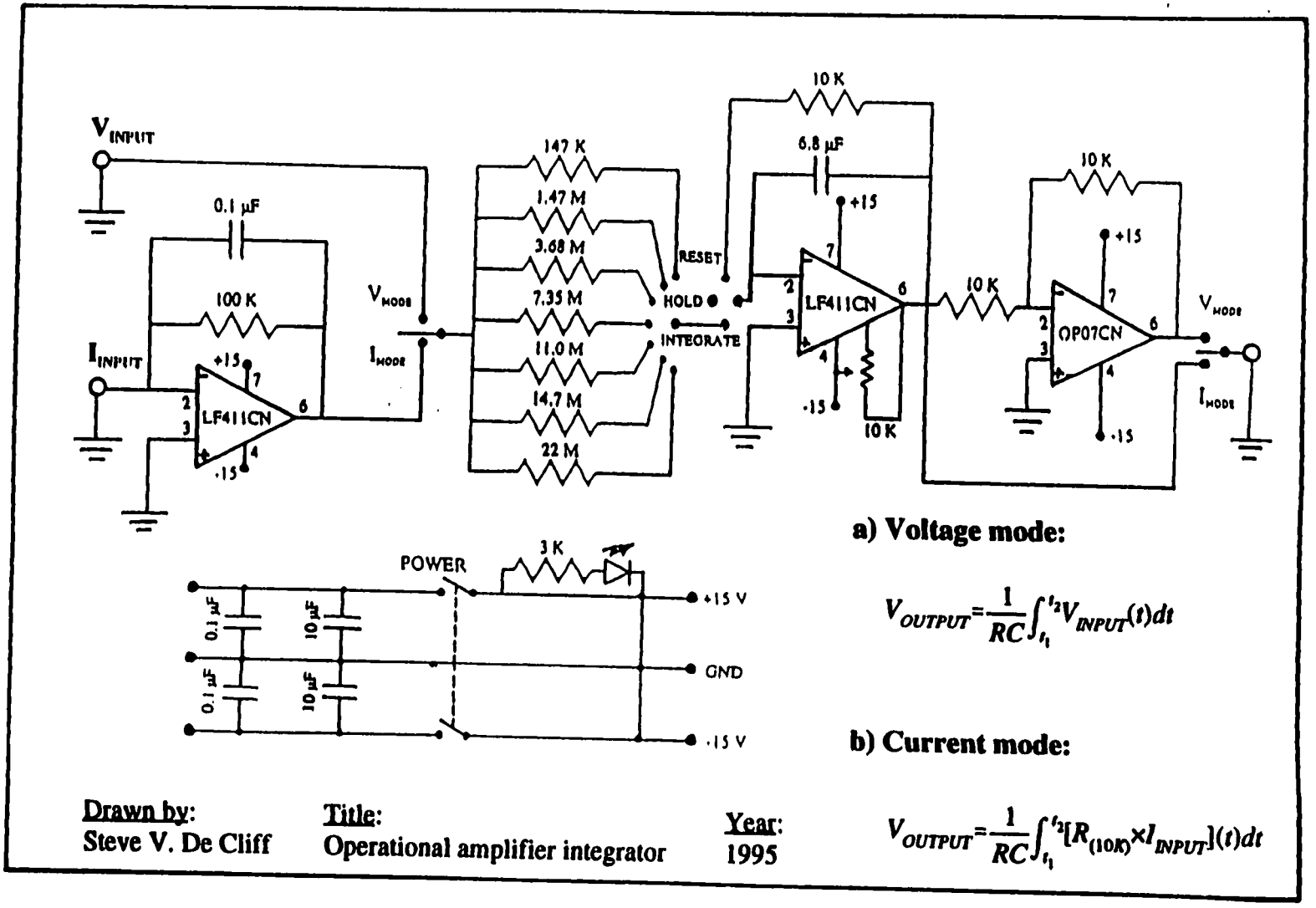

Figure 3-6:

Circuit of an integrator using an operational amplifier operating etheir in voltage or current mode.

In this chapter, we have presented the essential aspects of the electronic design and the instrumentation. The next chapters are all devoted to the presentation and discussion of experimental results of our research work.

* * *

Chapter 4:

Influence of Surface Pre-Treatment and Anions on the Electrochemical Quartz Crystal Microbalance (EQCM): Studies at Electrodeposited Platinum Electrodes (EDPE)

4.1. INTRODUCTION

A large volume of literature has been devoted to the applications of the electrochemical quartz crystal microbalance (EQCM) technique since its development as a technique that could be applied to *in-situ* studies of electrochemical processes. Much of this work has been well-reviewed recently [50-54,56]. However, the number of investigations of *sub-monolayer* surface processes (for example ionic adsorption and surface oxidation) at bare noble metal electrodes in background electrolytes, has been relatively few. Platinum electrodes have been used in only a few investigations, in part because until recently Au coated crystals were available commercially whereas Pt coated quartz crystals were not. It is clear from the

literature concerning Pt electrodes on the EQCM that there is still disagreement concerning the results obtained (for simple background electrolytes) and their interpretation [82,151-155]. It is also true that there is still considerable speculation concerning the factors which might influence the response of the EQCM (as discussed in Chapter 2), for any metal electrode, because of the fact that when operated in solution, the shear motion of the crystal results in the propagation of a shear wave into solution (Figure 2-7) and this leads to a (normally) constant offset of the frequency. However, if the nature of the electrode surface changes, and the interaction between electrode surface and solution shear wave (Figures 2-7 and 2-8) also changes, then there may be a frequency shift as a result of this rather than as a result of a mass change. It is generally assumed that the "no-slip" condition applies, meaning that the first layer of solution adjacent to the electrode oscillates with the electrode. However, it has been suggested that this condition may be affected by the state of the surface (whether or not it is hydrophobic for example) and by variables such as the degree of surface roughness [56,132,156,157] and so on . There is also some question about whether or not the adsorption of ions at the electrode surface may be observed and measured with the EQCM. It is with these questions in mind that the literature on studies of Pt electrodes in background electrolyte with the EQCM is summarised below.

In view of the earlier discussion of the possible causes of non-ideal behaviour (Chapter 2), and the paragraph above it is clear that the nature of the surface and the way in which it is prepared may be an important consideration in influencing the results obtained with an

EQCM. The literature on Pt EQCM electrodes can be divided simply into two categories:

① Studies performed on electrodes that have been vapour deposited or sputtered (and as a consequence have low roughness factors).

② Studies of electrodes that have been electro-deposited (and as a consequence have large roughness factors) typically 25-30 or greater.

Before discussing the mass responses observed for Pt electrodes, it is necessary to re-introduce the electrochemistry of Pt as seen in background electrolytes which was discussed in Chapter 1, section 1.3. It is fortunate that there is an extensive literature on the electrochemistry of Pt, partly because of its excellence as an electrocatalyst for a wide variety of important industrial applications. The historical development of the understanding of the electrochemistry of Pt has been well reviewed by Christensen and Hamnett in a book which contains many useful references to the original work [158]. The standard cyclic voltammogram of Pt is that observed in 0.5M H_2SO_4 and a literature example is shown in Figure 1-3 in Chapter 1. The voltammogram of Pt may be split into three regions of potential, all of which are referred to the Normal Hydrogen Electrode or N.H.E.

① The region of H adsorption/desorption (0.0 to 0.4V),

② The "double layer region" (0.4 to 0.8V) on a positive going scan but ca. 0.6V to 0.4V on a negative going scan because of the hysteresis between oxide formation and

reduction.

③ The region of surface oxidation.

Since one aspect of this chapter is concerned with anion effects, it is important to note that in the H adsorption region, there are two peaks that are clearly resolved. They correspond to different states of H adsorption at the surface (a more detailed discussion is presented later). The distribution of peaks changes with anion concentration and identity [40] but the total amount of charge associated with H deposition remains the same. In the double layer region of potential there are, in general, no Faradaic processes that occur in background electrolyte. However, various studies using for example, FTIR [159-161], and radioisotope labelling[162] indicate that anions can adsorb in this region and that the amount of anion adsorption should increase as potential increases. In the region of surface oxidation, the overall current profile shows a detailed structure that is a criterion of solution cleanliness. The different peaks have been suggested to correspond to different arrangements of PtOH at the electrode surface [39]. Once formed, there is a driving force for PtOH to undergo the process described as place exchange or turnover. Here, an OH inserts itself into the lattice, a process which is driven both by the field and by lateral interactions. It is this place exchange process that leads to irreversibility of the oxide formation process and causes the reduction of Pt oxide to occur at a potential that is significantly more negative than the oxide formation process. The oxide formation region is also sensitive to anion adsorption effects. Strongly adsorbing anions are able to displace the onset of oxidation of the surface to more positive values, examples of this

phenomenon will be seen later in Chapter 6 on chloride adsorption (and a similar effect is observed for organic adsorbates such as thiourea as we will see in Chapter 5). Based on this simple review of electrochemistry at Pt we might expect to see mass changes over all the potential scale as a result of anion adsorption effects.

4.2. LITERATURE REVIEW OF MASS RESPONSES FOR Pt ELECTRODES

In considering the mass responses that have been reported to accompany voltammetric studies of Pt electrodes in the literature, the data can be discussed in terms of the same three regions of potential described earlier. Almost all of these studies have been performed in either H_2SO_4 or $HClO_4$ as electrolytes:

- Mass responses in the H adsorption region fall into two types:

  a) If the potential is scanned negative from the double layer region so that the coverage of adsorbed H grows to a monolayer then the mass is seen to decrease consistently. The mass is at a minimum at the negative potential limit. This type of response appears to be associated with vapour deposited Pt electrodes that have low roughness factors [153,155]. Figures 4-1 and 4-2 show this feature. Note that mass increases down the page in these figures.

  b) As the potential proceeds from the double layer region into the region of under-potentially deposited H, the mass decreases but then it passes through a minimum and

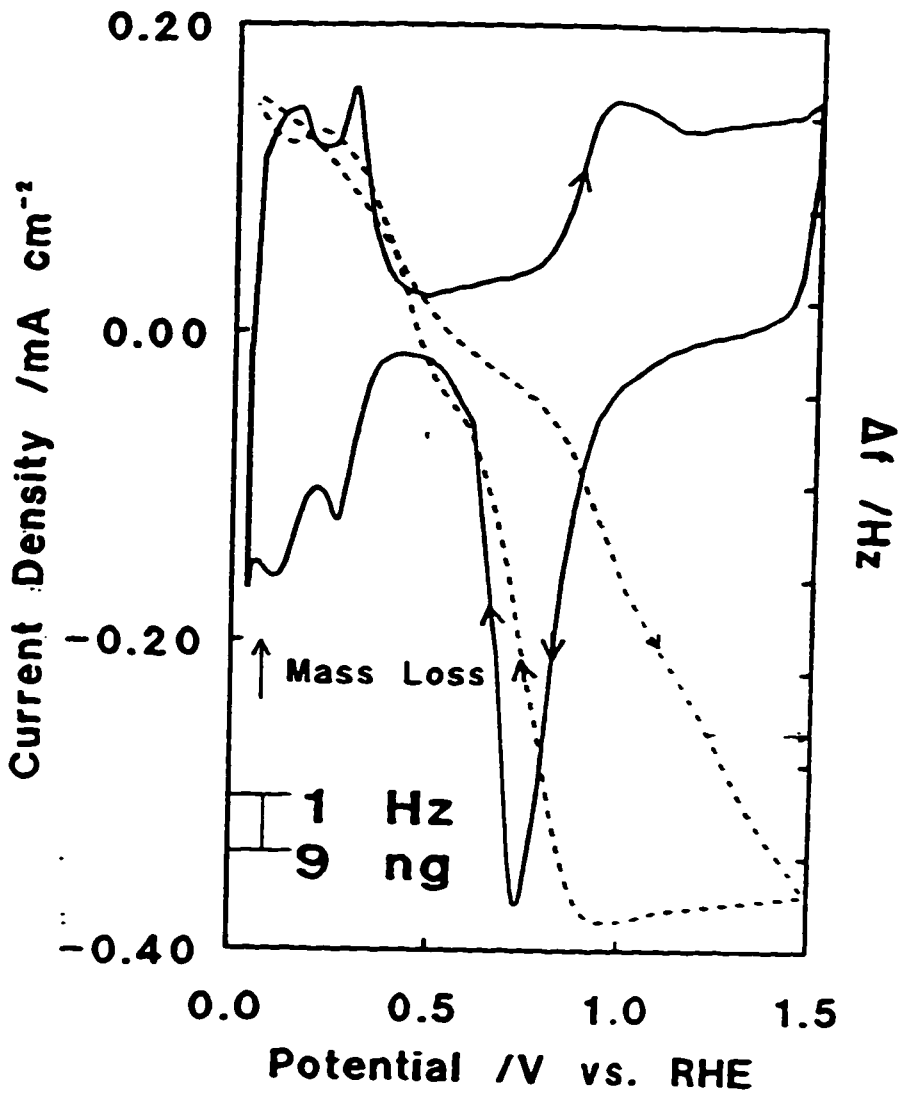

Figure 4-1:

Cyclic voltammogramm (___) and associated frequency change (...) of a Pt -coated quartz crystal in 0.1 M H_2SO_4 + 3 mM NaCl : scanning rate, 50 mV/s (*from Birss et al* [155]).

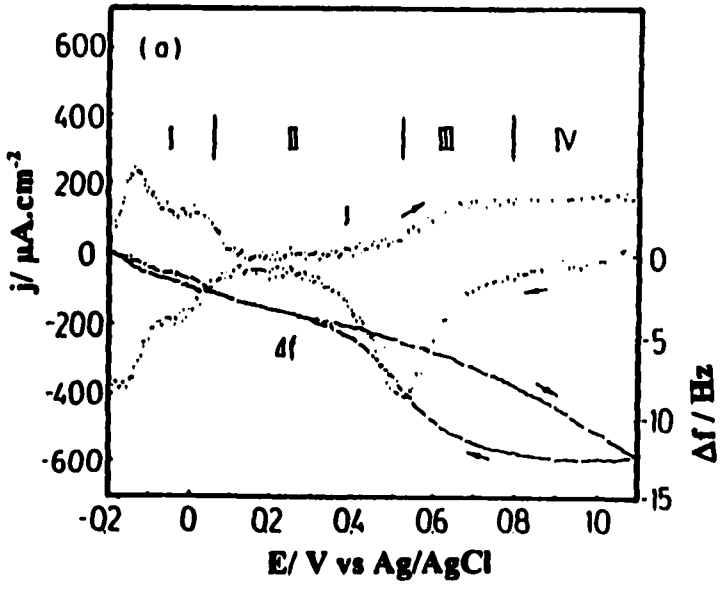

Figure 4-2:

(a) Cyclic voltammogram of a platinumEQCM electrode in 0.1 M $HClO_4$ along with simultaneously recorded frequency change. Sweep rate is 50 mV/s. (b) Frequency change vs charge plot (*from Shimazu and Kita* [153]).

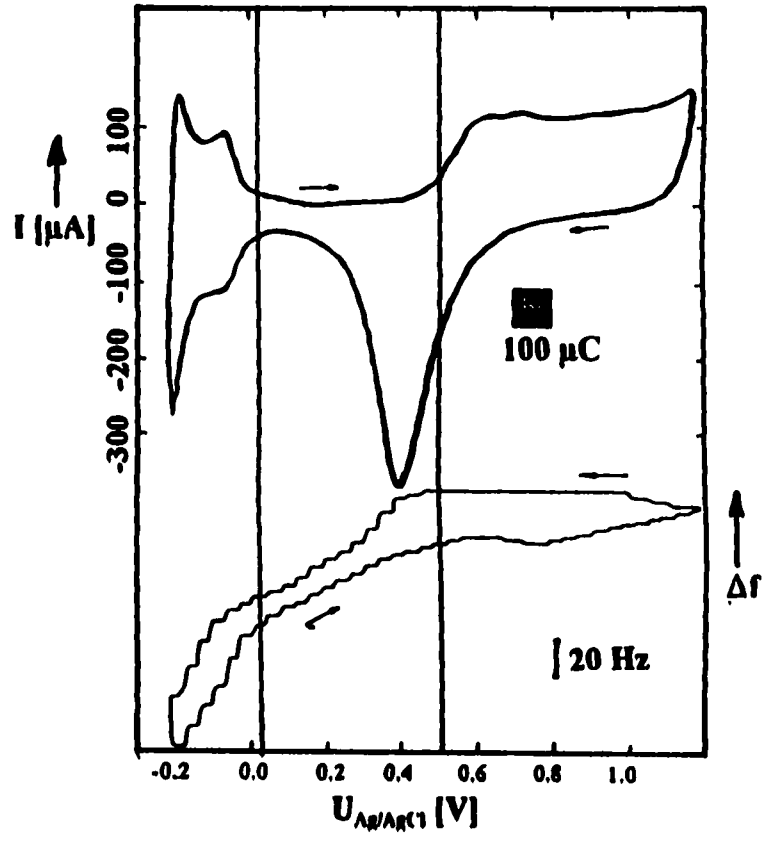

Figure 4-3:

Potentiodynamic recordings of current and frequency on a polycrystalline Pt electrode in contact with a sulfuric acid electrolyte solution (*from Stöckel and Schumacher* [151]).

increases again as the coverage of adsorbed H approaches a maximum. This type of response appears to be associated with electro-deposited electrodes (i.e. the electrodes that are used in this work) having large roughness factors [82,89]. These responses are shown and discussed in detail later in this chapter.

❷ In the double layer region the mass responses either increase continually as the potential is taken to more positive values, or are fairly flat.

❸ In the oxide formation region the mass response shows a steady increase as the potential increases (and the surface is oxidised) followed by a steady decrease as the electrode surface is reduced.

Most responses on freshly prepared Pt electrodes (i.e. when the electrode has not been subjected to extensive cycling) are broadly similar, irrespective of the method of preparation of the platinum and its degree of surface roughness. Figures 4-1 to 4-2 illustrate this. The one exception is the response of Schumacher and Stöckel [50,151] which is the exact opposite of other responses (Figure 4-3). In other words Schumacher and Stöckel [50,151] observed a steady mass increase with increasing coverage of adsorbed H, the increase being much larger than that expected from development of a monolayer of H. This change was attributed to a transition between a hydrophilic surface in the region of H adsorption to a hydrophobic surface in the double layer region with the transition between the two surfaces creating interfacial slip [so that the coupling between surface and solution (see Figures 2-7 and 2-8) is altered] and hence an anomalous frequency response.

The different studies of Pt electrodes have also been subjected to varying degrees of analysis and particular attention has been paid to different aspects in each paper - some focus on ion adsorption, while others focus on oxide formation. This last aspect will not be considered here.

If we consider the region of H adsorption first, Wilde and Zhang [82,89] observed the response noted above for electrodeposited electrodes with the mass passing through a minimum at partial coverage of H followed by a small increase of mass as the H coverage approached a monolayer. This latter increase was reported to be enhanced by ageing (cycling) of the electrode but was not observed in NaOH solutions [82,89].

Birss, Segal and Chang [155] found the typical response for vapour deposited electrodes in sulphuric acid solutions (Figure 4-1) with a steady *decrease* in mass of 5 g mol^{-1} of electrons as the H coverage increased. On the most simplistic basis, the development of a monolayer of H would be expected to give a mass *gain* of 1g mol^{-1} of electrons and so it was suggested that water desorption and bisulphate (HSO_4^-) desorption may be occurring in parallel with H adsorption.

Shimazu and Kita [153] have carried out what is probably the most detailed analysis of mass responses at Pt electrodes which were deposited (presumably by vapour deposition, although this was not specified) onto a thin Si layer on the quartz. The electrode was plasma cleaned after rinsing in ethanol but no information was provided on the surface roughness of the electrode. The authors recorded data on a computer and subtracted double layer charging

current (assumed to be constant across the whole potential range) from the charge and plotted frequency versus charge. In 0.1 M $HClO_4$, the frequency /charge plot was divided into 4 regions with the mass change in each region expressed as mass change per mol of surface Pt atoms (Figure 4-2). Regions I-II-III were taken to be H adsorption, double layer charging and initial oxide formation region respectively, with the charge in region III corresponding to the one electron surface oxidation of the electrode to give PtOH. The observed mass change in regions I, II and III was 17.4 $g.mol^{-1}$ and this was assumed to be due to Pt-H converting to PtOH (with an expected mass change of 16 $g.mol^{-1}$). These authors attributed changes in the mass response to adsorption of water because their data were found to be largely unaffected by the nature of the anion, although they did note some differences in sulphuric acid and NaOH solutions. Raudonis, Plausinaitis and Daujotis [156] also noted the differences between published reports of EQCM responses at Pt electrodes and suggested that they result from the different methods of pre-treatment and cycling of Pt electrodes. They were able to treat an electrode by extensive cycling (thousands of cycles) (Figure 4-4). In doing so they found that the response of a cycled electrode changed gradually. The initial response emulated that of a vapour deposited electrode and then after a number of cycles (2000) resembled that of an electrodeposited electrode. After 10000 cycles the response resembled that obtained by Stöckel and Schumacher [50,151] (compare Figure 4-3 and curve 3 in Figure 4-4).

The work presented here was designed to elucidate further the factors affecting the response of a platinised platinum electrode on the EQCM and to analyse the effects of

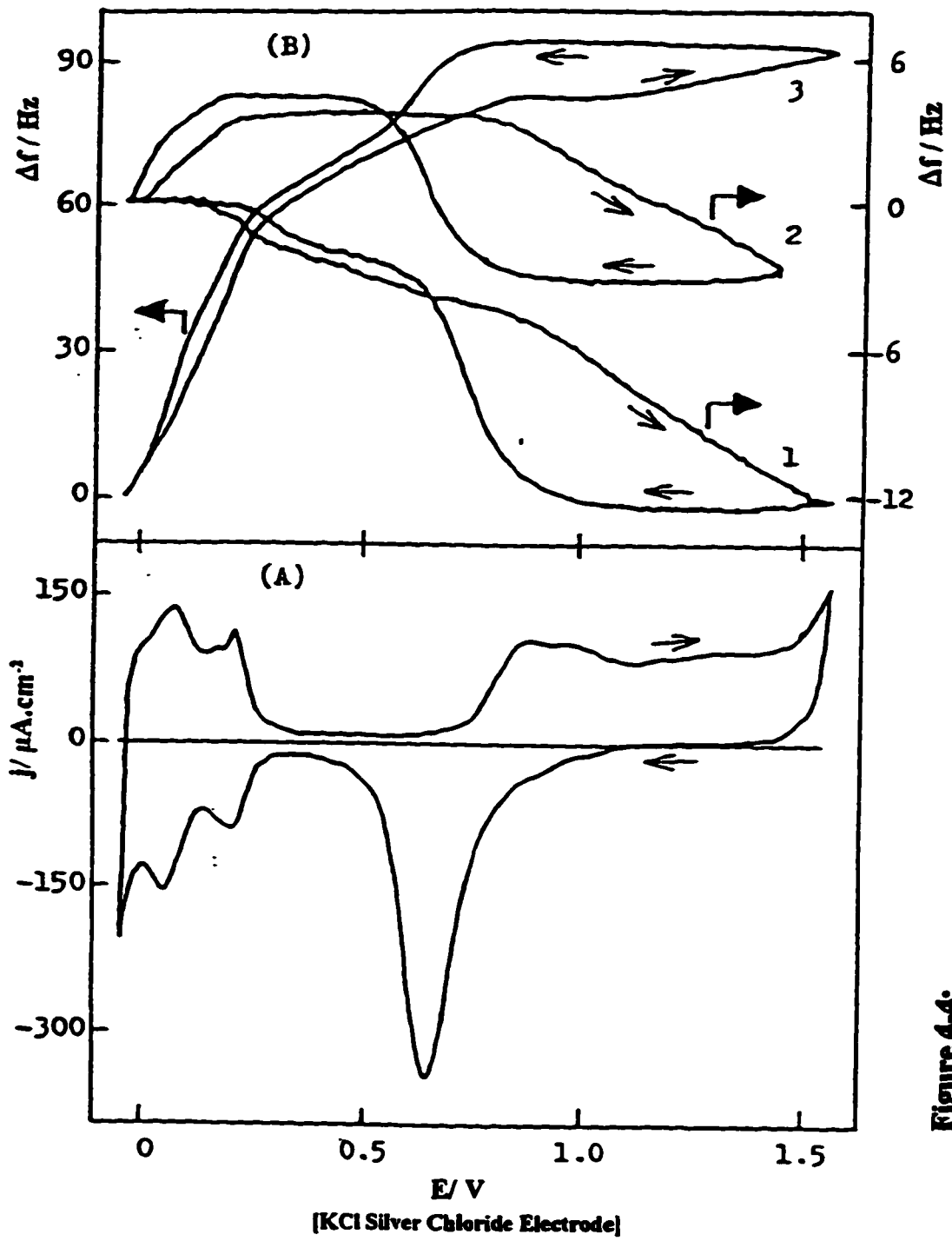

Figure 4-4:

Stabilized cyclic voltammogram (A) and the influence of the number of oxidation-reduction cycles on frequency responses (B) for a quartz supported platinum electrode recorded at 100 mV/s, 0.2 M H_2SO_4. (B) Curve 1: 100 cycles, curve 2: 2000 cycles, curve 3: 10000 cycles (*from Raudonis et al* [1156]).

electrode roughness, pretreatment and anion. In addition, in contrast to previous studies an assessment of the behaviour of the crystals was also performed by impedance analysis.

4.3. CYCLIC VOLTAMMETRY AND MASS RESPONSES FOR ELECTRODEPOSITED Pt ELECTRODES: EFFECT OF ANION CONCENTRATION AND NATURE

Platinum electrodes were prepared as described in the experimental section in Chapter 3, i.e. by electrodeposition from $PtCl_6^{2-}$, and typically have large roughness factors. After a brief electrochemical cleaning procedure to ensure the complete removal of any chloride that might remain from the electroplating process, the electrodes were examined in 0.2M H_2SO_4. A typical cyclic voltammogram for a freshly plated electrode is shown in Figure 4-5. This response is taken to be the reference EQCM response for the work presented in this chapter, in view of the fact that the voltammogram of a Pt electrode in sulphuric acid solution represents the literature standard on cleanliness. Note that in this and all other Figures generated in this laboratory, mass increases *up* the page, which is the opposite of the conventions used in Figures 4-1 to 4-4 (where a frequency scale is used rather than a mass scale).

The voltammetry of the Pt electrode has been described before in terms of the three regions of underpotentially deposited H, a double layer region and the oxide formation region. The mass response may be discussed in terms of the same three regions and the features seen

in the mass response are typical of those for an electrodeposited Pt electrode, as prepared in this laboratory (Figure 4-5). We will begin the discussion by treating the double layer potential region as the initial region of reference and considering the mass changes as the potential is either increased or decreased from this point. If the potential is decreased from a value of 0.2V in the double layer region (an arbitrarily chosen value that is referred to the S.C.E.) there is a decrease in mass which becomes steeper (at point A) as the first region of strongly bound hydrogen is encountered, the mass also reaches a minimum (point B) which coincides with the first H upd peak and then increases again until a second minimum (point C) is reached that coincides with the current peak due to weakly bound H upd. Thereafter, as the potential is made more negative, the mass increases still further until the negative scan limit is reached. On the positive going scan the same features are seen but displaced slightly, and when the potential returns to 0.2V there is a negligible difference in the mass responses, as should be expected for a reversible process.

If we now consider the changes that occur as the potential is *increased* from 0.2V, there is a steady increase in mass as the potential becomes more positive over the double layer region of potential and then the increase in mass changes slope at point D as irreversible surface oxidation (characterised by the place exchange process where OH is self-inserted into the Pt lattice [39]) begins. This increase continues until scan reversal. There is little change as the potential direction reverses until the oxide reduction peak occurs and then there is a decrease in mass which results in the mass returning to its original value at 0.2V. There is no

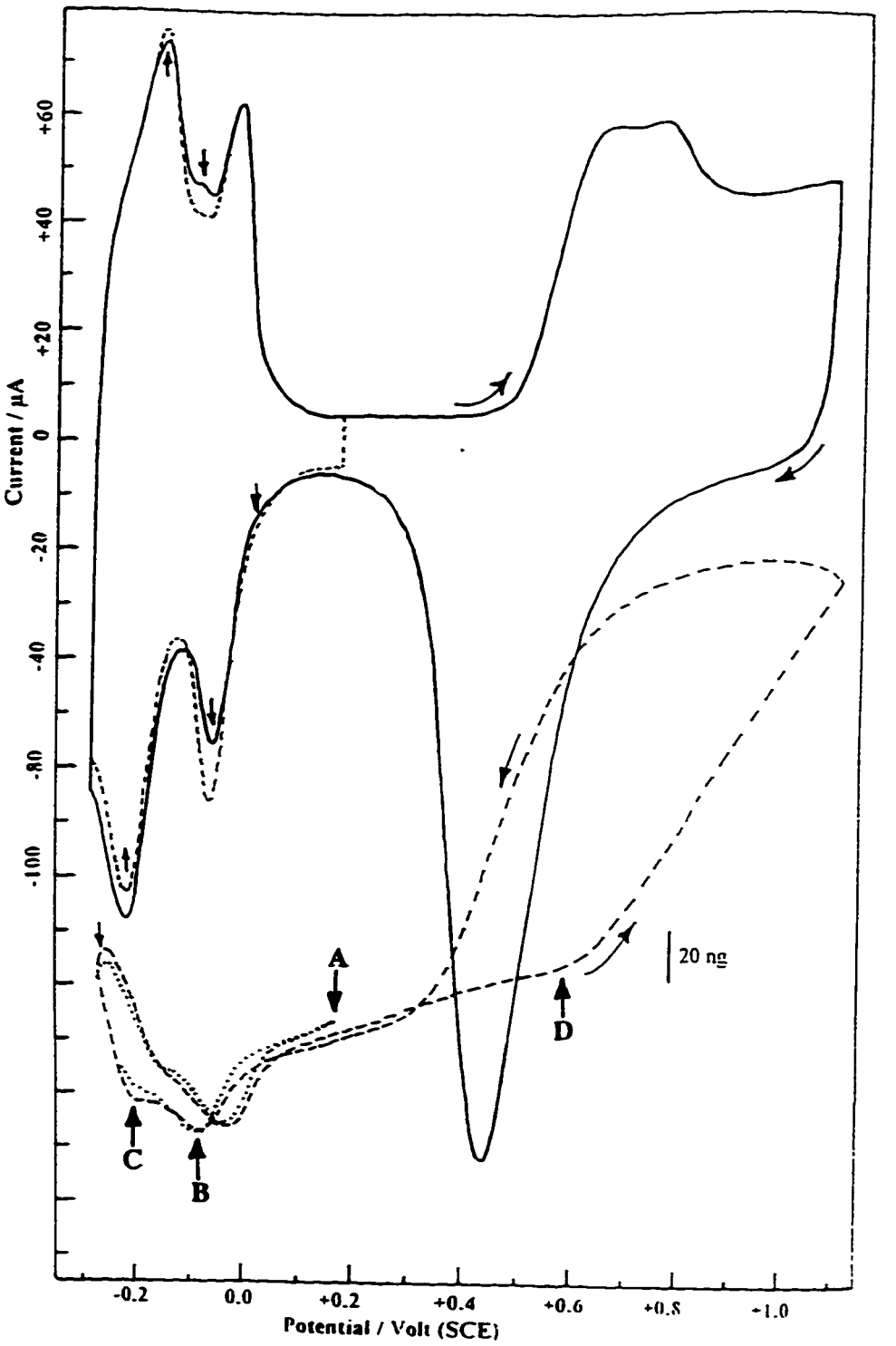

Figure 4-5:

Cyclic voltammogram (full lines) and mass responses (dashed lines) for a fresh Pt in 0.2 M H_2SO_4 electrolyte solution. One cycle was performed in the hydrogen adsorption/ desorption potential region. Scan rate: 20 mV/s; pH: 1.10; Electrode area: 6.3 cm^2

discrepancy between the mass at the beginning and end of the cycle, and this suggests that there is no significant dissolution of the Pt electrode upon one cycle.

The main focus of the work in this thesis has been an examination of the factors that affect the mass response that is presented in Figure 4-5. Factors such as the identity and concentration of the anion, the pH and the state of preparation of the Pt electrode have been studied.

The effect of the *concentration* of the anion is revealed in Figure 4-6, when the concentration of H_2SO_4 was decreased to 0.01M. Under these circumstances the voltammetric peaks are less sharp for underpotentially deposited H and the same is true of the mass features which are still present, although less well defined, than they are at the higher concentration of sulphuric acid. The double layer and oxide formation regions are similar also. Thus a simple inspection of the two Figures reveals little effect of the anion concentration on the mass response. Similar conclusions were reached when the same experiment was performed in 1.0 M H_2SO_4 (data not shown).

If the *identity* of the anion is changed from sulphate to perchlorate then both the voltammetry and the mass response undergo changes. This can be seen in Figure 4-7. If we discuss the voltammetry first and compare Figures 4-5 and 4-7, we see that the H upd peaks are less well-defined in perchloric acid than they are in sulphuric acid, in addition, in the double layer region of potential the current is not constant as it was in sulphuric acid but

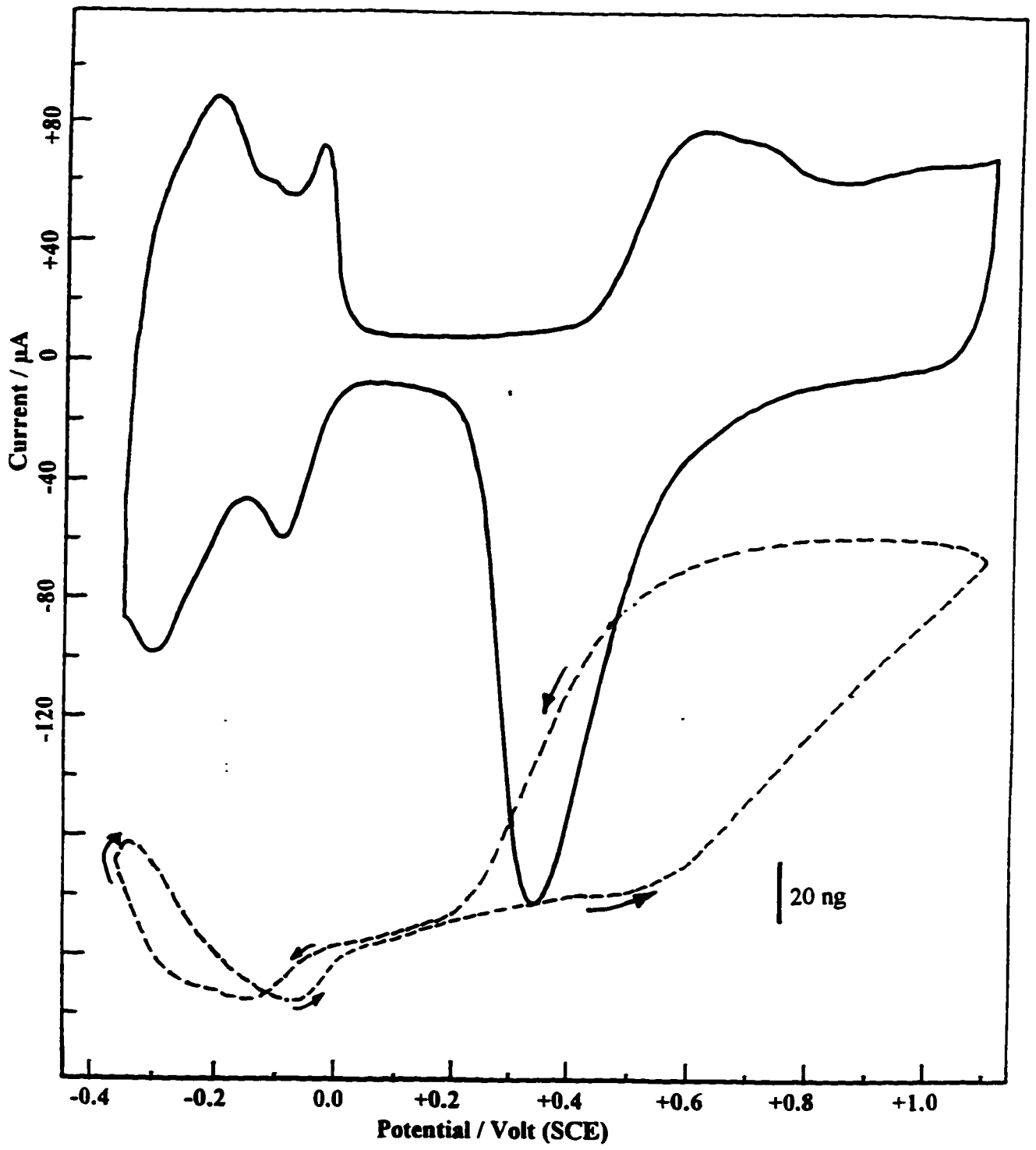

Figure 4-6:

Cyclic voltammogram (full lines) and mass responses (dashed lines) for a fresh Pt in 0.01M H_2SO_4 electrolyte solution. Scan rate: 20 mV/s; Electrode area: 4.1 cm^2

increases across the whole double layer region. These changes may be ascribed to the differences in the extent of specific adsorption of the anion. Sulphate is generally accepted to adsorb more strongly than perchlorate and so it may be the case that sulphate inhibits the formation of a layer of OH adsorbed onto the Pt prior to the surface oxidation whereas perchlorate does not inhibit this process.

Turning now to the mass response we can see that the effect of perchlorate leads to two principal differences. If we treat the result in the same way as before and consider the effect of decreasing the potential from 0.2V, we do still see a decrease in mass as we proceed to more negative potentials and H upd coverage starts but there seems to be just one minimum in this region rather than the two seen previously in sulphuric acid. The other principal difference is the fact that mass in the double layer region is flat in perchloric acid whereas in sulphuric acid a slow increase is seen. This supports the suggestion that the initial stages of oxidation occur through the loss of a proton from adsorbed surface water to site ahead because the loss of a proton is unlikely to lead to a detectable mass change. The use of perchloric acid and the consequent flat double layer region of potential also show the onset of irreversible surface oxidation more clearly than in sulphuric acid, as the increase in mass is much more dramatic.

As with sulphuric acid, if the *concentration* of perchloric acid is decreased, then we find no significant effects on the overall form of the mass response as Figure 4-8 reveals for a concentration of 0.01M $HClO_4$. The electrode used in this study was different from that in

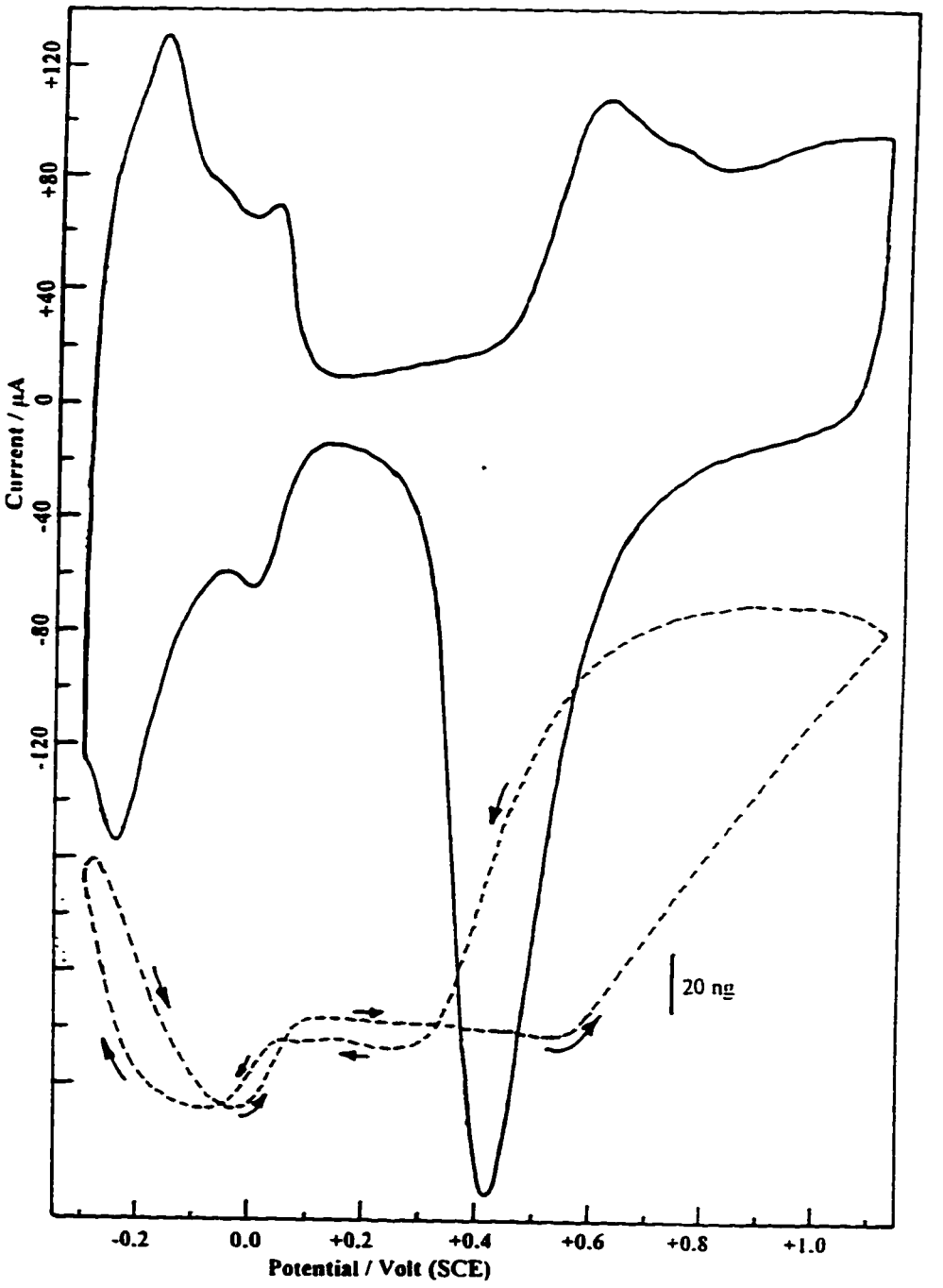

Figure 4-7:

Cyclic voltammogram (full lines) and mass responses (dashed lines) for a fresh Pt in 0.1M $HClO_4$ electrolyte solution. Scan rate: 20 mV/s; pH: 1.10; Electrode area: 5.7 cm^2

Figure 4-7 so the comparison is not exact but the lower concentration of perchloric acid gives rise to sharper H upd peaks and a flatter mass region in the H upd region of potential but as for the higher concentration of perchloric acid the slight changes in slope that occur at positions that coincide with the H upd peaks are less clear.

Finally in this series of results we discuss the response observed in a solution of KOH. The voltammogram and mass response are shown in Figure 4-9. The voltammogram shows the same general features of H upd peaks and oxide formation and reduction. The overall form of the mass response is not especially different from the acidic electrolytes. The main difference is that in the H upd region of potential, there is no minimum in the mass as there is for both $HClO_4$ and H_2SO_4. Instead the mass minimum is at the extreme negative limit of the scan and shows what is apparently a two stage increase as the potential proceeds to the double layer region. As with the weakly adsorbing perchlorate electrolyte, the mass is largely flat through the double layer region and then begins to increase again only when the oxide is formed on the electrode surface.

Thus to summarise this series of results for a freshly plated Pt electrode it can be seen that the mass response may be divided into three regions:

① The oxide region is largely unchanged in form for the three electrolytes.

② The double layer region is affected by the anion, being flat for KOH and $HClO_4$ and sloping (increasing with increasing potential) for H_2SO_4 which has the most strongly

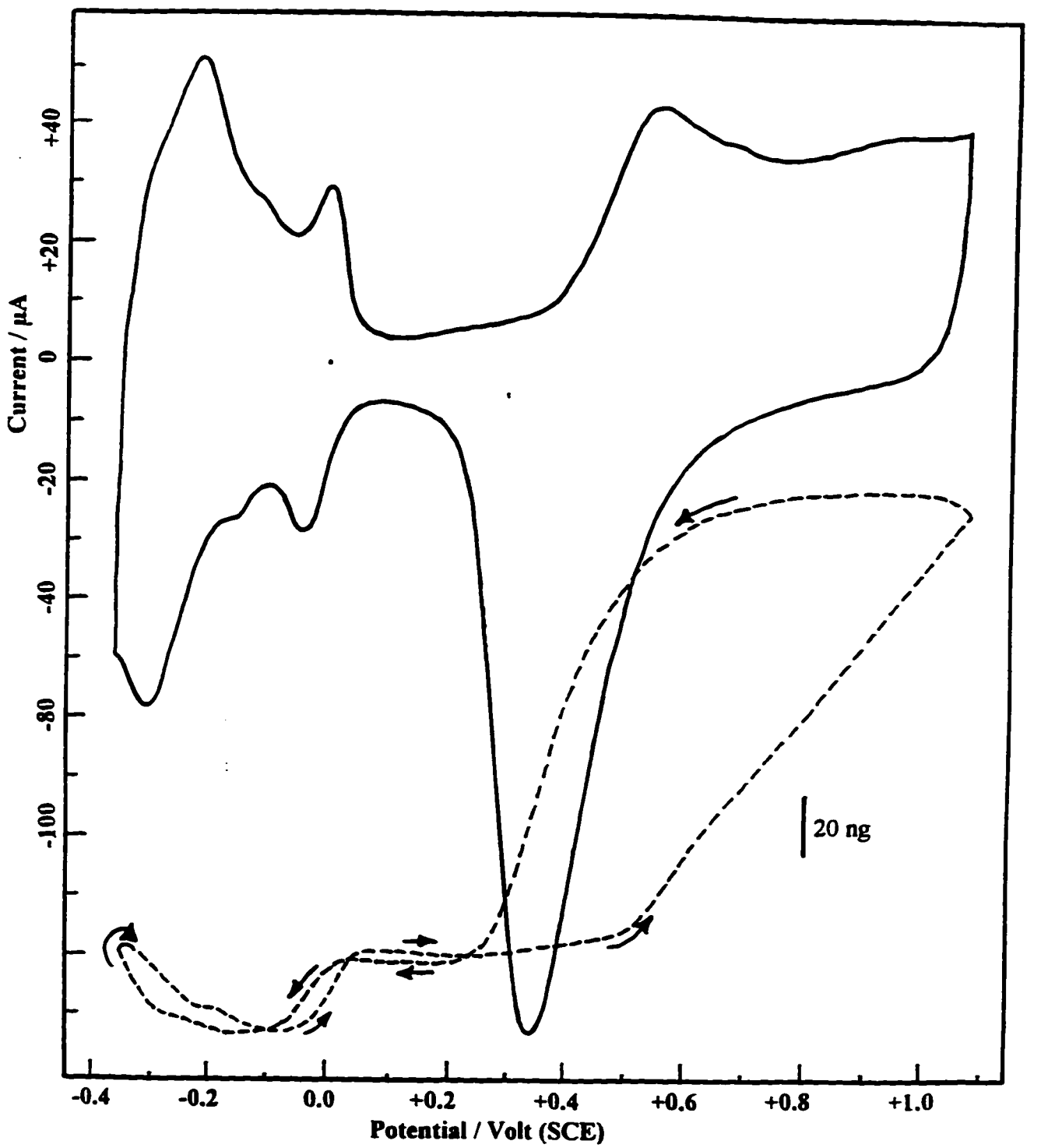

Figure 4-8:

Cyclic voltammogram (full lines) and mass responses (dashed lines) for a fresh Pt in 0.01M $HClO_4$ electrolyte solution. Scan rate: 10 mV/s; Electrode area: 4.8 cm^2

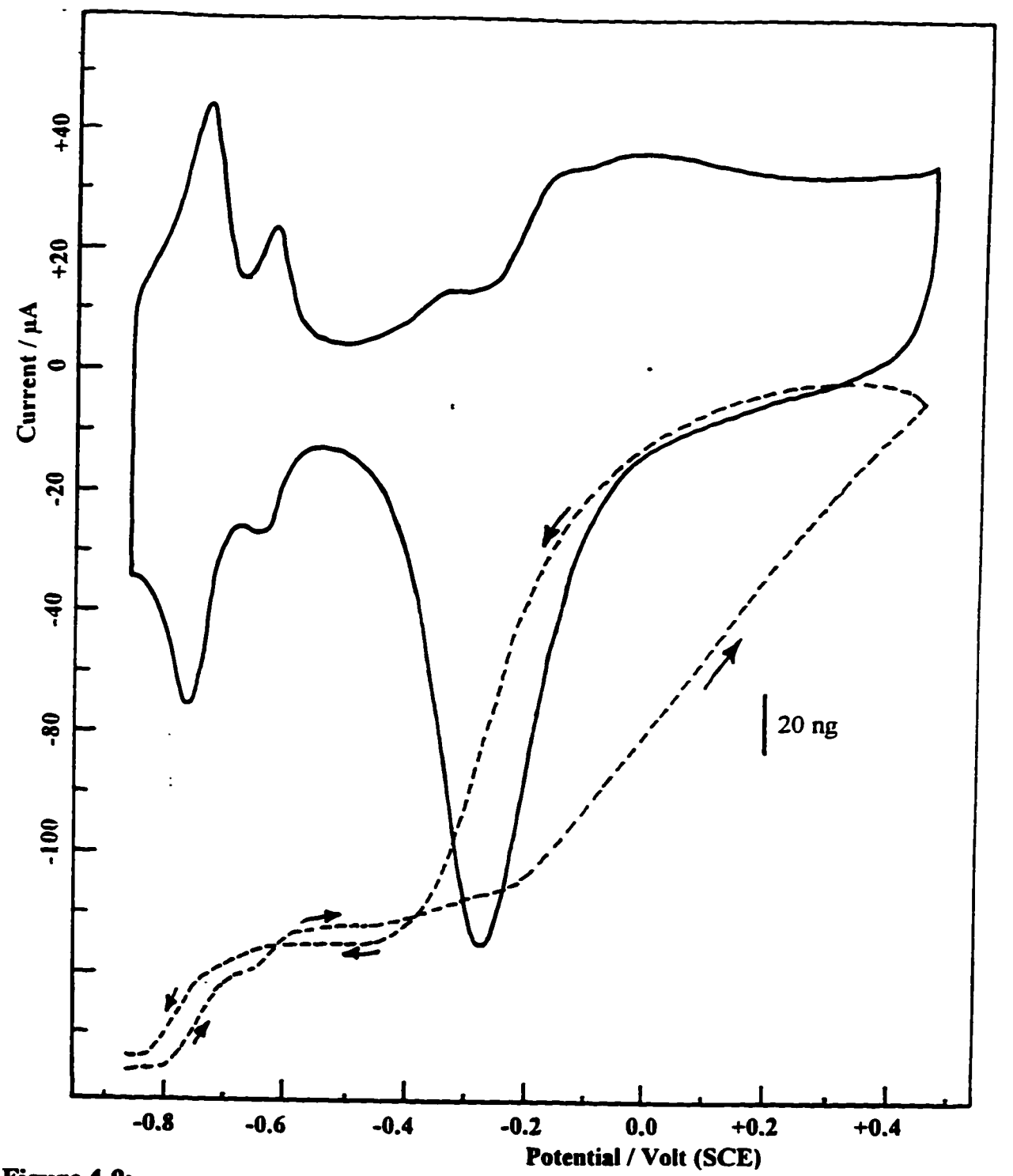

Figure 4-9:

Cyclic voltammogram (full lines) and mass responses (dashed lines) for a fresh Pt in 0.1M KOH electrolyte solution. Scan rate: 10 mV/s; Electrode area: 4.1 cm^2.

adsorbing anion of the three.

③ The structure of the mass response in the H upd region appears to reflect the H upd peaks in sulphuric acid having minima which correspond to the upd peaks. In perchloric acid where the current peaks are less well-defined then the mass peaks are less well defined too. In KOH the mass minimum is at the extreme negative limit of the scan.

There does not appear to be any *significant* effect of anion concentration on the mass responses, although it is well-known that the H upd peak distribution is influenced by the anion concentration [40].

4.4. THE INFLUENCE OF EXTENDED CYCLING ON THE MASS RESPONSE OF ELECTRODEPOSITED Pt ELECTRODES

During the course of this thesis it was noted that in certain experiments, unusual mass (frequency) changes were seen and that these unusual mass (frequency) changes typically arose after the Pt electrode had been subjected to extensive cycling in different electrolytes (including experiments which were carried out in thiourea solutions (chapter 5) and halide solutions (chapter 6). In general, the more the electrode was used, the more the mass response was seen to change. This observation agrees, at least in part, with that of Raudonis *et al* [156] which was published during the course of this work. In order to investigate this effect more fully, the effect of cycling in 0.2M H_2SO_4 was investigated.

The first results that will be discussed will be the voltammetric data. Prolonged cycling of these electrodeposited electrodes does not change the *form* of the cyclic voltammogram. However, the electrode area (and hence the roughness factor) does decrease with prolonged cycling. This is most likely to be a result of small amounts of dissolution of the electrode upon oxidative-reductive cycles and it may be more pronounced for these electrodes (compared to bulk Pt electrodes) because they are electrodeposited and are likely to be more open and porous in structure. However, it should be noted that there is (as can be seen from all the Figures 4-5 to 4-9), no significant mass loss observed on any one voltammetric cycle, because the mass response returns to its initial position after a cycle. A typical plot of electrode area and roughness factor as a function of cycling is shown in Figure 4-10 for two electrodes. The principal difference between the two electrodes in question is that the starting roughness factor was much higher in one case (Figure 4-10 upper curve, ▲) as a result of a longer time of plating. Despite the large differences in starting area a steady decline in area with cycling is seen for both electrodes, although the roughness factor at the end of both experiments is significantly different. (The roughness factor was assessed according to the method described in Chapter 1).

Figure 4-11 shows a cyclic voltammogram and mass response for a Pt electrode in its initial state after preparation and cleaning. The mass response (note the different scale for the x axis) is similar to that seen in Figure 4-5. Figure 4-12 shows the effect of cycling for 3380 cycles at 10 mV/s in 0.2M H_2SO_4. There are no differences in the shape of the voltammogram

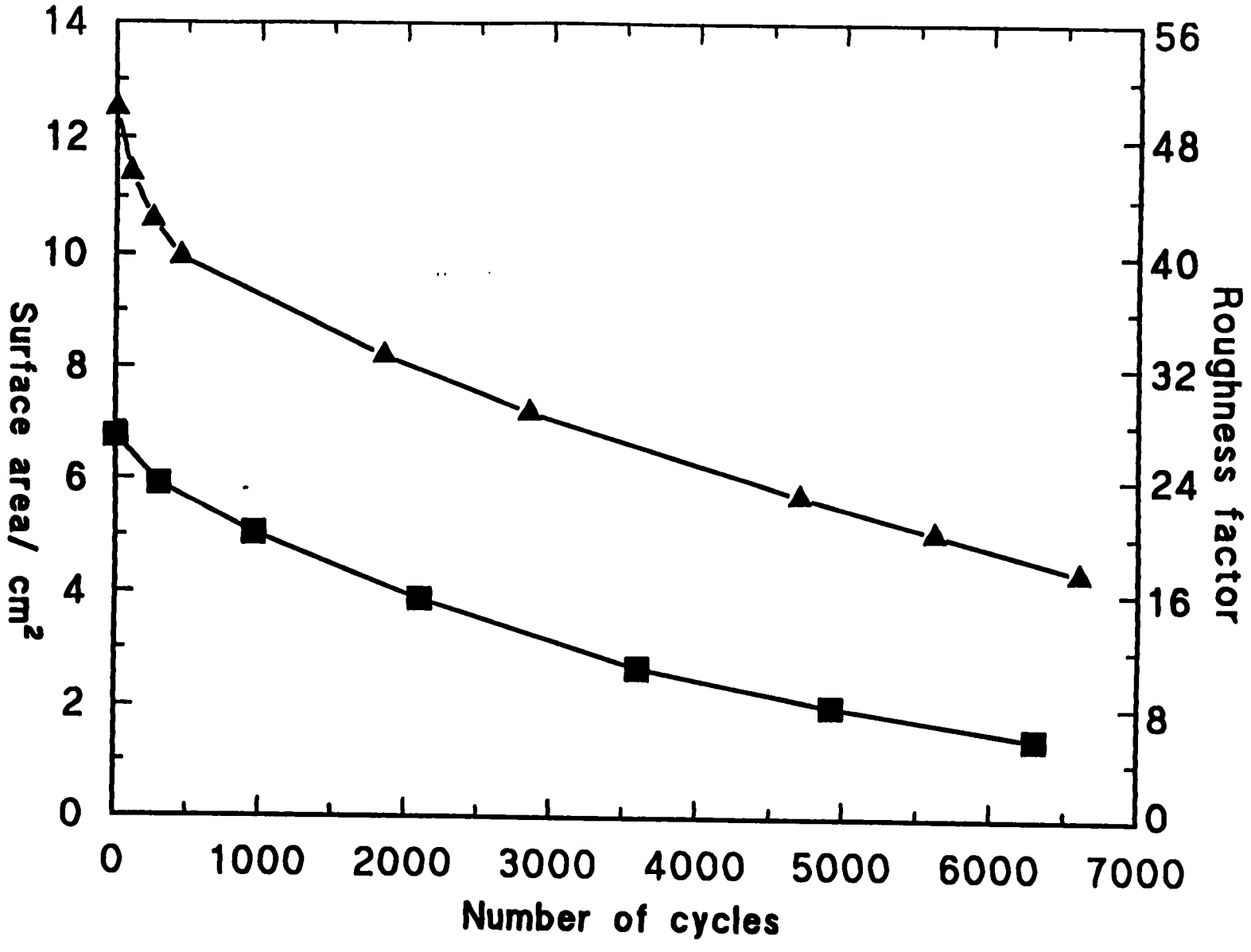

Figure 4-10:

Ageing effect investigated by cycling in 0.2 M H_2SO_4 two Pt with different starting roughness. ▲: Pt with a high roughness; ■: Pt with a low roughness.

and no dramatic differences in the mass response, but the mass increase seen at the lower limit of the scan has clearly increased. After further extensive cycling, to a total of 4930 cycles, the response of Figure 4-13 is obtained. Now the mass increase in the H adsorption region is much more dramatic and has increased to the point where it is in fact much larger than the increase seen in the oxide formation region. The second change is in the double layer region of potential where the mass response actually shows a mass *decrease* instead of showing a slow increase with potential as it did for a fresh electrode (Figure 4-11). The oxidation region remains largely unaffected by cycling, at least in terms of its overall shape. There is no apparent difference in the voltammogram, except for the decrease in area that was illustrated earlier in Figure 4-10. For this electrode, the area was found to decrease from 10.4 cm to 5 cm after the 4930 cycles. (Note that during the cycling the voltammograms that were recorded at different times were recorded in a fresh electrolyte and not in the solution used for cycling).

These results (Figures 4-11 to 4-13) show the dramatic effect of cycling on the mass response (at least that recorded in 0.2M H_2SO_4). The most important initial conclusion that can be made is that it is not sensible to regard the large change seen over the H upd region as a mass change. Any phenomena that are expected to be observed here (for example anion desorption or the development of a monolayer of adsorbed H) would not be expected to give such a large mass change, and certainly not one which is larger than the change seen for development of a monolayer of oxide on the electrode. It can also be stated that the response seen here does not completely agree with that of Raudonis *et al* [157] (Figure 4-4). In their case,

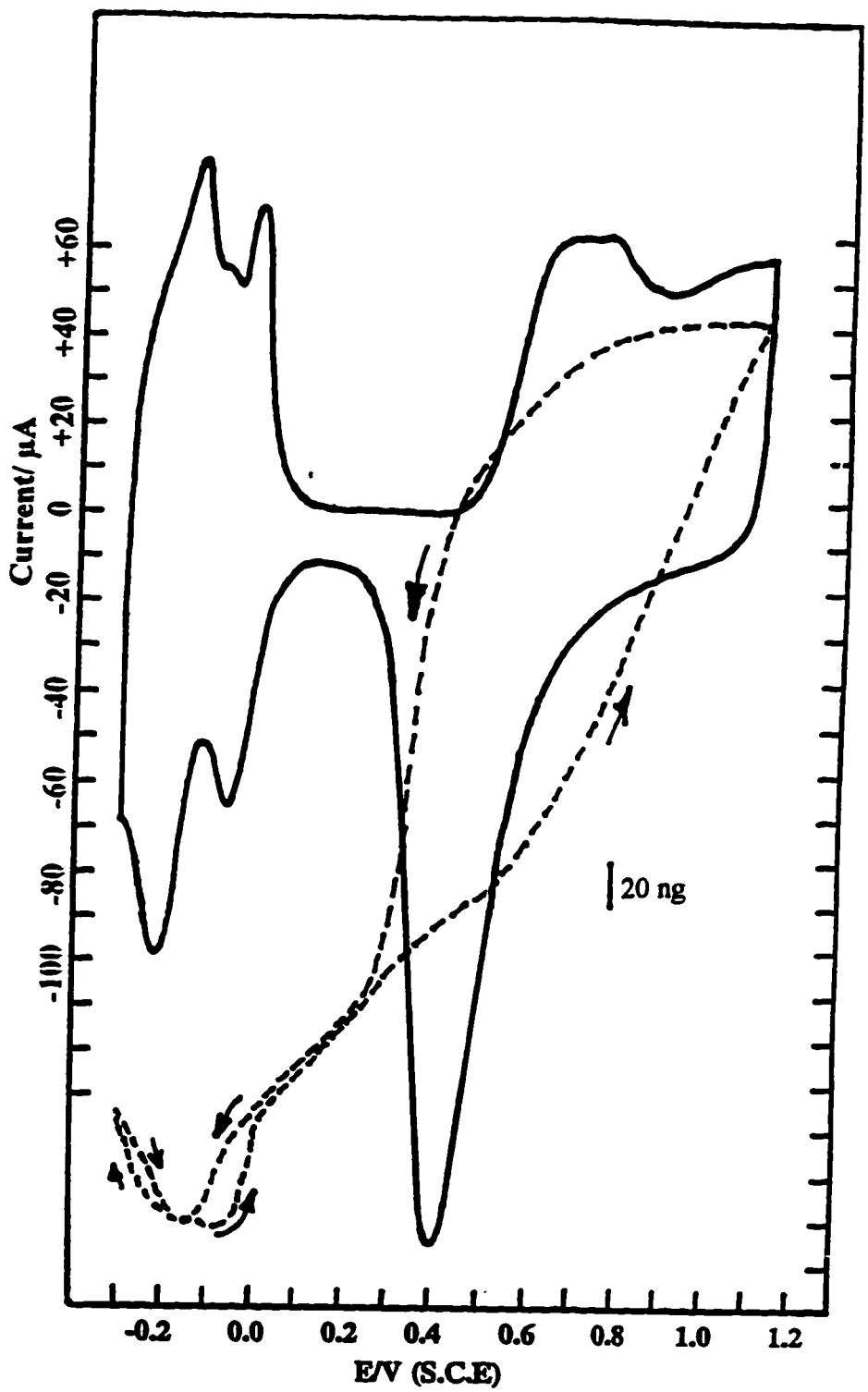

Figure 4-11:

Cyclic voltammogram (full lines) and mass responses (dashed lines) for a fresh Pt (the same as for figures 4-12 and 13) slightly aged (50 cycles) by cycling in 0.2 M H_2SO_4 at 10 mV/s. Electrode area: 10.2 cm^2. Recorded at 20 mV/s.

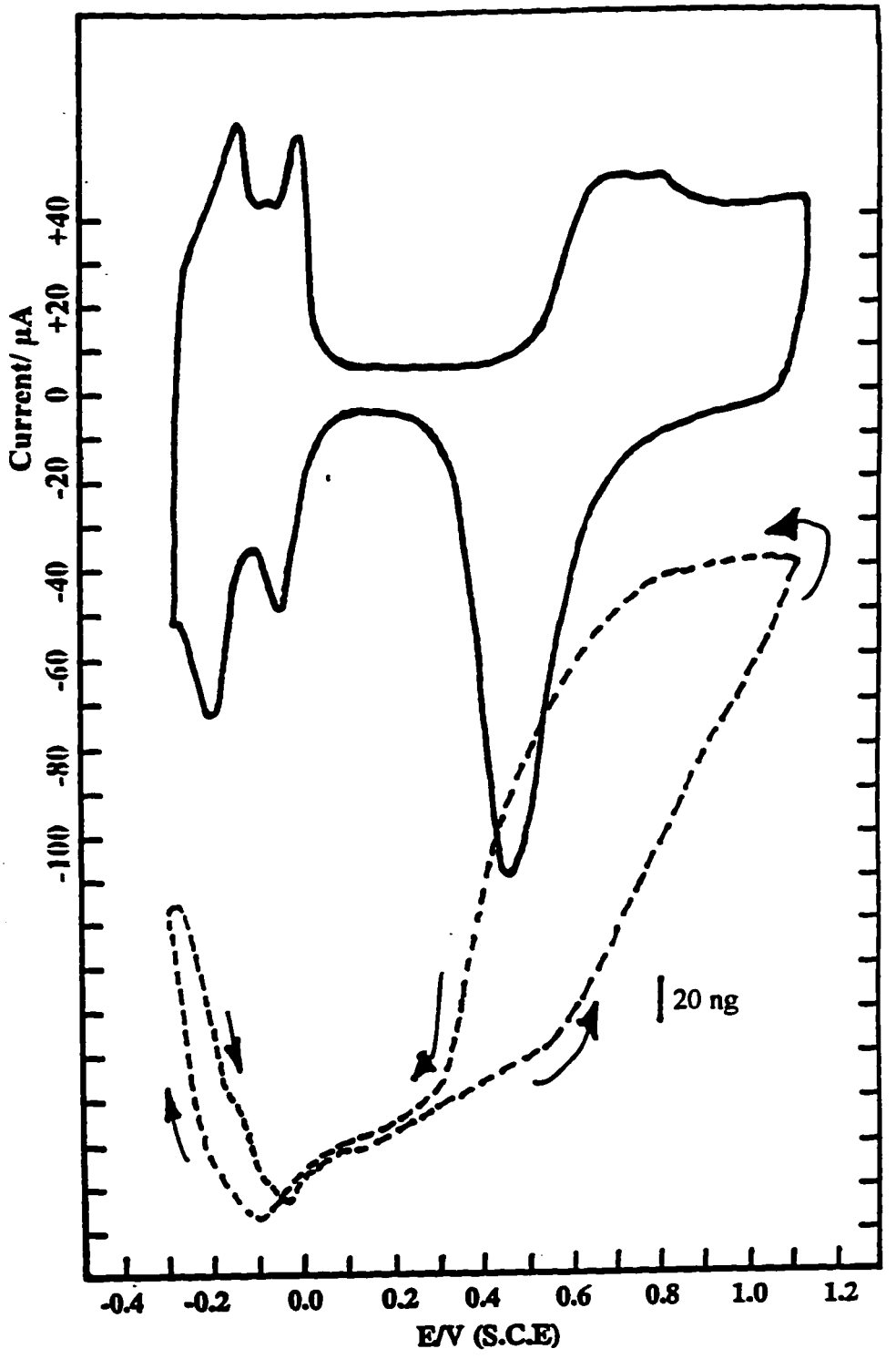

Figure 4-12:

Cyclic voltammogram (full lines) and mass responses (dashed lines) for a Pt moderately aged (3380 cycles) by cycling in 0.2 M H_2SO_4 at 10 mV/s (the same Pt as for figures 4-11 and 13). Electrode area: 7.5 cm^2. Recorded at 10 mV/s.

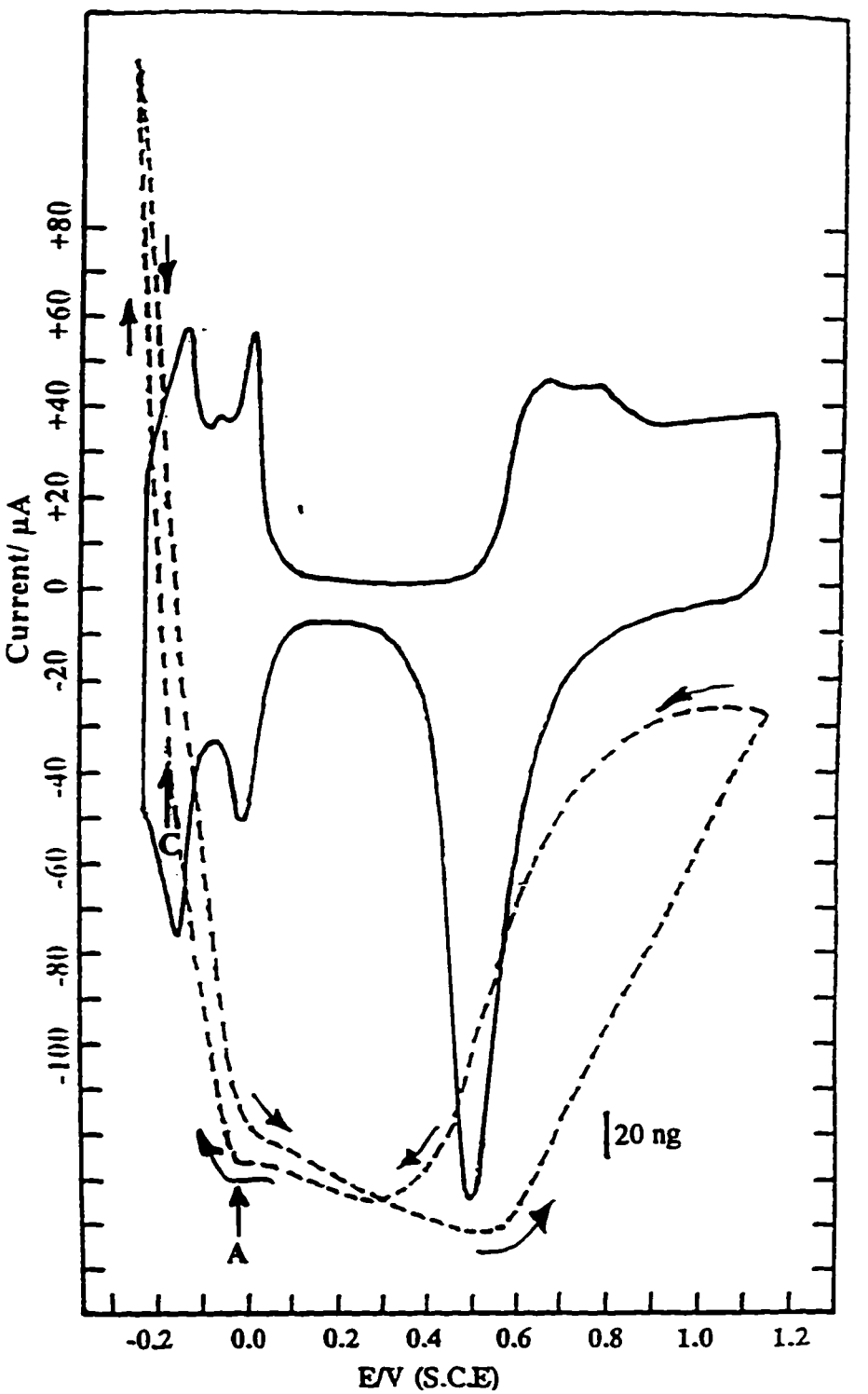

Figure 4-13:

Cyclic voltammogram (full lines) and mass responses (dashed lines) for a completely aged Pt (4930 cycles) by cycling in 0.2 M H_2SO_4 at 10 mV/s (the same Pt as for Figures 4-12 and 14). Electrode area: 5.05 cm^2. Recorded at 10 mV/s.

extended cycling did lead to a large increase in mass over the H adsorption/desorption region but in the oxide formation region the mass response was reversed from a gain to a decrease. This last feature was not observed here. However, the number of cycles used here was half the 10,000 cycles which they found necessary to produce a reversal of mass. Unfortunately it is unclear from their paper whether or not the electrode area changed in their experiment. The following conflicting statements appear in their manuscript: *"The most striking result..... is that the voltammetric features of the Pt electrode remain constant with repetitive potential cycling whereas the frequency properties can change enormously."* and. *"It should be emphasised that the cyclic voltammograms of the quartz supported Pt electrode, which have been recorded simultaneously in our experiments,....., do* (emphasis added) *change with time."*

Thus it is not clear if they refer to a change in area or roughness factor with cycling. The other principal difference between the experiment in their paper and that presented here is that the starting roughness factor of their electrode was reported to be 6-7 which is much less than any of the electrodes that have been used in this study.

Having observed this unusual effect of cycling the question now arises as to the nature of this effect - what causes it and what factors influence it ? Although it is difficult to see from the Figures presented above, examination of a similar response of an aged electrode plotted on a less sensitive scale for the voltage axis illustrates that the two stage response of the mass in the H adsorption region (from B to C and then from C to the lower limit of the voltage scan

as shown in Figure 4-5) is still present for the aged electrode, it is the sizes of the stages that are magnified after prolonged cycling. The magnification of the mass response is especially unusual because of the fact that while the mass response is magnified, the electrode area is actually *decreased* by a significant factor so that the real increase in mass response when expressed per unit electrode area is even more dramatic than it appears from a simple comparison of the sizes of the mass responses at the beginning and end of the cycling experiment.

The next stage of the investigation was to examine the effect of anion on the response of what we shall refer to as an "aged" Pt electrode. The presence of a large mass (frequency) in the region of H adsorption or desorption in 0.2M H_2SO_4 will be taken as an indication that an electrode is fully aged.

4.5. CYCLIC VOLTAMMETRY AND MASS RESPONSES FOR AN "AGED" ELECTRODE - EFFECT OF ION IDENTITY AND pH

The first and most important point about the ageing effect is that the cyclic voltammogram (for a given electrolyte) shows no changes in features after ageing . As mentioned above, the only significant changes are that the actual electrode area decreases with cycling and so the currents passed are smaller and the calculated roughness factor is also smaller. The data of Figure 4-10 also revealed another important effect and that is that the

ageing effect is apparently not a function of the final roughness factor. In the experiments shown in Figure 4-10, both electrodes showed signs of ageing, but at the end of the ageing process, their electrode areas were substantially different. The final area of one electrode was 4.75 cm^2 whereas the starting area of the other electrode was 6.9 cm^2 and fell to 1.5 cm^2. Thus the ageing effect does not appear to be dependent on absolute roughness.

The next series of results show the mass responses observed in different electrolytes after ageing. Since there is always some variability between electrodes (especially because they are electroplated) and since, as revealed earlier in this chapter, there is little apparent effect of the anion concentration on the mass response of a fresh electrode, the anion concentration was not varied in this set of results.

The effect of ageing in sulphuric acid solutions has already been presented in Figures 4-11 to 4-13 but an interesting insight into the process can be revealed from a comparison of fresh and aged electrodes in alkaline solutions. The response of a freshly plated electrode in 0.1M KOH was shown in Figure 4-9. Figure 4-14 shows the response of an aged electrode in 0.1M KOH. Note that the electrode is not the same electrode that was used in Figure 4-9. Figure 4-14 shows that there are some changes in the mass response in alkaline solutions after ageing (i.e. by cycling in sulphuric acid solution) but they are insignificant when compared to the changes seen in sulphuric acid solution after ageing. The principal difference between the two figures is that there is a slight increase in mass in the H adsorption region in the

alkaline solution after ageing, otherwise the results are quite similar. The lack of any dramatic difference between a fresh (Figure 4-9) and an aged electrode (Figure 4-14) is an important observation and more information was obtained by simply adding sulphate to the alkaline solutions. When the mass response was recorded in a solution of 0.1M KOH with 0.1M Na_2SO_4 there was no difference between the responses in the presence and absence of sulphate irrespective of whether or not the electrode was aged or fresh (results not shown). This is an important observation because of the fact that when the pH is changed, the difference in potential between the potential of zero charge and the potential where H adsorption/desorption takes place becomes much larger because the potential of H adsorption shifts to more negative values with pH. The potential of zero charge was discussed in Chapter 1 and although there is still much debate about the exact location of the pzc at Pt electrodes, it is generally taken to be around 0.2V vs. N.H.E. or -0.04V vs. SCE [163]. There is also some debate about whether or not the pzc shifts with pH. However, it is known that added sulphate ions have no effect on the H adsorption/desorption peaks in the cyclic voltammogram in alkaline solutions (whereas they certainly do have an effect in acid solutions)[40]. The negative shift of the H adsorption peaks means that electrode carries a much more negative charge in this region than it does in acid solutions because the potential is much more negative than the pzc. Thus anion adsorption is less likely because of electrostatic effects.

This experiment shows that the ageing effect is not simply associated with adsorbed H at the electrode surface but that it is also apparently a function of the charge that the electrode

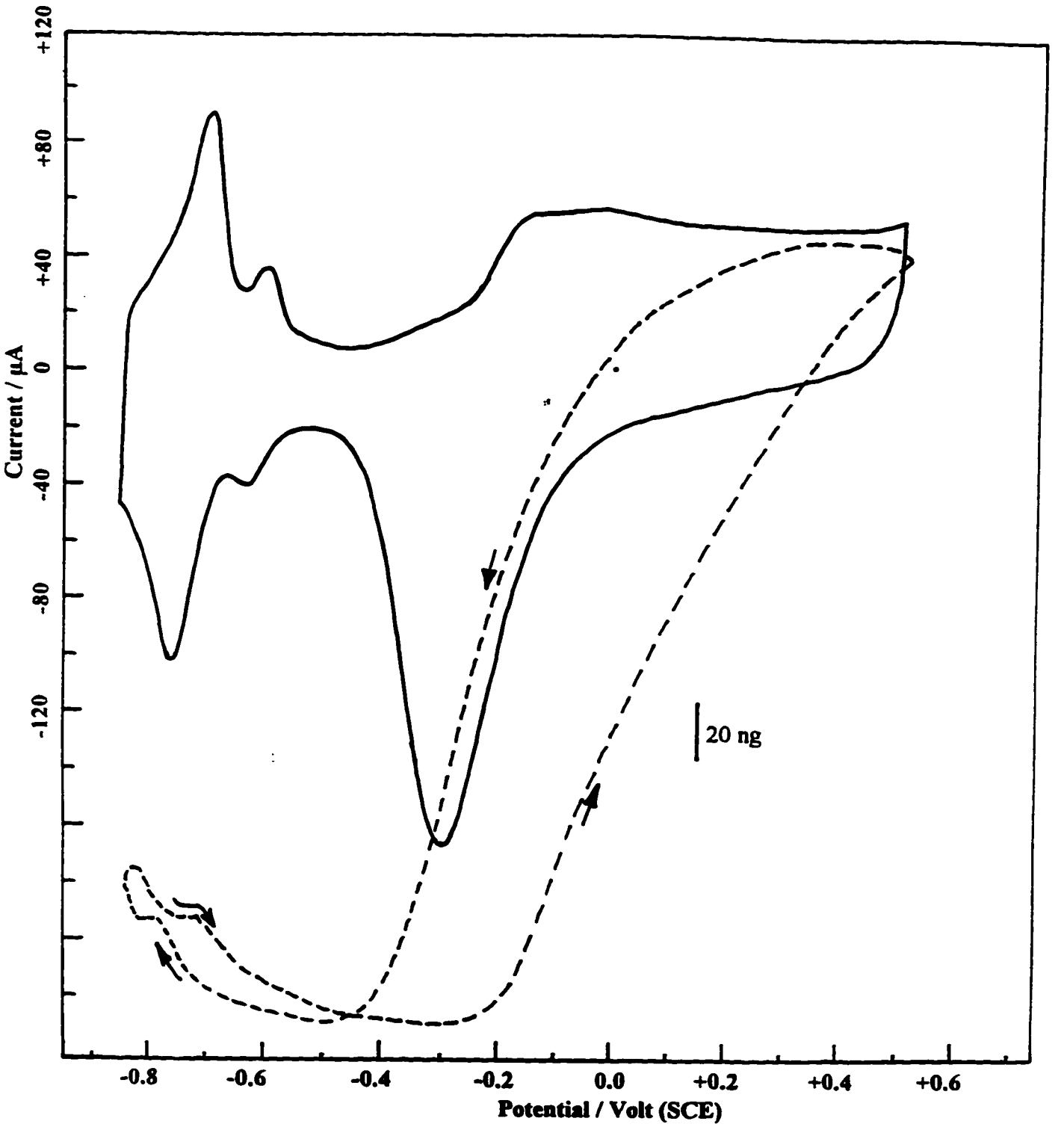

Figure 4-14:

Cyclic voltammogram (full lines) and mass responses (dashed lines) for a completely aged Pt electrode recorded in a 0.1 M KOH solution, pH 12.85. Scan rate: 20 mV/s.

carries, relative to the pzc. This aspect was probed a little further using phosphate buffer solutions adjusted to two different pH values. Figure 4-15 shows the cyclic voltammogram and mass responses for a freshly plated Pt electrode in an 0.2M phosphate buffer at pH 7.45. Taking a potential of -0.2V (in the double layer region of potential) as the reference point the mass is seen to decrease as H coverage increases, and there is no significant increase at the end of the scan. The double layer region of potential reveals an increase in mass as the potential increases above -0.2V and the oxide region seems very similar to different earlier figures in this chapter. Figure 4-16 shows the effect of ageing on the same electrode in the same electrolyte. There is now a significant increase in frequency (mass) as the potential decreases from -0.2V, although the increase is similar in size to that seen when the electrode surface is oxidised, and so it is less significant, in relative terms, than the increase seen in sulphuric acid solutions after ageing. This same electrode was then immersed in a phosphate buffer at a higher pH (9.10) and the experiment repeated. Figure 4-17 reveals that the increase of pH by just under 2 units appears to have resulted in a frequency (mass) increase that is certainly more than the same electrode in a solution of pH 7.45 *before* ageing, but is less than the same electrode in pH 7.45 *after* ageing.

The frequency (mass) increase in the region of H adsorption is less than the increase in the oxide region, whereas at pH 7.45 the increases were comparable. The experiments in phosphate buffer and KOH with and without added sulphate have indicated that the charge carried by an electrode (represented by the difference between the actual potential and the potential of zero charge) is an important influence on whether or not the ageing effect is seen.

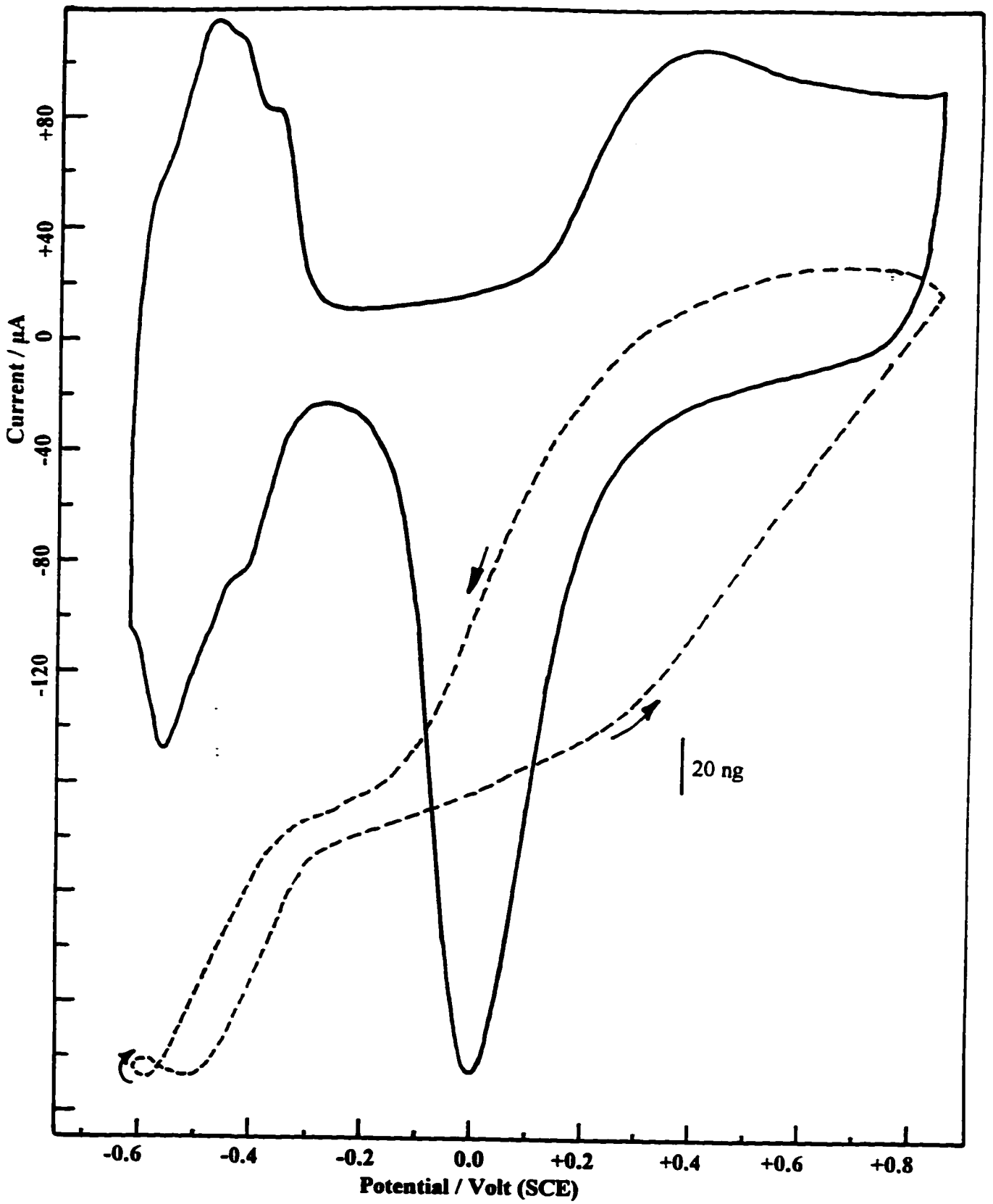

Figure 4-15:

Cyclic voltammogram (full lines) and mass responses (dashed lines) for a fresh Pt electrode recorded in a 0.2 M Na_2HPO_4 solution, pH 7.45. Scan rate: 20 mV/s.

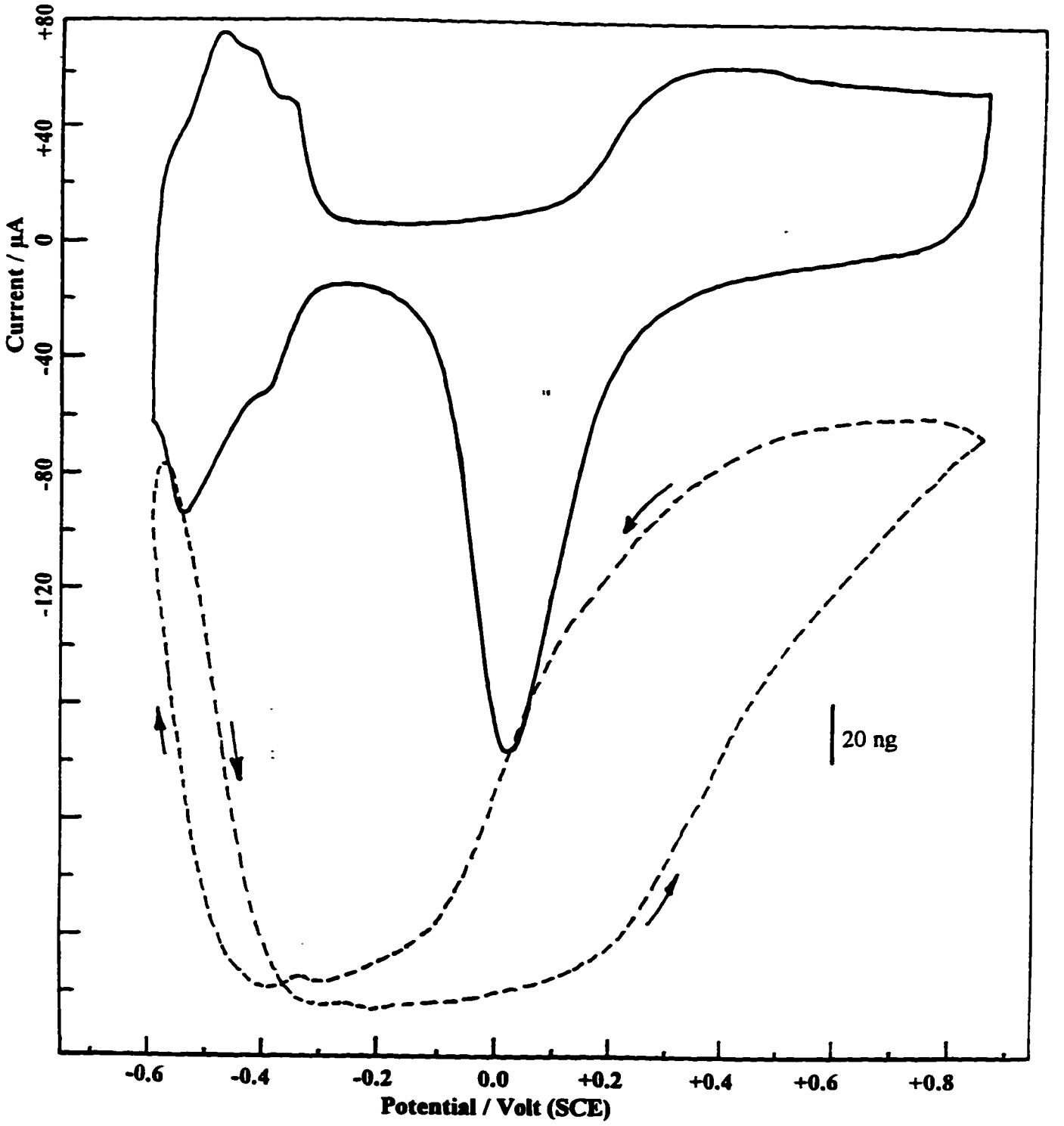

Figure 4-16:

Cyclic voltammogram (full lines) and mass responses (dashed lines) for an aged Pt electrode recorded in a 0.2 M Na_2HPO_4 solution, pH 7.45. Scan rate: 20 mV/s.

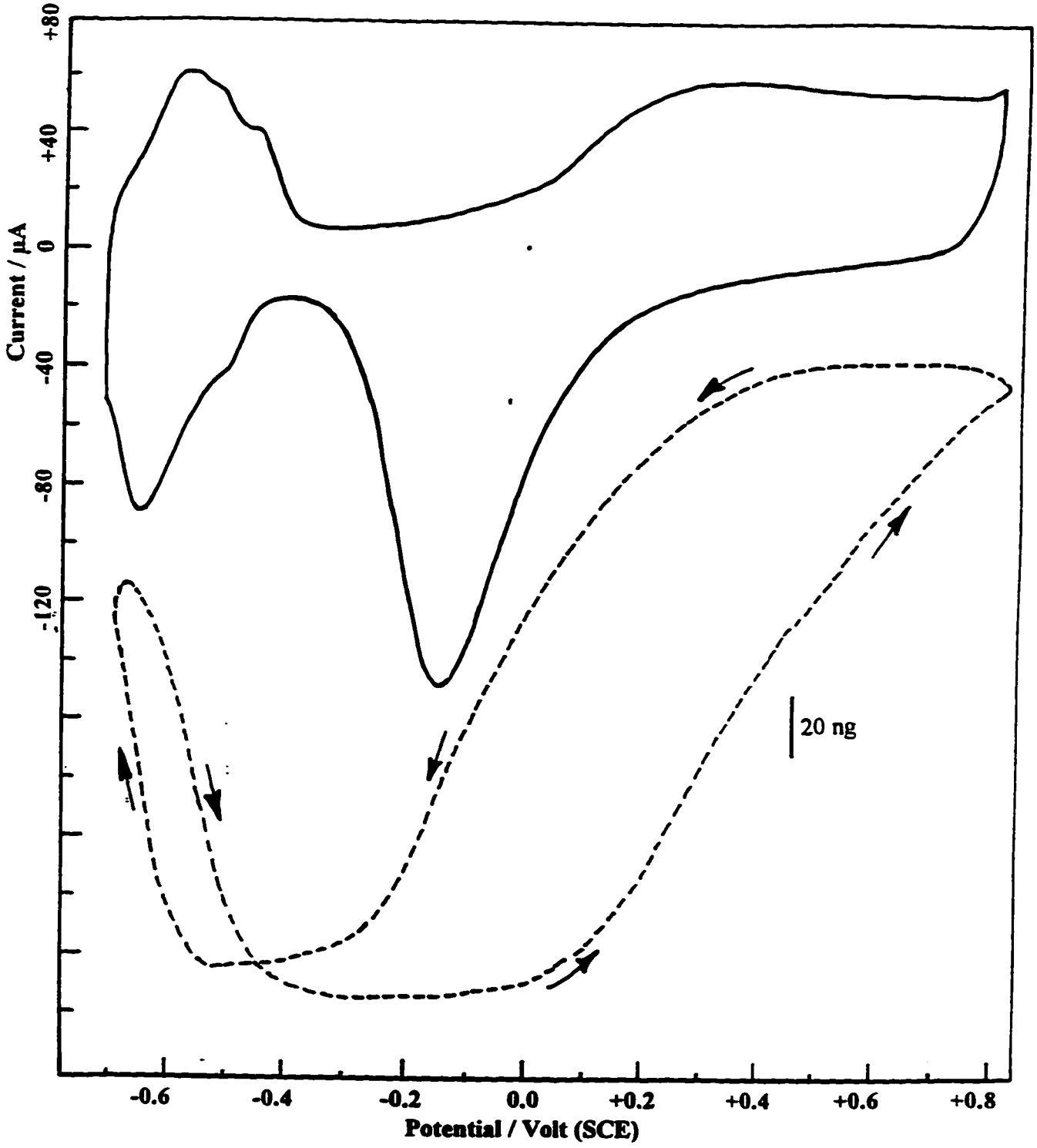

Figure 4-17:

Cyclic voltammogram (full lines) and mass responses (dashed lines) for an aged Pt electrode recorded in a 0.2 M Na_2HPO_4 solution, pH 9.10. Scan rate: 20 mV/s.

As the pH of the electrolyte increases and the potential of the electrode in the H adsorption region becomes more and more negative then the unusual increase in frequency (mass) in the H adsorption region gradually becomes smaller (as seen for example in Figure 4-13). This increase is unusual in the sense that such a mass change is much too large to be attributed to the mass change expected for a monolayer of H, in contrast to the mass change observed in the oxide region, which is of the expected size.

4.6. IMPEDANCE ANALYSIS OF ELECTRODEPOSITED Pt ELECTRODES

In an effort to shed more light onto the causes of ageing at Pt electrodes, several electrodes were subjected to an impedance analysis, as described in Chapter 2. The impedance spectrum of the quartz crystal was analysed before and after ageing and in different electrolytes, although it should be noted again that the experiments were not performed under potential control, the electrodes were at open circuit during the measurement. With regard to the discussion of impedance analysis that was presented in Chapter 2, several points are worthy of repetition. First, the results are displayed as the conductance spectrum, where G/Ω^{-1} is displayed as a function of frequency. Second, the three simplest pieces of information that are revealed by the data are the position of the frequency of maximum conductance, f_{Gmax} (which may be correlated with the resonance frequency of the crystal, in other words the quantity that the normal EQCM experiment reveals), the conductance (or resistance) at this point and the quality factor, Q, of the crystal. The quality factor of the crystal represents the

energy flow out of the crystal and can be estimated crudely by examination. A tall thin peak represents a high quality factor, where as a shorter broader peak (typically with a lower value of G) represents a low quality factor.

Several different electrodes were examined by impedance analysis and in the first set of results that are shown in Figure 4-18, the impedance spectra of a freshly plated electrode in three different electrolytes, 0.1M $HClO_4$, 0.2M H_2SO_4 and 0.1M KOH are shown. The data do not indicate any difference at all in the response of the electrode in the three different electrolytes and the three curves cannot be distinguished from each other. Thus the behaviour of the Pt electrode at open circuit is not affected by the electrolyte that is present. A similar conclusion was reached from a study of an aged Pt crystal in the same three electrolytes, the data are also shown in Figure 4-18. The next set of Figures (4-19 a to d) show the effect of ageing (i.e. repetitive cycling in sulphuric acid solutions) on the conductance spectrum for four different electrodes. As noted earlier, ageing results in a decrease in electrode area through a decreased roughness factor (Figure 4-10) and in addition, there is a mass loss as Pt is dissolved from the electrode surface with extended cycling. Analysis of the Figures 4-18 and 4.19 reveals three effects on the conductance spectrum:

① The conductance maximum shifts to a higher frequency upon ageing. $f_{G_{max}}$ increases. This is expected in view of the fact that mass is lost through Pt dissolution upon cycling. The Sauerbrey equation indicates that a loss in mass will result in a gain in frequency.

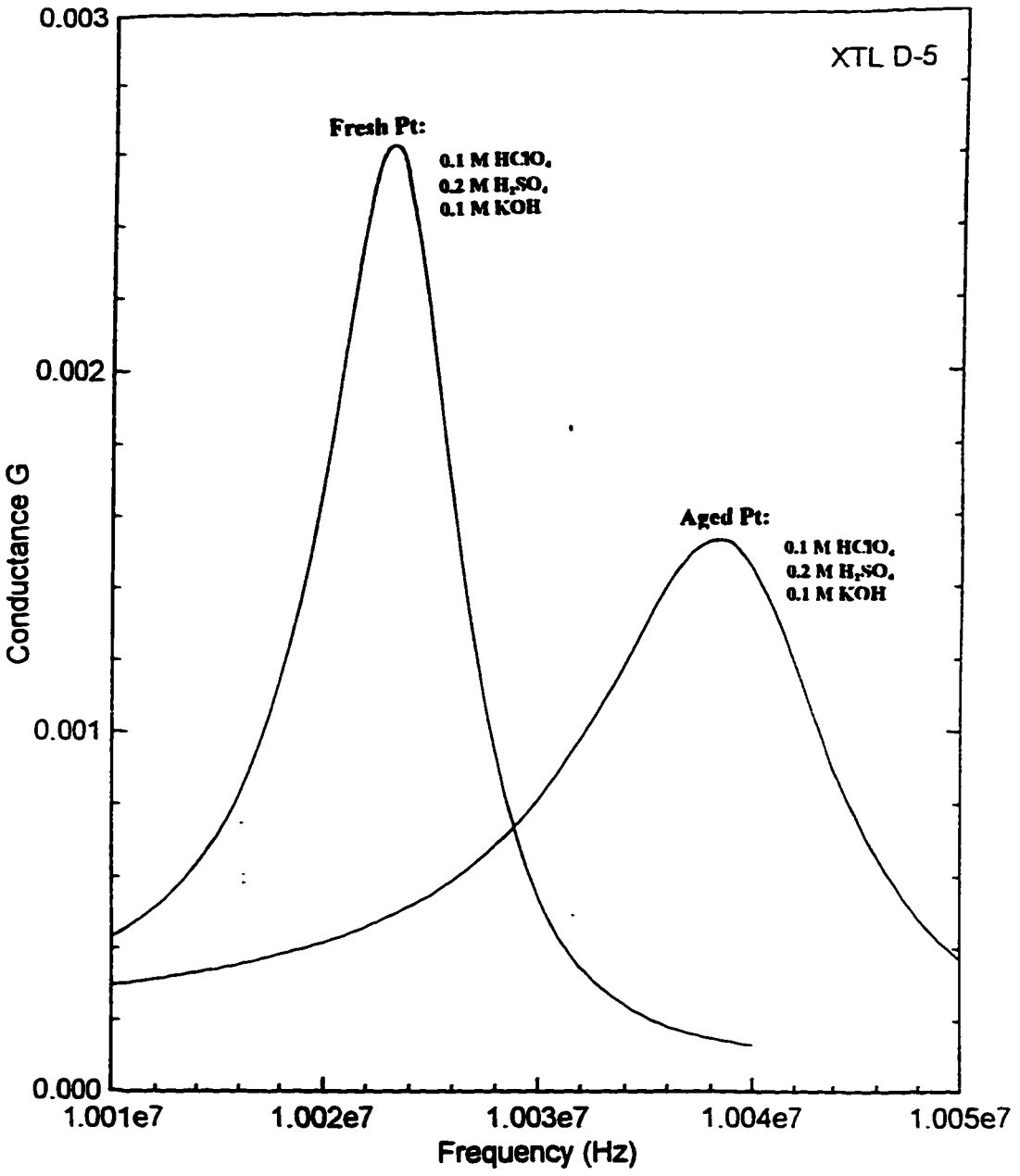

Figure 4-18:

Conductance plots for a fresh and aged Pt surrounded by three different electrolyte solutions: 0.1 M $HClO_4$, 0.2 M H_2SO_4 and 0.1 M KOH.

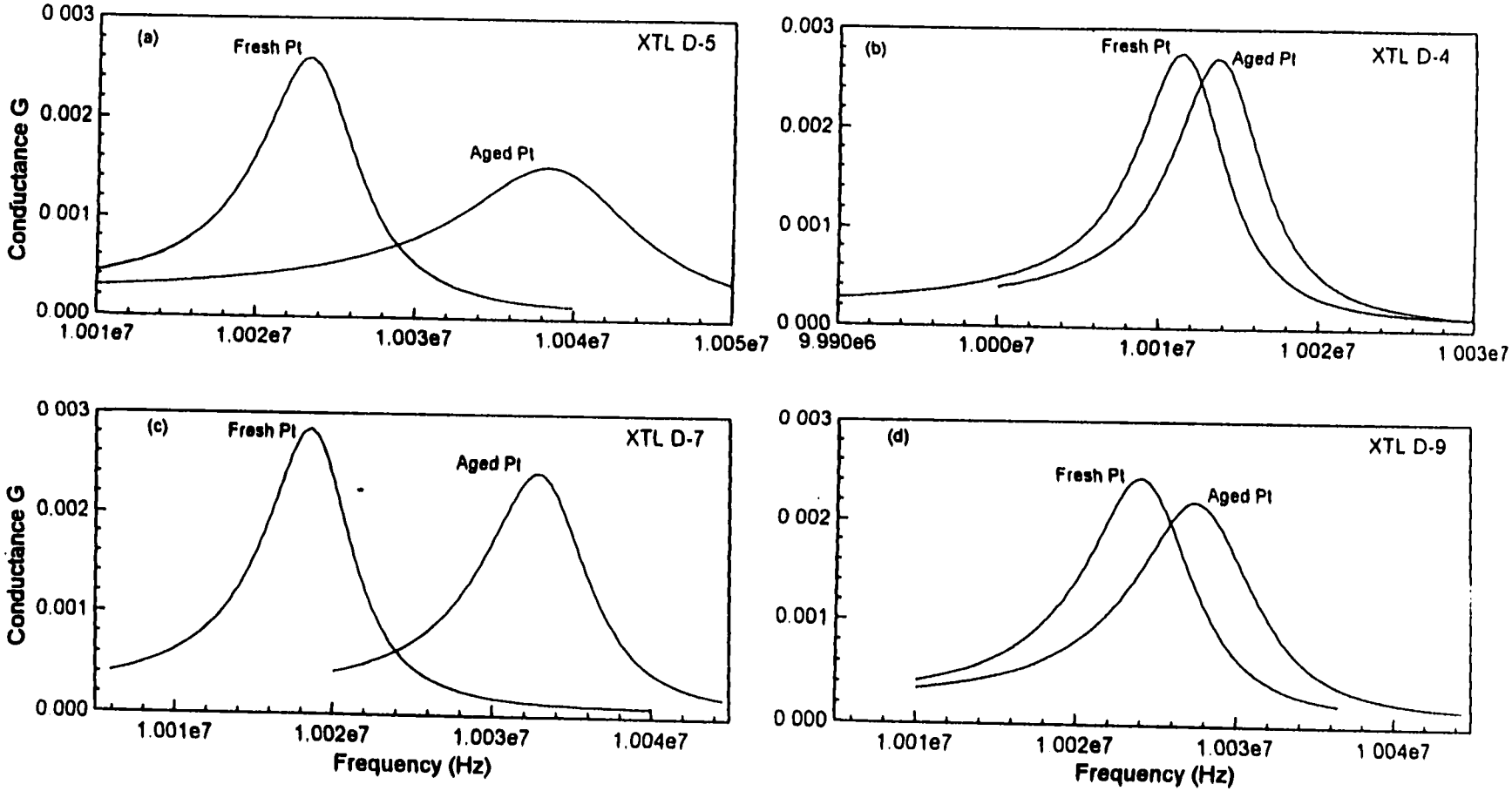

Figure 4-19:

Conductance plots for a series of Pt electrodes in their different states of ageing. Some corresponding quantitative parameters are summarized in the tables 4-1 and 4-2.

In addition of mass lost considerations, the translations of the admittance plots may arise from the contribution of the inductance element L_2. This element represents the kinetic energy of the entrained liquid layer. In effect, a quick calculation based on the concept of the Sauerbrey equation and the value for the mass sensitivity indicates that this shift cannot be due only to the loss of mass.

② In addition to the shift of the frequency of the conductance maximum, there is also a decrease in the value of the conductance at the maximum. Alternatively we may say that the resistance at the frequency of maximum conductance is seen to increase upon cycling or ageing.

③ Finally, ageing or cycling also has an effect on the quality factor, Q. The quality factor, as evaluated by equation 2.47, is seen to decrease slightly after ageing, and this is a result of the fact that the width of the peak at half maximum increases after ageing. The increase in the width of the peak at half maximum is a result of changes in surface structure caused by the ageing process.

The data from a series of experiments on four different Pt electrodes is presented in Table 4.1. The information is summarised in Table 4.2. The quality factors, Q, are calculated using equation 2.47. The resistance values are simply the inverse of the conductance value at $f_{G_{max}}$. The roughness factors (ϕ) are also included for comparison. All the data refer to experiments performed in 0.2M H_2SO_4. The fact that the ageing effect leads to an increase of $f_{G_{max}}$ is expected, as noted above, so that the main point of interest comes from the changes in

Table 4-1:

Some quantitative parameters from B-G plots for a series of Pt quartz crystals.

a) CRYSTAL D-5:

Fresh Pt in 0.2M H_2SO

B-G plots	Frequency / MHz	Real R /Ω	Imag X /Ω	Impedance: |Z| = 1/|Y| /Ω	Phase angle: θ /Deg.
f_{Gmax}	10.0234	380.70	-47.44	383.64	-7.10
f_{Bmax}	10.0189	300.23	-366.61	473.86	-50.68
f_{Bmin}	10.0268	528.66	341.11	629.16	32.83

Aged Pt in 0.2M H_2SO_4

B-G plots	Frequency / MHz	Real R /Ω	Imag X /Ω	Impedance |Z| = 1/|Y| /Ω	Phase angle θ /Deg.
f_{Gmax}	10.0384	603.09	-169.36	626.42	-15.68
f_{Bmax}	10.0308	416.46	-551.56	691.13	-52.94
f_{Bmin}	10.0444	1084.00	337.66	1135.37	17.30

b) CRYSTAL D-4

Fresh Pt in 0.2M H_2SO_4

B-G plots	Frequency / MHz	Real R /Ω	Imag X /Ω	Impedance |Z| = 1/|Y| /Ω	Phase angle θ /Deg.
f_{Gmax}	10.0114	358.09	-50.50	361.63	-8.11
f_{Bmax}	10.0076	283.47	-338.17	441.26	-50.03
f_{Bmin}	10.0145	488.84	316.85	582.54	32.95

(Contd.on next page)

Aged Pt in 0.2M H_2SO_4

B-G plots	Frequency / MHz	Real R /Ω	Imag X /Ω	Impedance |Z| = 1/|Y| /Ω	Phase angle θ /Deg.
f_{Gmax}	10.0137	359.83	-53.50	363.79	-8.46
f_{Bmax}	10.0099	288.68	-344.07	449.13	-50.00
f_{Bmin}	10.0169	502.55	330.95	601.73	33.37

c) CRYSTAL D-7:

Fresh Pt in 0.2M H_2SO_4

B-G plots	Frequency / MHz	Real R /Ω	Imag X /Ω	Impedance |Z| = 1/|Y| /Ω	Phase angle θ /Deg.
f_{Gmax}	10.0185	350.96	-26.00	351.92	-4.24
f_{Bmax}	10.0148	301.22	-334.11	-47.96	449.85
f_{Bmin}	10.0214	433.21	323.19	36.72	540.48

Aged Pt in 0.2M H_2SO_4

B-G plots	Frequency / MHz	Real R /Ω	Imag X /Ω	Impedance |Z| = 1/|Y| /Ω	Phase angle θ /Deg.
f_{Gmax}	10.0327	402.85	-58.65	407.10	-8.28
f_{Bmax}	10.0283	329.82	-392.12	512.39	-49.93
f_{Bmin}	10.0363	544.13	363.50	654.38	33.74

d) CRYSTAL D-9:

Fresh Pt in 0.2M H_2SO_4

B-G plots	Frequency / MHz	Real R /Ω	Imag X /Ω	Impedance |Z| = 1/|Y| /Ω	Phase angle θ /Deg.
f_{Gmax}	10.0239	398.12	-66.19	403.58	-9.44
f_{Bmax}	10.0196	318.42	-374.90	491.88	-49.66
f_{Bmin}	10.0275	564.89	337.99	658.28	30.89

(Contd.on next page)

Aged Pt in 0.2M H_2SO_4

B-G plots	Frequency / MHz	Real R /Ω	Imag X /Ω	Impedance |Z| = 1/|Y| /Ω	Phase angle θ /Deg.
f_{Gmax}	10.0275	443.81	-73.70	449.89	-9.43
f_{Bmax}	10.0225	332.10	-412.37	529.47	-51.15
f_{Bmin}	10.0315	669.98	372.70	766.67	29.08

Table 4-2:

Comparison between quantitative values from cycling effect (roughness factor ϕ) and parameters from impedance analysis (quality factor Q, resistance R) for a series of Pt quartz crystals (*).

XTL	Fresh Pt Electrode				Aged Pt Electrode			
	ϕ	f_{PWHH} /MHz	R /Ω	Q	ϕ	f_{PWHH} /MHz	R /Ω	Q
D-4	19.8	0.0069	358	1451	16.4	0.0070	359	1430
D-5	19.8	0.0079	380	1269	8.0	0.0136	603	738
D-7	25.2	0.0066	350	1518	16.0	0.0080	402	1254
D-9	20.6	0.0079	398	1269	15.2	0.0090	443	1114

(*) Values of f_{Gmax}, f_{Bmin}, f_{Bmax} and R are extracted from table 4-1.

the resistance at $f_{G_{max}}$ and from the changes in Q. For all crystals, although the effect is dependent on the degree of ageing and the size of the decrease in the roughness factor, the resistance at $f_{G_{max}}$ increases, and the quality factor decreases and there is an apparent correlation between the extent of the decrease in ϕ and the size of the decrease in Q. The value of R_m (i.e. R in the motional branch of the equivalent circuit of the QCM or EQCM - see Figure 2-9) is associated with the dissipation of energy due to friction within the crystal, any losses associated with the mounting system and with losses to the environment. The first two sources of energy dissipation should not change with ageing of the Pt electrode and so the change in R_m can be associated with a change in energy dissipation to the electrolyte as the electrode ages. Typical values of R_m for a quartz crystal in air are about 100 Ω so that the increase of R to over 300 Ω for all of the electrodes here represents the increased viscous damping resulting from the immersion of the crystal in the electrolyte. What is surprising is that the ageing of the crystal and a decrease in the surface roughness apparently increase the effectiveness of the coupling between the electrode surface and the electrolyte, resulting in greater energy dissipation and hence a larger value of R_m (and a smaller value of G in the conductance spectrum).

When the equation 2.48 is examined, it can be seen that the quality factor depends upon both L_m and R_m in the motional branch of the equivalent circuit. L_m represents added mass, and so ageing and the dissolution of the Pt will result in a decrease in L_m and we have seen above that an increase in R_m is observed and these two factors together lead to a decrease in the

quality factor, Q, with increased cycling. The data presented here are interesting in that they reveal the overall effect of ageing on the interaction of a Pt electrode with the contacting electrolyte, but it should be remembered that all experiments were recorded at open circuit and so the conclusions apply to the Pt surface as a whole, rather than the Pt surface covered with adsorbed Hydrogen or Oxygen.

4.7. SEM MICROGRAPHS OF Pt CRYSTALS

In the final set of experiments to be reported in this chapter, a series of Scanning Electron Micrographs were recorded to see if there was any correlation between the morphology of a crystal (at least on the scale visible in SEM) and the existence of the ageing effect. Typical pictures of gold electrodes are shown in Figure 3-1 in Chapter 3. The micrographs show the crystal as they are received from the manufacturer. Several micrographs of freshly plated Pt electrodes are presented in Figure 4-20 with the micrographs being recorded directly after a clean electrode is plated and subjected to the minimum amount of cycling required to produce a clean cyclic voltammogram. The same number of SEM pictures of aged Pt electrodes are also presented (Figure 4-21). However, it should be noted that it was not possible to obtain an SEM picture of the *same* Pt crystal before and after ageing. This is because of the fact that the crystals were sealed onto the glass cell (Chapter 3) using silicone sealant and the removal of the crystal generally results in the crystal being broken or cracked so that it cannot be re-used. While this is unfortunate, it became apparent from examination of a range of micro-

graphs of freshly plated crystals and crystals that had been aged, either by cycling in sulphuric acid solutions or after experiments in halide or thiourea solutions, that no correlation could be found between the appearance of the electrode surface in the micrograph and the existence of ageing as indicated from a voltammogram and mass response recorded in H_2SO_4. Thus it seems that the changes in surface roughness that occur in the experiments performed here do not lead to changes that are easily visible from SEM micrcographs, at least under the conditions used here.

The identification of changes in structure would be better performed on the same crystal before and after the ageing process.

4.8. DISCUSSION AND GENERAL CONCLUSIONS

The results presented in this chapter reveal several interesting aspects concerning the performance of electrodeposited Pt electrodes on the EQCM. First, if we consider freshly prepared electrodes then there are clearly changes in frequency (mass) that can be related to changes at the interface of the Pt electrode, as seen in Figure 4-5. For example, as noted by Stöckel and Schumacher [50,151], there does seem to be a transition between the double layer region and the region of adsorbed H and this is identified by a change in the mass slope (point A, Figure 4-5). There are also changes that are seen as the coverage of H upd increases and the potential moves from the region of strongly bound H to that of weakly bound H (points

XTL D-2 (fresh)

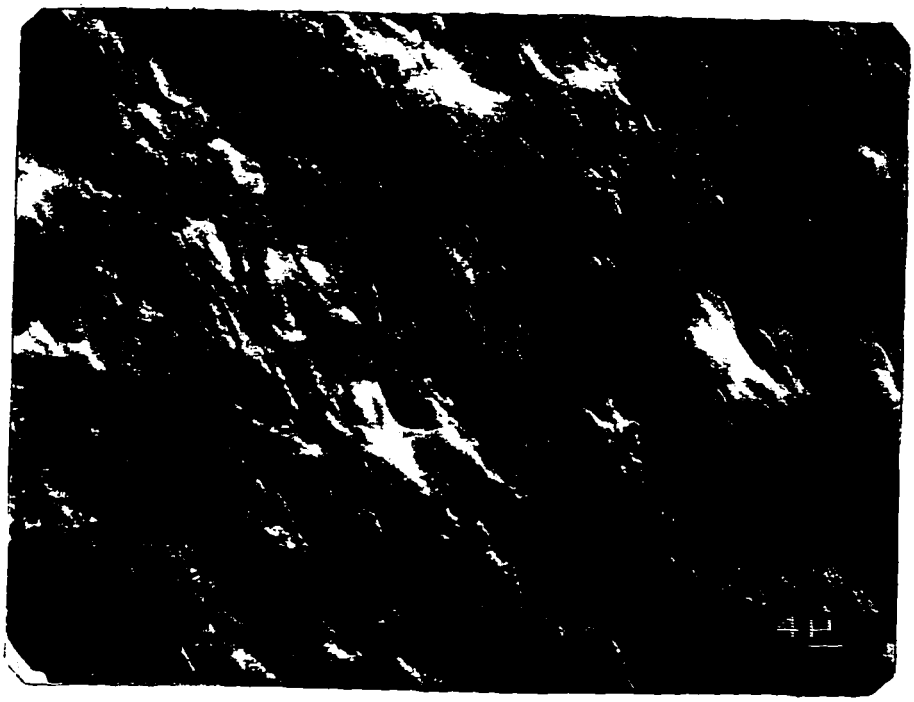

XTL Z-3 (fresh)

Figure 4-20:

SEM micrographs for two Pt-coated quartz crystals before ageing (freshly plated Pt electrodes).

XTL 2 (aged)

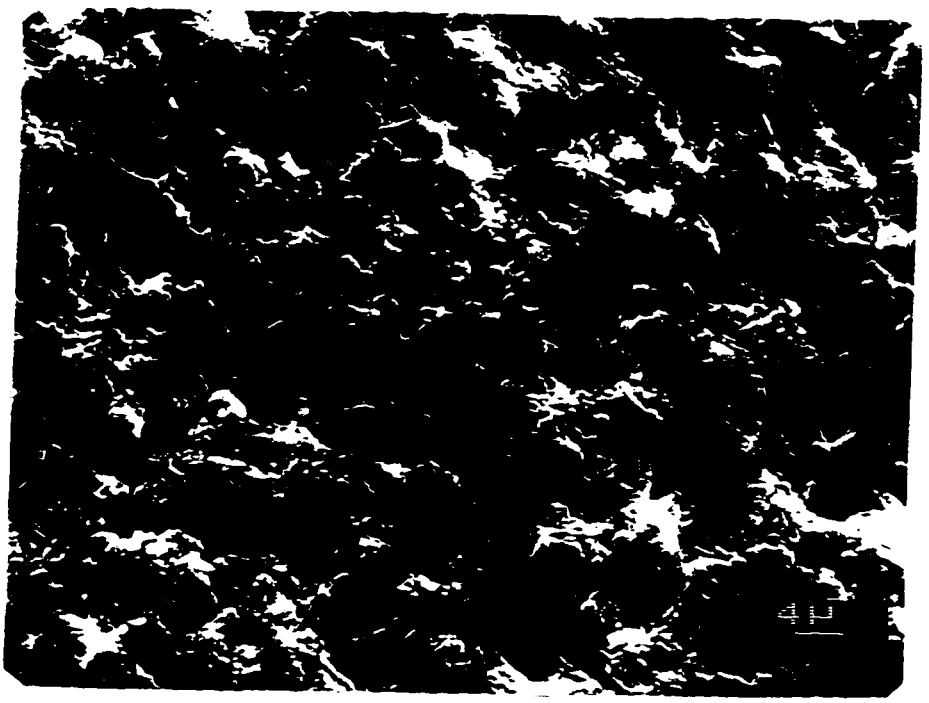

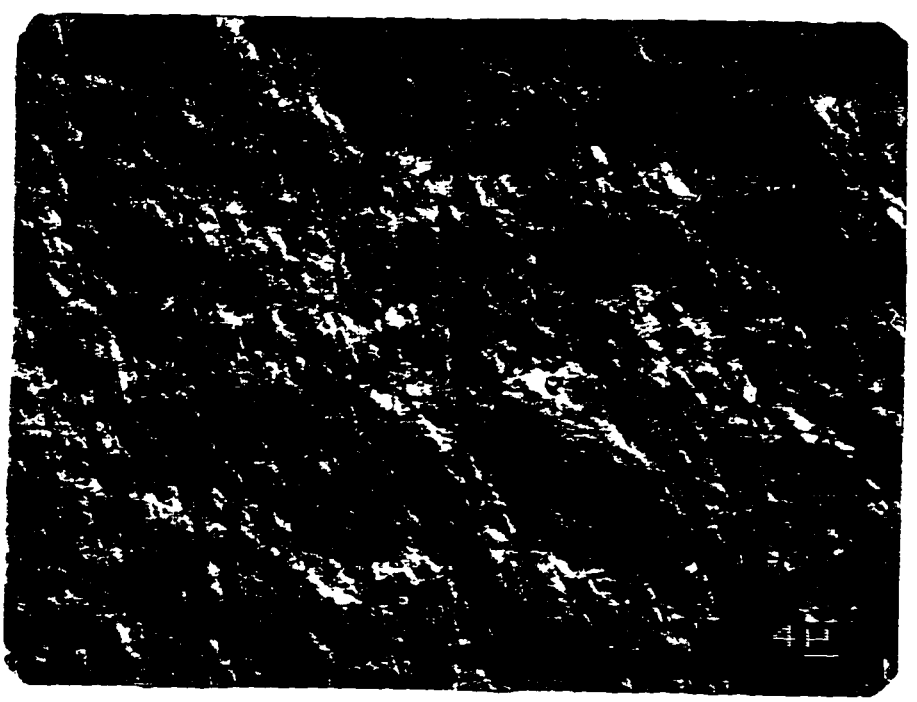

XTL Z1-36 (aged)

Figure 4-21:

SEM micrographs for two Pt-coated quartz crystals after ageing (Pt electrodes "aged" in 0.2 M H_2SO_4).

B and C). The frequency changes in this region are also influenced by the anion that is present and this is not surprising because of the fact that both the nature and concentration of the anion affects the distribution of the H upd peaks. Previous published work in this area has largely ignored these aspects of the EQCM response, or has treated the H upd region as a whole but it is clear that there is significant structure in the frequency response in this region. It seems unlikely that the processes that are observed are in fact mass changes, (i.e. corresponding to the formation of adsorbed H and changing anion concentrations, either in solution or in the surface) and this is clearly the case in alkaline solutions where there are no adsorbed anions. It is more likely that these changes are associated with changes in the interface and the way in which it interacts with the solution.

The results presented in this chapter, and in particular the ageing effect provide a good illustration of the unique ability of the EQCM to detect phenomena at the electrode/solution interface that are often undetectable by other techniques. It is more difficult to provide an explanation of these phenomena. This discussion will focus on the ageing effect in the H adsorption region and possible causes for it. There are two aspects to the discussion. The first is the fact that the ageing effect seems to decrease as pH increases. The second is that the ageing effect, as observed here, is associated with decreasing surface roughness. The changes that might occur as the pH increases are presented below after a discussion of the nature of adsorbed H at Pt electrodes.

4.8.1. The Nature of Adsorbed H at Pt Electrodes

Before moving to the effect of pH on the Pt electrolyte interface, it is important to discuss the nature of the two types of adsorbed hydrogen that are observed at the electrode surface, because it is in the potential region where the adsorbed H is present that the ageing effect is seen. The two types of hydrogen that are present lead to the two current peaks and are referred to as strongly bound hydrogen (the most positive peak) and weakly bound hydrogen (the most negative peak) respectively. Although there is still some debate, spectroscopic studies have suggested that strongly bound hydrogen might correspond to "sub-surface" hydrogen, i.e. an H atom that sits in the Pt lattice and whose electron is donated to the conduction band of the metal [158,163-170]. This hydrogen does not interact with the water at the interface.

The fact that this form of H is not absorbed on close packed Pt single crystals (where it presumably cannot penetrate the lattice) was also used to reinforce the identification of strongly bound H with "sub-surface" H. On the other hand, the weakly bound hydrogen does interact with the solution and in-situ specroscopic studies have suggested that the configuration is a water dimer hydrogen bonded to three adsorbed hydrogens (Figure 4-22). This hydrogen is thought not to sit "on top" of one atom of platinum but may be coordinated to several Pt atoms [158,163-170].

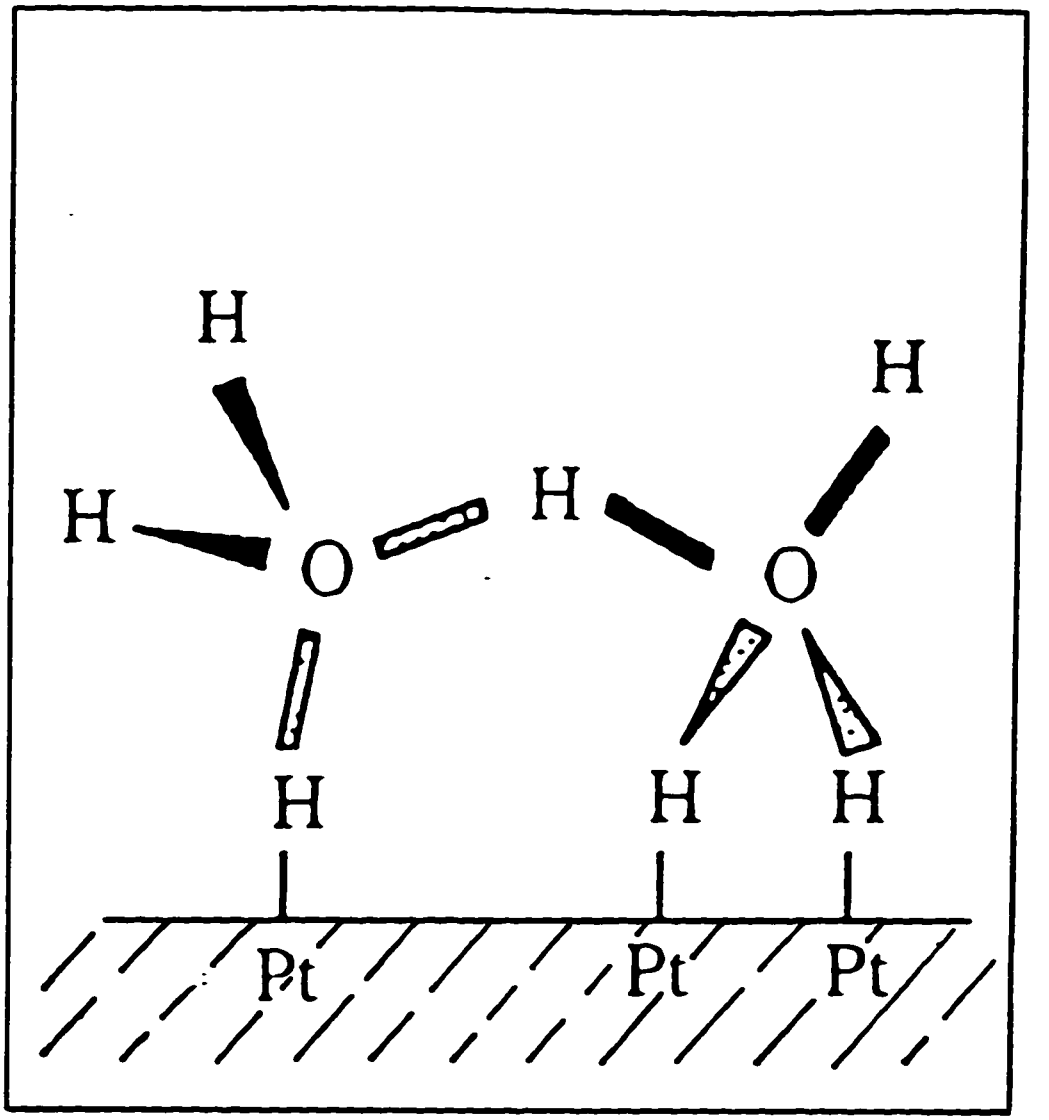

Figure 4-22:

Structure of weakly bound hydrogen adsorbed on platinum

***(from Bewick and Russel* [165]).**

4.8.2. The Effect of pH on the Structure of the Pt Electrolyte Interface in the Presence of Adsorbed H

The data in this chapter also provide some clues to help explain the ageing phenomenon. First, it is seen in acid solutions but not in a very basic solution and as the pH increases, the size of the ageing effect decreases. In view of the fact that there is indeed adsorbed hydrogen present at the electrode surface over the whole pH range, it is clear that the presence of adsorbed H is not the only requirement for the ageing effect to be seen. Unfortunately the role of anions cannot be clearly established with the data available. It is well known that, in acid solution, anions are present at the electrode surface in the same region of potential as the adsorbed H and that they affect the distribution of the H upd peaks [40]. However, in alkaline solution, the difference between the pzc of the Pt electrode and the potential where adsorbed H is present is significantly larger than it is in acid and so the electrode carries a larger negative charge than is the case in alkaline solutions. No anion adsorption is expected (from electrostatic considerations) in alkaline solution and it is known that anions (such as perchlorate and sulphate) do not affect the H upd peaks in alkaline media [40] and the results in this chapter have shown that anions have no effect on the mass response in basic solutions. Thus it is not possible to make any strong conclusions concerning the role of anions on the ageing effect.

The fact that the Pt electrode carries a large negative charge in alkaline solution in the region of H adsorption will have a second influence on the interface, in addition to inhibiting

anion adsorption. This effect is on the solvent. The normal picture of the solvent at the electrode is that the solvent dipoles will be oriented by the field. In acid solutions and in the H adsorption/desorption region the potential is close to the pzc whereas in alkaline solutions the greater negative charge on the electrodes is expected to result in the orientation of the water molecules so that (if the molecule is viewed as a dipole) the dipole δ of the H atoms should be oriented towards the surface. Recent (EXAFS) X-Ray studies at single crystal Ag electrodes have reinforced this picture of the water re-orientation as the potential (net charge) on an electrode changes from positive to negative [171]. This may make hydrogen bonding with neighbouring water molecules more difficult than is the case in acidic solutions. In view of this discussion, it is possible that one cause of the gradual decrease in the ageing effect with pH is a decrease in the interaction between adsorbed H and water molecules at the interface because of a change in the orientation with pH.

4.8.3. The Role of Surface Roughness in Ageing

The pH studies thus provide an insight into the ageing process, but they do not give an answer to the question of why the cycling process leads to such a change in the mass response in acid solutions. It is known that the electrodes are slowly dissolved in this process and that the roughness factor decreases but no significant structural changes could be seen from SEM pictures, and the effect does not seem to depend on absolute roughness. As noted earlier, this unusual effect of a large change in mass over the H region has been reported by others [151,156].

In one instance [156] the change was developed by cycling what was apparently a smooth electrode but no information was provided on the final state of the electrode, nor was any explanation advanced for the changes. In the other instance [151], the change was seen apparently immediately, although very little detail was provided about the electrode. These authors did however suggest a hydrophobic/hydrophilic transition might be implicated and referred to the hydrogen bonding between weakly adsorbed H and water. Careful examination of Figures where ageing occurs shows that the large mass increase (frequency decrease) begins just after the peak corresponding to strongly adsorbed H and so most of the frequency change can be associated with the gradual development of weakly bound H which can hydrogen bond to water. The data in this chapter thus suggest that the ageing effect is most likely to arise from the hydrogen bonding between weakly bound H and water at the electrode surface with anions perhaps providing a further degree of structure to the solvent next to the electrode. As pH increases the larger negative charge on the electrode in the H upd region will result in the removal of anions and in the re-orientation of water at the surface which will lead to a less structured interfacial region because hydrogen bonding to water by weakly adsorbed H will be less likely. The remaining puzzle is why this effect is seen after cycling. Literature data seem to show that the effect is not generally seen on smooth electrodes [153-156] and the data here suggest that the effect is also not generally seen on rough electrodes. Without further evidence or more detailed and specific information on the experiments performed in the literature, then we can only suggest that the coupling between electrode surface and solution is most effective not at a smooth electrode or a very rough electrode but at a moderately rough electrode. This

state can be reached either by cycling a rough electrode so that its area decreases or by cycling a smooth electrode so that its area (and roughness) increases. STM studies of Pt electrodes that were initially smooth has shown that regular ridge-like patterns are formed after oxidation-reduction cycles [172] but there does not seem to have been a similar study performed at rough electrodes.

This work has highlighted the need for careful structural characterisation of EQCM electrodes and for detailed surface preparation methods to be described in the literature. As well as the variation of mass/frequency responses with electrode treatment noted here, it is interesting to note that different methods of platinization have been found to yield very different catalytic activities (for reduction of perchlorate ions) [173], thus structural features of Pt electrodes are relevant to more than just EQCM responses.

4.8.4. Final Conclusion

The data presented in this chapter suggest that the large frequency changes observed at "aged" Pt electrodes in the region where adsorbed H is present at the surface are associated with the formation of a degree of structure of the solvent at the interface. This is most likely to be due to H bonding between the weakly adsorbed H and water and may also be influenced by anions. The effect decreases with pH because the charge carried by the electrode in the region of weakly adsorbed H becomes more and more negative and this results in anion

desorption and re-orientation of water so that H bonding to adsorbed H becomes more difficult. The development of this structure appears to be inhibited either by a large degree of roughness (as noted here) or (as deduced from literature results) by a smooth surface. However, further investigations into the role of surface roughness are clearly required. It is interesting to note that the theoretical treatments of the EQCM immersed in solutions (Chapter 2) show that the frequency change is proportional to the square root of the product of viscosity and density of the contacting solution. Thus if the increased structuring of the interfacial region increases either of these factors then we would expect a frequency decrease or an "apparent" mass increase and this is what is observed on ageing.

* * *

Chapter 5:

Adsorption and Oxidation of Thiourea at Electrodeposited Platinum Electrodes

5.1. INTRODUCTION - APPLICATIONS OF THIOUREA

Several authors have shown that thiourea (TU) is strongly adsorbed at many noble metal electrode surfaces, such as gold[174,175], mercury[176,177], silver[178-180] and platinum[181] in a wide range of electrolytes. Thiourea acts as a polishing agent in electrodeposition and its use as an anti-corrosive material has been established for a long time for the benefit of the industry[182,183]. It is also able to facilitate the reduction of certain metal ions through the formation of complexes and has been of interest as a complexing agent for gold as an alternative to cyanide in electrowinning processes[184]. Thus there is much interest in the study of its adsorption at different electrode surfaces. The strong electrosorption that the molecule shows is mainly due to the high value of the permanent dipole moment[185] as well as to the strong interaction of the sulphur in TU with the metal electrode. In addition

to adsorption effects, there has also been significant recent interest in the oxidation of thiourea. The principal interest arises in the area of electrochemical detectors for liquid chromatography (LC). The method of pulsed amperometric detection (PAD) or pulsed electrochemical detection (PED) has been applied to the detection of many different species that cannot easily be detected at constant potentials because of electrode fouling. PAD uses a potential pulsing regime that involves adsorption, detection and cleaning potentials to prevent deterioration of the electrode response[174,175,181].

Organosulphur compounds are a class of compounds that have wide uses (for example in the area of pesticides) and thiourea provides a useful model compound for the studies of the appropriate PAD regime for detection of organosulphur compounds because of its solubility, low volatility and lack of odour[175], although it should be noted that it has been identified as a carcinogen [186].

5.1.1. Literature Review - Oxidation of Thiourea to Formamidine Disulfide

One of the earliest studies of the oxidation-reduction of TU was that of Preisler and Berger in 1947 [187]. These authors used a direct measurement (potentiometric study) of electrode potentials to evaluate the standard potential of the thiourea system. They considered the reaction: 2RSH - 2H = RSSR to be reversible, implying that thiourea (represented here by RSH) is oxidised to form formamidine disulphide, and showed that

measured electrode potentials fitted the Nernst equation:

$$E_h = \frac{RT}{2F} \ln \frac{[RSSR]}{[RSH]^2} \qquad (5.1)$$

The E_0' value was estimated to be 0.420V (vs the N.H.E) in acidic solutions. The mechanism suggested by Preisler and Berger[187] proposed that TU is oxidized via its tautomeric form and that two radicals dimerise to give formamidine disulphide as the overall oxidation product, the reduction of this species leading to the formation of two molecules of thiourea. The structures of thiourea and its tautomeric form and of formamidine disulphide are shown in Figure 5-1.

The concept of the reversible oxidation of TU to formamidine disulphide as a one-electron process (per TU) initiated by Preisler and Berger[187] was used by Santhanam and Krishnan[188] in their coulometric (constant potential) study of TU oxidation at a stationary platinum gauze electrode in varied electrolytes. The potentials chosen varied between 0.6 and 0.7V (vs S.C.E.) and various electrolytes were used, ranging from acids to bases, but only in hydrochloric, sulphuric and perchloric acids was quantitative oxidation of TU found to occur. It was also noted that the electrolysis of TU in sodium hydroxide medium revealed some passive behaviour, attributed to the formation of a film of oxidant product.

Up to this point, most work considered the oxidation of TU to be a simple one

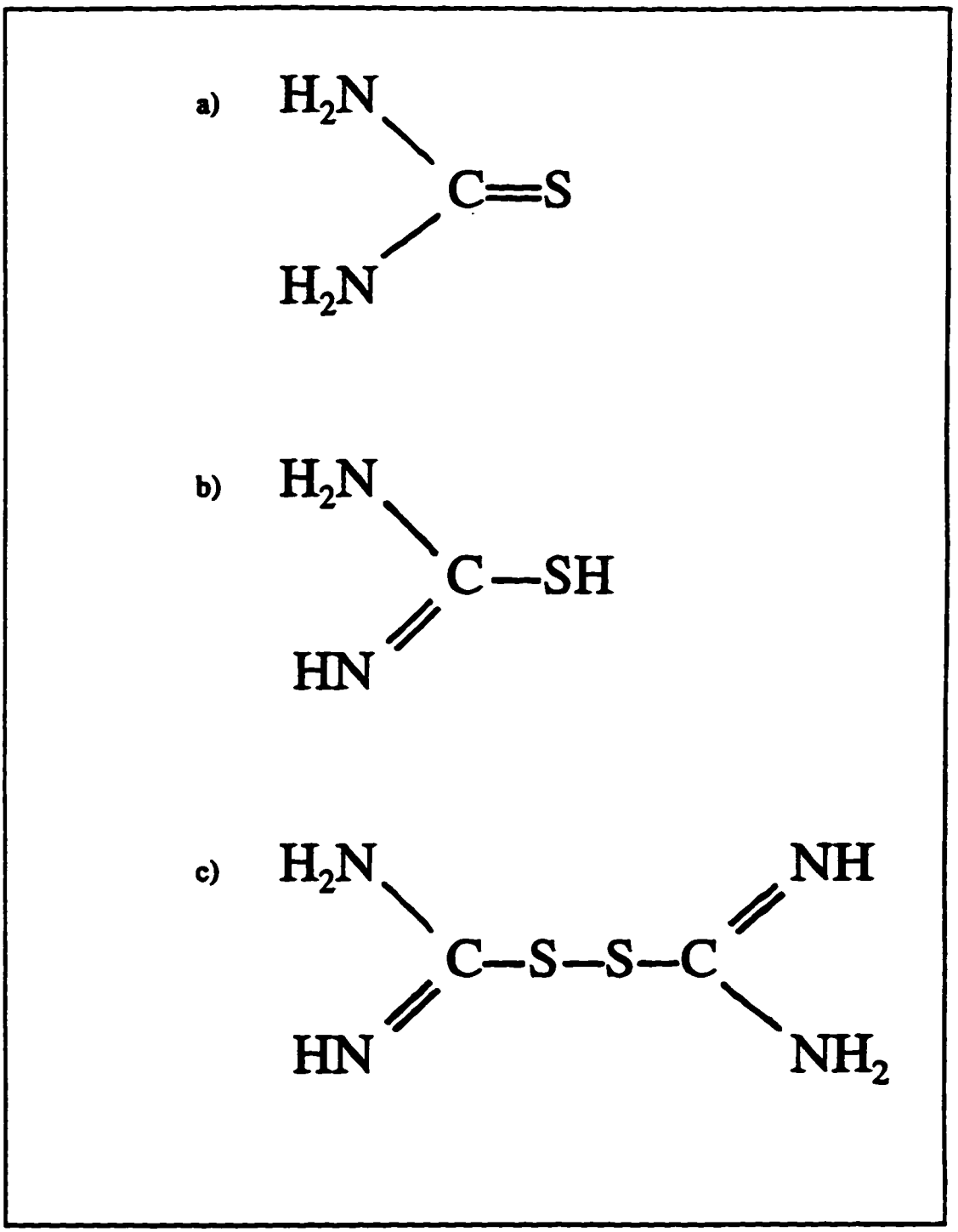

Figure 5-1:

(a) Structures of thiourea, (b) one of the tautomeric form of thiourea, and (c) the formamidine disulphide.

electron process but further complexities were revealed in the work of Kuz'mina and Songina[189]. By using a rotating disk platinum electrode in O-containing acid electrolytes (sulphuric, nitric and acetic acids) and in hydrochloric media, these authors concluded that the oxidation of TU in O-containing acids is affected by the adsorption of the oxidation products, indirect oxidation of TU at rather high potential, and formation of Pt oxides on the surface of the electrode. They concluded that for stepwise oxidation of TU, the first step was that of the oxidation to the disulphide, followed by a slow step and then further oxidation with O-participation.

5.1.2. Role and Mechanism of the Adsorption of Thiourea.

The mechanism of the oxidation of TU was proposed by Reddy and Krishnan[190] in 1969 for a stationary platinum electrode in aqueous solutions of hydrochloric acid. Hydrochloric acid allows oxidation of TU at lower potentials than other acids. Unfortunately, the current density values (recorded up to potential values of 0.7V (S.C.E.)) obtained by Reddy and Krishnan were never reproducible. They attributed this result to a possible adsorption of the product on the surface, in accordance with the previous study by Kuz'mina and Songina. Also, the data indicated that the electrochemical oxidation of TU at platinum electrodes is an irreversible process. The oxidation process was concluded to be barrier free[191] and from this conclusion, Reddy and Krishnan considered that the activation energy of the reverse reaction (cathodic) was close to zero

and wrote the following overall reaction:

$$2(NH_2)_2CS \rightarrow H_2N^{\cdot}C(:NH)S^{\cdot}S^{\cdot}C(:NH)NH_2 + 2H^+ + 2e^- \quad (5.2)$$

By comparing the infrared spectrum and TLC (thin-layer chromatography) results for the oxidation and cathodic products with spectra for the compounds prepared by chemical methods[187], Reddy and Krishnan confirmed formamidine disulphide and TU as oxidation and reduction products, respectively. They then suggested that the formation of formamidine disulphide involved the conversion of the tautomeric form of TU into a free radical with the combination of free radicals to give the disulphide. The existence of the tautomeric form of TU had been demonstrated earlier by Sheinker *et al* [192].

Gorbachev *et al* [193] further investigated the role of adsorption in the oxidation of TU by recording polarisation curves at a smooth rotating platinum electrode in 2N HCl. Two important conclusions are revealed by the work by Gorbachev *et al*: first, the fractional effective reaction order that is an indication of an effect of adsorption on the kinetics of the electrochemical oxidation of TU; second, the fact that the rate of stirring of the electrolyte does not affect the anodic current density was taken as a demonstration that, in the given range of polarisation potentials, the rate of oxidation of TU is limited by chemical polarisation. Gorbachev *et al* confirmed again the mechanism of oxidation of TU previously proposed by Reddy and Krishnan, oxidation of TU to form adsorbed radicals

that then combine to produce the disulphide, and the irreversible character of the process.

Thiourea is essentially only stable at Pt in the range of potentials where the Pt electrode is covered by adsorbed H. (The $E_0^{'}$ value of 0.420V vs N.H.E is equivalent to 0.178V on the S.C.E scale). The mechanism of adsorption of TU (and other similar organic compounds) on the platinum surface was first established by Conway, MacDougall and Kozlowska [194,195]. These authors used a technique that consisted of measuring anodic adsorption transient currents at a platinum electrode held at a series of constant potentials (in the region where H atoms are present at the electrode surface) in a solution into which different amounts of thiourea were added. Cyclic voltammograms were then recorded. The facts that *anodic* transient currents were observed, that the magnitude of the transient current decreased with increasing potential (and consequent decrease of coverage of adsorbed H), and that the transient charge and the charge associated with the adsorption of hydrogen were identical, led Conway *et al* to conclude that the chemisorption of S-containing molecules proceeds by the *anodic displacement* of H previously adsorbed on the electrode. The adsorption mechanism proposed by these authors is:

$$RSH + PtH \rightarrow PtRSH_{ads} + H^{+}_{aq} + e^{-} \qquad (5.3)$$

This differs from the mechanism of adsorption of many other compounds such as alcohols

which are themselves dehydrogenated upon adsorption. These authors also observed a faradaic current associated with the oxidation of TU once the potential passed into the double layer region at Pt electrodes.

It appears from all the references mentioned above that thiourea undergoes a strong adsorption at platinum. On the basis of radiotracer results, Horanyi has classified strong adsorption phenomena into two types[196-199]: those that do not give a significant change in the molecular state of the adsorbate during the adsorption (oxidation or reduction do not take place during the adsorption), and those that are characterized by an irreversible or reversible oxidation or reduction of adsorbed species, the rate of the process being dependent on the potential. When the potential is restricted to the H adsorption region at Pt, the adsorption of TU at Pt falls into the former category.

5.2. *CYCLIC VOLTAMMETRY IN THIOUREA SOLUTIONS*

The initial study of the electrochemistry of TU involved a brief investigation of the oxidation of TU by cyclic voltammetry in a solution of moderately low concentration. A cleaned Pt electrode was placed in a solution of 1mM thiourea and held at a fixed potential of 0.0V (in the hydrogen adsorption region) for times ranging from 0 to 10 minutes. A single cyclic voltammogram was then recorded together with a mass response, with the potential being scanned down from 0.0V initially (Figure 5-2, solid line).

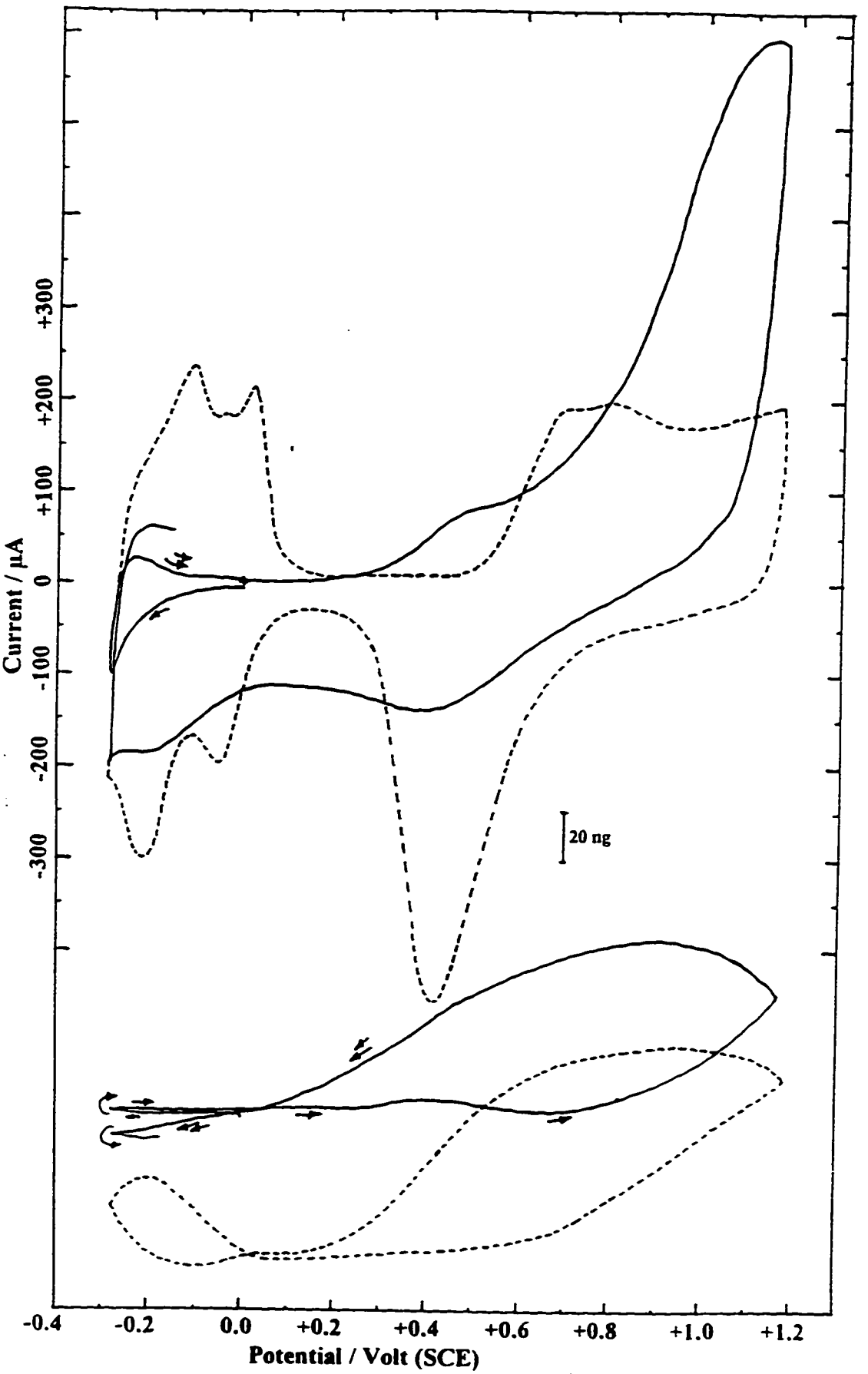

Figure 5-2:
Cyclic voltammogram (top) and mass response (bottom) of a clean Pt electrode in 0.2 M H_2SO_4 (dashed lines). The electrode was then placed in a 1 mM thiourea solution and held at a fixed potential of 0.0 V (in hydrogen adsorption region) for times ranging from 0 to 10 minutes. Scan rate: 50 mV/s.

The voltammogram (solid line) reveals almost complete blocking of the hydrogen adsorption/ desorption peaks and hence that the electrode surface is almost completely covered with thiourea. However, once the potential moves into the double layer region, a rise in current begins at about 0.2V and then a small plateau is reached at ca. 0.6V. This peak will be discussed later. The current then rises again to a second peak just before the scan reversal. The fact that the current reaches this second (more positive) peak is associated with the development of the oxide at the Pt surface. It has been noted from previous studies of oxidation of thiourea at Au in alkaline solutions[175] that full development of the oxide makes the electrode significantly less active toward the oxidation of thiourea. The same may apply here. Thus when the oxide is fully or largely developed the thiourea oxidation current begins to fall. This will be seen more clearly in later Figures.

The negative going scan reveals several further points of interest. First, that the large oxidation peak involves both oxidation of thiourea and oxidation of the electrode surface itself because there is a very broad oxide reduction peak centred at about 0.4V-0.5V. Second, after the reduction of the oxide and before H adsorption, there is a reduction current that is larger than the normal double layer current (a background scan is shown as a dotted line for comparison). This may be attributed to reduction of products of the thiourea oxidation process (see below). At the end of the first cycle, the larger H adsorption current indicates that some thiourea has been removed from the electrode

surface. However, the actual current due to H adsorption may be distorted by the extra reduction current due to reduction of thiourea oxidation products. Nevertheless the full cycle indicates that material has been removed from the electrode surface during the scan and that re-adsorption of thiourea is not complete on the time scale of this experiment. Thiourea is only stable in the potential range of H adsorption and so the time in which adsorption may take place without reaction is quite small in this experiment.

The mass response that accompanies the voltammetry does not show many features, but several points can be discussed. First, the response is completely flat as the potential is taken negative from 0.0V to the lower scan limit and then back to ca. 0.2V. In this potential region, the surface is covered with a monolayer of thiourea and since there are no faradaic processes taking place and thiourea does not desorb, the surface does not change and so the mass response is constant. This is in contrast to the response in background electrolyte where the coverage of the electrode with adsorbed H varies over this potential range, and where, as we have seen in Chapter 4, there can be large changes in the frequency response, depending on the treatment of the electrode. (The dotted line shows the background response for the electrode used in this experiment). It is only after 0.2V where the oxidation current begins to appear in the voltammogram, that any mass change is seen. In fact, there is a very small increase which is followed by a tiny decrease as the first oxidation region is encountered. It is reasonable to assume that the oxidation current after 0.2V corresponds to oxidation of adsorbed thiourea (which should be present

intact on the electrode surface after adsorption in the H adsorption region) perhaps with a component of oxidation of solution species. Although there may be removal of an adsorbate here, there is no significant mass change and so it is likely that re-adsorption occurs once surface sites are freed. Such a situation would lead to a small mass change, if any. Literature data suggest that the first stage of oxidation involves a one electron oxidation of thiourea (or a tautomeric form of it) to a radical (which may be adsorbed) with subsequent formation of formamidine disulphide through dimerisation. Disulphides can also adsorb strongly to electrode surfaces (and the formamidine disulphide has been suggested to be a poisoning species at Pt in alkaline media[181]). Thus the flat mass profile could result from adsorbate removal and replacement either by product or by fresh reactant.

As the potential is taken to more positive values and the large oxidation current passes, then the mass increases. The oxidation current can be attributed to two processes as noted above. The first will be oxidation of thiourea or the disulphide and the second will be the generation of oxide on the Pt surface (since the characteristic oxide reduction peak, although broader than normal, is seen on the negative going scan). Thus the mass increase is probably a result of oxide formation, but may also be balanced with some removal of adsorbed residues. When the potential is decreased again, the reduction of the oxide gives rise to a broad mass decrease, but at the end of the scan the mass is slightly less than at the beginning, indicating a slight loss of material from the surface, in

agreement with the conclusions deduced from the voltammetry.

Figure 5-3 shows another cyclic voltammogram which illustrates that the thiourea oxidation process is reversible to some extent and that the product of thiourea oxidation in the double layer region of potential can be reduced. In this experiment, the electrode was held at -0.25V for 5 minutes in a 2.5 mM solution of thiourea, and then the potential was cycled between -0.25V and 0.5V at 20 mV/s for 4 cycles. The initial scan shows a sharp peak (note that the TU concentration is higher than for the experiment in Figure 5-2) and a reverse peak is also visible on the negative going scan. Thus the products of TU oxidation can be reduced. On subsequent cycles both peaks decrease in size which suggests that a large component of the current comes from the adsorbed species or that the product of the oxidation adsorbs on the electrode and poisons it so that the potential must be taken to higher values than 0.5V to remove the adsorbed product.

5.3. EXAMINATION OF ADSORBED RESIDUE AT Pt ELECTRODES

In the next experiment, an electrode that had been treated as described in section 5.2 above (the experiment of Figure 5-2) was rinsed thoroughly and then the electrolyte (which contained thiourea) was replaced with fresh sulphuric acid which did not contain any thiourea. This allows an examination of the electrochemistry of any adsorbed residue present on the electrode surface after cyclic voltammetry in thiourea solutions. The

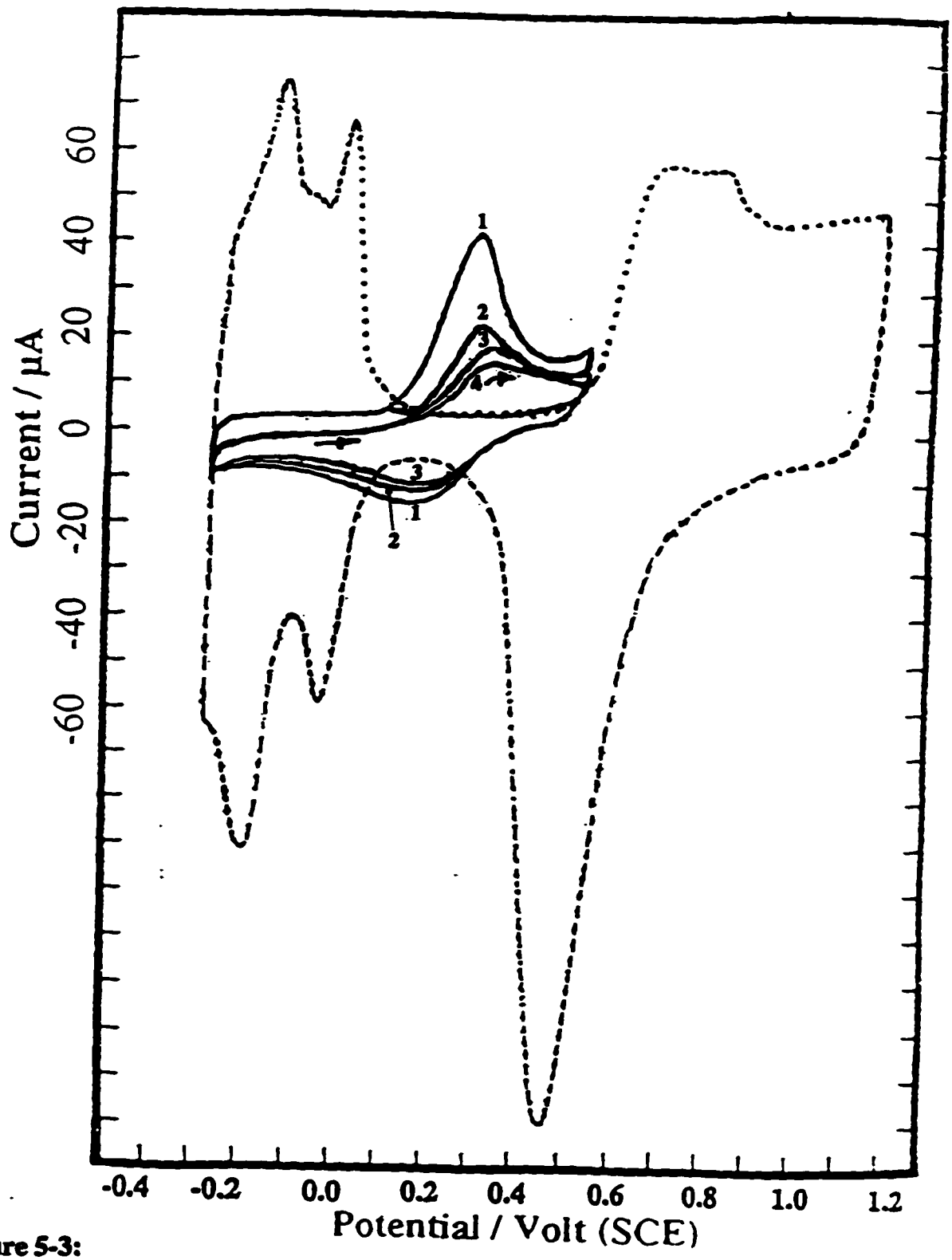

Figure 5-3:

Cyclic voltammogram of a 2.5 mM thiourea after the Pt electrode was held at -0.25 V for 5 minutes. The potential was cycled between -0.25 V and 0.5 V at 20 mV/s. Also shown in the figure is a cyclic voltammogram of the same Pt electrode clean in 0.2 M H_2SO_4 solution (dotted lines). The numbers refer to successive cycles.

potential was then cycled for 5 scans from 0.0V beginning in the negative direction. Figure 5-4 shows the first (solid line) and fifth scans.

The initial voltammogram shows that after the experiment of Figure 5-2, there is still substantial coverage of the electrode with an adsorbed residue, even after rinsing and electrolyte replacement because the H adsorption/desorption current is still suppressed to a significant extent. There is also a net reduction current in this region around 0.0V. This may be due to traces of oxygen present in solution after the replacement of the thiourea containing solution with the fresh electrolyte. The major difference in the voltammetry when compared to the response with thiourea present in solution (Figure 5-2) is the absence of the plateau oxidation current in the region between 0.2V and 0.6V. The current simply increases smoothly to the large peak at 1.05V. The absence of the plateau may be related to the fact that in Figure 5-2 the electrode is covered (initially) with adsorbed TU whereas in Figure 5-4 the effect of the cycle in Figure 5-2 may result in a different adsorbate (perhaps an adsorbed product such as the disulphide) on the electrode. This adsorbate may require higher potentials for oxidation.

The large oxidation peak at the end of the positive going scan occurs at a lower potential than that of Figure 5-2 (the peak is not fully visible in Figure 5-2 but is in Figure 5.4 and in both cases the upper potential limit is the same). Since it is accepted that the two electron oxidation of the Pt surface inhibits TU oxidation, the fact that the peak

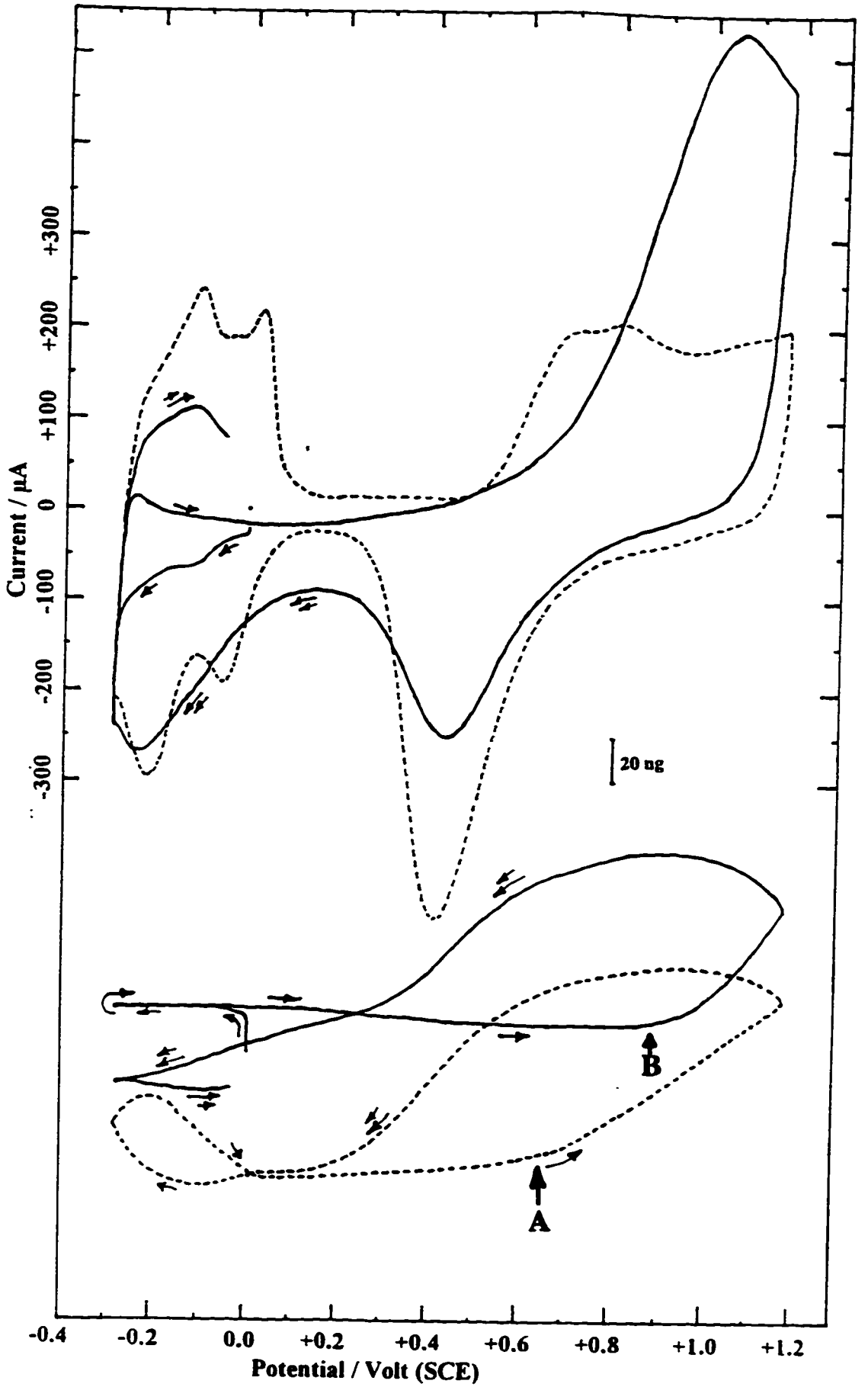

Figure 5-4:
Cyclic voltammogram (top) and mass response (bottom) of Pt electrode that has been treated as described in figure 5-2 (1 mM thiourea held at potential 0.0 V, then the cell rinsed and a new fresh electrolyte solution put in). Dashed figures correspond to a clean Pt. Scan rate: 50 mV/s.

occurs earlier suggests less significant blocking of oxide formation in the solution where thiourea is not present in the bulk. This is likely to be due to the fact that any surface sites that are freed from adsorbate by oxidation in a solution containing thiourea may be subject to further adsorption. The oxidation of adsorbates from surface sites in background electrolyte is less likely to lead to re-adsorption, unless it is of products. As before, the presence of an oxide reduction peak on the reverse scan indicates that the oxidation current includes contributions from both oxidation of thiourea (or other adsorbed residues) and oxidation of the electrode surface. The oxide reduction current is larger than in Figure 5-2 which also shows that oxide formation is less inhibited when there is no TU in the electrolyte. There is again a substantial reduction current passed after the oxide reduction peak and before the H adsorption current. As for Figure 5-2, this current is due to reduction of the products of thiourea oxidation but probably also contains an oxygen reduction component in this case.

Figure 5-4 also shows the fifth cyclic voltammogram (dashed line), as it was found that five cycles were necessary to generate a clean cyclic voltammogram.

The mass responses for the first and fifth cycles are also shown. The first cycle reveals little mass change over the range of potential until ca. 0.75V and this is then followed by a mass increase. Given that a reasonable amount of oxidation charge is passed before this potential is reached it seems that the initial stages of the oxidation

process lead to no change in mass. This suggests that the adsorbed residue remains on the surface even after oxidation since, in contrast to Figure 5-2, there is no bulk thiourea present to adsorb if adsorbates are removed. There is a mass increase after 0.80V and this can be attributed to oxide formation although if a residue is also removed from the surface then the overall mass change may be a result of a mass increase (due to oxide formation) combined with a mass decrease (due to loss of adsorbed species into solution).

On the negative going scan there is a steady mass decrease due, at least in part, to oxide reduction but at the end of the cycle the mass is less than at the start. Thus there has been a net loss of material from the electrode. This loss is larger than when there is TU present in solution. After 5 cycles the mass response takes on the form similar to that of a clean Pt electrode indicating that all the adsorbed residue has been removed from the surface. Clearly, the fact that five cycles are needed for complete adsorbate removal suggests that removal of adsorbed thiourea or of the adsorbed products is difficult. An experiment at a much slower scan rate might show adsorbate removal in fewer cycles.

One final observation relates to the onset of oxide formation at the clean electrode (dotted line) and at the electrode with adsorbed species (solid line). It is well known that oxide formation at Pt and Au occurs through initial formation of adsorbed OH (which is often very active for oxidation processes, particularly at gold electrodes in alkaline media) and then at higher potentials the OH is inserted into the metal lattice. This latter process

(known as place exchange[39] or turnover and discussed in Chapter 4) can be identified in EQCM experiments because the generation of OH (from adsorbed water) does not lead to a mass change[80,200] whereas the place exchange process does. Since the Pt electrode was aged and had a flat double layer mass change, the onset of irreversible surface oxidation is easily located where the mass begins to increase again after the double layer region. This is shown by point A in Figure 5-4. A comparison of this response with the mass response accompanying the first cycle (solid line) shows that there is no mass increase in that case until above 0.8V (Point B in the Figure). Thus the presence of the adsorbed residue inhibits the oxidation of the surface and the initial stages of the oxidation current (which begins at about 0.6V in the first cycle) can be attributed to oxidation of adsorbed residues rather than to the oxidation of the electrode surface. However, when the oxidation of the surface starts, the mass increase is steeper than for the background electrolyte (compare the slopes of the mass responses after points A and B), probably as a result of the increased electric field driving the oxidation process. It is also noticeable that the peak in the current occurs shortly after the mass increase which also agrees with the suggestion that the irreversibly formed oxide is not very active for oxidation of thiourea.

5.4. ADSORPTION OF THIOUREA IN THE H ADSORPTION REGION OF POTENTIAL

In an effort to be able to examine the oxidation of adsorbed residues at the electrode surface in the absence of readsorption, experiments were carried out with a low bulk concentration of thiourea. The adsorption process was first followed with time using both cyclic voltammetry and mass responses. The profiles that resulted are shown in Figure 5-5 for a bulk thiourea concentration of just 1 μM. The potential was held at -0.15V for differing periods of time and then the voltammogram and mass responses were recorded as the potential was cycled between from -0.15V to 0.2V and then down to the normal lower limit of the scan. This ensures that no hydrogen evolution takes place and that there is no oxidation of adsorbed thiourea, but it allows the adsorption to be studied through an examination of the suppression of the H upd peaks.

The figure shows that as the time of holding increases (left to right) there is a progressive decrease of the H adsorption/desorption current as thiourea blocks surface sites (since the upper potential for the scan is insufficient to remove any adsorbed species). The upper part of the Figure 5-5 shows two changes in the mass response as the coverage of thiourea grows. First, the structure associated with the H adsorption/ desorption region is gradually removed, making the mass response flatter, and second there is a slow increase in mass as thiourea is adsorbed. The removal of the mass changes

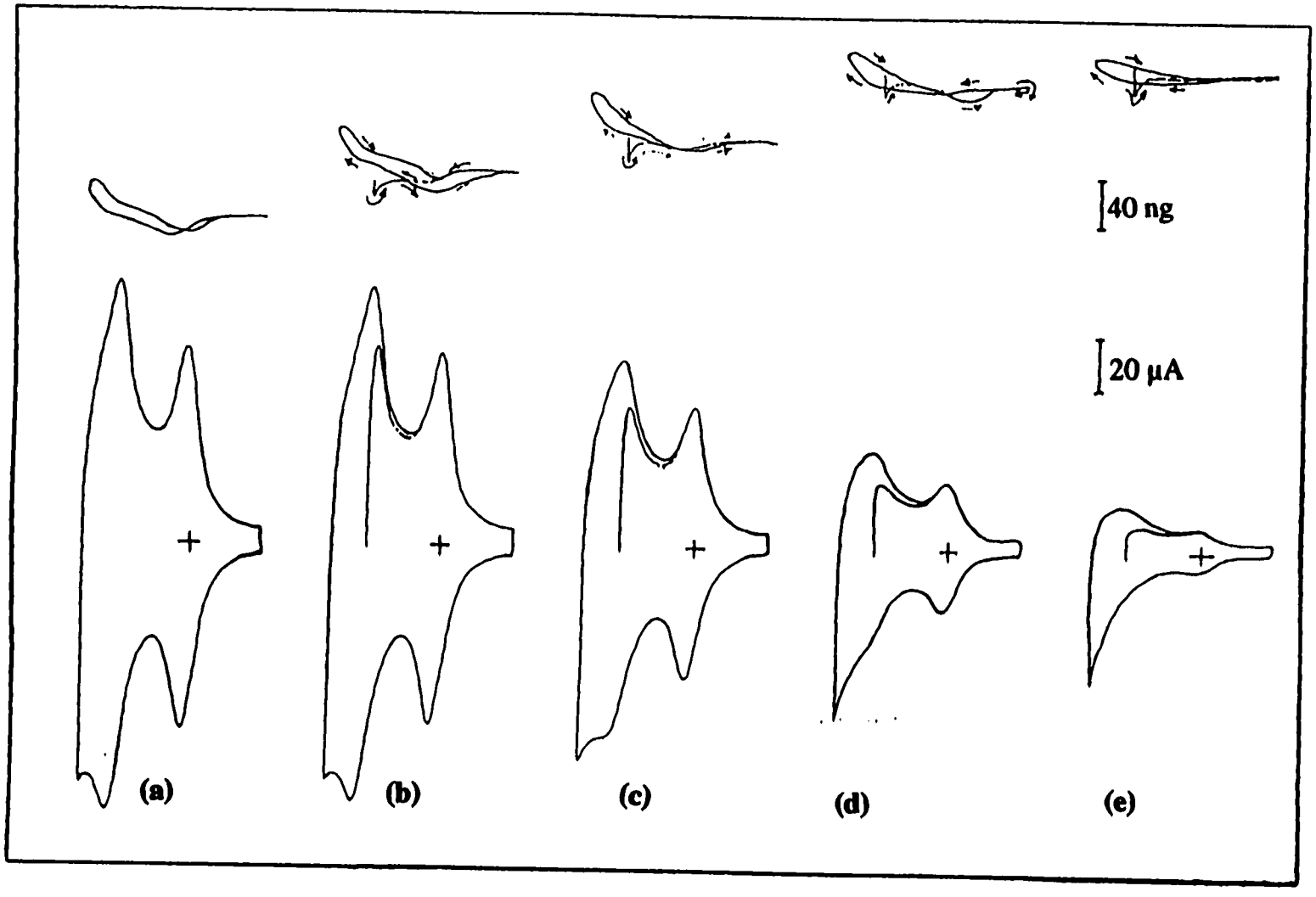

Figure 5-5:

Cyclic voltammograms (bottom) and mass responses (top) after holding the potential at -0.15 V: a) Background electrolyte (0.2 M H_2SO_4); b) 1 µM TU/ 0.2 M H_2SO_4, holding time: 1 minute; c) 1 µM TU/ H_2SO_4, holding time: 15 minutes; d) 1 µM TU/ H_2SO_4, holding time: 30 minutes; e) 1 µM TU/ H_2SO_4, holding time: 40 minutes. Scan rate: 20 mV/s.

associated with H adsorption/ desorption with time is expected, since the electrode surface becomes covered with a layer of thiourea over the whole potential range investigated and no electrochemical changes take place. No mass changes would be expected in this case. The change of mass of an electrode with the adsorption of thiourea shows a mass increase upon adsorption. This is in agreement with the data of Figure 5-4 which show a decrease as TU or adsorbates derived from it are removed (if the beginning and end of the first cycle of that Figure are compared). Mass increases are not always seen upon adsorption because the adsorbate may displace anions and adsorbed water and produce a net mass decrease if the adsorbate is of low molecular weight, but in this case an increase is seen. However, it is likely that adsorbed anions are displaced as well as adsorbed water because the mass changes that are seen at clean Pt are removed by thiourea adsorption.

5.5. CYCLIC VOLTAMMETRY AND MASS RESPONSES IN THIOUREA SOLUTIONS OF LOW CONCENTRATION

Figure 5-2 shows that the mass response in the presence of thiourea in solution is not especially informative and the main interest in this section of the thesis is in the effect that adsorbed thiourea has on the mass response and the changes that occur as the adsorbate is removed. Thus in an effort to examine mass responses when thiourea is removed but when there is no re-adsorption (at least of fresh reactant) and to avoid transfer of the electrode in air or under conditions of open circuit between a thiourea

containing solution and a solution containing background electrolyte alone, experiments were carried out with a very low concentration (1 μM) of thiourea in solution. This should ensure that no re-adsorption of TU occurs during the time needed for a potential cycle, as suggested by Figure 5-5.

5.5.1. Adsorption in the H Upd Region Followed by Oxidation

In these experiments, thiourea was allowed to adsorb at a fixed potential for a time long enough to obtain monolayer coverage (as judged from the experiment in Figure 5-5). The potential was then scanned positive in order to oxidise the adsorbed material from the surface and the mass and current were recorded.

Figure 5-6 shows the results of one such experiment where the electrode was immersed in a 1 μM solution at a potential of -0.150V for 2 hours. The potential was then scanned positive (solid line). Prolonged holding of the potential at a constant value could also lead to the accumulation of other impurities on the electrode surface. However, similar experiments in background electrolyte showed that the H adsorption/desorption peaks were suppressed by only 5-10% in this time, whereas with TU, monolayer coverage is found. The presence of strongly adsorbing thiourea should also lead to minimal adsorption of other impurities, which should be present at lower concentration levels in a clean solution.

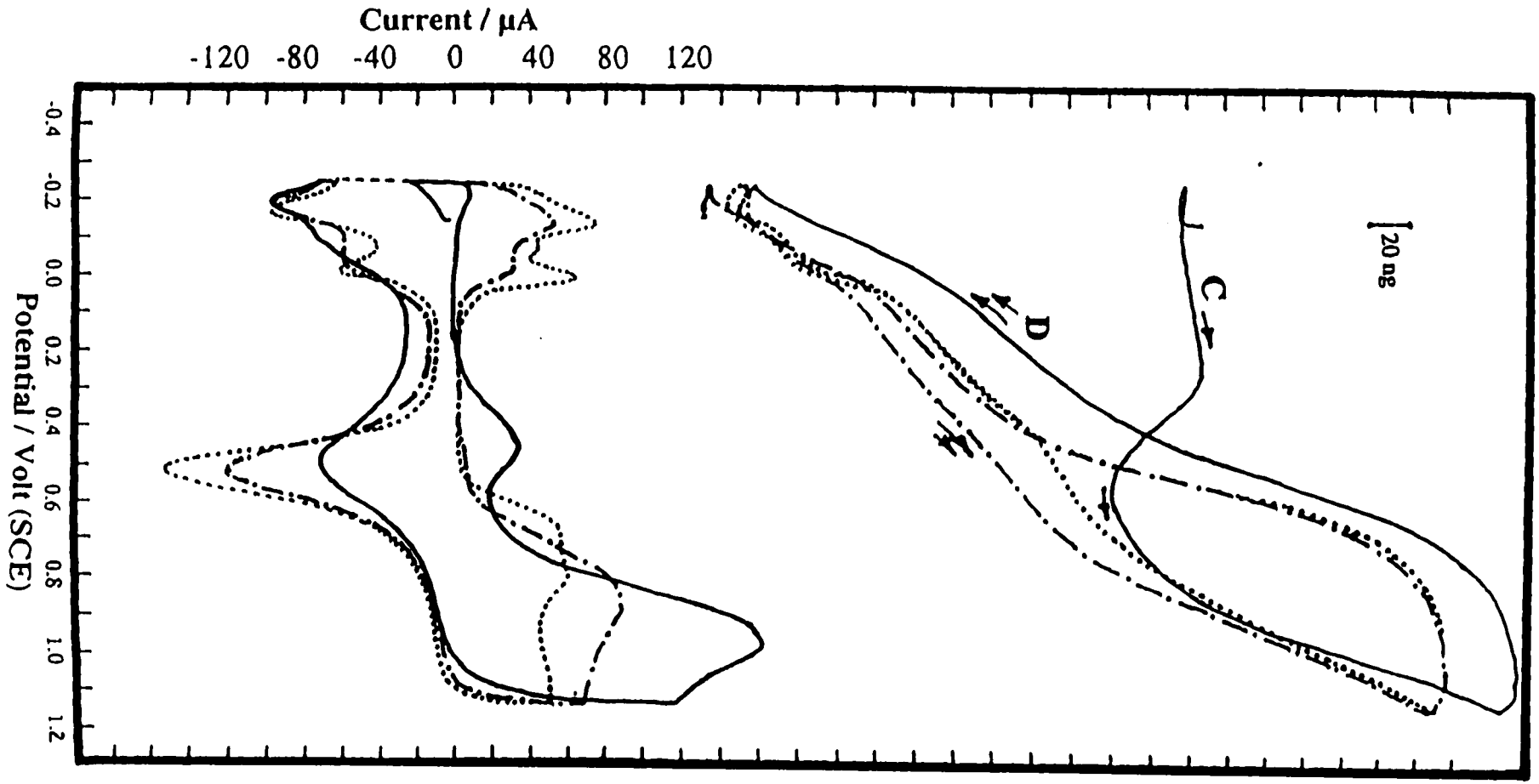

Figure 5-6:

Cyclic voltammogram (bottom) and mass response (top) for 1 µM thiourea after the potential was held at -0.15 Volt for 2 hours. Dashed figures are for the same Pt clean in the same electrolyte with thiourea present in the solution. Scan rate: 20 mV/s.

The voltammetric response of Figure 5-6 (lower part) will be discussed first. In the voltammogram, the first part of the scan from -0.150V towards the negative limit (solid line) indicates that the coverage of thiourea on the surface of the electrode is not complete, as some current that may be attributed to H adsorption /desorption is still visible. Because the adsorption involves anodic displacement of adsorbed H[194,195] and at -0.150V the H coverage is not unity, this is not unexpected. However, a substantial fraction of the surface *is* covered with thiourea. There is no significant oxidation current until about 0.2V when the current rises to give a sharp peak at 0.45V. The current then rises again at 0.6V into a large oxidation peak but then declines as the upper scan limit is approached. On the negative-going scan, there is the familiar peak due to oxide reduction but this is less than the peak observed for a clean electrode (compare solid and dotted lines). As noted earlier, there is also a significant reduction current that is still passed even after the oxide reduction peak and before the H adsorption current occurs (roughly in the region between 0.3V and 0.0V on the negative going scan). This is attributable to reduction of the oxidation products of thiourea, as discussed earlier.

When the second cycle (-.-.-.) begins, the large currents for the H adsorption/ desorption peaks are visible and indicate that a large fraction of adsorbate has been removed, but there is still some blockage of the surface by adsorbed residues because the H upd current is less than for a clean electrode (.....). The next difference between first and second cycles is that there is no oxidation peak in the double layer region at 0.45V.

The current does rise slowly after 0.4V and then more sharply after 0.6V. In comparing the currents, the peak current (and the peak potential) for the most positive oxidation peak on the second cycle are both less than for the first cycle. On the negative going part of the second cycle the current for oxide reduction is larger and the reduction current between 0.3V and 0.0V is less. Both these observations indicate that the coverage of the electrode with thiourea is decreasing and that there has been a gradual removal of surface adsorbates. Thus, more of the surface is oxidised and there are less oxidation products from thiourea to be reduced between 0.3V and 0.0V. The fifth voltammetric cycle (.....) is comparable to that of a clean Pt electrode, indicating that all adsorbed residues have been removed.

The following general conclusions may be made from the voltammetric response in a solution containing 1μM thiourea. First, the presence of thiourea that has been allowed to adsorb in the H adsorption/desorption region of potential (and thus should be present as undissociated thiourea) leads to an oxidation peak at 0.45V. The large subsequent oxidation peak suggests that even after oxidation at 0.45V there are still adsorbed residues on the surface that can be further oxidised. The peak at 0.45V does not lead to complete removal of adsorbed species from the surface because the charge associated with the oxide reduction peak on the subsequent negative going scan is less than the value expected for a clean electrode, indicating blockage of surface oxidation by an adsorbed residue. The broad reduction current (0.3V to 0.0V) after the oxide reduction

peak indicates the reduction of oxidation products or adsorbed residues. More than two full cycles are necessary for full removal of adsorbed residues but on the second cycle the oxidative removal of adsorbates does not occur unless the potential is greater than 0.6V. The fact that a clean CV can be obtained in several cycles indicates that thiourea in solution makes a negligible contribution to the voltammetric features seen on the first two cycles, although it is likely that some of the current (particularly at the highest potentials) results from reactions of products generated close to the electrode surface. There are several oxidation products of thiourea that are possible, including the disulphide, a sulphinic acid, or sulphate and urea[174,175,181] although the production of some of these species will be favoured in alkaline solutions. However, no conclusions may be made about the nature of the products formed here without further experiments.

The mass response over the first two cycles also shows several important features. First, on the first cycle (solid line) and as noted earlier, it is flat up to the point in the initial stages of the cycle where there is no Faradaic current taking place at a surface that is largely covered with thiourea. Since there are no changes in the surface over this potential range then there should be no change in the mass response. There is, as noted previously, a small mass increase that is seen once the oxidation current appears at 0.20V and above and then a broad mass decrease is associated with the oxidation peak at 0.45V. This can be compared with the response seen in Figure 5-2 where a similar current peak is present but there is no mass change. This is a strong indication that adsorbate removal

does lead to a mass decrease but that in Figure 5-2, re-adsorption of reactant/product occurs giving no mass change overall. Here where reactant is present at a much lower concentration (1μM vs. 1 mM) and where re-adsorption of reactant is much less likely, there is clearly a net loss of adsorbed material.

The mass then passes through a minimum as the oxidation current increases and then increases steadily as the upper potential limit is reached. The mass then decreases throughout the rest of the negative going scan. Most of this decrease is a result of oxide reduction, but it is clear that there is now a significant difference between the mass in the double layer region on the negative-going half of the scan and on the positive-going half of the scan (points D and C respectively). At point C the surface is covered with TU, but at point D the surface is closer to a clean Pt surface and the mass is substantially less than when thiourea is present and continues to decrease as the potential proceeds into the H adsorption/desorption region.

The mass that accompanies the second cycle (-.-.-.) is very similar to that for a clean Pt electrode. But the CV shows that there is still some blockage of H adsorption and thus some adsorbates present on the surface. The mass differences between the second cycle and the fifth cycle are much less significant and are only just larger than experimental error or drift expected between scans.

5.5.2. Adsorption in the Double Layer Region of Potential Followed by Oxidation

The same type of experiment as that shown in Figure 5-6 was also carried out, but with an adsorption potential for the thiourea of 0.2V. At this value, which is at the start of the double layer region of potential, the adsorption process cannot occur through anodic displacement of adsorbed hydrogen as it does for adsorption at -0.15V. There may be some oxidation of the TU as it adsorbs at this potential, or alternatively it may undergo dehydrogenation. The results are shown in Figure 5-7 for scan rate of 10 mV/s. The principal features of the voltammogram are similar to those of Figure 5-6 in general, but it is noticeable that the prominent peak seen at 0.45V on cycle 1 in Figure 5-6 is not seen here, although there is a broad shoulder in this region. The difference between the voltammetric characteristics for the experiments where adsorption was performed at 0.20V and -0.15V may well indicate that the product of adsorption is slightly different in the two regions of potential (double layer region and H upd region). This is not surprising since the mechanisms of adsorption will be slightly different at the two potentials as noted above. Thus the peak at 0.450V may correspond to oxidation of adsorbed thiourea but when adsorption is performed at 0.20V then the thiourea undergoes dehydrogenation or other oxidation and although the surface coverage is almost identical in the two cases, the adsorbate resulting from adsorption in the double layer region is removed mainly at higher potentials in the oxide formation region.

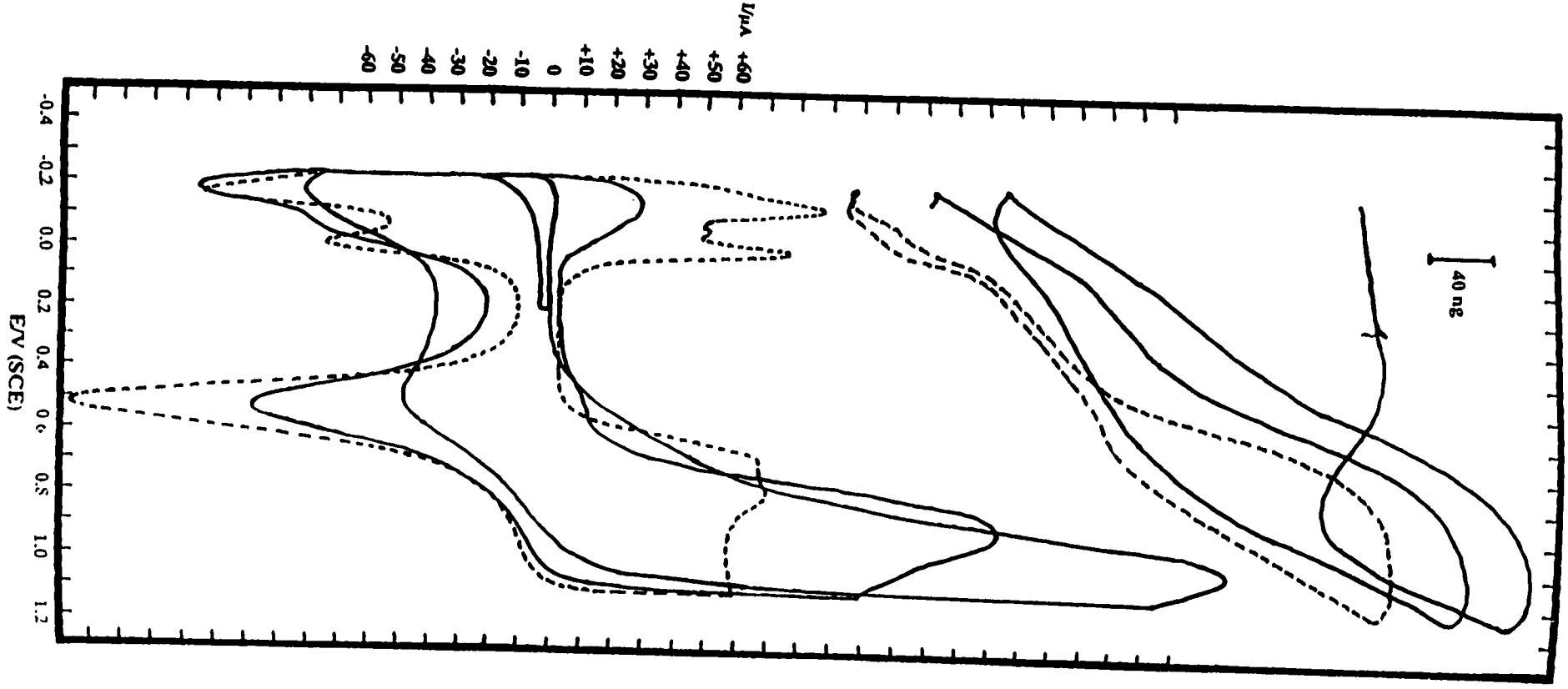

Figure 5-7:

Cyclic voltammogram (bottom) and mass response (top) for 1 μM thiourea after the potential was held at +0.20 volt for 2 hours. Dashed figures are for the same Pt clean in the same electrolyte with thiourea present in the solution. Scan rate: 10 mV/s.

The mass response is also very similar to the previous Figure. There is still a mass decrease that accompanies the oxidation current in the double layer region of potential and so there is still adsorbate removal here even though the current peak is less prominent. Otherwise it is still seen that several cycles are required to ensure complete removal of the adsorbed species at the electrode surface. The overall picture of the mass response in Figures 5-6 and 5-7 is very similar. Adsorbate removal gives a mass decrease but removal is not complete after one scan. After the first scan the mass response is very similar to that for a clean Pt and it is difficult to identify where adsorbate removal occurs on the second and subsequent cycles.

5.6. OPEN CIRCUIT POTENTIAL DECAY EXPERIMENTS: REACTION OF TU WITH THE OXIDISED Pt SURFACE

In EQCM experiments, especially when cyclic voltammetry is used and where an adsorbate or reactant is subject to oxidation during the cycle, it may be the case that the mass response that is observed is dependent on the processes that have occurred at earlier potentials in the sweep. Thus supplementary information can be obtained using potential step or open circuit potential decay methods where the mass, current and potential are monitored with time. This is especially useful in the study of the reaction between thiourea and the oxidised Pt surface. Earlier work in this laboratory on the oxidation of methanol and formic acid at Pt[39,158] showed that both reactants react rapidly with an

oxidised Pt surface, particularly when OH is present before irreversible oxidation of the surface. It has also been suggested that the irreversibly formed oxide at Au is not especially active for oxidation of TU[175] and this may also be true here which is why the current in the highest regions of potential (in Figures 5-2 and 5-4) passes through a peak and then declines, the decline being assumed to be a result of the beginning of the irreversible formation of the oxide at the electrode surface.

In a series of open circuit potential decay experiments, the Pt electrode was held at various constant potentials for a period of 5 minutes and then the circuit was opened and the potential and mass changes monitored after thiourea was injected into the solution. The potentials were chosen to be in the region where the electrode surface is oxidised, but also to span the whole range of surface oxidation from the initial stages to irreversible oxidation. The values chosen ranged from 0.65V to 1.14V, and each potential was reached by a step from a constant potential in the double layer region of potential to ensure that the initial state of the electrode surface before the step corresponded to a reduced Pt surface. The mass and potential were allowed to stabilise after the circuit was opened. Before thiourea was injected an injection of a similar volume of background electrolyte was made to ensure that the act of injection itself was not responsible for any of the subsequent responses that were seen. The injection of thiourea solution consisted of 1 ml of 0.05M thiourea in background electrolyte that was added to 50 mL of background electrolyte giving a final bulk concentration of thiourea of 1mM. However, the injection

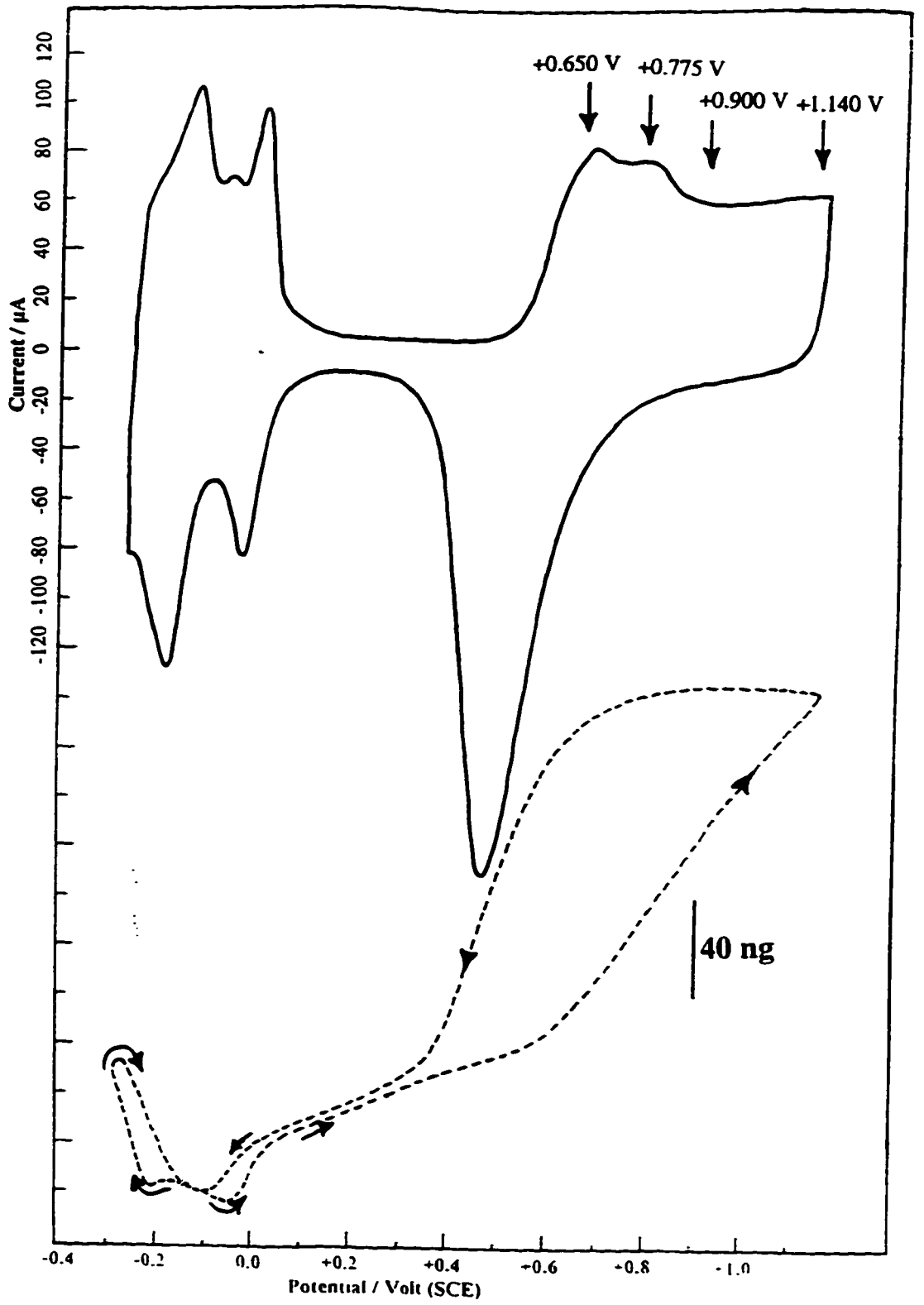

Figure 5-8:

Cyclic voltammogram (top) and mass response of an electrodeposited Pt with identification of the main potentials where the oxidation of Pt occurs. Scan rate: 20 mV/s. Background electrolyte: 0.2 M H_2SO_4.

was performed using a plastic delivery tube that was positioned close to the electrode surface and so the local concentration of TU close to the surface is likely to be higher than the final bulk concentration. Figure 5-8 shows the cyclic voltammogram and mass response for the electrode (in background electrolyte) that was used for these experiments, and the arrows indicate the potentials that were used for injection. The potential and mass transient results are collected in Figure 5-9. The potential decay curves and mass responses observed before the injection will be discussed first.

For the two highest potentials used (1.140V and 0.900V) there was a slow decrease of potential once the circuit was opened suggesting a partial reduction of the oxidised surface. Smaller decreases in potential were also seen when the circuit was opened at 0.75V and 0.65V, in fact, all potentials decreased to a value of 0.58V ± 0.02V. At the same time, mass decays were also seen. These were largest for the highest potentials and almost negligible for the two lowest potentials. The mass changes that are seen before TU injection are close to those expected for these changes in potential if the mass response in Figure 5-8 is inspected. Thus after opening the circuit at 1.140V, there is reduction of the oxidised surface and there is less reduction after the circuit is opened at 0.9V but there is still (particularly after the potential was opened at 1.140V) a significant fraction of the oxide still present at the surface at 0.58V. This can be seen by following the mass response from 1.140V to 0.58V on the negative going scan in Figure 5-8. For the two potentials 0.650V and 0.775V, there is a negligible mass response prior to reduction.

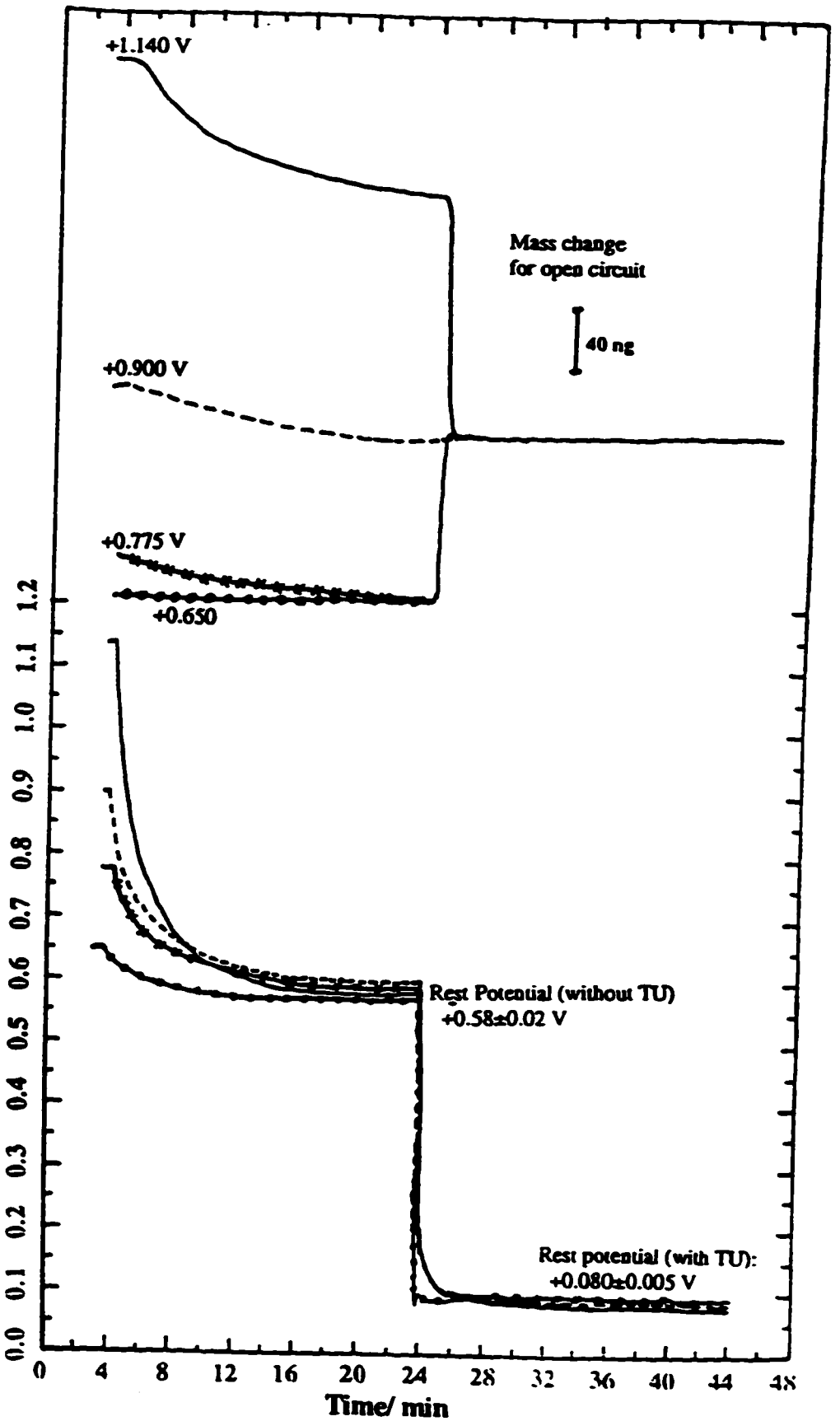

Figure 5-9:

Potential (bottom) and mass (top) transients for a Pt electrode. The electrode was first held at various constant potentials for a period of 5 minutes and then the circuit the circuit opened and the potential and mass changes are monitored after thiourea was injected. 1 mL of 0.05 M thiourea was injected. In 50 mL background electrolyte (final concentration: 1 mM thiourea).

After injection of thiourea with the electrode at open circuit, the potential decreased in all cases to a value that was roughly constant at 0.080 ± 0.005V. This indicates that thiourea is capable of reacting with the oxidised Pt surface, whether or not the surface is PtOH (as would be the case for the two lowest potentials) or the irreversibly formed oxide where OH or O is inserted into the Pt lattice. The final state of the surface at 0.080V is expected to correspond to a reduced Pt surface covered with an adsorbed residue that is derived from thiourea.

The mass responses are interesting and have been drawn in the diagram so that the final mass (at the final rest potential of 0.080V) is assumed to be the same, irrespective of the starting potential when TU was injected. In this case the data fall into three categories:

① For the highest potential, the addition of TU is seen to yield a net mass decrease.

② For the intermediate potential of 0.90V, there is no overall mass change after addition of thiourea.

③ When the potential was lower, there is a net mass increase after TU is added.

In general, the data correspond to expectations, if they are compared to the mass responses of Figure 5-6. That figure allows a comparison of the mass of a clean electrode (.....) at different potentials with the mass of a TU coated electrode in the H adsorption

region where the mass is flat, around point C in Figure 5-6. Careful inspection of the Figure shows that the mass of a clean Pt electrode is only larger than the mass of the TU coated electrode when a significant fraction of the electrode surface is oxidised. For the case of the two lowest potentials (0.650V and 0.775V) the mass of the electrode is expected to increase when the transition is made between a clean Pt electrode at those potentials and a thiourea coated electrode. In the case of 0.900V as the starting potential, the fact that there is a negligible mass change is reasonable because it is at about this potential that the mass of the clean electrode is comparable to that of a thiourea coated electrode (point C). At higher potentials than this the mass of a clean electrode is larger than the mass of a thiourea coated electrode at point C. Thus the overall transient data reinforce the picture of the effect of thiourea adsorption as represented in Figure 5-6. It is also clear that thiourea can react with both PtOH and the irreversibly oxidised surface so that thiourea is oxidised and the oxidised surface is reduced (and the potential decays to a value of 0.08V). However, the transients were not recorded on a time scale that was fast enough to give detailed information about the rates of the reaction.

5.7. MASS TRANSIENTS FOR TU ADSORPTION

In the open circuit potential decay experiments described above, the mass transients correspond to the changes observed when an oxidised surface is reduced in a reaction with TU. However, mass transients were also recorded for the adsorption process

at the two potentials used earlier, namely -0.15V (H adsorption region) and 0.20V (double layer region) where, especially at -0.15V, TU does not react. Current transients were also recorded. In these experiments, the final bulk concentration of thiourea after injection was 0.1 mM. The combined data are shown in Figure 5-10. At both potentials there is an anodic oxidation transient, as noted previously by Conway *et al* [194, 195] However, the time scale used in these experiments was much longer than that of Conway *et al* [194,195] who found that the anodic displacement of adsorbed H was completed within about 5s after addition of TU to give a final bulk concentration of 3 mM. The lower concentration used here presumably leads to an increase of the time scale required to give monolayer coverage. At 0.2V the current continues at a low level for some time and this may reflect a small steady state oxidation current. At -0.15V the current transient should contain a fixed amount of charge because it corresponds to anodic displacement of a fixed amount of H at the electrode surface.

The mass transients are also informative. As expected from the mass data shown in Figure 5-6, there is a mass increase upon adsorption at both potentials. The increase when the adsorption potential is -0.15V is larger than the increase when the potential is 0.20V. At 0.20V, the mass stabilises quickly to a plateau value whereas when the adsorption potential is -0.15V the principal part of the increase is rapid and then there is a further slow increase over a period of 10 minutes. The difference in mass profile between the two responses is hard to explain but there may be an effect of mass transport

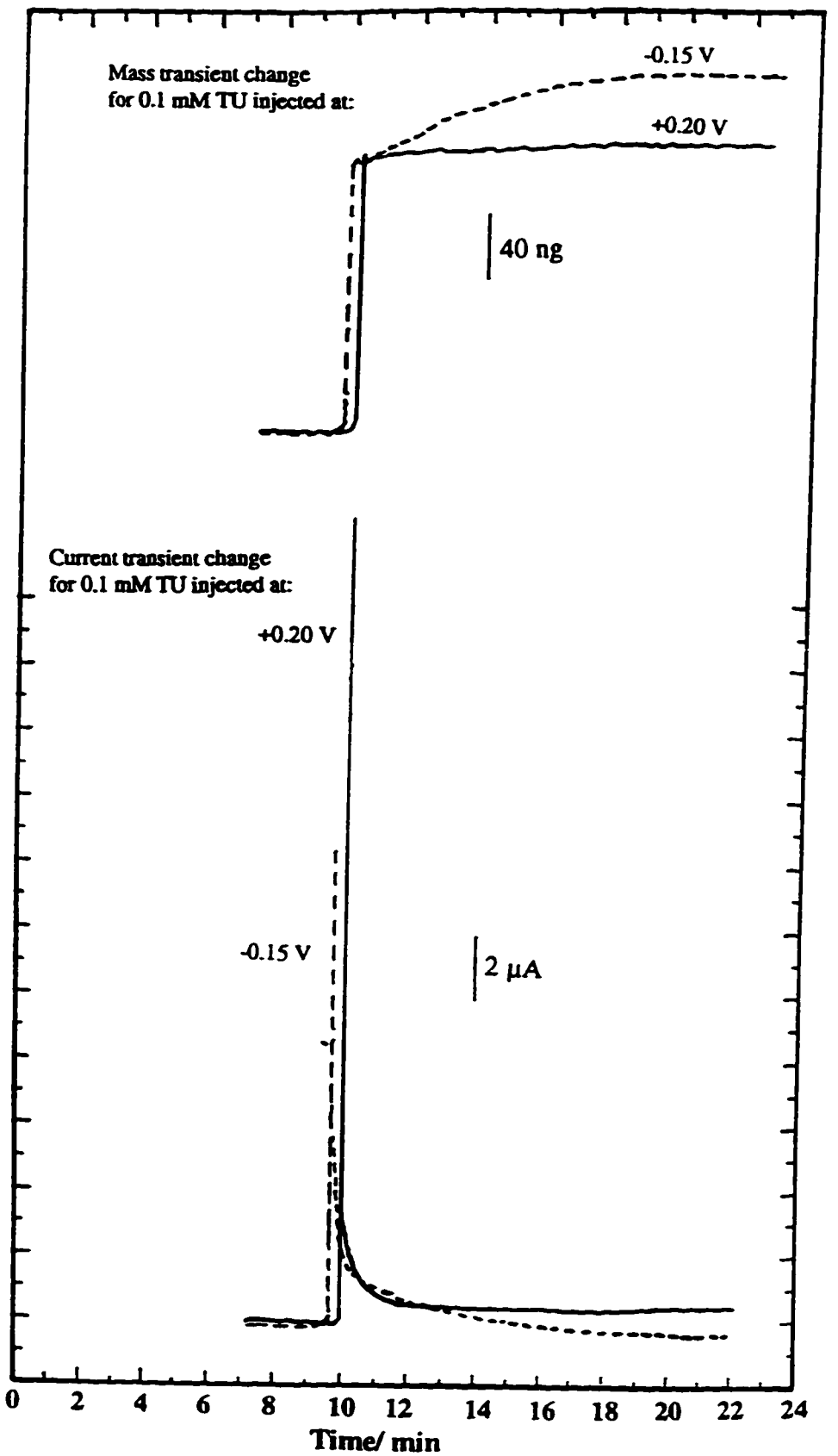

Figure 5-10:
Current (bottom) and mass (top) transients for thiourea injected in background electrolyte to give a final concentration of 0.1 mM thiourea. Transients are performed for potentials -0.15 V and +0.20 V.

because the solution was unstirred and the precise location of the injection may have been different between the two experiments. Nevertheless, the transient experiments lead to the same conclusion as the voltammetry. Adsorption of thiourea leads to a mass increase at the electrode surface whether it takes place in the double layer region of potential or in the H adsorption region.

5.8. DISCUSSION AND GENERAL CONCLUSIONS

The following general conclusions can be drawn from the work presented in this chapter.

5.8.1. Adsorption of Thiourea

Cyclic voltammograms, mass responses and mass transients recorded at constant potentials show that the adsorption process leads to a mass gain, whether or not this is in the double layer region of potential (where it is likely that TU reacts upon adsorption) or in the H adsorption region of potential where TU is adsorbed intact on the surface. As noted above, an adsorption process does not necessarily lead to an increase in mass because displacement of solvent and anions can also take place. The adsorption of thiourea may also change the coupling between the surface and the solution - impedance experiments would be necessary to identify this effect.

5.8.2. Oxidation of Thiourea - Double Layer Region of Potential

The experiments in this Chapter are not detailed enough to obtain mechanistic information about the oxidation of thiourea. However, some conclusions may be made. First, the peak in the double layer region of potential is more prominent when adsorption of thiourea has taken place in the H adsorption region (Figures 5-2, 5-3 and 5-6). This suggests that it corresponds to oxidation of adsorbed thiourea, although there may be some small component of oxidation of solution species as well.

The minimal mass change over the double layer region of potential when thiourea has been allowed to adsorb at the electrode surface in the H adsorption region (Figure 5-2) reveals that oxidation processes in this region results in adsorption of fresh reactant onto freed surface sites when TU is present in solution (Figure 5-2). It is only when there is a tiny bulk concentration of thiourea (1 μM) and re-adsorption is slow that a mass decrease is observed in association with the oxidation peak (Figure 5-6).

When the adsorption potential for thiourea is in the double layer region of potential, the oxidation peak in the double layer region is also less prominent (Figure 5-7). This is also true when there is merely an adsorbed product on the electrode (Figure 5-4). Figures 5-10 and 5-3 suggest that there is oxidation of thiourea at 0.2V and so the product of adsorption at 0.2V may well be the disulphide. It seems that the oxidation of the

disulphide is more difficult than that of thiourea and does not occur to the same extent in the double layer region, hence the smaller oxidation peak in this region. However, there is still some oxidation and it does lead to a mass loss when there is no TU in solution (Figure 5-7).

5.8.3. Oxidation of Thiourea - Pt Oxide Region of Potential

The large currents seen in the region where Pt oxide is normally present at the electrode surface (Figures 5-2, 5-6) illustrate that thiourea (and the products of its oxidation) can be oxidised at an oxidised Pt surface.

The extra information provided by the mass responses is the ability to locate where the irreversible oxidation of the Pt surface begins when the oxidation current is due to a mixture of surface oxidation and thiourea oxidation and thus cannot be used for this purpose (point B - Figure 5-4). The mass reveals blockage of surface sites by the adsorbed TU and that the rate of surface oxidation is higher when the onset is at a higher potential (Figure 5-4). The onset of irreversible surface oxidation (Figure 5-4, point B) is also correlated with a decrease in the thiourea oxidation current. The open circuit potential decay experiments reveal that TU can react with both the irreversibly formed surface oxide and the PtOH (the latter is thought to be more active for the oxidation) causing a reduction of the oxide and a mass change that depends on the starting potential (Fig. 5-9).

There is clearly much more information that can be obtained from the application of EQCM experiments to systems where adsorption occurs, such as kinetics of adsorption (perhaps in a flow cell system), providing rapid changes in frequency can be measured accurately and the application of a comparison of mass and charge may be more helpful than current and charge. Nevertheless this short study has shown that the EQCM is a useful technique for the study of strongly adsorbing molecules at electrodes.

* * *

Chapter 6:

Adsorption of Chloride on Electrodeposited Platinum Electrodes

---

6.1. INTRODUCTION

The last two decades have seen an extensive study of the electrolysis process of the halides, mainly the chloride[201-203]. The study of the adsorption of chloride is dictated by the industrial and economic importance of the chlor-alkali process in the chemical industry. As the process consumes vast amounts of electricity there is a considerable economic benefit to be gained from an understanding of the mechanism of chlorine evolution and from the development of electrodes which are resistive to the aggressive action of chloride and chlorine, and which evolve chlorine at low overpotentials, thus decreasing energy consumption. There has also been much interest in this process from

an environmental point of view. Therefore, researches have been made in order to design electrodes for efficient production of chlorine and NaOH and to better understand the fundamental electrochemistry of chlorine evolution. The dimensionally stable anode (DSA) based on a mixture of RuO_2/TiO_2 oxides is one result of this research effort and is now in widespread use for the chlor-alkali process[201].

6.1.1. Electrochemistry of Halide Anions

Adsorption of halide anions (Cl^-, Br^-, I^-) at Pt electrodes has been studied by many researchers such as Breiter[204,205], Bagotzky[206] and Conway[207-210]. One particularity of these studies is that they have demonstrated that halide anions can adsorb at very low concentrations (even lower than 10^{-7} molar) at smooth Pt surfaces in very clean solutions[208]. Halide adsorption is visible at Pt from two effects. First in the H upd region, the competitive adsorption of halides causes a redistribution of the H upd peaks. Second, in the oxide formation region at Pt, the presence of adsorbed halides suppresses oxide formation by blockage of surface sites and shifts the onset of surface oxidation to more positive potentials.

The isotherms for competitive electrochemical adsorption of OH^- and O species in the surface oxide film, relative to that of X^- ions (where X^- represents a halide), have been evaluated quantitatively by Novak and Conway[208], by means of a micrometer titration

procedure. According to these authors, chloride selectively blocks the initially deposited OH monolayer at Pt while bromide and iodide block the formation of the surface oxide non-selectively over a wide range of potentials. In other words, bromide and iodide block the initial OH monolayer and the irreversibly formed oxide where OH is inserted into the Pt lattice. The state of charge (electrosorption valency - which represents the amount of charge that is transferred to the anion upon adsorption) is then different for bromide and iodide in relation to that of adsorbed chloride, the latter ion exhibiting lateral interactions due to the partial charge of the adsorbed chloride, whereas bromide and iodide are assumed to have zero charge when present on the surface.

Among all the halide reactions, the reaction of chlorine evolution is one of the most investigated because of its technological impact in the field of the electrocatalysis and in the environment, as noted above. Despite a large amount of literature devoted to the chlorine/chloride system, the story of the mechanism of chlorine evolution has not been entirely clarified. For example, the review paper on oxide electrodes by Trasatti[203] has listed a minimum of 10 mechanisms depending on the type of electrode used. However, there is a fact that all the mechanisms proposed include *a common step of the adsorption as the primary step*, but what happens to the adsorbed chloride remains somewhat uncertain.

The following mechanistic steps have been proposed by several authors for Cl^-/Cl_2

system and may be generalized for the other X^-/X_2 systems:

1) $X^- \rightleftharpoons X_{ad} + e$ (1a)

$X_{ad} + X^- \rightarrow X_2 + e$ (1b)

2) $2X^- \rightleftharpoons 2X_{ad} + e$ (2a)

$2X_{ad} \rightarrow X_2$ (2b)

Both these mechanisms involve a neutral halogen atom. The standard potential for $Cl^-/Cl_2(g)$ system is +1.359 V (NHE). This potential is higher than that of Br^-/Br_2 (aq) and I^-/I_2 (aq) systems, which are +1.087 V and +0.615 V, respectively. This suggests that iodide should be more likely to adsorb than bromide, and that chloride should be least adsorbing. Knowing these potentials and the surface oxidation behaviour of Pt, one might suggest that the evolution of X_2 (Cl_2, Br_2 and I_2) should take place on an electrode surface completely covered by at least a monolayer of oxygen (Pt-OH or Pt-O). This is not the case. It has been demonstrated for the Cl^-/Cl_2 system that chloride can adsorb at a Pt electrode that is completely free from any oxide, and the kinetics of this system showed that chloride adsorbs *competitively* with the formation of the oxide film. For Br^-/Br_2 and I^-/I_2 systems, another factor that will influence the adsorbability of bromide and iodide is the solubility of the corresponding halogen. The solubilities of these two compounds at 25°C are 0.18 M and 0.0020 M for bromine Br_2 and iodine I_2, respectively[211]. Therefore, if any saturation is suspected for these systems, one must take into account the standard

potentials for the half-reactions $Br_2(l) + 2e^- = 2Br^-$ and $I_2(s) + e^- = 2I^-$. These potentials are +1.065 V and +0.5355 V for saturated $Br^-/Br_2(l)$ and $I^-/I_2(s)$ systems, respectively [211].

6.1.2. EQCM Literature Review on Halide Anions

Surprisingly, there have been few detailed EQCM studies of the adsorption of halides at Pt electrodes. The iodide/iodine system has been investigated by Shu and Bruckenstein[79] using an EQCM apparatus and a rotating ring disk electrode, both with a platinum electrode. Another EQCM study of halide anions is that of Deakin[212] for Br^- and I^- but this study was carried out at a gold electrode. One EQCM study of chloride anions on a Pt electrode is that of Hillman *et al* [213] who studied chloride electrolysis at high concentrations (0.9 M NaCl in 0.1M HCl) in order to investigate what they called "*the bubble growth/ nucleation*" phenomenon. i.e. a study of the formation of bubbles upon evolution of Cl_2 was their objective, rather than the investigation of the adsorption of halides. Their cyclic voltammetric study involved chlorine and hydrogen evolution but some conclusions were reached concerning adsorption of chloride. Birss, Chang and Segal[155] also briefly investigated the electrochemistry of chloride at a Pt electrode at a concentration of 3.5 mM in 0.1M H_2SO_4 (one cv only was shown).

The present EQCM study is an attempt to understand the effect of adsorbed halide ions on the mass responses at large area electrodeposited Pt electrodes. It is known that

the halide adsorption influences the H upd peak distribution and suppresses oxide formation, but previous studies using the EQCM have either not focussed on these aspects, or used high concentrations of chloride so that H upd and oxide formation currents are obscured by the large currents due to H_2 evolution or Cl_2 evolution.

6.2. EFFECT OF THE POTENTIAL ON THE ADSORPTION OF CHLORIDE

6.2.1. Adsorption of Chloride at Concentrations Equal to and Below 1mM

As noted above, the adsorption of chloride ions at Pt electrodes is apparent even at very low concentrations (10^{-7} M) and is revealed by the shift and re-distribution of the H upd current peaks[208], although the coverage of adsorbed H does not change. It has been shown in Chapter 4 that the ions of background electrolyte do not have a significant effect on the mass response in the H upd region, and so a comparison of the behaviour of chloride ions with those of the background electrolyte may be instructive. The adsorption was investigated, principally for the H adsorption region of potential, for two concentrations of chloride (10^{-4} M and 10^{-3} M) which were added to the background electrolyte of 0.2M H_2SO_4.

Figure 6-1 shows the background response of a freshly plated Pt electrode in 0.2M H_2SO_4 for reference purposes, together with a full cv and mass response for the same

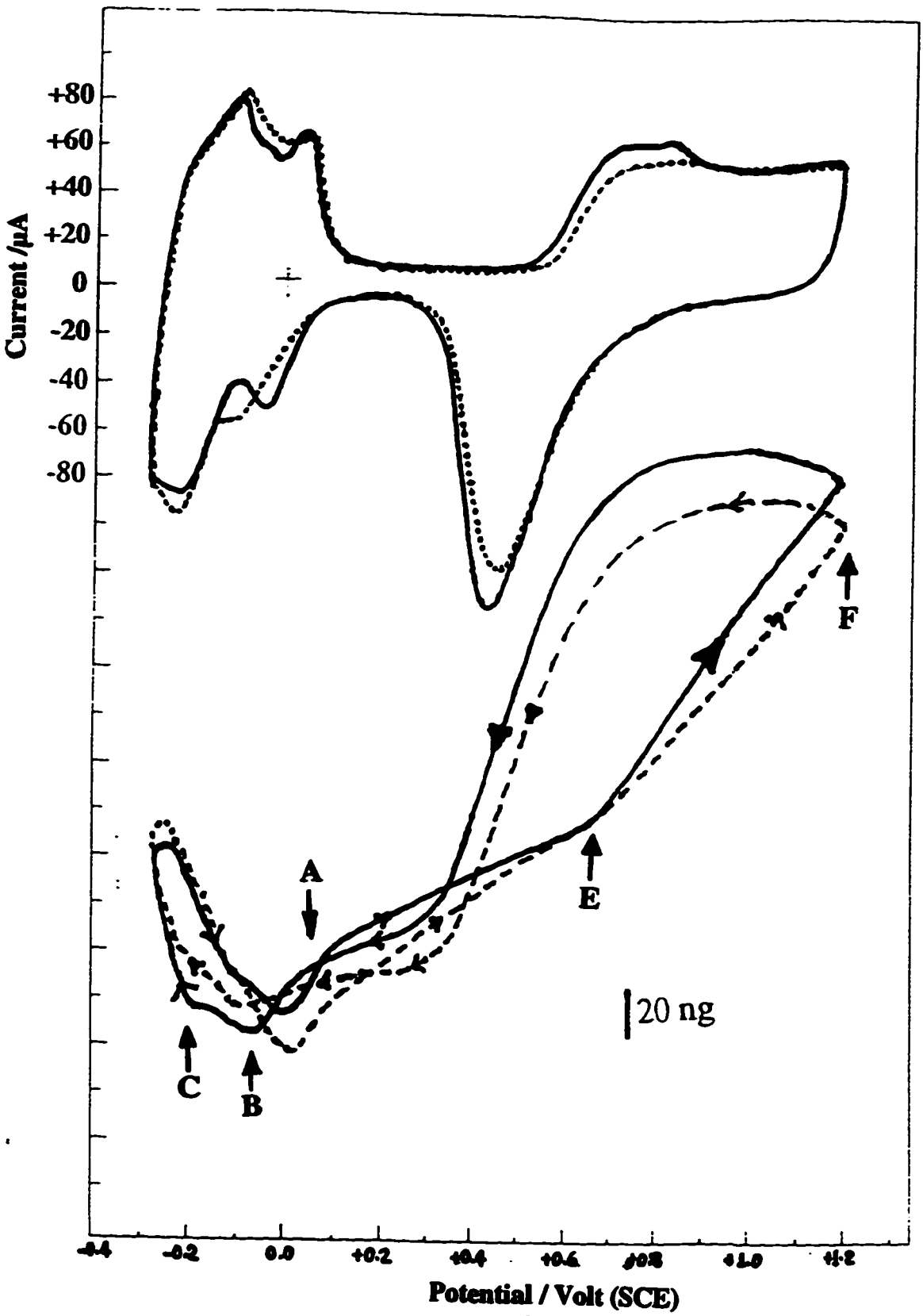

Figure 6-1:

Cyclic voltammetry (top) and mass response (bottom) for an electrodeposited Pt electrode in 0.2 M H_2SO_4 (full lines) and in 10^{-4} M KCl/ 0.2 M H_2SO_4 (dashed). Scan rate 20 mV/s.

electrode recorded in a solution to which sufficient chloride had been added to give a final concentration of 10^{-4} M. Note that the mass responses are displayed at relative positions that are arbitrary. The position of the responses is not meant to imply that where the curves cross the mass is the same.

In general, the voltammogram shows the expected effects. There is a slight shift of the H upd peaks as a result of adsorbed Cl^- (compare dotted and solid lines) and at the other potential extreme, the onset of surface oxidation is delayed by a small amount because of the presence of adsorbed chloride. The smaller oxide reduction peak in the presence of the halide shows that less oxide was formed in this case for a scan to the same upper limit.

The mass responses are a little more complex to examine and so Figure 6-2 shows the H upd region in more detail for the chloride containing solution. The background response in the absence of chloride (Figure 6-1) shows the features described earlier in Chapter 4 if the response is considered beginning at 0.2V and proceeding in the negative direction. The onset of H upd formation causes a change in the slope of the decreasing mass (point A) and then there is a minimum of mass at point B, coincident with the first current peak. The mass then increases and changes slope again at point C coincident with the second, most negative current peak. These changes are reversed when the potential scans in the positive direction.

If the same region is examined in Figure 6-2, it can be seen that the transition between the double layer region of potential and the H upd region (point A in Figure 6-1) is almost not discernible in the chloride solution when the potential is scanned in the negative direction, but the mass minimum (B) is present and is shifted to a more negative potential, in parallel with the shift in the first H upd peak (this is revealed in Figure 6-1). The change in slope at point C also shifts slightly in the presence of chloride. The mass changes in the positive going scan are also slightly affected by chloride with the most noticeable change being a more pronounced minimum (point D, Figure 6-2) in the presence of chloride. There is negligible hysteresis in the double layer region in the presence of chloride when the potential is restricted to the upper limit shown in Figure 6-2 to ensure that no significant surface oxidation occurs.

The full cv (Figure 6-1) also allows an investigation of the effect of adsorbed chloride on oxide formation and reduction. In fact the mass response reveals little effect at this level, in agreement with the voltammogram. The dotted line in the mass response in the region of surface oxidation seems to show a slower growth of the oxide in the presence of chloride as the slope of the mass increase (point E to point F) is less than for the absence of chloride. The increase in mass from point E to the upper limit of the scan is also smaller than when chloride is absent showing that less oxide is formed. This is in agreement with the smaller oxide reduction peak in the voltammogram. One final point is of interest. That is that the mass response for chloride solutions does not show any loss

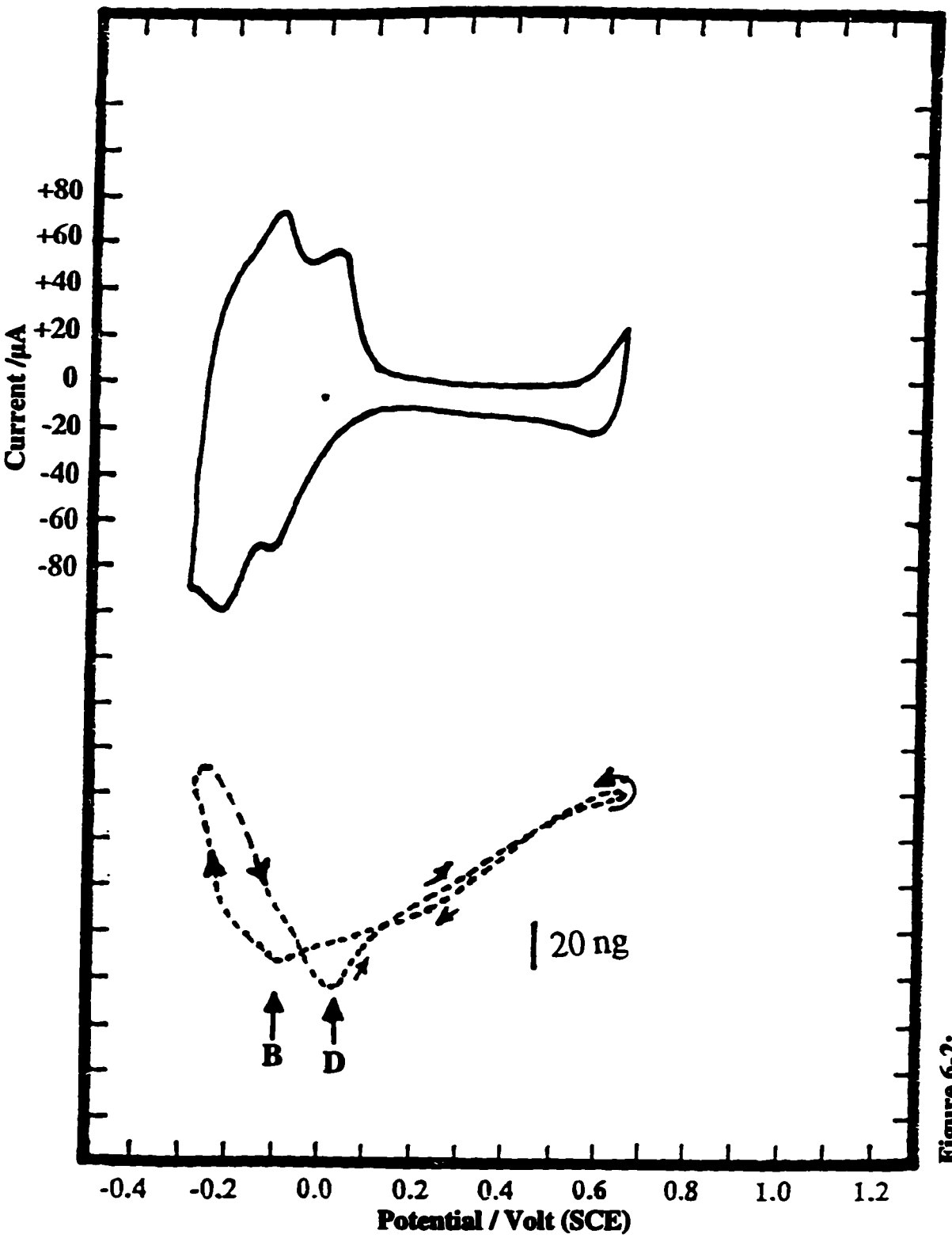

Figure 6-2: Cyclic voltammogram (top, full lines) and mass response (bottom, dashed lines) for an electrodeposited Pt electrode in 10^{-4} M KCl/ 0.2 M H_2SO_4. The potential was taken between the hydrogen adsorption/ desorption and the double-layer onset. Scan rate: 20 mV/s.

of material into solution because it forms a complete loop.

When the concentration of chloride is increased to 10^{-3} M, the results of Figure 6-3 are obtained when the potential is restricted to the H upd and double layer regions of potential. The H upd current peaks show further shifts with increasing adsorbed chloride (although this is difficult to see). The mass response still shows a decrease as the potential proceeds negatively from 0.2V, but the transition between the double layer and the beginning of H upd coverage (point A in Figure 6-1) is hardly detectable. After a steady decrease the mass reaches a flat region (G) as the first H upd peak is seen and then increases as the second peak is reached. Otherwise there are no dramatic changes as the chloride concentration has increased by a factor of 10. The mass response over the double layer region reveals a steady increase and it is interesting to note that although there is some surface oxidation in this Figure (shown by the small oxidation current at the upper limit) the reduction of this current is very broad and very hard to distinguish from the double layer current. The reduction of the initial stages of surface oxidation seems to be inhibited by the presence of adsorbed chloride.

From these three Figures, we can conclude that as noted for background electrolyte effects, there is some effect of chloride adsorption on the mass response at bulk concentrations of 10^{-3} M and 10^{-4} M (1 mM and 0.1 mM), but these changes are small and subtle, and interpretation of results is complicated by the fact that different electro-

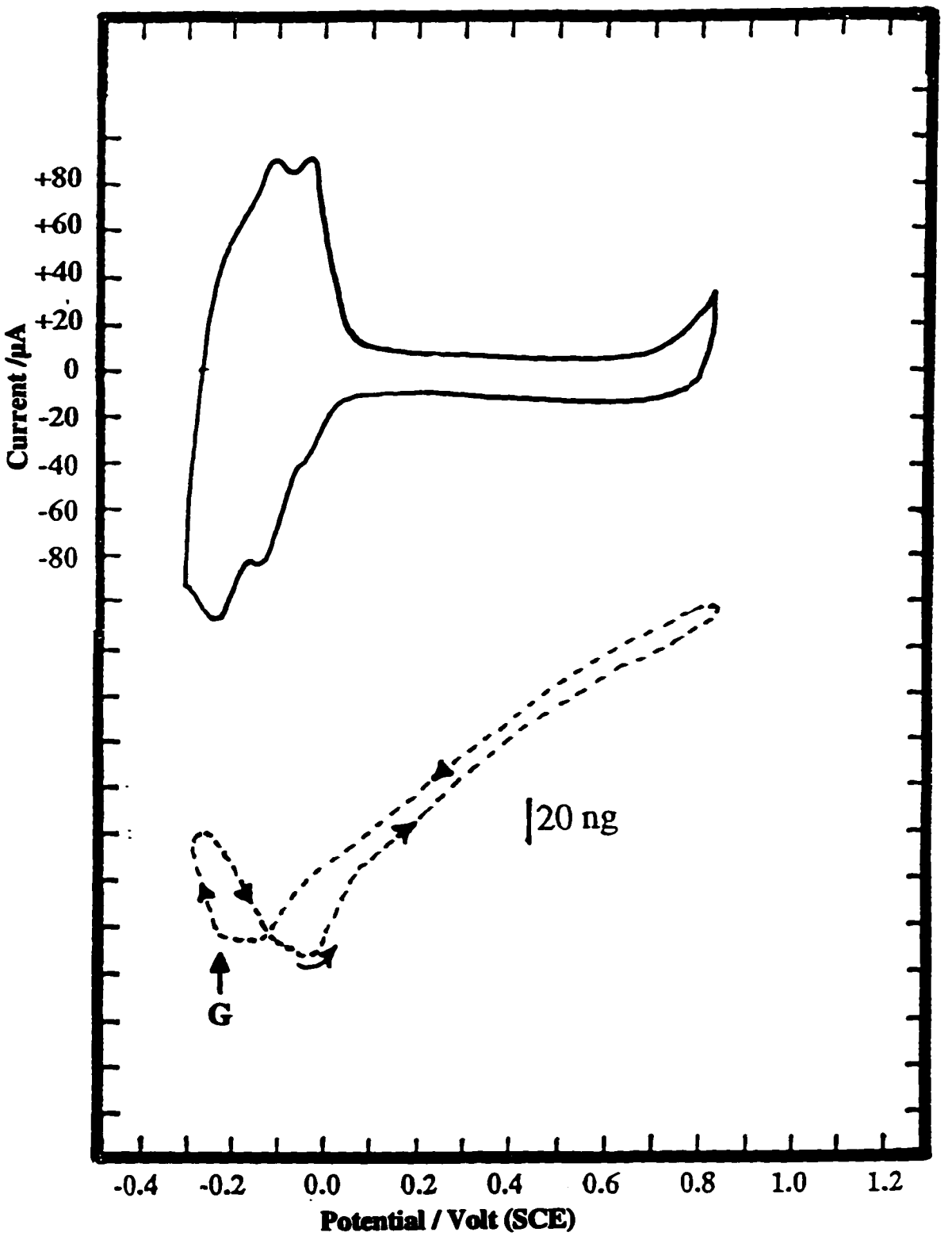

Figure 6-3:

Cyclic voltammogram (top, full lines) and mass response (bottom, dashed lines) for an electrodeposited Pt electrode in 10^{-3} M KCl/ 0.2 M H_2SO_4. The potential was taken between the hydrogen adsorption/ desorption and the double-layer onset. Scan rate: 20 mV/s.

deposited electrodes are slightly different in their mass responses. For these concentrations of chloride, the mass response is very stable to cycling and may be extended to potentials in the double layer region and cycled many times with very little effect.

6.2.2. Adsorption of Chloride at Concentrations Above 1mM

When the concentration of chloride ion is increased above 1mM, more significant changes begin to appear in the mass responses, especially at more positive potentials. The results of two cycles to an upper potential limit of 1.15V in a solution containing 2.5 mM chloride are shown in Figure 6-4. The H upd peaks are seen to be compressed further towards the negative potential limit and a third small peak is visible close to 0.0V. This is consistent with previous work[206]. Oxide formation is shifted to more positive potentials and there is less oxide formed than for the same electrode in the absence of chloride (compare the relative heights of the H upd peaks and the oxide reduction peak with those of the background scan in Figure 6-1).

The mass response also shows some changes when compared to the result at 1mM Cl^-. The structure in the H upd region is further compressed and reduced in size but the response is still perfectly stable if the upper limit of the scan is restricted to the end of the double layer region. When this range is exceeded, the mass increases again as oxide is

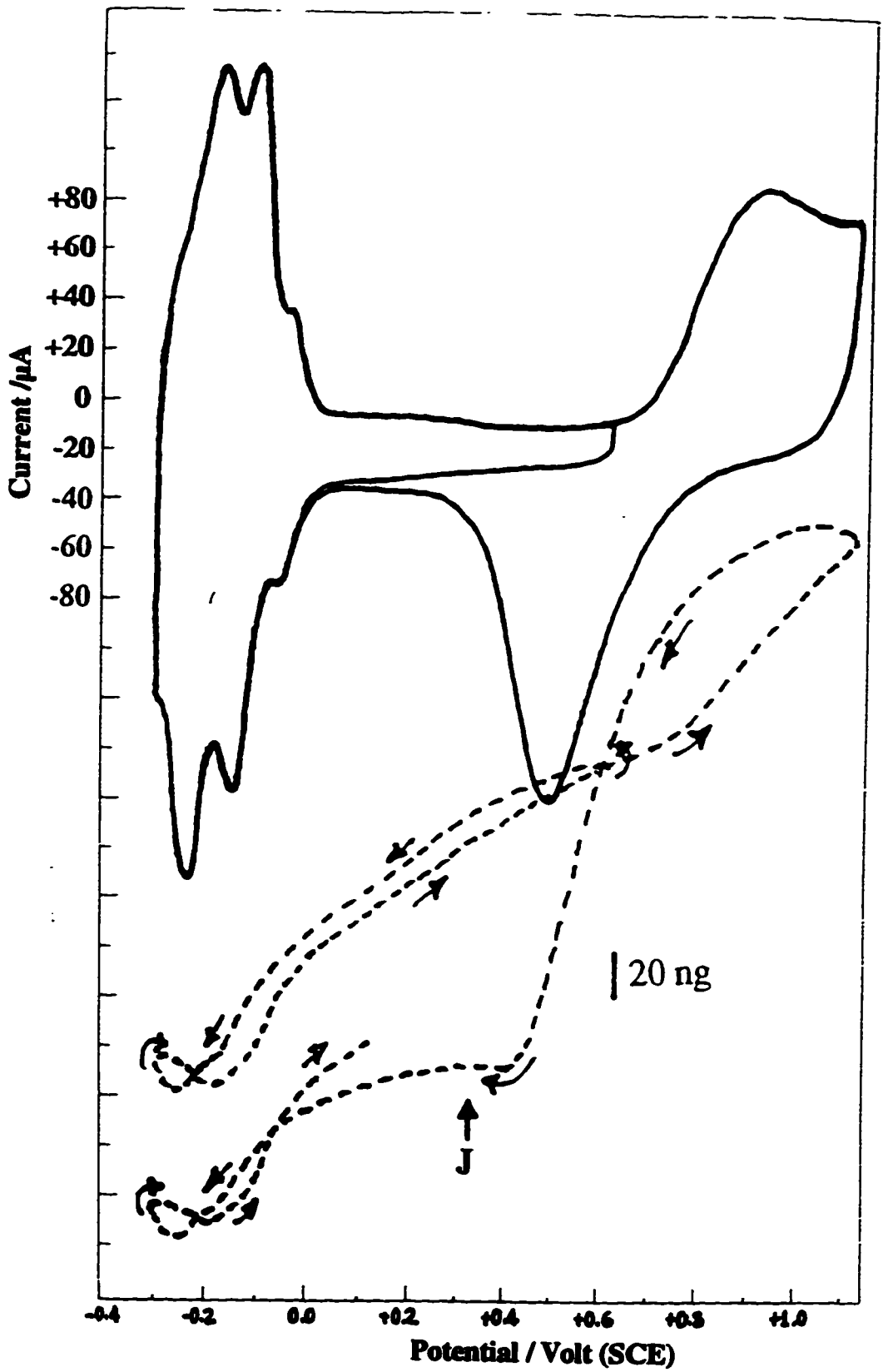

Figure 6-4:

Cyclic voltammogram (top, full lines) and mass response (bottom, dashed lines) of an electrodeposited Pt electrode in 2.5 mM KCl/ 0.2 M H_2SO_4. Scan rate: 20 mV/s.

formed and decreases as the potential direction is reversed and oxide reduction occurs. This decrease is rapid and then reaches a small plateau (labelled J) before declining further to the end of the scan. Now, in contrast to earlier results the mass loop does not close after one full cycle to an upper potential limit of 1.15V, suggesting a loss of material into solution after a full cycle.

When the chloride concentration is increased to 12.5 mM, the voltammogram (Figure 6-5) shows further changes that are expected from literature comparisons, especially the further shift of H upd peaks to more negative potentials and a shift of the oxide formation current to a point that is 0.2V more positive than the onset point in the background electrolyte. This gives a much broader double layer region. As a consequence of this, and the fact that the upper potential limit was held to the same value as for the background electrolyte, less oxide is formed in this case, as the oxide reduction peak shows.

In the mass response, several further changes are visible in addition to those noted at the lower concentration of 2.5 mM. The extra chloride has removed the mass increase normally seen at the negative scan limit together with the structure that is present in this region in background electrolyte. As a consequence, the mass minimum is at the extreme lower scan limit. There is a sharp increase as the potential increases and a change in slope as the potential reaches the double layer region.The electrode can be cycled between -

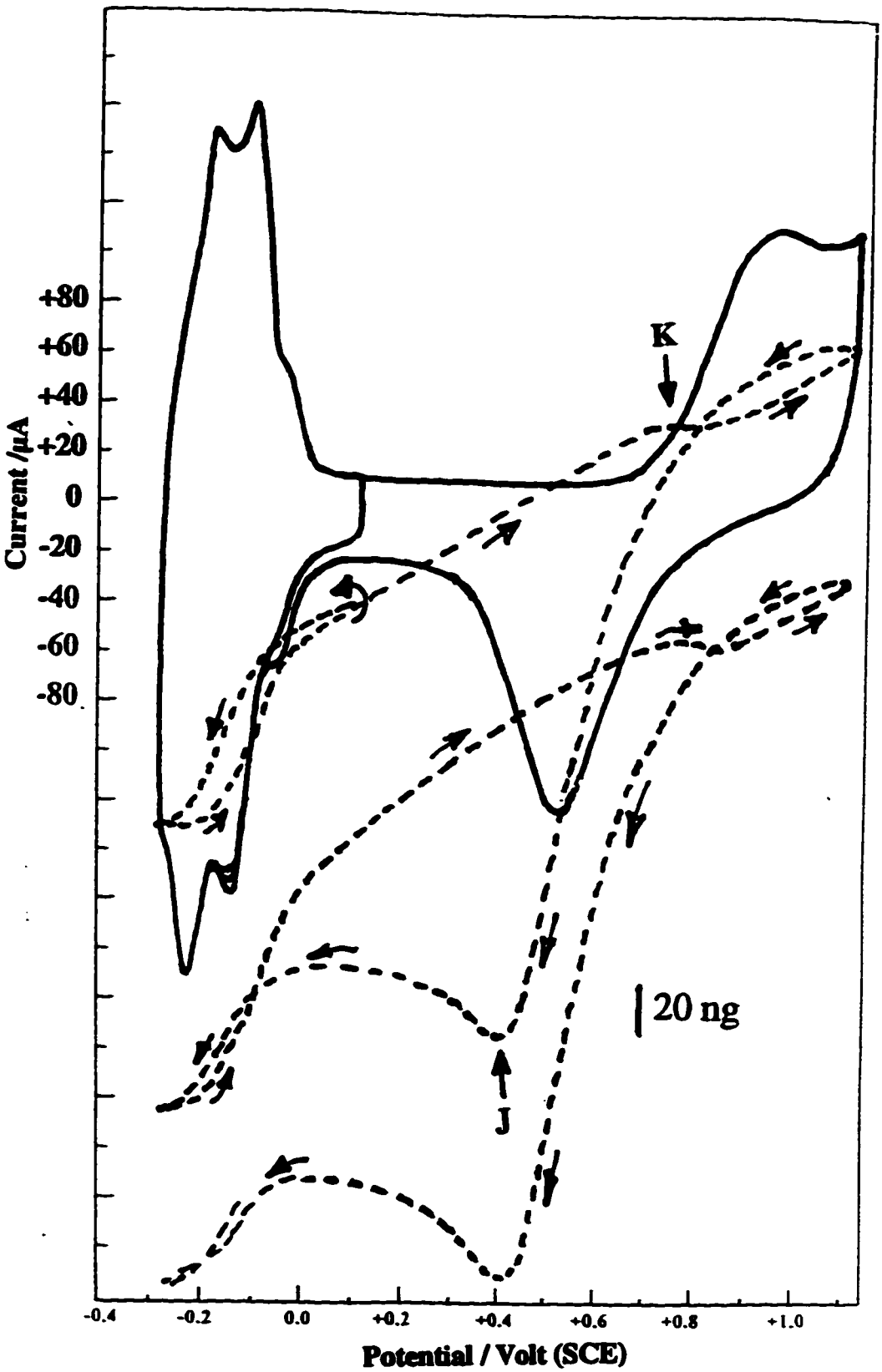

Figure 6-5:

Cyclic voltammogram (top, full lines) and mass response (bottom, dashed lines) of an electrodeposited Pt electrode in 12.5 mM KCl/ 0.2 M H_2SO_4. Scan rate: 20 mV/s.

0.25 V and 0.15V (a potential that is just inside the double layer region) for several cycles with no change whatsoever in the mass response. As the potential enters the double layer region there is a steady increase in mass, until the surface oxidation begins. At this point there is a small plateau in the mass response (K) and then the mass increases again until the scan direction reverses. However, this increase is less than that seen for 2.5 mM chloride (Figure 6-4) and then as the potential reverses, the mass decreases, slowly at first but then more rapidly as oxide reduction occurs. A minimum is reached just after the peak of the oxide reduction current, but then rather than the plateau (J) that was seen at this point in Figure 6-4 for 2.5 mM chloride, the mass increases again slightly before decreasing to the lower scan limit. The mass at the end of the cycle is significantly less than it was at the start. A second full cycle shows the same features, except that the overall mass loss after the second cycle is less than that after the first cycle.

A doubling of the chloride concentration to 25 mM produces a further change of the mass. The result seen in Figure 6-6 is obtained. There are now three H upd peaks that are clearly visible and as the figure shows, the mass could be cycled to 0.65V with the mass response being reproducible. The amount of oxide formed is not affected to any great extent by the extra chloride present. The mass response shows one change from the result seen at the lower concentration of 12.5 mM. There is still an increase over the H upd region and an increase at a lower rate over the double layer region, but the onset of oxidation of the Pt surface actually causes a mass decrease and then no further increase as oxide coverage increases (as was the case for all the lower concentrations used so far).

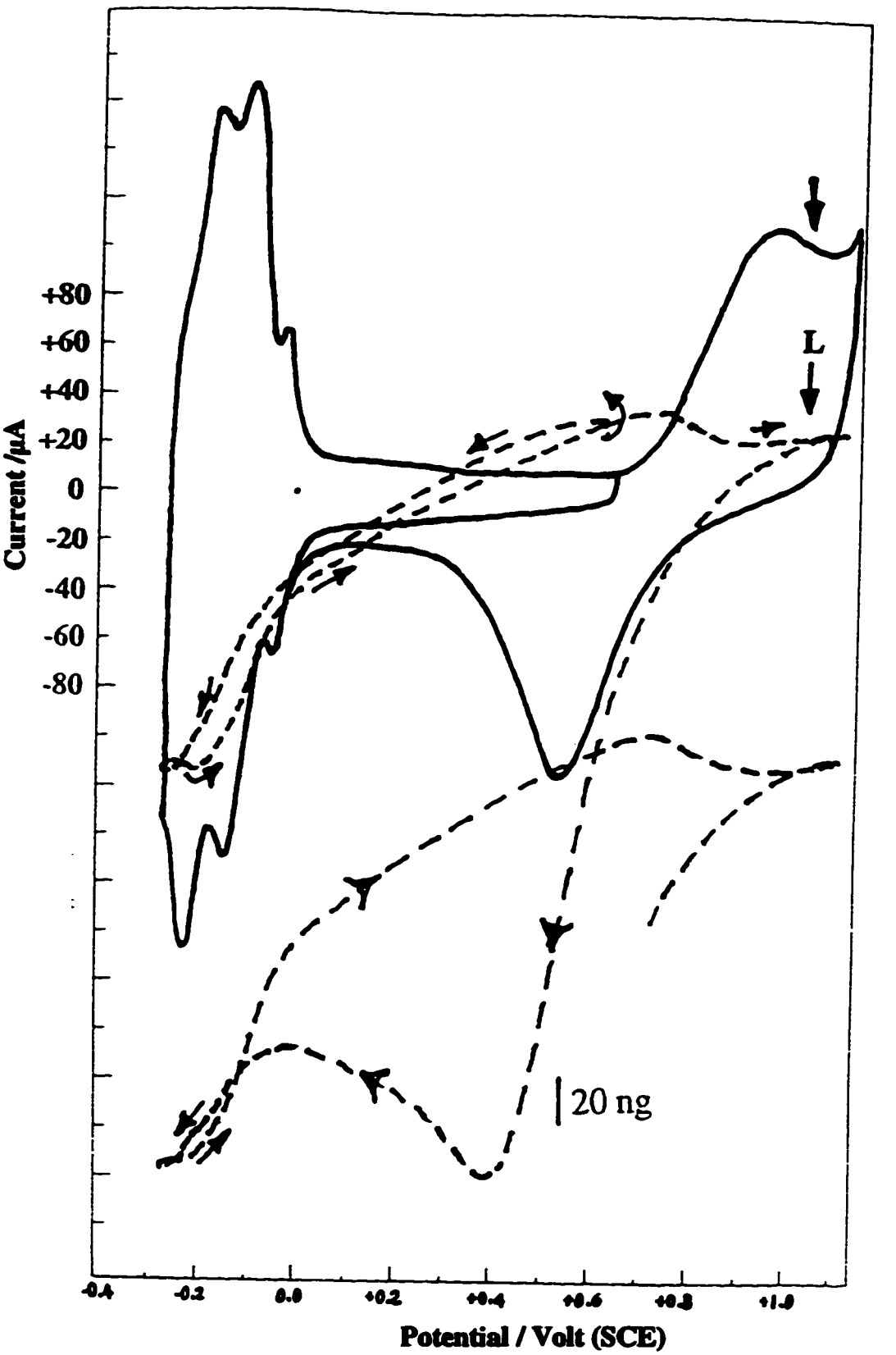

Figure 6-6:

Cyclic voltammogram (top, full lines) and mass response (bottom, dashed lines) of an electrodeposited Pt electrode in 25 mM KCl/ 0.2 M H_2SO_4. Scan rate: 20 mV/s

In fact the development of the oxide leads to no mass change at all, just a plateau (L). The remainder of the cycle shows the mass loss as the potential is scanned negative and then the minimum and the slight recovery after the oxide reduction peak and before the final decrease. The mass loss over the cycle is larger than it was for the 12.5 mM chloride solution, but as for that solution, a second cycle does not produce as large a mass loss over the cycle (data not shown in the Figure).

The next experiment in this series is shown in Figure 6-7. At 50 mM added chloride in 0.2M H_2SO_4, there are no significant changes in the voltammogram but another change is seen in the mass response. This is again associated with the oxide region and now, after the potential passes from double layer region and surface oxidation starts, the decrease in mass has increased relative to the lower concentration and the plateau region has shortened. The mass in the region of the H upd and double layer potential ranges is no different from the lower chloride. The overall mass loss over the cycle has increased again with chloride concentration.

For all the Figures seen so far, there has been little evidence of chlorine production in the voltammetry, particularly as the upper potential limit was kept at 1.15V. When the chloride concentration is increased to 0.322M there is definite voltammetric evidence of the evolution of chlorine and the reduction of molecular chlorine. This is revealed by the large sharp current increase at the upper scan limit (labelled M) and the sharp reduction

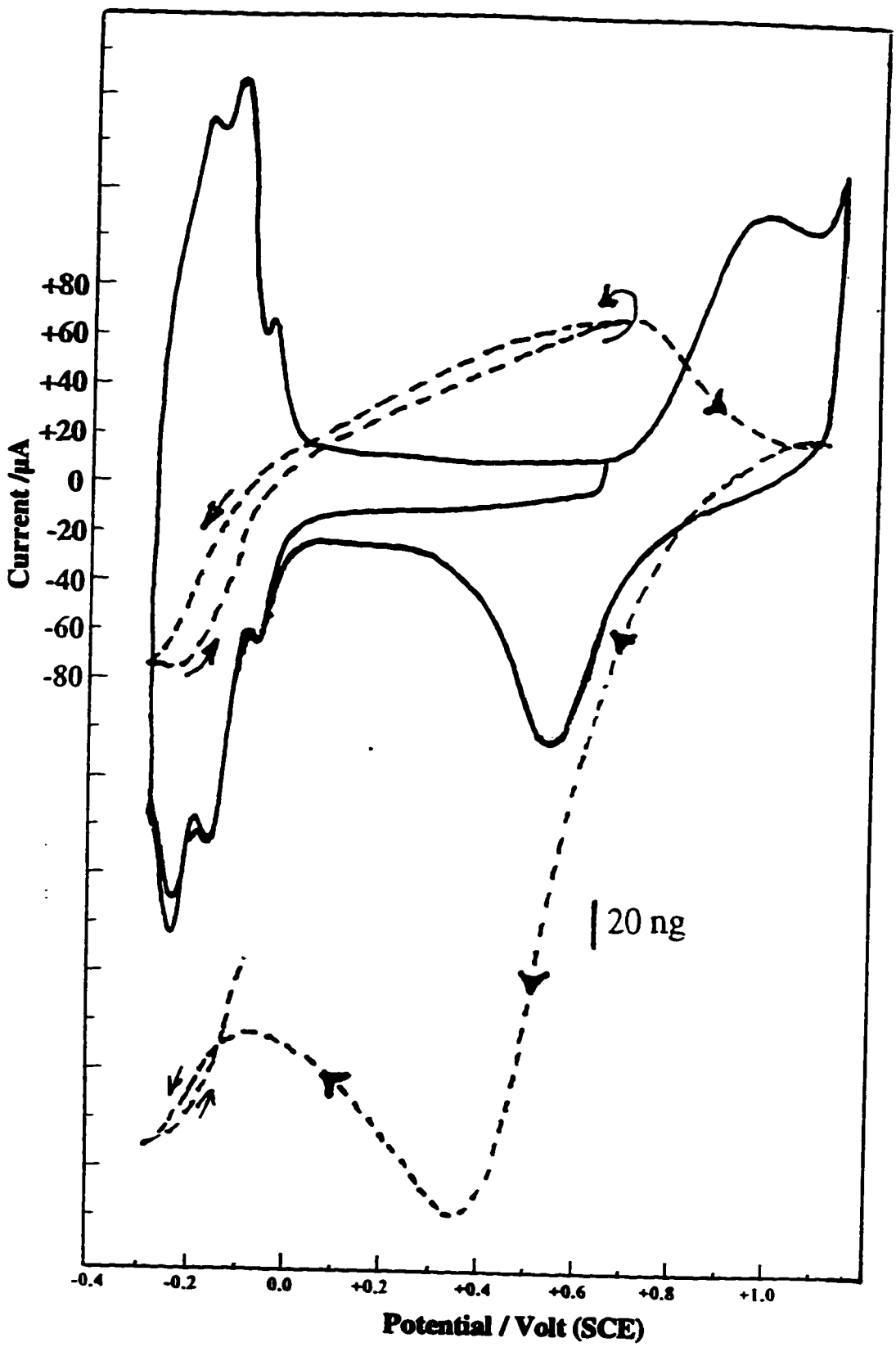

Figure 6-7:
Cyclic voltammogram (top, full lines) and mass response (bottom, dashed lines) of an electrodeposited Pt electrode in 50 mM KCl/ 0.2 M H_2SO_4. Scan rate: 20 mV/s

peak (labelled N) seen immediately after the scan is reversed (Figure 6-8). There are no other significant changes in the voltammetry. In fact, the mass also reveals few differences between the previous result at 50 mM and this one, except for the fact that the mass decrease which occurs as the oxidation current rises after the double layer region is larger than at the lower concentrations, although it does seem to slow down as chlorine evolution appears in the voltammogram. The large decrease continues after the scan reversal and actually disappears off the scale at the bottom of the diagram. The difference in this experiment is that after the first cycle the potential was reversed but the full cycle was not repeated, instead the potential was only allowed to proceed until the end of the double layer region of potential and then it was cycled for nine further cycles over the region of H upd and the double layer. The effect of this experiment is that the mass slowly increased with this cycling and then stabilised after 7 cycles, although the final mass trace still reveals a significant mass loss when compared to the first cycle.

6.3. DISCUSSION AND GENERAL CONCLUSIONS

The series of experiments in this chapter are not concerned with the mechanism of chlorine evolution but more with the adsorption of Cl^- and its effects in different regions of potential. As usual with Pt, the electrochemistry may be divided into three regions of potential and the discussion applied to each region in turn.

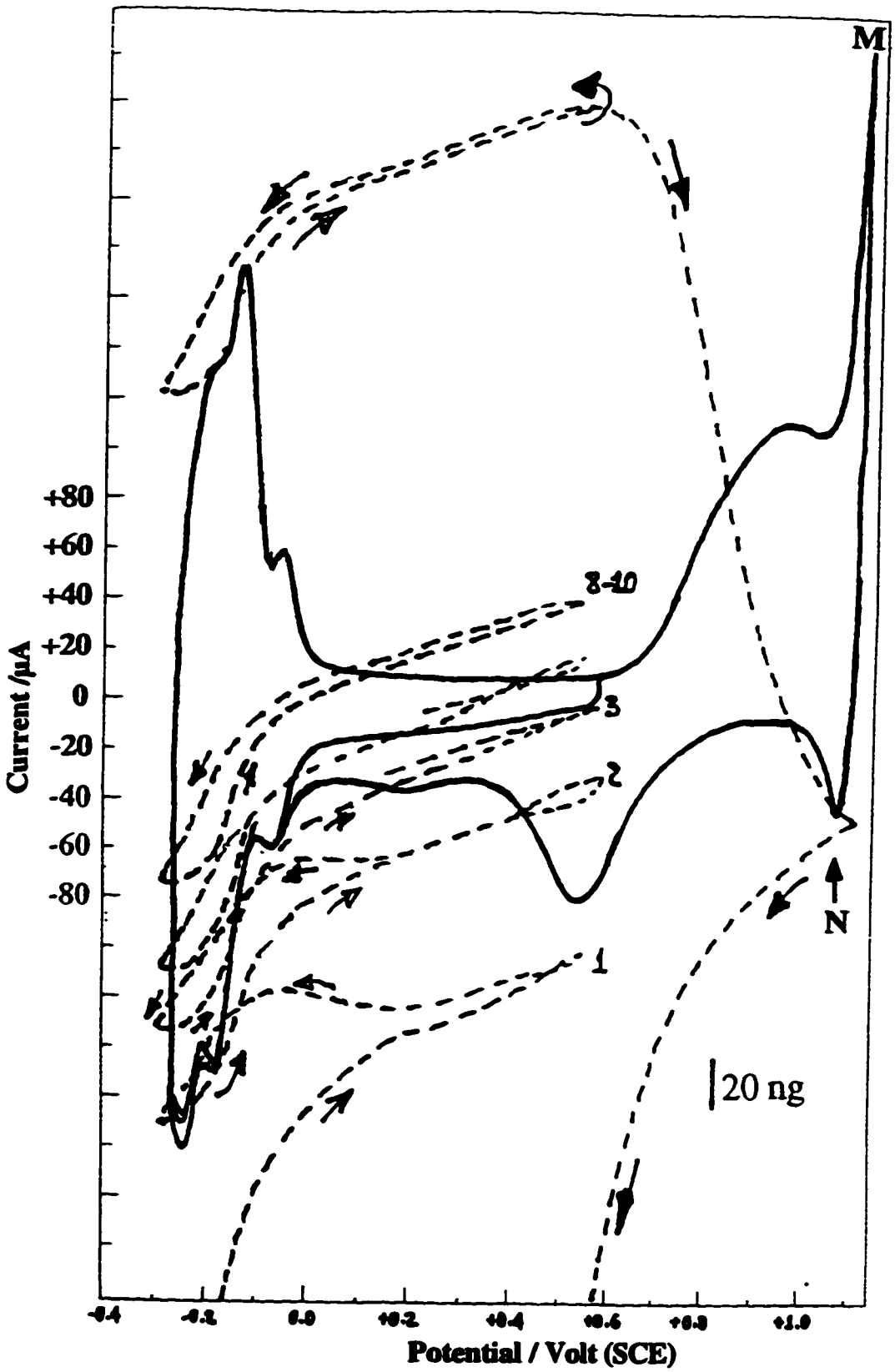

Figure 6-8:

Cyclic voltammogram (top, full lines) and mass response (bottom, dashed lines) of an electrodeposited Pt electrode in 0.322 M KCl/ 0.2 M H_2SO_4. Scan rate: 20 mV/s

6.3.1. Chloride Adsorption in the Region of Adsorbed Hydrogen

Chapter 4 has presented some results of studies of the mass changes in this region and it seems that the mass (or frequency) changes are associated with the interaction between adsorbed H and water and that there may be an influence of anions as well. There are several changes that occur in the H adsorption region in background electrolyte :

① An increase in the slope of the mass decrease (point A, Figure 6-1) when H coverage begins.

② A mass minimum (point B, Figure 6-1) at the first H upd peak.

③ A mass increase (point C, Figure 6.1) as the coverage of weakly bound H upd increases.

The presence of adsorbed chloride produces several changes in the mass responses. In the concentration range from 0.1 to 2.5 mM the first effect of chloride is that the change in slope at point A (Figure 6-2) becomes more difficult to see and there is a flattening of the response at point G (Figure 6-3). The increase in mass (frequency) negative of point C also gets smaller, and by the time the concentration of Cl^- reaches 2.5 mM, there is only a tiny increase in the mass at the very end of the scan. When 12.5 mM Cl^- is reached, the mass minimum is at the negative potential limit and the mass decreases all the time as the H coverage increases (i.e. when the potential is taken negative from the

double layer potential region). The H upd peaks are compressed into a smaller region of potential by the time that this concentration of Cl^- is reached. The shift of these peaks to more negative potential reflects a weakening of the Pt-H bond, as noted by Bagotzky *et al* [206]. However, it is important to note that there is still a change in mass slope as the potential reaches the H upd region in Figure 6-5 and so the mass (frequency) change in this region does appear to relate directly to the presence of adsorbed H at the electrode surface.

The changes that occur in this region are complex, even in background electrolyte and so without further experiments few firm conclusions can be drawn. However chloride is a strongly adsorbing anion and given the fact that the pzc of Pt is close 0.0V[162], it is likely that chloride is present over the whole of the H upd range (Bagotzky[206] and co-workers suggested that complete removal of anions is reached at the potential of hydrogen evolution). The changes seen as the chloride ion concentration increases may reflect the fact that chloride, being largely unsolvated and not an oxo-anion (like perchlorate and sulphate) cannot assist in the formation of hydrogen bonds between weakly adsorbed H and water. This may be why the mass (frequency) increase at potentials negative of point C (Figure 6-1), and associated in Chapter 4 with H bonding between weakly adsorbed H and water, is removed as the chloride concentration increases. In this regard, it would be interesting to see the effect of chloride adsorption on the mass response for an aged electrode.

6.3.2. Chloride Adsorption in the Double Layer Region of Potential

In the double layer region itself there is a steady increase in the mass with potential for all chloride concentrations as well as for the background electrolyte (0.2M H_2SO_4 (Figure 6-1). It is also noticeable that when oxide formation is blocked and shifted to more positive potentials, the mass increase in the double layer region simply continues to increase over the extra potential region (see Figure 6-5 for example). However, the fact that the mass (frequency) also increases with potential in the background electrolyte (Figure 6-1) - at least for H_2SO_4 solutions as noted in Chapter 4 - makes it difficult to establish whether or not any part of this increase is due to increasing adsorption of chloride with potential. (Isotherms produced previously suggest that coverage should increase with potential over the range of chloride concentrations used here[206]). Experiments involving injection of chloride ions into the background electrolyte at fixed potentials, or potential step experiments with mass transients might resolve this question.

6.3.3 - Effect of Adsorbed Chloride in the Region of Oxide Formation

The most unusual results relate to the initial stages of the oxide formation process on the positive going scan. It is seen that as the bulk chloride concentration increases, the onset of surface oxidation leads to a mass increase (Figure 6-4, 2.5 mM Cl^-), a mass plateau (K) followed by a mass increase (Figure 6-5, 12.5 mM Cl^-) and a mass decrease

followed by a plateau (L) (Figure 6-6, for 25 mM Cl^- and Figure 6-7, for 50 mM Cl^-) and finally a mass decrease (Figure 6.8, for 25 mM Cl^-). In each case, the voltammetry shows clearly that oxide is formed because the oxidation and reduction currents associated with the process are visible.

It is important to note at this point that the observation of a mass change does not necessarily mean, for example, that there is only one process occurring. Thus when a mass loss is seen upon surface oxidation, there may still be a mass gain which is part of this process, but it may be obscured by a larger mass loss that occurs at the same time. It is likely that in this region there are several processes leading to mass changes and that the balance between them shifts with chloride concentration and this causes the overall mass response to vary.

A discussion of the electrochemical processes occurring in this region is helpful. We know that at all concentrations of chloride, some oxide is formed, because the oxide reduction peak is visible and there is little chlorine evolution except at the highest concentration of chloride used (peaks M and N in Figure 6-8). Li *et al* [213] reported chloride desorption, leading to a mass loss, between the potentials of 0.6V and 1.1V, but their data were obtained in solutions that were 1M in chloride ion. They also suggested that while a monolayer of adsorbed chloride was present, roughly 25% of a monolayer of Cl_{ad} was deposited at the same time. Chloride coverage in the experiments here is likely

to be less than a monolayer but desorption of adsorbed chloride should be a possible component of the mass changes seen.

The other process that may contribute to the mass changes is dissolution of the Pt electrode. Li *et al* [213] reported dissolution of Pt in their EQCM study, as identified by mass losses and by the detection of Pt in solution by atomic absorption analysis. However, they noted that the dissolution only occurred upon reduction of Pt oxide and that it decreased after a series of cycles which they attributed to removal of spikes and protrusions at the electrode surface which left a smoother surface that was less prone to dissolution. The electrode surfaces in that study however were prepared by vacuum deposition and so can be expected to be much smoother than those used here. The large mass decreases seen on the positive going scan at the higher chloride concentrations (Figure 6-8) suggest that dissolution is occurring here even on the positive going scan. This may be because of the rougher, more porous nature of these electrodes. In experiments where the potential was restricted to the double layer region and then extended into the oxide formation region (Figures 6-5 to 6-8) the reduction current after the oxide reduction peak can be seen to be larger than the double layer current. This could be due to slow oxide reduction but this observation, together with the mass increase seen in the same region (Figures 6-6 to 6-8) suggest reduction of dissolved Pt. The slowly decreasing recovery of mass when the potential is restricted to the double layer region for several cycles (Figure 6-9) also indicates that solution species are reduced but that this

reduction must compete with loss of dissolved species into solution by diffusion.

With a knowledge of the electrochemical processes that can occur, the changes seen in Figures 6-4 to 6-8 can now be explained. In Figure 6-4 (2.5 mM chloride) the extent of adsorption of chloride will be lowest and it is likely that the amount of dissolution is least too. Thus as the potential reaches the oxide formation region, the mass gain will be mainly due to oxide formation, with perhaps small amounts of chloride desorption or dissolution to offset this. Then when the potential is reversed the oxide is reduced and there is likely to be more dissolution thus giving the mass decrease. At J there is probably some re-oxidation of the dissolved Pt (which may be formed as a chloro-complex) which leads to the small recovery. There is a net loss of mass from the electrode at the end of the first cycle because the dissolved Pt is not all recovered.

The increase of concentration to 12.5 mM produces a plateau (K, Figure 6-5) before the mass increase due to surface oxidation. The expected increase in coverage of adsorbed chloride may give a larger decrease here due to adsorbed chloride and perhaps a small amount of dissolution but then the mass increase due to oxide becomes the dominant feature and a net increase occurs until the upper potential limit is reached. Scan reversal leads to oxide reduction and dissolution until the chloro-complex can be reduced (just after oxide reduction) so that the mass shows a broad gain in this region. The net mass loss over the cycle is larger than at the lower chloride concentration.

When the chloride concentration doubles to 25 mM the early stages of surface oxidation give a mass loss followed by a plateau (L - Figure 6-6). This may come from loss of adsorbed chloride and some dissolution that is then roughly balanced by the mass increase because of oxide formation. The first two processes will grow with increasing concentration of chloride but the last process will get smaller (as the oxide reduction peak shows). There are no other differences on the negative going scan except for larger mass losses because of dissolution. At 50 mM chloride, the mass decrease on oxide formation is larger and the plateau at the end of the positive going scan is shorter, reflecting the increased dominance of desorption and dissolution (mass losses) over oxide formation (mass gain). The evolution of the mass response is also assisted by the gradual shift of the onset of oxide formation to more positive potentials so that the process that gives rise to a mass gain occurs later. Less oxide is formed and so the actual mass increase associated with the oxide formation is smaller too.

Finally, when the chloride concentration reaches 0.322 M, dissolution and desorption (with the former likely to be the largest contributor) completely outweigh any mass increase due to oxide formation. It is interesting to note that the mass decrease seems to slow down as Cl_2 evolution begins.

In conclusion, the mass changes seen at a Pt electrode in the region of oxide formation can be explained by a balance between the processes of desorption of adsorbed

chloride, dissolution of the electrode, probably as a chloro-complex and oxide formation. The first two processes lead to a mass decrease and gain in importance with chloride concentration, whereas the oxide formation process which gives a mass increase is increasingly blocked and becomes less important with increasing chloride concentration.

* * *

REFERENCES

1. A.J. Bard and L.R. Faulkner, in "*Electrochemical Methods: Fundamentals and Applications*", (Ed: John Wiley), John Wiley and Sons, New York.Chichester, Brisbane, Toronto, Singapore, 1980.

2. B.E. Conway, in "*Theory and Principles of Electrode Processes: Modern Concepts of Chemistry*", (Eds: B. Crawford, Jr., W.D. McElroy and C.C. Prices), The Ronald Press Company, New York, 1965.

3. P. Delahay, in "*Double Layer and Electrode Kinetics*", John Wiley and Sons, New York, London and Sydney, 1965.

4. a) A.N. Frumkin, O.A. Petri and B.B. Dmaskin, in "*Comprehensive Treatise of Electrochemistry*", (Eds: J.O'M. Bockris, B.E. Conway and E. Yeager), Plenum Press, New York and London, Vol. 1, 1980, pp 221.

   b) S. Trasatti, in "*Modern Aspects of Electrochemistry*", (Eds: J.O'M Bockris and B.E. Conway), Plenum Press, New York and London, Vol. 13, 1979, pp 81.

5. B.E. Conway, *Prog. Surf. Sci.*, **16**, (1984) 1.

6. A.N. Frumkin, *Z. Phys. Chem.*, **103**, (1923) 43.

7. M.S. Metsik, V.D. Perevertaev, V.A. Liopo, G.T. Timoshtchenko and A.B. Kiselev, *J. Colloid. Interf. Sci.*, **43**, (1973) 662.

8. G.E. Van Gils, *J. Colloid. Interf. Sci.*, **30**, (1969) 272.

9. D.M. Kolb, in *"Advances in Electrochemistry and Electrochemical Engineering"*, (Eds: H. Gerischer and C.W. Tobias), John Wiley and Sons, New York, Vol.11, 1978, pp 25.

10. D.M. Kolb, M. Przasnyski, H. Gerischer, *J. Electroanal. Chem.*, **54**, (1974) 25.

11. J.N. Jovicevic, V.D. Jovic and A.R. Despic, *Electrochim. Acta*, **29**, (1984) 1625.

12. J.N. Jovicevic, V.D. Jovic and A.R. Despic, *Electrochim. Acta*, **30**, (1985) 1455.

13. T. Yamanaka and K. Tanabe, *J. Phys. Chem.*, **80**, (1976) 1723.

14. A.C. Zettlemoyer, F.J. Micale, K. Klier, in *"Water. A Comprehensive Treatise"*, (Ed: F. Franks), Plenum Press, New York, Vol. 5, 1975.

15. E. McCafferty, V. Pravdic and A.C. Zettlemoyer, *Trans. Faraday Soc.*, **66**, (1970) 1720.

16. R.G. Gast, E.R. Landa and G.W. Meyer, *Clays Clay Miner.*, **22**, (1974) 31.

17. A.V. Volkov, A.V. Kiselev and V.I. Lygin, *Kolloid. Zh.*, **38**, (1976) 330.

18. H. Jeziorowski, H. Knözinger, W. Meye and H.D. Müller, *J. Chem. Soc. Faraday Trans. 1*, **69**, (1973) 1744.

19. P.A. Rebinder and E.K. Venstrem, *Acta Physicochim. URSS*, **19**, (1944) 36.

20. F.P. Bowden and L.Young, *Research*, **3**, (1950) 235.

21. F.P. Bowden and D. Tabor, in *"The Friction and Lubrication of Solids"*, Oxford University Press, London, 1950, Chap. 7.

22. F.P. Bowden and D. Tabor, *Properties of the Metallic Surfaces, Inst. Metals,*

1953, pp 97.

23. J.O'M. Bockris and R. Parry-Jones, *Nature*, **171**, (1953) 930.

24. M.A. Habib and J.O'M. Bockris, in "*Comprehensive Treatise of Electrochemistry*", (Eds: J.O'M. Bockris, B.E. Conway and E. Yeager), Plenum Press, New York and London, Vol.1, 1980, pp 135.

25. R. Parsons, in "*Trends in Interfacial Electrochemistry*", (Eds: A. Fernando Silva, D. Reidel), 1986, pp 373.

26. D.C. Grahame, *Chem. Rev.*, **41**, (1947) 441.

27. M.A. Feltham and M. Spiro, *Chem. Rev.*, **71**, (1971) 177.

28. I. Bakos and G. Horányi, *J. Electroanal. Chem.*, **397**, (1995) 105.

29. T.N. Andersen and R.S. Perkins, in "*Modern Aspects of Electrochemistry*", (Eds: J.O'M Bockris and B.E. Conway), Butterworths, London, Vol. 5, 1969, pp 208.

30. J.O'M. Bockris, S.D. Argade and E. Gileadi, *Electrochim.. Acta*, **14**, (1969) 1259.

31. A.N. Frumkin, *Adv. Electroch. Eng.*, **3**, (1963) 307.

32. A.N. Frumkin, N.A. Balashova and V.E. Kazarinov, *J. Electrochem. Soc.*, **113**, (1966) 1011.

33. A.N. Frumkin, *J. Electrochem. Soc.*, **107**, (1960) 461.

34. A.N. Frumkin and O.A. Petrii, *Electrochim. Acta*, **15**, (1970) 391.

35. E. Gileadi, S.D. Argade and J.M'O. Bockris, *J. Phys. Chem.*, **70**, (1966) 2044.

36. A.N. Frumkin, O.A. Petrii and Yu.G. Kotlov, *Elektrokhimiya*, **5**, (1969) 476.

37. N.A. Balashova and N.T. Gorokhova, *Elektrokhimiya*, **8**, (1972) 760.

38. A.N. Frumkin, Zh.N. Malysheva, O.A. Petrii and V.E. Kazarinov, *Elektrokhimiya*, **8**, (1972) 599.

39. H. Angerstein-Kozlowska, B.E. Conway and W.B.A. Sharp, *J. Electroanal.Chem.*, **43**, (1973) 9.

40. B.E. Conway, H. Angerstein-Kozlowska and F.C. Ho, *J. Vac. Sci. Technol.*, **14**, (1977) 351.

41. B.E. Conway, H. Angerstein-Kozlowska, F.C. Ho, J. Klinger, B. MacDougall and S.Gottesfeld, *Faraday Disc. Chem. Soc.*, **56**, (1973) 199.

42. T. Biegler, D.A.J. Rand and R. Woods, *J. Electroanal. Chem.*, **29**, (1971) 269.

43. H. Angerstein-Kozlowska, in "*Comprehensive Treatise of Electrochemistry*", (Eds: E.Yeager, J.O'M. Bockris, B.E. Conway and S. Sarangapani), Plenum Press, New York, Vol. 9, 1984, pp 15.

44. A.A. Michiri, A.G. Pshchenichnikov and R.Kh. Burshtein, *Elektrokhimiya*, **8**, (1972) 354.

45. J.F. Alder and J.J. McCallum, *The Analyst*, **108**, (1983) 1169.

46. J. Hlavay and G.G. Guilbault, *Anal. Chem.*, **49**, (1977) 1890.

47. S. Bruckenstein and M. Shay, *Electrochim. Acta*, **30**, (1985) 1295.

48. K. Keiji Kanazawa and Joseph G. Gordon II, *Anal. Chem.*, **57**, (1985) 1770.

49 J.H. Kaufman, K.K. Kanazawa and J.B. Street, *Phys. Rev. Lett.*, **53**, (1984) 2461.

50. R. Schumacher, *Angewandte Chemie Int. Ed. Engl.*, **29**, (1990) 329.

51. M.Thompson, A.L. Kipling, W.C. Duncan Hewitt, L.V. Rajakovic and B.A. Cavic Vlasac, *The Analyst*, **116**, (1991) 881.

52. Daniel A. Buttry, in "*Electroanalytical Chemistry*", (Ed: A.J. Bard), Marcel Decker, New York, Vol. 17, 1991.

53. D.A. Buttry and M.D. Ward, *Chemical Reviews*, **92**, (1992) 1355.

54. C. Lu and A.W. Czanderna, in "*Applications of Piezoelectric Quartz Crystal Microbalances*", (Eds: C. Lu and A.W. Czanderna), Elsevier, Amsterdam, Oxford, New York, Tokyo, Vol.7, 1984.

55. D.A. Buttry, in "*Applications of the Quartz Crystal Microbalance to Electrochemistry: Electroanalytical Chemistry*", (Ed: A.J. Bard), Marcel Dekker, New York, Vol. 7, 1991.

56. M.D. Ward, in "*Principles and Applications of the Electrochemical Quartz Crystal Microbalance (Physical Electrochemistry: Principles, Methods and Applications)*", (Ed: Israel. Rubinstein), Marcel Dekker, New York, Basel, Hong Kong, (1995), pp 293.

57. B. Beden, J.M. Léger and C. Lamy, in "*Modern Aspects of Electrochemistry*", (Eds: R.E. White, J.O'M. Bockris and B.E. Conway), Plenum Press, Vol. 22, 1992.

58. A. Bewick, "*Trends in Interfacial Electrochemistry*", (Ed: A.F. Sylva), D. Reidel Publishing Company, New York, (1986) pp 331; and (1992) pp 97.

59. C. Lang, F. Hahn and B. Beden, *Portug. Electrochim. Acta*, **7**, (1989) 435.

60. A. Hamnett, P.A. Christensen, S.J. Higgins, *Portug. Electroch. Acta*, **7**, (1989) 591.

61. A. Bewick and S. Pons, "*Advances in Infrared and Raman Spectroscopy*", (Eds: R.S.H. Clark and M.E. Hester), Heyden, London, Vol.12, 1985, pp 1.

62. B. Beden, *NATO ASI Ser., Ser. C.*, **320**, (1990) 103.

63. R.G. Greenler and T.L. Slager, *Spectrochim. Acta*, **29A**, (1973) 193.

64. O. Wolter and J. Heitbaum, *Ber. Bunsenges. Phys. Chem.*, **88**, (1984) 2.

65. S. Bruckenstein and J. Comeau, *Faraday Disc. Chem. Soc.*, **56**, (1974) 285.

66. S. Wilhelm, W. Vielstich, H.W. Buschmann and T. Iwasita, *J. Electroanal. Chem.*, **229**, (1987) 377.

67. S. Wilhelm, T. Iwasita and W. Vielstich, *J. Electroanal. Chem.*, **238**, (1987) 383.

68. M. Watanabe, M. Uchida and S. Motoo, *J. Electroanal. Chem.*, **229**, (1987) 395.

69. K.V. Ramesh, P.R. Sarode, S. Vasudevan and A.K. Shukla, *J. Electroanal. Chem.*, **223**, (1987) 91.

70. E. Roch and J. Heitbaum, *J. Electroanal. Chem.*, **205**, (1986) 151

71. J.B. Goodenough, A. Hamnett, B.J. Kennedy and S.A. Weeks, *Electrochim. Acta*, **32**, (1987) 1233.

72. M. Shibada and S. Motoo, *J. Electroanal. Chem.*, **209**, (1986) 151.

73. E.M. Belgsir, H. Huser, J.M. Léger and C. Lamy, *J. Electroanal. Chem.*, **225**,

(1987) 281.

74. K.B. Kokoh, P. Parpot, E.M. Belgsir, J.M. Leger, B. Beden and C. Lamy, *Electrochim. Acta*, **38**, (1993) 1359.

75. K.B. Kokoh, J.M. Léger, B.Beden, H. Huser and C. Lamy, *Electrochim. Acta*, **37**, (1992) 1909.

76. G. Guilbault, *Ion Selective Electrode Reviews*, **2**, (1980) 3.

77. S. Bruckenstein and M. Shay, *J. Electroanal. Chem.*, **188**, (1985) 131.

78. M.R. Deakin, T.T. Li and O.R. Melroy, *J. Electroanal. Chem.*, **243**, (1988) 343.

79. Z. Shu and S. Bruckenstein, *J. Electroanal. Chem.*, **317**, (1991) 263.

80. C.P. Wilde and M. Zhang, *Electrochim. Acta*, **39**, (1994) 347.

81. C.P. Wilde and M. Zhang, *J. Chem. Soc. Faraday Trans.*, **89**, (1993) 385.

82. C.P. Wilde and M. Zhang, *J. Electroanal. Chem.*, **340**, (1992) 241.

83. H.E. Hager, R.D. Ruedisueli and M.E. Buehler, *Corrosion*, **42**, (1986) 345.

84. W.D. Hinsberg, C.G. Willson and K.K. Kanazawa, *J. Electrochem. Soc.*, **133**, (1986) 1448.

85. C. Gabrielli, M. Keddam and H. Takenouti, *Corrosion Science*, **31**, (1990) 129.

86. S. Bruckenstein and S. Swathirajan, *Electrochim. Acta*, **30**, (1985) 851.

87. M.R. Deakin and O.R. Melroy, *J. Electroanal. Chem.*, **239**, (1988).

88. Y. Tang and T.E. Furtak, *Electrochim. Acta*, **36**, (1991) 1873.

89. C.P. Wilde and M. Zhang, *J. Electroanal. Chem.*, **327**, (1992) 307.

90. C.P. Wilde and M. Zhang, *Langmuir*, **10**, (1994) 1600.

91. C.P. Wilde and M. Zhang, *J. Electroanal. Chem.*, **338**, (1992) 359.

92. H.J. Schmit, *Anal. Chim. Acta*, **273**, (1993) 561.

93. C.K. Baker and J.R. Reynolds, *Synth. Met.*, **28**, (1989) C21.

94. C.K. Baker and J.R. Reynolds, *J. Electroanal. Chem.*, **251**, (1988) 307.

95. P.T. Varineau and D.A. Buttry, *J. Phys. Chem.*, **91**, (1987) 1292.

96. D. Orata and D.A. Buttry, *J. Amer. Chem. Soc.*, **109**, (1987) 3574.

97. M.R. Deakin and H. Byrd, *Anal. Chem.*, **61**, (1989) 290.

98. R.R. McCaffrey, S. Bruckenstein and P. Prasad, *Langmuir*, **2**, (1986) 228.

99. G.G. Guibault, *Anal. Chem.*, **55**, (1983) 1682.

100. M. Thompson, C.L. Arthur and K.D. Gurbaksh, *Anal. Chem.*, **58**, (1986) 1206.

101. C.P. Wilde, A. Hu, C.M. Rondeau and M. Wood, *J. Electroanal. Chem.*, **353**, (1993)19.

102. H. Muramatsu, K. Kajiwara, E. Tamiya and I. Karube, *Anal. Chim. Acta*, **188**, (1986) 257.

103. E.S. Grabbe, R.P. Buck and O.R. Melroy, *J. Electroanal. Chem.*, **223**, (1987) 67.

104. S.Z. Yao and Z.H. Mo, *Anal. Chim. Acta*, **193**, (1987) 97.

105. W.Z. Wei, L.H. Nie and S.Z. Yao, *Anal. Chim. Acta*, **269**, (1992) 149.

106. J.L. Jones and J.P. Meiure, *Anal. Chem.*, **41**, (1969) 484.

107. J.L. Jones and J.P. Meiure, *Talanta*, **16**, (1969) 149.

108. P.L. Konash and J.G. Bastiaans, *Anal. Chim.*, **52**, (1980) 1929.

109. T. Nomura, *Anal. Chem.*, **124**, (1981) 81.

110. T. Nomura, T. Nagamure, K. Izutsu, T.S. West, *Bunseki Kagaku*, **30**, (1981) 494.

111. T. Nomura and M. Iijima, *Anal. Chim. Acta*, **131**, (1981) 97.

112. P. Curie and J. Curie, C.R. Acad. Sci., **91**, (1880) 294.

113. E.A. Gerber and A. Ballato, "*Precision Frequency Control: Acoustic Resonator and Filters*",(Eds: E.A. Gerber and A. Ballato), Academic Press Inc, Vol. 1, 1985.

114. E.A. Gerber and A. Ballato, "*Precision Frequency Control: Oscillators and Standards*", (Eds: E.A. Gerber and A. Ballato), Academic Press Inc, Vol. 2, 1985.

115. G. Sauerbrey, *Z. Phys.*, **155**, (1959) 206-212.

116. G. Sauerbrey, *Z. Phys.*, **178**, (1964) 457-471.

117. S.J. Lasky and D.A. Buttry, *J. Am. Chem. Soc.*, **110**, (1988) 6258.

118. S.J. Lasky and D.A. Buttry, *ACS Symp. Ser.*, **403**, (1989) 237.

119. S.J. Martin and J.C. Frye, *Appl. Phys. Lett.*, **57**, (1989) 2630.

120. B.A. Martin and H.E. Hager, *J. Appl. Phys.*, **65**, (1989) 2630.

121. M.D. Ward and E.J. Delawski, *J. Anal. Chem.*, **63**, (1991) 886.

122. R. Schumacher, J. Gordon and O. Melroy, *J. Electroanal. Chem.*, **216**, (1987) 127.

123. R. Schumacher, G. Borges and K. Kanazawa, *Surf. Sci.*, **163**, (1985) L621.

124. A. Muller, M. Wicker, R. Schumacher and R.N. Schindler, *Ber. Bunsen-Ges. Phys. Chem.*, **92**, (1988) 1395.

125. K.E. Heusler, A. Grzegorzewski, L. Jackel and J. Pietrucha, *Ber. Bunsen-Ges. Phys.Chem.*, **92**, (1988) 1218.

126. W. Stockel, R. Schumacher, *Ber. Bunsen-Ges. Phys. Chem.*, **345**, (1987) 91.

127. E.P. EerNisse, *Proc. 29th Annual Symposium Frequency Control Atlantic City*, Electronics Industries Association, Washington DC, New Jersey, (1975) pp 1.

128. G.T. Cheek and W.E. O'Grady, *J. Electroanal. Chem.*, **277**, (1990) 341.

129. E.P. EerNisse, *J. Appl. Phys.*, **43**, (1972) 1330.

130. E.P. EerNisse, *J. Appl. Phys.*, **44**, (1972) 4482.

131. D.M. Ullevig, J.M. Evans and M.G. Albrecht, *Anal. Chem.*, **54**, (1982) 2341.

132. L.V. Rajakovic, B.A. Cavic-Vlasak, V. Ghaemmaghami, K.M.R. Kalury, A.L. Kipling and M. Thompson, *Anal. Chem.*, **63**, (1991) 615.

133. A.L. Kipling, M. Thompson, *Anal. Chem.*, **62**, (1990) 1514.

134. M. Thompson, C.L. Arthur and G.K. Dhaliwal, *Anal. Chem.*, **58**, (1986) 1206.

135. J. Benziger, F. Pascal, S. Bernasek, M. Soriaga and T. Hubbard, *J. Electroanal. Chem.*, **198**, (1986) 65.

136. W.G. Cady, "*Piezoelectricity*", Dover: New York, 1964.

137. V.E. Bottom, "*Introduction to Quartz Crystal Unit Design*"; Van Nostrand Reinhold: New York, 1982.

138. H. Muramatsu, E. Tamiya and I. Karube, *Anal. Chem.*, **60**, (1988) 2142.

139. R. Beck, U. Pittermann and K.G. Weil, *Ber. Bunsen-Ges. Phys. Chem.*, **92**, (1988)

1363.

140. A.L. Kipling, M. Thompson, *Anal. Chem.*, **62**, (1990) 1514.

141. Z. Tiean, N. Liehua, Y. Shouzhou, *J. Electroanal. Chem.*, **293**, (1990) 1.

142. C.E. Reed, K.K. Kanazawa, J.H. Kaufman, *J. Appl. Phys.*, **68**, (1990) 1993.

143. S.J. Martin, V. Edwards Granstaff and G.C. Frye, *Anal. Chem.*, **63**, (1991) 2272.

144. C. Fruböse, K. Doblhofer and D.M. Soares, *Ber. Bunsen-Ges. Phys. Chem.*, **97**, (1993) 475.

145. M. Yang, Michael Thompson and W.C. Duncan-Hewitt, *Langmuir*, **9**, (1993) 802.

146. D.M. Soares, W. Kautek, C. Fruböse and K. Doblhofer, *Ber. Bunsen-Ges. Phys. Chem.*, **98**, (1994) 219.

147. E.J. Calvo, C. Danilowicz and R. Etchenique, *J. Chem. Soc. Faraday Trans.*, **91**, (1995) 4083.

148. M. Zhang and C.P. Wilde (supervisor), in "*PhD Thesis: Chemistry: Electrochemical Quartz Crystal Microbalance (EQCM) Studies of Electrocatalytic Reactions*", ©M. Zhang, University of Ottawa, Ottawa, Canada, (1994) p.67-69.

149. S. Bruckenstein, M. Michalski, A. Fensore, Z. Li and A.R. Hillman, *Anal. Chem.*, **66**, (1994) 1847.

150. S. Bruckenstein, A. Fensore, Z. Li and A.R. Hillman, *J. Electroanal. Chem.*, **370**, (1994) 189.

151. W. Stöckel and R. Schumacher, *Ber. Bunsenges. Phys. Chem.*, **91** (1987) 345.

152. M. Hachkar, T. Napporn, J.M. Léger, B. Beden and C. Lamy, *Electrochim. Acta*, **41**, (1996) 2721.

153. K. Shimazu and H. Kita, *J. Electroanal. Chem.*, **341**, (1992) 361.

154. T. Frelink, W. Visscher and J.A.R. Vanveen, *Langmuir*, **12**, (1996) 3702.

155. V.I. Birss, M. Chang and J. Segal, *J. Electroanal. Chem.*, **355**, (1993) 181.

156. R. Raudonis, D. Plaušinaitis,V. Daujotis, *J.Electroanal. Chem.*, **358**, (1993) 351.

157. M. Yang and M. Thompson, *Langmuir*, **9**, (1993) 802.

158. P.A. Christensen and A. Hamnett, in "*Techniques and Mechanisms in Electrochemistry*", Blackie Academic and Professional, 1994.

159. M.A. Habib and J. O'M. Bockris, *J. Electrochem. Soc.*, **132** (1985) 108.

160. F.C. Nart and T. Iwasita, *J. Electroanal. Chem.*, **308** (1991) 277.

161. T. Iwasita and F.C. Nart, *J. Electroanal. Chem.*, **295** (1990) 215.

162. A. Wieckowski, in "*Modern Aspects of Electrochemistry*", (Eds: R.E.White, J.O'M. Bockris and B.E. Conway), Plenum Press, New York, Vol. 21, 1990.

163. J.F. Llopis and F. Colom, in "*Encyclopedia of the Electrochemistry of the Elements*", Ed: A.J. Bard, Vol. VI, Marcel Dekker, New York, 1976.

164. A. Bewick and K. Kunimatsu, *Surf. Sci.*, **101**, (1980) 131.

165. A. Bewick and J.W. Russel, *J. Electroanal. Chem.*, **132**, (1982) 329.

166. J. Nichols and A. Bewick, *J. Electroanal. Chem.*, **243**, (1988) 445.

167. H. Ogasawa and M. Ito, *Chem. Phys. Lett.*, **221**, (1994) 213.

168. A. Peremans and A. Tadjeddine, *Phys. Rev. Lett.*, **73**, (1994) 3012.

169. A. Peremans and A. Tadjeddine, *J. Chem. Phys.*, **103**, (1995) 7197.

170. A. Bewick, K. Kunimatsu, J. Robinson and J.W. Russell, *J. Electroanal. Chem.*, **119**, (1981) 175.

171. J.G. Gordon, O.R. Melroy and M.F. Toney, *Electrochim. Acta*, **40**, (1995) 3.

172. K. Itaya, S. Sugawara and K. Higaki, *J.Phys. Chem.*, **92**, (1988) 6714.

173. I. Bakos and G. Horányi, *J.Electroanal. Chem.*, **347**, (1993) 383.

174. P.J. Vandeberg, J.L. Kowagoe and D.C. Johnson, *Analytica Chimica Acta*, **260**, (1992) 1.

175. P.J. Vandeberg and D.C. Johnson, *J. Electroanal. Chem.*, **362**, (1993) 129.

176. R. Philipp and U. Retter, *Electrochim. Acta*, **40**, (1995) 1581.

177. Z.Q. Tian, W.H. Li, B.W. Mao, J.S. Gao, *J. Electroanal. Chem.*, **379**, (1994) 271.

178. A. Baars, J.W.J. Knapen, M. Sluyters-Rehbach and J.H. Sluyters, *J.Electroanal. Chem.*, **368**, (1994) 293.

179. B.H. Loo, *Chem. Phys. Lett.*, **89**, (1982) 346.

180. S.H. Macomber and T.E. Furtak, *Chem. Phys. Lett.*, **90**, (1982) 59.

181. T.Z. Polta and Dennis C. Johnson, *J. Electroanal. Chem.*, **209**, (1986) 159.

182. K. Nakamoto, in "*Infrared and Raman Spectra of Inorganic and Coordination Compounds*", 3rd Ed., (Wiley- Interscience), New York, 1978.

183. L.L. Shreir, in "*Corrosion*", (Ed: L.L. Shreir), 2nd Ed., Newnes-Butterworths,

London, 1976.

184. T. Groenewald, *J. Appl. Electrochem.*, **5**, (1975) 71.

185. D. Kumler and G.M. Fohler, *J.Am.Chem.Soc.*, **64**, (1942) 1944.

186. U.S. Department of Health and Human Service, *4th Ann. Report on Carcinogens*, U.S. Government Printing Office, Washington D.C., 1985.

187. P.W. Preisler and L. Berger, *J. Amer. Chem. Soc.*, **69**, (1947) 322.

188. K.S.V. Santhanam and V.R. Krishnan, *Z.Phys.Chem.*, **34**, (1962) 312.

189. N.N. Kuz'mina and O.A. Songina, *Chem. Abstr.*, **57**, (1962) 2857.

190 S.J. Reddy and V.R. Krishnan, *J.Electroanal.Chem.*, **27**, (1970) 473.

191. L.I. Krishtalik, *Electrochim. Acta*, **13**, (1968) 1045.

192. Yu.N. Sheinker, I.Ya. Postoviskii and I.M. Voronova, *Zhur.Fiz.Khim.*, **33**, (1959) [see *Russ.J.Phys.Chem., Abs.*, **33**, Nos 1-6].

193. S.V. Gorbachev, A.F. Atanasyants and Yu.M. Senatorov, *Russ. J. Phys. Chem.*, **46**, (1972) 1395.

194. B. MacDougall, B.E. Conway and H.A. Kozlowska, *J.Electroanal.Chem.*, **32**, (1971) App.15.

195. B.E. Conway, B. MacDougall, H.A. Kozlowska, *Farad. Trans.I*, **68**, (1972) 1566.

196. G. Horányi, *J.Electroanal.Chem.*, **51**, (1974) 163.

197. G. Horányi, D. Hegedüs and E.M. Rizmayer, *J. Electroanal. Chem.*, **40**, (1972) 393.

198. G. Horányi, G. Inzert and E.M. Rizmayer, *J. Electroanal. Chem.*, **98**, (1979) 105.

199. G. Horányi, E.M. Rizmayer, E.P. Simon and J. Szammer, *J. Electroanal. Chem.*, **323**, (1992) 329.

200. C.P. Wilde and M. Zhang, *J.Chem.Soc Faraday Trans.*, **90** (1994) 1233.

201. D.M. Novak, B.V. Tilak and B.E. Conway, in "*Modern Aspects of Electrochemistry*", (Eds: J.O'M. Bockris, B.E. Conway and R.E. White), Plenum Press, New York, Vol. 14, 1982, pp 195.

202. F. Hine, B.V. Tilak and K. Viswanathan, in "*Modern Aspects of Electrochemistry*", (Eds: J.O'M. Bockris, B.E. Conway and R.E. White), Plenum Press, New York, Vol. 18, 1986, pp 249.

203. S. Trasatti, *Electrochim. Acta*, **32**, (1987) 369.

204. M.W. Breiter, *Electrochim. Acta*, **8**, (1963) 925.

205. W. Böld and M.W. Breiter, *Electrochim. Acta*, **5**, (1961) 145.

206. V.S. Bagotzky, Y.B. Vasillyev, J. Weber and J.N. Pirtskhaleva, *J.. Electroanal. Chem.*, **27**, (1970) 31.

207. B.E. Conway and D.M. Novak, *J.Chem. Soc. Faraday Trans.* I, **75**, (1979) 2454.

208. D.M. Novak and B.E. Conway, *J. Chem. Soc. Faraday Trans.* I, **77**, (1981) 2341.

209. B.E. Conway and L. Bai, *J. Electroanal. Chem.*, **198**, (1986) 149.

210. B.E. Conway and G. Ping, *J. Chem. Soc. Faraday Trans.* I, **87**, (1991) 2705.

211. D.A. Skoog and D.M. West, in "*Fundamentals of Analytical Chemistry*", Saunders

College Publishing, Fourth edition, 1982.

212. M.R. Deakin, T.T. Li and O.R. Melroy, *J. Electroanal. Chem.*, **243**, (1988) 343.

213. F.-B. Li, A.R. Hillman, S.D. Lubetkin and D.J. Roberts, *J. Electroanal. Chem.*, **335**, (1992) 345.

* * *